

PREPARATION AND SURFACE MODIFICATION OF NOBLE METAL
NANOPARTICLES WITH TUNABLE OPTICAL PROPERTIES FOR SERS
APPLICATIONS

A THESIS SUBMITTED TO
THE GRADUATE SCHOOL OF NATURAL AND APPLIED SCIENCES
OF
MIDDLE EAST TECHNICAL UNIVERSITY

BY

MURAT KAYA

IN PARTIAL FULFILLMENT OF THE REQUIREMENTS
FOR
THE DEGREE OF DOCTOR OF PHILOSOPHY
IN
CHEMISTRY

MARCH 2011

Approval of the thesis:

**PREPARATION AND SURFACE MODIFICATION OF NOBLE METAL
NANOPARTICLES WITH TUNABLE OPTICAL PROPERTIES FOR SERS
APPLICATIONS**

submitted by **MURAT KAYA** in partial fulfillment of the requirements for the degree of **Doctor of Philosophy in Chemistry Department, Middle East Technical University** by,

Prof. Dr. Canan Özgen
Dean, Graduate School of **Natural and Applied Sciences**

Prof. Dr. İlker Özkan
Head of Department, **Chemistry**

Prof. Dr. Mürvet Volkan
Supervisor, **Chemistry Dept., METU**

Examining Committee Members:

Prof. Dr. O. Yavuz Ataman
Chemistry Dept., METU

Prof. Dr. Mürvet Volkan
Chemistry Dept., METU

Prof. Dr. E. Hale Göktürk
Chemistry Dept., METU

Prof. Dr. Macit Özenbaş
Metallurgical and Materials Eng. Dept., METU

Prof. Dr. A. Rehber Türker
Chemistry Dept., Gazi University

Date: 16/03/2011

I hereby declare that all information in this document has been obtained and presented in accordance with academic rules and ethical conduct. I also declare that, as required by these rules and conduct, I have fully cited and referenced all material and results that are not original to this work.

Name, Last name: Murat Kaya

Signature

ABSTRACT

PREPARATION AND SURFACE MODIFICATION OF NOBLE METAL NANOPARTICLES WITH TUNABLE OPTICAL PROPERTIES FOR SERS APPLICATIONS

Kaya, Murat

Ph.D., Department of Chemistry

Supervisor: Prof. Dr. Mürvet Volkan

March 2011, 170 pages

Metal nanostructures exhibit a wide variety of interesting physical and chemical properties, which can be tailored by altering their size, morphology, composition, and environment. Gold and silver nanostructures have received considerable attention for many decades because of their widespread use in applications such as catalysis, photonics, electronics, optoelectronics, information storage, chemical and biological sensing, surface plasmon resonance and surface-enhanced Raman scattering (SERS) detection.

This thesis is composed of three main parts about the synthesis, characterization and SERS applications of shape-controlled and surface modified noble metal nanoparticles. The first part is related to a simple synthesis of shape controlled solid gold, hollow gold, silver, gold-silver core-shell, hollow gold-silver double-shell nanoparticles by applying aqueous solution chemistry. Nanoparticles obtained were used for SERS detection of dye molecules like brilliant cresyl blue (BCB) and crystal violet (CV) in aqueous system.

The second part involves the synthesis of surface modified silver nanoparticles for the detection of dopamine (DA) molecules. Determination of a dopamine molecule attached to a iron-nitrilotriacetic acid modified silver (Ag-Fe(NTA)) nanoparticles by using surface-enhanced resonance Raman scattering (SERRS) was achieved. The Ag-Fe (NTA) substrate provided reproducibility and excellent sensitivity. Experimental results showed that DA was detected quickly and accurately without any pretreatment in nM levels with excellent discrimination against ascorbic acid (AA) (which was among the lowest value reported in direct SERS detection of DA).

In the third part, a lanthanide series ion (Eu^{3+}) containing silver nanoparticle was prepared for constructing a molecular recognition SERS substrate for the first time. The procedure reported herein, provides a simple way of achieving reproducible and sensitive SERS spectroscopy for organophosphates (OPP) detection. The sensing of the target species was confirmed by the appearance of an intense SERS signal of the methyl phosphonic acid (MPA), a model compound for nonvolatile organophosphate nerve agents, which bound to the surface of the Ag- Eu^{3+} nanostructure. The simplicity and low cost of the overall process makes this procedure a potential candidate for analytical control processes of nerve agents.

Key words: noble metal nanoparticles, surface modification, surface enhanced Raman scattering (SERS), neurotransmitters, dopamine, chemical warfare agents

ÖZ

AYARLANABİLİR OPTİK ÖZELLİKLERE SAHİP METAL NANOPARÇACIKLARIN HAZIRLANMASI, YÜZEYLERİNİN MODİFİYE EDİLMESİ VE SERS UYGULAMALARI

Kaya, Murat

Doktora, Kimya Bölümü

Tez Yöneticisi: Prof. Dr. Mürvet Volkan

Mart 2011, 170 sayfa

Metal nanoyapılar, morfoloji, bileşim ve çevre değişiklikleriyle geniş bir yelpazede ayarlanabilen, ilginç fiziksel ve kimyasal özelliklere sahiptirler. Altın ve gümüş nanoyapılar, katalizör, fotonik, elektronik, optoelektronik, bilgi depolama, kimyasal ve biyolojik algılama, yüzey plazmon rezonans algılama, görüntüleme ve yüzeyde güçlendirilmiş Raman saçılması (YGRS) gibi birçok alanda yaygın olarak kullanılabilmeleri nedeniyle uzun yıllardan beri büyük ilgi görmektedir.

Bu tez, şekil kontrollü ve yüzeyleri modifiye edilmiş soy metal nanoparçacıkların sentezlenmesi, karakterizasyonları ve YGRS uygulamalarını içeren üç kısımdan oluşmaktadır. İlk bölüm, altın, içi boş altın, gümüş, altın-gümüş çekirdek kabuk ve altın-gümüş çift kabuk nanoparçacıklarının kontrollü şekilde, basit sulu çözelti kimyası uygulanarak sentezlenmesi ve karakterize edilmesi ile ilgilidir. Sentezlenen nanoparçacıklar, sulu sistemde parlak kresil mavi (BCB) ve kristal viyole (CV) gibi model boya moleküllerinin YGRS ile tayini için kullanılmıştır.

İkinci bölüm, dopamin (DA) moleküllerinin tespiti için yüzeyi modifiye edilmiş gümüş nanoparçacıklarının sentezini içermektedir. Yüzeyde güçlendirilmiş rezonans Raman saçılması (YGRS) yöntemi kullanarak Ag-Fe(NTA) nano yapısına bağlı dopamin molekülünün tayini sağlanmıştır. Hazırlanan Ag-Fe(NTA) substratı ile dopamin molekülünün belirlenmesinde tekrarlanabilirlik ve mükemmel hassasiyet sağlanmıştır. Deneysel sonuçlar, dopaminin askorbik asit ortamında, herhangi bir ön hazırlık olmadan nanomolar seviyesinde hızlı ve doğru bir şekilde mükemmel bir ayırımla, dopaminin YGRS ile tespiti için rapor edilen en düşük derişim değerlerinden daha aşağıdaki değerlerde, tayin edilebildiğini göstermektedir.

Üçüncü ve son bölümde ise, ilk defa, YGRS yüzeyi olarak moleküler tanımlamada kullanılmak üzere bir lantanit dizi iyonu (Eu^{3+}) içeren gümüş nanoparçacıklarının yeni bir yöntemle hazırlanması anlatılmıştır. Burada bildirilen işlem, organofosfatların (OPPs) duyarlı YGRS spektroskopisi ile tekrarlanabilir şekilde tayin edilmesini sağlamaktadır. Hedef türlerin varlığı, uçucu olmayan organofosfatlı sinir ajanları için model bileşik olan metil fosfonik asitin Ag- Eu^{3+} nano yapı yüzeyi ile elde edilmiş yoğun YGRS sinyali ile teyit edilmiştir. Genel sürecin basitliği ve düşük maliyeti bu yöntemi sinir ajanlarının kontrol süreçleri için potansiyel bir aday yapar.

Anahtar Kelimeler: soy metal nanoparçacıklar, yüzey modifikasyonu, yüzeyde güçlendirilmiş Raman saçılması (YGRS), nörotransmitter, dopamin, kimyasal silah ajanları

To my family

ACKNOWLEDGEMENT

I would like to express my sincere thanks to Prof. Dr. Mürvet Volkan for her priceless support, guidance and encouragement during my graduate studies. I have learnt many important lessons from her not only about scientific research but also about life. I am deeply honored to have a chance to work with her, and to be alumni of her research group.

My appreciation and thanks to Prof. Dr. O.Yavuz Ataman, Prof. Dr. Macit Özenbaş and Prof. Dr. E. Hale Göktürk for their guidance as committee members.

Thanks also extended to Murat Işık, Emre Yusuf Yazıcıoğlu, Mehmet Zahmakıran, Sezgin Bakırdere, and Seher Karabıçak for being such good friends and their endless help and motivation. I also would like to thank all C-50 and C-49 members for their friendship.

I would like to thank to TUBITAK for grant TBAG-104T361 and TBAG-108T368.

The last but not the least, my special appreciation and great gratitude is devoted to my family for their endless support and my love Serap for her patience, moral support and encouragement in every moment of my life.

TABLE OF CONTENTS

ABSTRACT.....	iv
ÖZ.....	vi
ACKNOWLEDGMENT.....	ix
TABLE OF CONTENTS.....	x
CHAPTERS	
1. INTRODUCTION	1
1.1. Nanostructures.....	1
1.2. General Methods for Synthesis of Nanoparticles.....	2
1.2.1. Top-Down Approach	2
1.2.2. Bottom-Up Approach.....	3
1.3. Characterizations of Metallic Nanoparticles	4
1.4. Metal Nanoparticles	7
1.4.1. Synthesis of Metal Nanoparticles.....	7
1.4.2. Noble Metal Nanoparticles	8
1.5. Hollow Nanostructures.....	9
1.6. Core-Shell Nanostructures	10
1.7. Optical Properties of Noble Metal Nanostructures	12
1.8. Raman Spectroscopy	18
1.9. Surface Enhanced Raman Scattering (SERS)	20
1.9.1. Different SERS-Active Media (SERS Substrates).....	22
1.9.2. Instrumentation	23
1.9.3. Surface Enhanced Resonance Raman Scattering (SERRS)	25
1.10. Surface Modification of Nanostructured Materials.....	27
1.11. Importance of Dopamine (DA) and Common Techniques Used in Dopamine Detection	28

1.12. Nerve Agents (Chemical Warfare Agents)	32
1.13. Scope of the Thesis	35
2. EXPERIMENTAL	36
2.1. Materials.....	36
2.2. Instrumentation	37
2.3. Synthesis of Hollow Gold Nanoparticles	38
2.3.1. Preparation of Cobalt Nanotemplates	38
2.3.2. Preparation of Hollow Gold Nanoparticles.....	39
2.4. Preparation of Solid Gold Nanoparticles	40
2.5. Synthesis of Hollow Gold-Silver Double-Shell and Solid Gold-Silver Core-Shell Nanoparticles	41
2.6. Synthesis of Silver Nanoparticles with Citrate Reduction.....	43
2.7. Surface Modification of Silver Nanoparticles with Iron-Nitrilotriacetic Acid Complex	43
2.8. Preparation of Europium (III) Ion Modified Silver (Ag-Eu ³⁺) Nanoparticles.....	44
2.9. Preparation of Substrates for SERS and SERRS Studies.....	44
3. RESULTS AND DISCUSSIONS	45
3.1. Preparation of SERS Substrates with Tunable Optical Property	45
3.1.1. Preparation of Hollow Gold Nanoparticles with a Tunable Interior Cavity.....	47
3.1.1.1. Preparation of Cobalt Nanotemplates	47
3.1.1.2. Effect of the Amount of Capping Agent (Sodium Citrate) and Reducing Agent (Sodium Borohydride) on the Particle Size of Cobalt Nanoparticles.....	49
3.1.1.3. Formation of Hollow Gold Nanoparticles (HAuNPs)	54
3.1.1.4. Optical Characterization of Prepared Hollow Gold Nanoparticles.....	58
3.1.2. Preparation of Hollow Gold-Silver Double-Shell Nanoparticles (HAuAgNPs).....	64
3.1.2.1. Surface Plasmons in Hollow Gold-Silver Double-Shell Nanoparticles...	67
3.1.3. Preparation of Solid Gold Nanoparticles	69
3.1.3.1. Effect of Particle Size on Optical Properties of AuNPs.....	70
3.1.4. Preparation of Gold Core-Silver Shell Nanoparticles	72

3.1.4.1. Characterization of the Gold Core-Silver Shell Nanoparticles	73
3.1.5. Production of Silver Nanoparticles with Citrate Reduction Method	77
3.1.6. SERS Studies	79
3.1.6.1. SERS Probe Molecules Used in Comparison Studies.....	79
3.1.6.2. SERS Studies with Prepared Nanostructures	81
3.2. Plasmonic-Based Chemical Sensing Methodologies for the Determination of Dopamine and Chemical Warfare Agents.....	89
3.2.1. Surface Modification of Silver Nanoparticles with Iron-Nitrilotriacetic Acid Complex for the Direct Measurement of Dopamine using SERRS	89
3.2.1.1. Preparation and Characterization of Fe(NTA) Modified Silver Nanoparticles.....	90
3.2.1.2. Optical properties of the Prepared Particles.....	95
3.2.1.3. SERRS Substrate Preparation and Dopamine Measurement	97
3.2.1.4. Importance of the Prepared Particles	99
3.2.1.5. Effect of pH of Complex on the SERRS Signal	101
3.2.1.6. Choice of the Form of SERRS Substrate	103
3.2.1.7. Optimization of the Complexation Period	104
3.2.1.8. Reproducibility of the Prepared Substrate	105
3.2.1.9. The Shelf-life (Stability) of the Prepared Substrate	107
3.2.1.10. Selectivity and Interference Studies	108
3.2.1.11. Sensitivity of the Surface Modified (Ag-Fe(NTA)) Nanoparticles as SERRS Substrate.....	110
3.2.2. Preparation of Silver Nanoparticles Modified with Europium (III) Ion for Sensitive and Selective Determination of Chemical Warfare Agents	113
3.2.2.1. Preparation of Europium (Eu ³⁺) Ion Modified Silver Nanoparticles	113
3.2.2.2. Characterization of Ag-Eu ³⁺ Nanoparticles	114
3.2.2.3. Detection of Methylphosphonic Acid (MPA) as Degradation Product of Nerve Agents by Using SERS.....	116
3.2.2.3.1. Raman Spectrum of Methylphosphonic Acid.....	118
3.2.2.3.2. SERS Measurements of Methylphosphonic Acid.....	119

3.2.2.4. Optimization of Complexation Period	122
3.2.2.5. Stability of the Ag-Eu ³⁺ Nanostructures	123
3.2.2.6. Reproducibility of the Prepared Substrate	124
3.2.2.7. Sensitivity of the Ag-Eu ³⁺ Nanostructures as SERS Substrate	126
4. CONCLUSIONS.....	128
REFERENCES.....	129
APPENDIX.....	146
CURRICULUM VITAE.....	166

LIST OF FIGURES

FIGURES

Figure 1. Schematic illustration of the top-down approach [22].	3
Figure 2. Schematic illustration of the bottom up approach [22].	4
Figure 3. Spatial resolution for observing materials [29].	5
Figure 4. Multiple shapes and sizes of nanoparticles produced with chemical methods [46].	8
Figure 5. General production procedure of hollow nanostructures.....	10
Figure 6. Possible core-shell nanostructures production mechanisms [74].	11
Figure 7. Optical absorption spectra of gold nanoparticles of different sizes [79].	13
Figure 8. Schematic of plasmon oscillation in a metal nanosphere.	14
Figure 9. Calculated higher-order charge cloud distortion around gold nanoparticles of sizes > 25 nm [80].	16
Figure 10. Calculated plasmon resonance spectra for different shell thicknesses of gold on a silica core of 60-nm radius [87].	18
Figure 11. Energy level diagram for Raman scattering; (a) Stokes scattering, (b) anti-Stokes scattering.	19
Figure 12. Schematic drawing of a typical SERS setup.....	21
Figure 13. Schematic diagram of representative instrumentation used for surface-enhanced Raman spectroscopy measurements; (a) Macro-Raman setup (b) Micro-Raman setup (Abbreviations: CCD, charge-coupled device; CL, collection lens; FL, focusing lens; NF, notch filter) [118].....	25
Figure 14. Surface modification of nanoparticles.	27
Figure 15. Chemical structure of a Dopamine molecule.	29
Figure 16. Hydrolysis pathways for G-Series nerve agents.....	33
Figure 17. Picture of Schlenk line used for producing air-free solution.	39

Figure 18. The experimental setup used for the production of the hollow gold nanoparticles (HAuNPs)	40
Figure 19. The experimental setup used for the production of the solid gold nanoparticles (AuNPs).....	41
Figure 20. The experimental setup used for the production of the hollow gold-silver double-shell nanoparticles (HAuAgNPs).	42
Figure 21. The experimental setup used for the production of the solid gold-silver core-shell nanoparticles (AuAgNPs).	42
Figure 22. Preparation of SERS and SERRS substrates.	44
Figure 23. Representations of nanostructures prepared.	46
Figure 24. FE-SEM image of cobalt nanoparticles. The average diameter of the cobalt nanoparticles was measured as 44 ± 4 nm by sampling 100 nanoparticles (0.4 M 100 μ L CoCl_2 , 0.1 M 400 μ L sodium citrate and 1 M 100 μ L NaBH_4 were used in the production of cobalt nanoparticles).....	48
Figure 25. EDX pattern of cobalt nanoparticles.....	48
Figure 26. FE-SEM image of cobalt nanoparticles. The average diameter of the cobalt nanoparticles (Table 3) was measured as 36 ± 6 nm by sampling 100 nanoparticles(0.4 M 100 μ L CoCl_2 , 0.1 M 600 μ L sodium citrate and 1 M 100 μ L NaBH_4 were used in the production of cobalt nanoparticles).	50
Figure 27. FE-SEM image of cobalt nanoparticles. The average diameter of the cobalt nanoparticles (Table 3) was measured as 25 ± 3 nm by sampling 100 nanoparticles (0.4 M 100 μ L CoCl_2 , 0.1 M 900 μ L sodium citrate and 1 M 100 μ L NaBH_4 were used in the production of cobalt nanoparticles).	51
Figure 28. FE-SEM image of cobalt nanoparticles. The average diameter of the Co nanoparticles (Table 4) was measured as 32 ± 4 nm by sampling 100 nanoparticles (0.4 M 100 μ L CoCl_2 , 0.1 M 400 μ L sodium citrate and 1 M 400 μ L NaBH_4 were used in the production of cobalt nanoparticles).	53
Figure 29. Preparation of hollow gold nanoparticles with a tunable interior cavity.	54
Figure 30. FE-SEM images of hollow gold nanoparticles produced with 44 ± 4 nm CoNP templates and with 50 μ L of 0.1 M chloroauric acid ($\text{HAuCl}_4 \cdot 3\text{H}_2\text{O}$).	55

Figure 31. FE-SEM images of hollow gold nanoparticles produced with 44 ± 4 nm CoNP templates and with $50\ \mu\text{L}$ of $0.1\ \text{M}$ chloroauric acid ($\text{HAuCl}_4\cdot 3\text{H}_2\text{O}$). The average diameter of the hollow nanoparticles was measured as 52 ± 9 nm by sampling 100 hollow gold nanoparticles.	56
Figure 32. EDX pattern of hollow gold nanoparticles.	56
Figure 33. FE-SEM image of the hollow interior of gold nanoparticles.	57
Figure 34. FE-SEM image of the hollow interior of gold nanoparticles.	58
Figure 35. UV–Vis spectra of (A) solid and (B) hollow gold nanoparticles. The sizes of the solid and hollow gold nanoparticles were 20 ± 2 and 52 ± 9 nm respectively. .	59
Figure 36. Appearance of (A) solid and (B) hollow gold nanoparticles. The sizes of the solid and hollow gold nanoparticles were 20 ± 2 and 52 ± 9 nm respectively.	60
Figure 37. Hollow nanoparticles prepared with different size of cobalt nanotemplates.	60
Figure 38. Appearance of hollow gold nanoparticles with different shell thickness and size, prepared using various sizes ((A) 25 ± 3 nm, (B) 36 ± 6 nm and (C) 44 ± 4 nm) of cobalt nanotemplates.	61
Figure 39. UV–Vis spectra of hollow gold nanoparticles prepared using various sizes ((A) 25 ± 3 nm, (B) 36 ± 6 nm and (C) 44 ± 4 nm) of cobalt nanotemplates.	61
Figure 40. Hollow nanoparticles prepared with different amount of $0.1\ \text{M}$ HAuCl_4	62
Figure 41. UV–Vis spectra of hollow gold nanoparticles with different shell thickness ($0.1\ \text{M}$ HAuCl_4).....	63
Figure 42. Preparation of hollow gold-silver double-shell nanoparticles with a tunable shell thickness.	64
Figure 43. FE-SEM image of hollow gold-silver double-shell nanoparticles produced with 52 ± 9 nm HAuNPs and $1\ \text{mM}$ AgNO_3 . The average diameter of the nanoparticles was measured as 87 ± 10 nm.	65
Figure 44. FE-SEM image of hollow gold-silver double-shell nanoparticles produced with 52 ± 9 nm HAuNPs and $1\ \text{mM}$ AgNO_3 . The average diameter of the nanoparticles was measured as 87 ± 10 nm.	66

Figure 45. EDX pattern of hollow gold-silver double-shell nanoparticles.	67
Figure 46. UV–Vis spectra of (A) hollow gold (52±9 nm) and (B) hollow gold-silver double-shell (87±10 nm) nanoparticle solutions.....	68
Figure 47. Appearance of (A) hollow gold (52±9 nm) and (B) hollow gold-silver double-shell (87±10 nm) nanoparticle solutions.....	68
Figure 48. FE-SEM image of 20±2 nm gold nanoparticles.	69
Figure 49. EDX pattern of 20±2 nm gold nanoparticles.....	70
Figure 50. UV–Vis spectra of gold nanoparticles with different size ((A) 20±2 nm and (B) 30±2 nm).....	71
Figure 51. Appearance of solid gold nanoparticles with different size (A) (20±2 nm and (B) 30±2 nm). Tunable colors generated by controlling the diameter of solid gold nanoparticles.	72
Figure 52. Preparation of gold-silver core-shell nanoparticles with a tunable shell thickness.....	72
Figure 53. FE-SEM images of gold-core silver-shell nanoparticles produced with 20±2 nm AuNPs and 1 mM AgNO ₃ . The average size of the prepared nanoparticles was measured as 51±8 nm.	73
Figure 54. EDX pattern of gold-core silver-shell nanoparticles.	74
Figure 55. UV–Vis spectra of (A) gold and (B) gold-core silver-shell nanoparticles.	75
Figure 56. Appearance of (A) solid gold (red in color) and (B) gold-core silver-shell nanoparticles (yellow in color).	75
Figure 57. UV–Vis spectra of gold-core silver-shell nanoparticles prepared with different shell thickness (10 ⁻³ M AgNO ₃).....	76
Figure 58. FE-SEM images of silver nanoparticles. The average diameter of the silver nanoparticles was measured to be 70±19 nm by sampling 100 nanoparticles.....	77
Figure 59. EDX pattern of silver nanoparticles.	78
Figure 60. UV-Vis spectrum of silver nanoparticles.	78
Figure 61. Chemical structures of dye molecules used in SERS measurements.	79

Figure 62. Raman spectrum of solid BCB. 632.8 nm radiation from a Helium–Neon laser was used with an excitation power of 10 mW and spectra was acquired with 10 s integration time.....	80
Figure 63. Raman spectrum of solid CV. 632.8 nm radiation from a Helium–Neon laser was used with an excitation power of 10 mW and spectra was acquired with 10 s integration time.....	81
Figure 64. Comparison of SERS spectra of 5×10^{-8} M BCB obtained with solid gold (AuNP) and hollow gold (HAuNP) nanoparticles. 632.8 nm radiation from a Helium–Neon laser was used with an excitation power of 10 mW and spectra was acquired with 10 s integration time.....	82
Figure 65. Comparison of SERS spectra of 5×10^{-7} M CV obtained with solid gold (AuNP) and hollow gold (HAuNP) nanoparticles. 632.8 nm radiation from a Helium–Neon laser was used with an excitation power of 10 mW and spectra was acquired with 10 s integration time.....	82
Figure 66. Comparison of SERS spectra of 5×10^{-8} M BCB obtained with hollow gold (HAuNP) and hollow gold-silver double-shell (HAuAgNP) nanoparticles. 632.8 nm radiation from a Helium–Neon laser was used with an excitation power of 10 mW and spectra was acquired with 10 s integration time.....	84
Figure 67. Comparison of SERS spectra of 5×10^{-8} M BCB obtained with gold (AuNP) and gold-core silver-shell (AuAgNP) nanoparticles. 632.8 nm radiation from a Helium–Neon laser was used with an excitation power of 10 mW and spectra was acquired with 10 s integration time.....	84
Figure 68. Comparison of SERS spectra of 5×10^{-7} M CV obtained with hollow gold (HAuNP) and hollow gold-silver double-shell (HAuAgNP) nanoparticles. 632.8 nm radiation from a Helium–Neon laser was used with an excitation power of 10 mW and spectra was acquired with 10 s integration time.	85
Figure 69. Comparison of SERS spectra of 5×10^{-7} M CV obtained with gold (AuNP) and gold-core silver-shell (AuAgNP) nanoparticles. 632.8 nm radiation from a Helium–Neon laser was used with an excitation power of 10 mW and spectra was acquired with 10 s integration time.....	86

Figure 70. Comparison of SERS spectra of 5×10^{-8} M BCB obtained with solid gold-core silver-shell (AuAgNP), hollow gold-silver double shell (HAuAgNP) and silver (AgNP) nanoparticles. 632.8 nm radiation from a Helium–Neon laser was used with an excitation power of 10 mW and spectra was acquired with 10 s integration time.	87
Figure 71. Structure of Fe(NTA) functionalized SERRS labels. Left: silver nanoparticle, middle: bifunctional Fe(NTA) host, right: analyte, dopamine molecule.	90
Figure 72. Schematic representation for the production of Ag-Fe(NTA) nanoparticles and possible cross-linking between silver nanoparticle and Fe(NTA) complex.	91
Figure 73. FE-SEM image of Fe(NTA) modified Ag NPs (31 ± 5 nm).	92
Figure 74. EDX pattern of Fe(NTA) modified Ag NPs.	93
Figure 75. FTIR spectra of (A) AB-NTA (N_{ω}, N_{α} -Bis(carboxymethyl)-L-lysine hydrate) and (B) Fe(NTA) modified Ag NPs.	94
Figure 76. UV-Vis spectrum of [Ag-Fe(NTA)DA] structure in water.	96
Figure 77. Schematic illustration of the production, and the application of Ag-Fe(NTA) substrate as molecular traps for surface-enhanced resonance Raman scattering (SERRS) of dopamine molecules.	97
Figure 78. SERRS spectrum of 1×10^{-5} M DA solution. 632.8 nm radiation from a Helium–Neon laser was used with an excitation power of 10 mW and spectra was acquired with 10 s integration time.	98
Figure 79. Influence of the surface coverage on the SERRS signal strength: A) SERS signal of 0.5 M DA obtained with silver colloid B) SERS signal of 10^{-4} M DA complexed with Fe^{3+} ion obtained with silver colloid C) SERRS signal obtained with Fe(NTA) modified silver nanoparticle, direct measurement of 10^{-5} M DA. 632.8 nm radiation from a Helium–Neon laser was used with an excitation power of 10 mW and spectra was acquired with 10 s integration time.	100
Figure 80. SERRS spectra of 1.0×10^{-5} M DA obtained with Ag-Fe(NTA) substrates at a final pH of (A) 7.0 and (B) 9.0. 632.8 nm radiation from a Helium–Neon laser	

was used with an excitation power of 10 mW and spectra was acquired with 10 s integration time.	102
Figure 81. Comparison of SERRS signal of 1.0×10^{-5} M DA obtained with (A) wet and (B) dry conditions. 632.8 nm radiation from a Helium–Neon laser was used with an excitation power of 10 mW and spectra was acquired with 10 s integration time.	103
Figure 82. Effect of the complexation time between Fe(NTA) modified silver nanoparticle and 10^{-5} M DA on the SERRS signal strength. SERRS signal of 10^{-5} M DA obtained with Fe(NTA) modified silver nanoparticle after A) as prepared B) 15 minutes. 632.8 nm radiation from a Helium–Neon laser was used with an excitation power of 10 mW and spectra was acquired with 10 s integration time.	104
Figure 83. b) SERRS spectra of 10^{-5} M DA by using Ag-Fe(NTA) nanoparticles prepared in different runs. 632.8 nm radiation from a Helium–Neon laser was used with an excitation power of 10 mW and spectra was acquired with 10 s integration time.	106
Figure 84. SERRS signal of 10^{-5} M DA acquired with Ag-Fe(NTA) nanoparticles as substrate A) the day B) after 5 days C) after 7 days D) after 15 days of their preparation. 632.8 nm radiation from a Helium–Neon laser was used with an excitation power of 10 mW and spectra was acquired with 10 s integration time.	107
Figure 85. SERRS spectrum of the (A) 1×10^{-5} M DA (B) 1×10^{-5} M DA in 1×10^{-4} M ascorbic acid (AA), (C) 1×10^{-5} M DA in 1×10^{-3} M AA (D) 1×10^{-6} M DA (E) 1×10^{-6} M DA in 1×10^{-3} M AA . 632.8 nm radiation from a Helium–Neon laser was used with an excitation power of 10 mW and spectra was acquired with 10 s integration time.	109
Figure 86. SERRS spectrum of 10^{-9} M DA solution. 632.8 nm radiation from a Helium–Neon laser was used with an excitation power of 10 mW and spectra was acquired with 10 s integration time.	111
Figure 87. FE-SEM images of Ag-Eu ³⁺ nanoparticles (39±5 nm).....	114
Figure 88. FE-SEM images of Ag-Eu ³⁺ nanoparticles.....	115
Figure 89. EDX pattern of Ag-Eu ³⁺ nanoparticles.....	116

Figure 90. A sketch of the production, and the application of Ag- Eu³⁺ substrate as molecular traps for surface-enhanced Raman scattering (SERS) of MPA molecules. 117

Figure 91. Raman spectrum of solid MPA. 632.8 nm radiation from a Helium–Neon laser was used with an excitation power of 10 mW and spectra was acquired with 10 s integration time..... 118

Figure 92. Comparison of SERS intensity of MPA acid measured with three different substrates ((A) 10⁻² M MPA on silver colloid substrate, (B) 10⁻² M MPA on silver island substrate, (C) 10⁻⁵ M MPA on Ag-Eu³⁺ substrate. 632.8 nm radiation from a Helium–Neon laser was used with an excitation power of 10 mW and spectra was acquired with 10 s integration time..... 120

Figure 93. Blank measurement of Ag–Eu³⁺ substrate. 632.8 nm radiation from a Helium–Neon laser was used with an excitation power of 10 mW and spectra was acquired with 10 s integration time..... 121

Figure 94. Effect of the complexation time between Ag-Eu³⁺ substrate and 1x10⁻⁵ M MPA on the SERS signal strength. SERS measurements of 1x10⁻⁵ M MPA with Ag-Eu³⁺ substrate were taken after A) 1 minute B) 5 minutes C) 10 minutes D) 15 minutes E) 30 minutes. 632.8 nm radiation from a Helium–Neon laser was used with an excitation power of 10 mW and spectra was acquired with 10 s integration time. 122

Figure 95. Complexation period between Ag-Eu³⁺ substrate and 1x10⁻⁵ M MPA solution..... 123

Figure 96. SERS signal of 10⁻⁵ M MPA obtained with Ag-Eu³⁺ substrate which were taken at the day of preparation and seven days after its preparation. 632.8 nm radiation from a Helium–Neon laser was used with an excitation power of 10 mW and spectra was acquired with 10 s integration time. 124

Figure 97. SERS spectra of 10⁻⁵ M MPA by using Ag-Eu³⁺ nanoparticles prepared in different runs. 632.8 nm radiation from a Helium–Neon laser was used with an excitation power of 10 mW and spectra was acquired with 10 s integration time. 125

Figure 98. Calibration curve of MPA (1×10^{-7} - 7×10^{-7} M MPA obtained with Ag-Eu³⁺ substrate). 126

Figure 99. SERS spectrum of 1×10^{-7} - 7×10^{-7} M MPA obtained with Ag-Eu³⁺ substrate. 632.8 nm radiation from a Helium–Neon laser was used with an excitation power of 10 mW and spectra was acquired with 10 s integration time. 127

LIST OF TABLES

TABLES

Table 1. Microscopes used in characterization of nanoparticles.....	6
Table 2. Several types of metallic nanostructures used for SERS	23
Table 3. Particle size of cobalt nanoparticles as a function of citrate amount	49
Table 4. Particle size of cobalt nanoparticles as a function of sodium borohydride amount.....	52

LIST OF ABBREVIATIONS

AA: Ascorbic acid

AB-NTA: Aminobutylated Nitrilotriacetic acid

AFM: Atomic force microscopy

AMPA: Alkyl methylphosphonic acid

a.u.: Arbitrary unit

BCB: Brilliant cresyl blue

CBW: Chemical and biological warfare

CCD: Charged coupled device

CNS: Central nervous system

CNT: Carbon nanotube

CT: Charge transfer

CW: Chemical warfare

CV: Crystal violet

d: Diameter

DA: Dopamine

DETA: Trimethoxysilylpropyl–diethylenetriamine

DL: Detection limit

DNA: Deoxiribo nucleic acid

DSC: Differential scanning calorimetry

EBL: electron beam lithography

EDX: Energy dispersive X-ray analysis

EF: Enhancement factor

EM: Electromagnetic field

EMPA: Ethyl methylphosphonic acid

EXAFS: Extended X-ray absorption fine structure

FE-SEM: Field emission scanning electron microscopy

FIB: Ball milling

FT-IR: Fourier transform infra red

GB: Sarin

GD: Soman

HGN: Hollow gold nanosphere

HPLC: High performance liquid chromatography

HRTEM: High resolution transmission electron microscopy

ICP-OES: Inductively coupled plasma optical emission spectrometry

IMPA: Isopropyl methylphosphonic acid

LDI-MS: Laser desorption ionization mass spectrometry

LSPR: Localized surface plasmon resonance

MPA: Methyl phosphonic acid

NF: Notch filter

NMR: Nuclear magnetic resonance

NP: Nanoparticle

NTA: Nitrilotriacetic acid

OPP: Organophosphates

ORC: Oxidation–reduction cycle

PD: Parkinson’s disease

PEG: Poly (ethylene glycol)

ppm: Parts per million

SAM: Self-assembled monolayer

SAXS: Small-angle X-ray scattering

SER: Surface-enhanced Raman

SERRS: Surface-enhanced resonance Raman scattering

SERS: Surface-enhanced Raman scattering

SP: Surface Plasmon

SPR: Surface plasmon resonance

STM: Scanning tunnelling microscopy

TEM: Transmission electron microscopy

TGA: Thermo gravimetric analysis

XPS: X-ray photoelectron spectroscopy

XRD: X-ray diffraction

UHV: Ultra high vacuum

CHAPTER 1

INTRODUCTION

1.1. Nanostructures

Nanoparticles can be defined as ultra fine particles in nanometer scale. This description is strongly related to the field of applications and the materials. Mostly the particles in the range of from 1 to 100 nm in which the physical characteristics of solid materials severely alter are named as nanoparticles. Nanotechnology offers the possibility to produce and control the objects within the scale of 1–100 nm with the aim of producing new materials which have particular properties in areas such as physics, chemistry, biology, engineering, medicine and healthcare, energy, materials science, information technology, and national security [1,2,3,4].

The properties of nanomaterials can be very different from those of bulk materials. When the dimension of a material drops below 100 nm, dramatic changes in its properties can occur. As the size of a solid particle decreases in the order of one millionth of a millimeter, the number of atoms constructing the particle becomes small and in the order of several hundreds or thousands. At this state, the fundamental properties can change drastically [1,2,3].

They show completely different electromagnetic or physicochemical properties from their bulk counterparts, although they are made of the same materials. The uniqueness of nanoparticles is mainly due to the considerable part of atoms present at the surface when checked against to the ones exist in the coincident bulk equivalent and the limitation of charge carrier motion to a small material volume. Through these two main features, the size and shape of nanocrystals are regularly connected to the physical and chemical properties [5,6,7,8,9].

1.2. General Methods for Synthesis of Nanoparticles

Nanoparticles from various materials can be prepared by relatively simple methods. In recent years, several types of methods have been published and reviewed for synthesizing monodisperse and uniform sizes of nanoparticles [10,11,12]. Currently, there are two kinds of approaches generally carried out to prepare nanoparticles, (A) The “top down approach”, which involves the constant division of bulk metals into nanoparticles and (B) The “bottom-up approach”, which involves the building up of nanoparticles from the atomic level [1,13,14].

1.2.1. Top-Down Approach

As the name implies, a top-down technique is where nanoparticles are cut from a larger structure (Figure 1), for example by lithographic techniques [15], UV [16], electron or ion beam [17], scanning probe [18], film deposition and growth [19], laser-beam processing [20]. Among these the two main methods are electron beam lithography (EBL) and focused-ion beam (FIB) lithography in top-down approach [17].

Both techniques have limiting resolution of 20 nm at the present state-of-the-art, so they are unable to produce particles as small as the bottom-up approaches. They are however more flexible in the shape of the resulting nanoparticles and can produce square, circular, triangular and elliptical particles as well as nanorings, antidots, etc. [21,22].

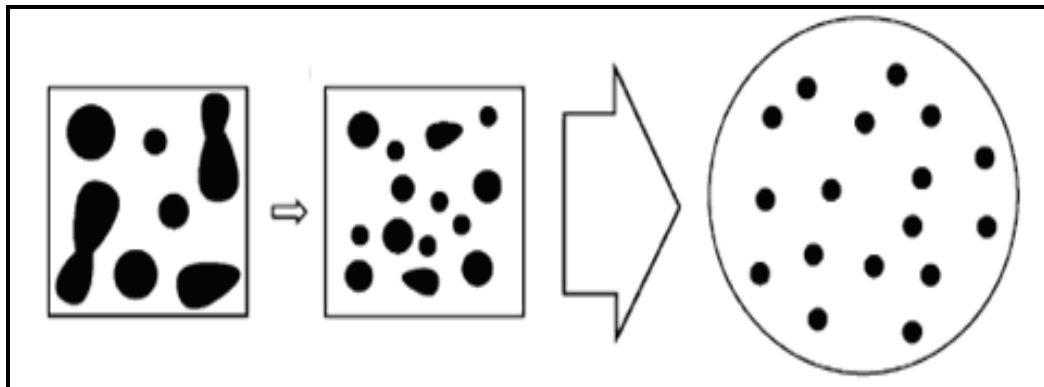


Figure 1. Schematic illustration of the top-down approach [22].

1.2.2. Bottom-Up Approach

In the bottom-up approach nanomaterials having particular morphology, properties and functions are well assembled by handling building blocks of desired materials. General synthesis method of nanoparticles by using bottom-up approach is given in Figure 2. Examples of this approach include the use of chemical synthesis [23,24], and laser induced assembly [25,26] like laser trapping, self-assembly, colloidal aggregation and 2-photon confocal processing. By using bottom-up processes it is possible to overcome the size limitations of the top-down approach when preparing nanoparticles.

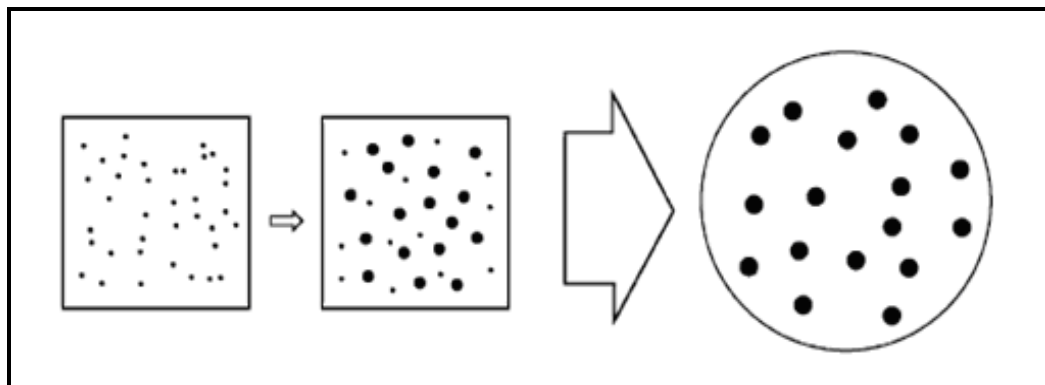


Figure 2. Schematic illustration of the bottom up approach [22].

1.3. Characterizations of Metallic Nanoparticles

Characterization methods for analysis and measurement of nanomaterials are essential in the development of nanotechnology; as their functions are influenced by their size, shapes, and structures [5,6]. Especially, development of precise analytical techniques for the characterization of local nanostructures at atomic levels such as their chemical composition and bonding state, defects, and impurities, is a key to elucidate the mechanism of nanophenomena. Recently, improvements in analytical equipment have allowed researchers to study and to understand the local nanostructures in functional materials at atomic levels (Figure 3) [27,28,29].

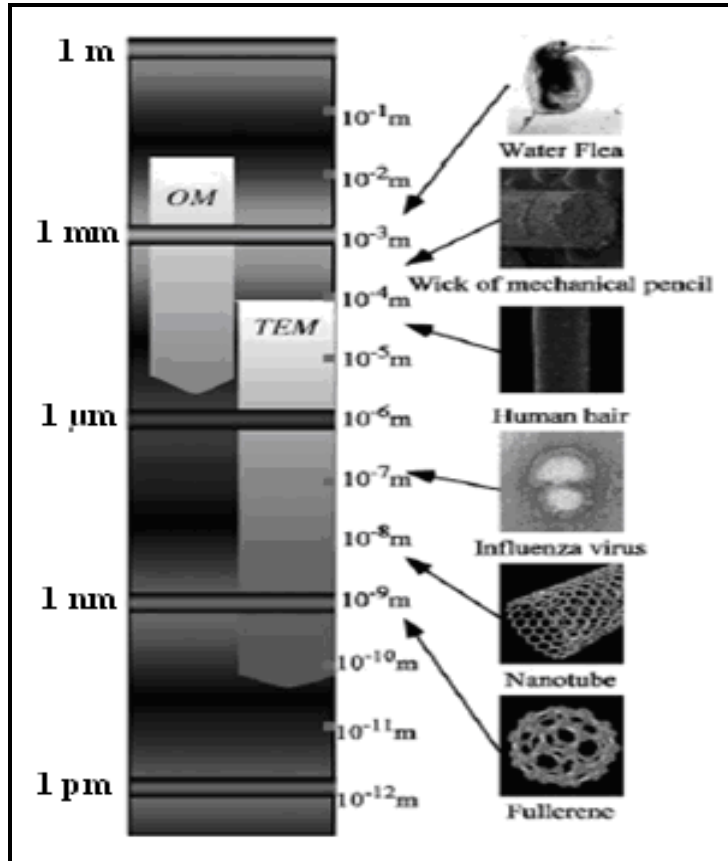


Figure 3. Spatial resolution for observing materials [29].

The most common technique used for characterization of nanoparticles is high resolution transmission electron microscopy (HRTEM) [30], which generates a photomicrograph of the core of the nanoparticles, providing information on the size distribution and dispersity of the sample. The mean number of atoms can be calculated from the mean diameter, d , of the cores. The core dimensions of the metallic nanoparticles have also been characterized using alternative techniques based on microscopy [31,32]. Comparison of microscopes used in characterization of nanoparticles is given in Table 1.

Table 1. Microscopes used in characterization of nanoparticles.

	Atomic Force Microscopy (AFM)	Transmission Electron Microscopy (TEM)	Scanning Electron Microscopy (SEM)	Optical Microscope
Maximum resolution	Atomic resolution	Atomic resolution	Several nanometers	Several hundreds of nanometers
Observation environment	In air, liquid and vacuum	In vacuum	In vacuum	In air and liquid
In situ observation	Possible	Impossible	Impossible	Possible
Preparation of sample	Easy	Difficult	Easy	Easy

UV-Visible (optical) spectroscopy is used for analysis of the intensely colored colloidal dispersions having characteristic surface plasmon absorption [13]. In a given preparation of nanoparticles, there is usually a mixture of different size nanoparticles. Different size nanoparticles have characteristic surface plasmon resonance peaks and thus their UV-visible spectra are also usually significantly different, which may also helps in determining the particle size [33,34]. Also UV-visible spectra together with infrared (IR) spectra [35] provides a way for the identification of the ligands. The localized elemental composition on the nanoparticles can be obtained from Energy Dispersive X- ray microanalysis (EDX) in conjunction with TEM and SEM [36,37].

1.4. Metal Nanoparticles

Metal nanoparticles have a wide variety of applications due to their properties. For instance, the quantum confinement effects on electronic magnetic and other relevant features can be investigated experimentally. Optoelectronics [38], photonics [39], information storage [40], surface enhanced Raman scattering (SERS) [41,42], photography, catalysis and biological labeling [43] are the main fields where metal nanoparticles are extensively used. The fundamental features of a metal nanoparticle are primarily specified by its composition, size, crystallinity, shape, and structure whichever can provide the adjustment of the properties of the resulting particles.

1.4.1. Synthesis of Metal Nanoparticles

There are a lot of chemical ways to produce metallic nanoparticles in different size and shape. By using these methods precursor of metals have been prepared in different form of nanostructures in the presence of a capping agent at room temperatures (Figure 4). Centrifugation and size-selective precipitation techniques are applied to isolate pure products [44,45,46].

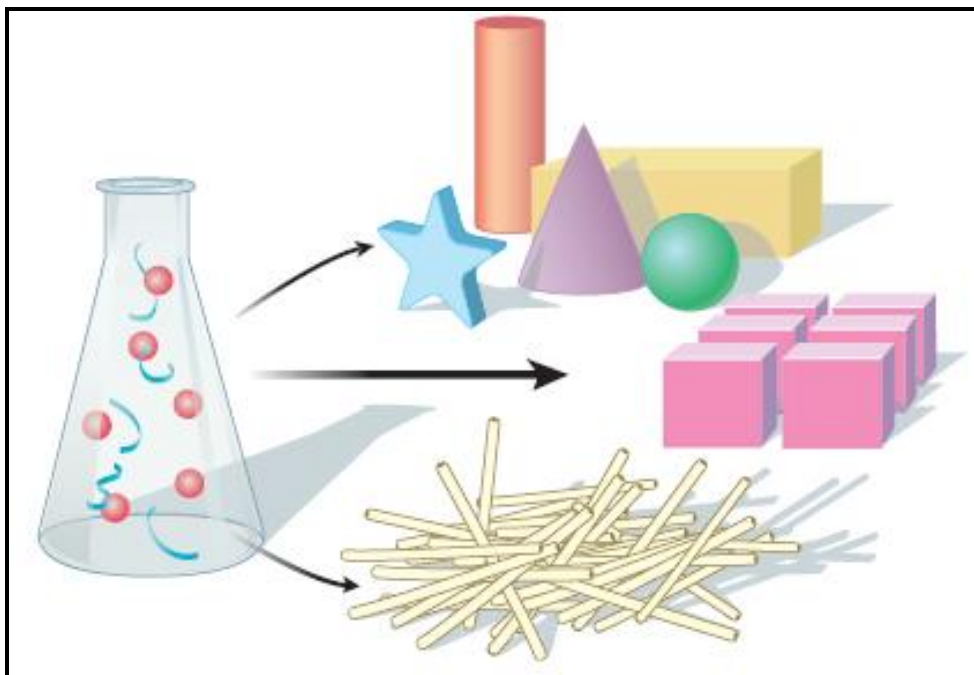


Figure 4. Multiple shapes and sizes of nanoparticles produced with chemical methods [46].

Citrate, alcohol, polyol, borohydride, photolytic, and radiolytic reductions, sonochemical approach, laser ablation, and metal evaporation-condensation are of the methods that have been used to prepare nanoparticles from precursor of metal ions. The conditions used in preparation of the nanoparticles have a direct effect on the electrochemical and optical properties of these particles [47,48,49,50,51,52].

1.4.2. Noble Metal Nanoparticles

Noble metal nanoparticles are known to be used as decorative pigments in stained glasses and artworks in the past due to their bright and charming colors [53]. Recently, the adjustable photophysical characteristic [54], their effective spectroscopic and optical properties and rapid improvements in synthesis of metal nanoparticles increased the importance of them in a broad range of applications from photonics [55] to biomedicine [56].

Superb surface plasmon absorption and scattering characteristics were observed for noble metal nanoparticles of especially silver (Ag) and gold (Au) in the visible and infrared regions of electromagnetic spectrum [57]. Local enhancement of electrical fields light illumination at the surface plasmon wavelengths were considered upon of these nanoparticles. The surface plasmon resonances are coalesced when the nanoparticles became adjacent eventuating in higher electric-field enhancements in between the gaps of the adjacent nanoparticles. In order to provide amplification of optical signals in fluorescence [58], and in Raman scattering [59,60,61] great efforts have been given to the preparation of noble metal nanoparticles based substrates.

1.5. Hollow Nanostructures

Hollow nanostructures of noble metals are particularly interesting to synthesize and investigate because they exhibit plasmonic properties completely different from those of solid nanoparticles (even of the same metal). An enhancement in the scattering of light is observed due to the prominent contrast between the refractive index values of the shell and core part of the hollow nanoparticles providing their use in especially optical and imaging applications [62]. Hollow nanostructures of different metals and materials like polymer and silica have been widely examined [63,64,65]. Generally researchers have focused on shell thickness and size of the hollow space. This tunable optical feature makes nanoshells attractive for applications to extinction or SERS-based sensing [66,67].

They were usually prepared by templating against solid particles. Polystyrene spheres, silica spheres, emulsion, liquid drops, microemulsion and metal nanoparticles, have been used as templates to produce hollow nanostructures. In their preparation, initially surfaces of the templates are covered with thin layers of the preferred material to obtain core-shell nanostructures. Then the template is

removed by etching or calcination procedure to produce hollow nanostructure. The size of the cavity is determined by the size of templates (Figure 5) [68].

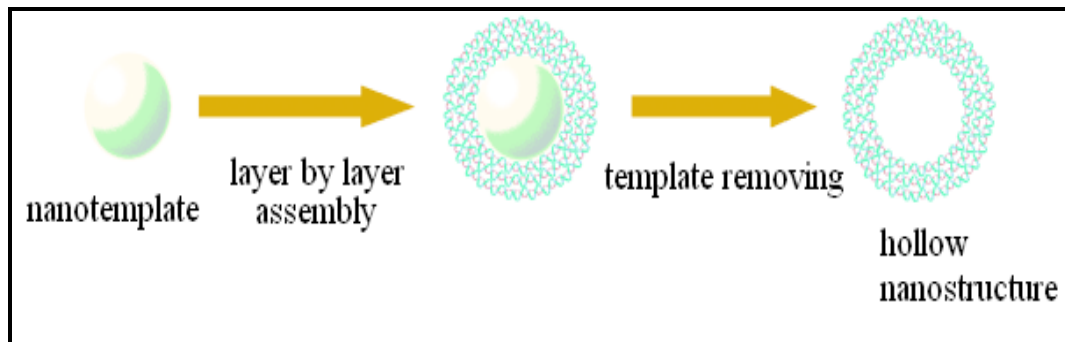


Figure 5. General production procedure of hollow nanostructures.

1.6. Core-Shell Nanostructures

In order to obtain the core shell-nanostructures different layers are regularly added to the initial core material. To produce core-shell nanostructure, the shell molecular precursors are added slowly to a solution containing the target nanostructure cores to avoid homogeneous nucleation of the shell material. Core-shell nanomaterials have been synthesized in a successful manner by using (1) seed mediated technique in which the core part of the nanostructures covered by desired material by coreaction or deposition to form the shell part [69,70] (Figure 6, 1a-c); (2) redox reaction, by exchanging the outmost part of the core with the shell material [71,72] (Figure 6, 2); and (3) thermal annealing of the shell part [73,74] (Figure 6, 3).

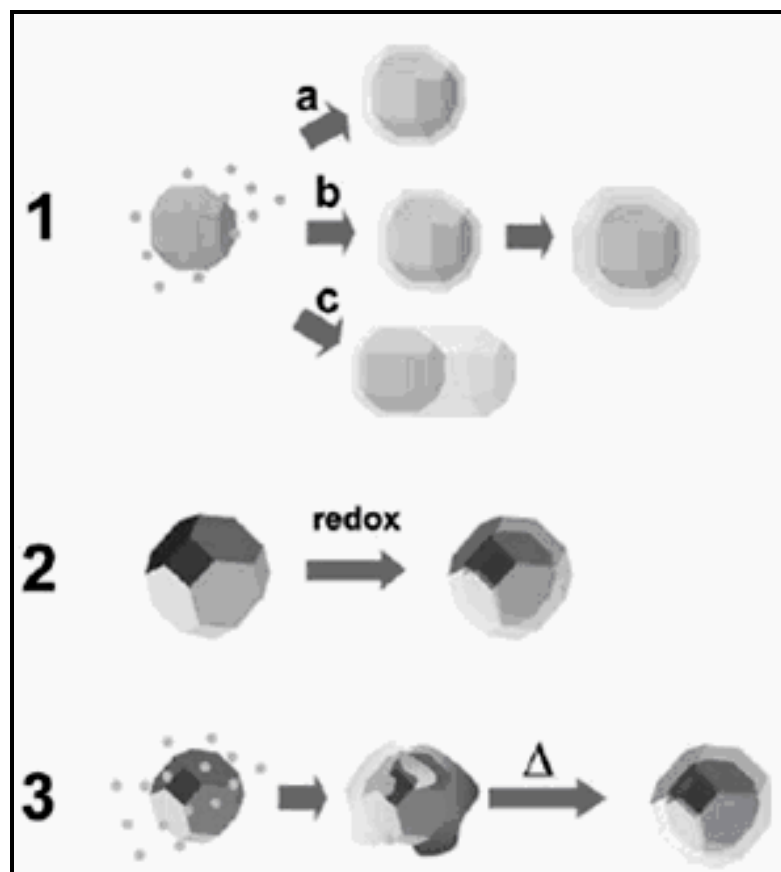


Figure 6. Possible core-shell nanostructures production mechanisms [74].

The production of core-shell nanostructures is of importance in materials chemistry due to the multifunctionalities and improved properties of these structures as compared to their mono-elemental counterparts. Core and shell components of the prepared nanoparticles enable them to achieve multitalented roles as optical probes, magnetic separators, and chemical identifications [75,76,77,78].

1.7. Optical Properties of Noble Metal Nanostructures

The optical properties of metallic nanostructures are mainly related to dielectric constant of metallic part and surroundings. A metal-dielectric boundary on the nanoscale order causes respected changes in the optical properties of metallic nanoparticles. As a result of this change a new sort of resonance which is called as surface plasmon resonance is observed. Surface plasmon resonance is localized near the boundary between the metal nanostructure and the surrounding dielectric. This action generates an increased electromagnetic field at the boundary [79,80,81].

Coherent oscillation of electrons is the result of the light absorbed by metallic nanoparticles, which is caused by coactions with the electromagnetic field. As a result of this interactions surface plasmon waves are produce. These localized plasmons are excited by light absorption in the nanoparticles, with the specific absorption bands called as plasmon bands [79,80,81].

The size and shape of the nanoparticle, the dielectric constant of metallic nanoparticle and surrounding effect the surface plasmon absorption band of the nanostructures. For nanoparticles smaller than 25 nm, small shift of the surface plasmon band peak position is observed with a broadening of the peak. For nanoparticles larger than 25 nm the red shift of absorption band is high when compared to smaller nanoparticles. The results of these phenomena are shown in Figure 7 [79,80,81].

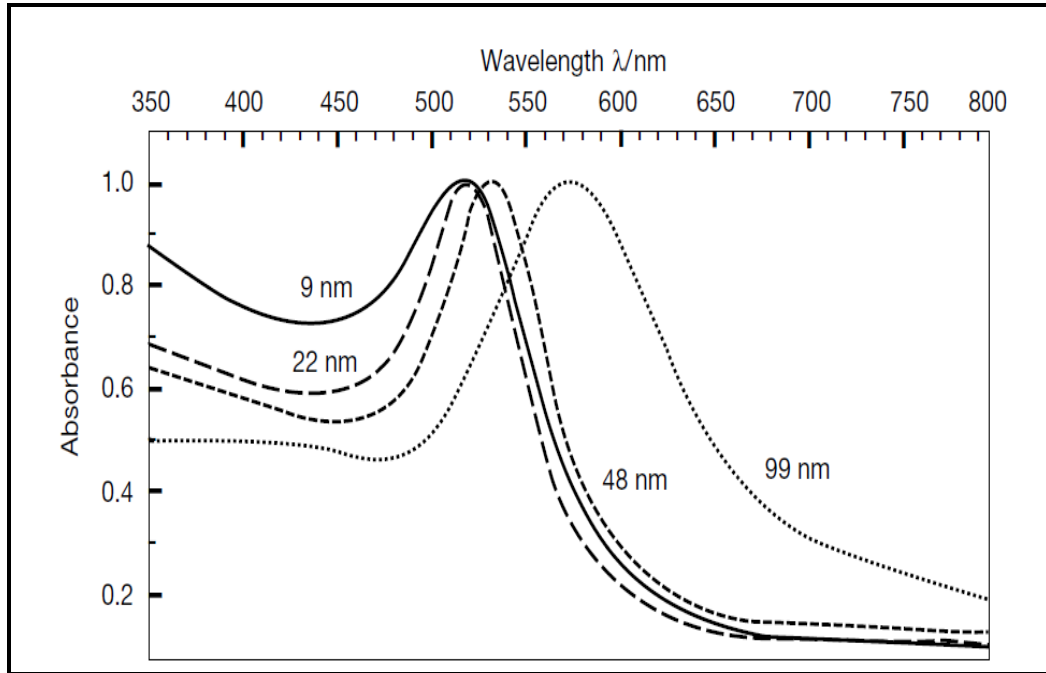


Figure 7. Optical absorption spectra of gold nanoparticles of different sizes [79].

Although a number of theoretical models have been proposed [80] the original classical model of Mie [82] is often used to describe the optical properties of the metal nanoparticles. In this model, frequently the oscillation of conduction electrons, also referred as plasmon oscillation, driven by the electromagnetic field of light called as dipole approximation are used to produce oscillating dipoles along the field direction where the electrons are driven to the surface of the nanoparticles as illustrated in Figure 8.

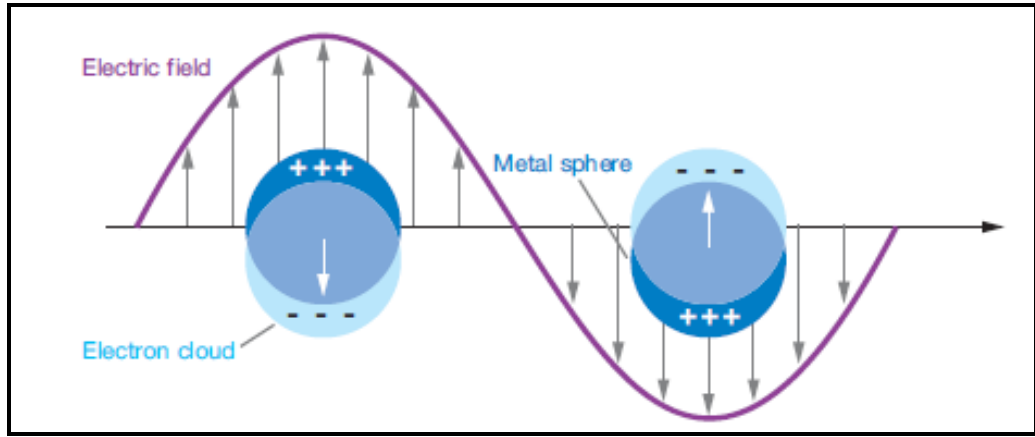


Figure 8. Schematic of plasmon oscillation in a metal nanosphere.

With respect to Mie explanation, metal nanosphere with particle size ($2R$) which is smaller than the wavelength of light λ , has an extinction coefficient k_{ex} (absorption and scattering) given by the following equation [83].

$$k_{\text{ex}} = \frac{24\pi^2 R^3 \epsilon_h^{3/2}}{\lambda} \frac{\epsilon_2}{[\epsilon_1 + 2\epsilon_h]^2 + \epsilon_2^2} \quad (1)$$

In the equation, the wavelength of light is shown with λ , and the dielectric constant of the surrounding medium is shown with ϵ_h where the terms ϵ_1 and ϵ_2 reveal the real and the imaginary parts of the dielectric constant of the metal, ϵ_m , ($\epsilon_m = \epsilon_1 + i\epsilon_2$). Dielectric constant of the metal is also dependent on the frequency of light (ω). If the imaginary part of the dielectric constant of the metal (ϵ_2) is so small, the resonance condition which results the absorption maximum is produced ($\epsilon_1 = -2\epsilon_h$). Dielectric constant of the metal ϵ is affected by the change in the size of nanoparticles which results in the change of the surface plasmon resonance which is generally explained as the intrinsic size effect [84].

One of them is the result of transition of electrons from inner d orbitals to the conduction band and second one is related to the free electrons which is explained by Drude model [82,83], stated as

$$\varepsilon_D(\omega) = 1 - \frac{\omega_p^2}{\omega^2 + i\gamma\omega} \quad (2)$$

where the plasmon frequency of the metal is given as ω_p and the damping constant which is related to the width of the plasmon resonance band is given as γ . The damping term (γ) is inversely proportional to the size of nanoparticle (r). According to equation 2, one can state that the size dependence of $\varepsilon_D(\omega)$ (real part of the dielectric constant of the metal (ε_1 in equation 1)) which results change in the surface plasmon resonance condition comes from the particle size dependence of γ .

For larger-size nanoparticles (>25 nm for gold particles), higher-order (such as quadrupolar) charge cloud distortion of conduction electrons becomes important, as shown in Figure 9.

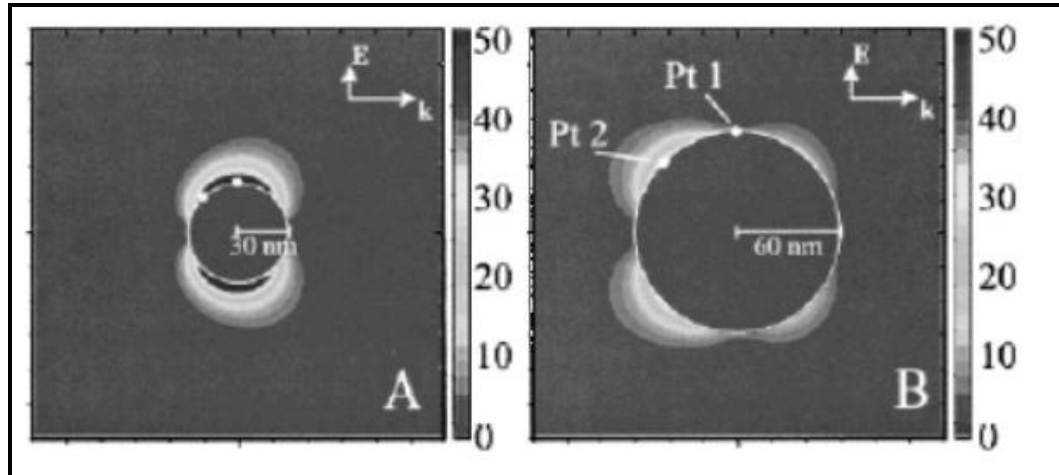


Figure 9. Calculated higher-order charge cloud distortion around gold nanoparticles of sizes > 25 nm [80].

The enlargement of the particle size results the shift of the plasmon band toward the lower energetic regions. This result is also explained as the extrinsic size effect [84]. According to the equation 1 given above, the appearance and the region of the plasmon absorption band also related to the dielectric constant ϵ_h of the surrounding medium. An increase in the ϵ_h results the shift of the absorption band toward the red regions besides a rise in the plasmon band intensity and band width. This action of increasing the plasmon absorption by using a higher ϵ_h is defined as immersion spectroscopy [83].

Core-shell nanoparticles which contain different materials at their core and shell part is considered as the another type of metallic nanoparticles and receiving considerable attention at recent times [81,85,86,87]. As varied materials are used at their core and shell part, core-shell nanostructures also referred to as heterostructures. Optical properties of the core-shell nanoparticles are also controlled by surface plasmon resonance like the other metallic nanostructures (nanospheres, nanorods, etc.) when the shell part of the structure is metallic.

The shift in plasmon resonance band is much longer in wavelengths than those in the corresponding solid counterparts. The dielectric constant for the core-shell nanospheres is calculated by the following equation (Eq. 3),

$$\varepsilon = \varepsilon_h + f \frac{\varepsilon_h [(\varepsilon_s - \varepsilon_h)(\varepsilon_c + 2\varepsilon_s) + \delta(\varepsilon_c - \varepsilon_s)(\varepsilon_h + 2\varepsilon_s)]}{[(\varepsilon_s + 2\varepsilon_h)(\varepsilon_c + 2\varepsilon_s) + 2\delta(\varepsilon_c - \varepsilon_s)(\varepsilon_s - \varepsilon_h)]} \quad (3)$$

where the dielectric constant of corepart is ε_c and shell part ε_s , and the host medium ε_h where particles are embedded in. δ is the volume ratio of core to overall particle [88].

In the metallic shell nanostructures, when the shell thickness decreases, holding the size of core constant, plasmon resonance band is red shifted. Also, plasmon resonance band is blue shifted when the size of shell thickness increases. The examples of these characteristics are given in Figure 10. So, it is possible to tune the plasmon resonance across the visible and IR part of the electromagnetic spectrum by changing the thickness of shell [87,88].

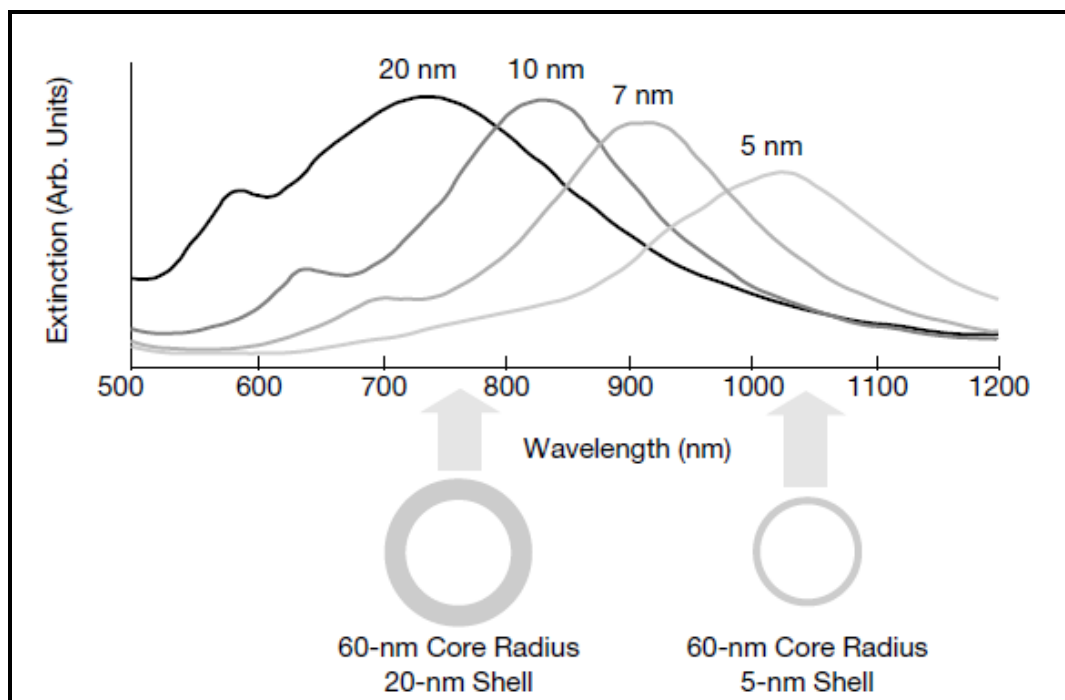


Figure 10. Calculated plasmon resonance spectra for different shell thicknesses of gold on a silica core of 60-nm radius [87].

1.8. Raman Spectroscopy

From the time of its discovery in 1927, Raman spectroscopy has been a very powerful characterization tool in a variety of fields such as materials science, biology, chemistry, physics and forensic science [89,90,91]. The Raman effect results from the interaction of vibrational motions of molecules with an electromagnetic wave, providing unique spectral fingerprint of vibrations in the molecules.

When a sample is irradiated with a laser, two types of scattering are observed: (a) Rayleigh scattering and (b) Raman scattering. Rayleigh scattering is intense and has the same frequency as the incident beam, whereas Raman scattering is very weak and has a frequency shifted from the incident frequency

(Stokes shift, lower in energy ($\nu_0 - \nu_m$) and anti-Stokes shift, higher in energy ($\nu_0 + \nu_m$) where ν_0 is the frequency of a photon which is absorbed by the molecule in the basic vibrational state and ν_m is the frequency of transferred energy). Energy level diagram for Raman scattering is shown in Figure 11 [92,93,94].

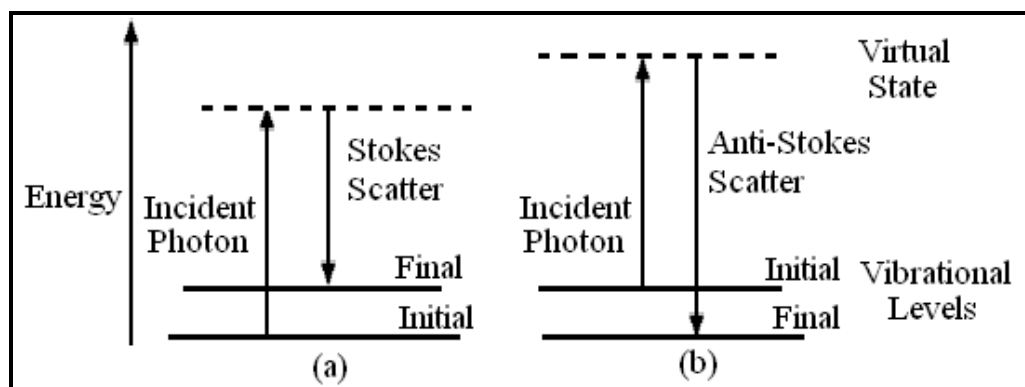


Figure 11. Energy level diagram for Raman scattering; (a) Stokes scattering, (b) anti-Stokes scattering.

Stokes and anti-Stokes spectra include the identical frequency data. When the Stokes spectrum is not directly observable the anti-Stokes spectrum can be used, for instance, owing to poor detector reply at lower frequencies [93,94].

In the classical theory, the coaction of the electromagnetic field with molecule gives rise to infrared absorption and Raman scattering [95]. Electromagnetic radiation can cause a change in the dipole moment of the molecule. The induced polarization μ is proportional to the strength of the electric field, E as given in the equation $\mu = PE$ where the proportionality, P , corresponds to the polarizability of the molecule [94,95].

The polarizability reflects the ease to distort the electron cloud of a molecule susceptible to an electromagnetic radiation. Higher Raman signal can be produced from higher radiation frequency and larger change in the polarizability. The polarizability of the molecule depends on the vibration mode of different molecular bonds and the surface plasmon assisted enhancement [92,93]. Raman signals from a highly polar moiety, such as the O-H bonds in water, are usually weak. An external electric field cannot induce a large change in the polarizability of the O-H bond. Therefore, Raman spectroscopy is insensitive to water, herein makes Raman spectroscopy or SERS an excellent fingerprinting technique for the detection of unknown in an aqueous solution [93,94].

1.9. Surface Enhanced Raman Scattering (SERS)

Identification of the chemical structure is a significant challenge in analytical chemistry besides the detection of trace amounts of substances. For that reason, the recent fact of a strongly increased Raman signal from molecules bounded to metallic nanoparticles gained great attention, approximately 50 years after the exploration of the Raman effect [96,97]. This phenomenon is known as surface-enhanced Raman scattering (SERS) and solved the low-sensitivity problem in traditional Raman spectroscopy. In other words, SERS has transformed Raman spectroscopy from the least sensitive vibrational spectroscopy to a single molecule detecting spectroscopy capable of giving detailed molecular information at ambient conditions [98,99]. SERS has the potential to join the sensitivity of fluorescence with the structural information ingredient of Raman spectroscopy. A typical SERS setup is given in Figure 12.

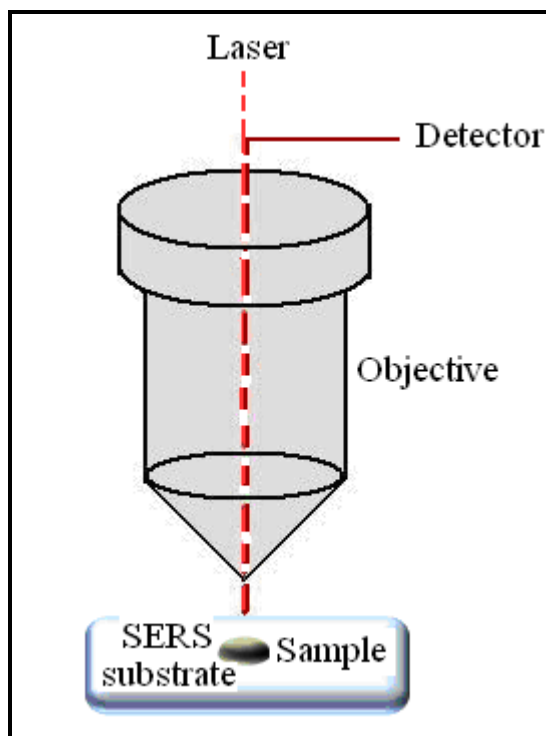


Figure 12. Schematic drawing of a typical SERS setup

There are mainly two types of enhancement process in the theoretical explanations of SERS mechanism. The first one is the electromagnetic model [100] which also referred as the field effect. In electromagnetic model, molecule feels huge local electromagnetic fields occurring near the surface of metal substrates. The second one is charge transfer or chemical model [101,102] and also referred to as the molecular effect. In chemical model polarizability of the molecule is influenced by coactions between the roughened metal surface and the molecule. The effect of the first model on the SERS enhancement have been widely investigated and quite well understood but the effect of the chemical model on SERS signal is not well known and is presently investigated by researchers [103, 104,105,106].

1.9.1. Different SERS-Active Media (SERS Substrates)

An extensive range of methods utilizing diverse sorts of solid and liquid SERS media increases the popularity of the SERS technique. For each certain application, a specific sample medium is used. Initially, roughened metal electrodes were studied as SERS substrates [107]. Metal colloids were then received extensive interest because of their easy preparation techniques [108,109]. Nanostructured substrates and metal films were then developed and used in extensive range of areas as SERS-substrate to obtain reproducible results [110,111].

The selection and production of the noble-metal nanostructures for fabrication of the SERS substrates is the most important feature in SERS measurements. Since SERS enhancement based on the localized surface plasmon resonance (LSPR) excitation, controlling the parameters affecting the LSPR to increase the signal power and reproducibility of measurement is important [112]. Surface-confined nanostructures, electrodes roughened by the oxidation–reduction cycle (ORC), colloidal nanoparticles, and metal island films provide the preferred optical properties. So mostly they are chosen as conventional SERS substrates [113,114]. Several metallic nanostructures used in preparation of SERS substrates are given in Table 2.

Table 2. Several types of metallic nanostructures used for SERS

Structures	Base Materials
Metal islands	Silver, other metals
Metal-coated nanospheres	Teflon, latex, polymer, nanospheres
Metal-coated nanoparticles	Alumina, fumed silica, titanium oxide
Metal-coated surfaces	Cellulose, silica gel, polystyrene
Metal-coated etched quartz	Quartz
Metal-coated gratings	Crossed gratings
Metal membranes	Silver membranes, other metals
Chemically etched metal	Metal
Physically roughened surfaces	Quartz, metal

1.9.2. Instrumentation

Gas, dye, and solid-state lasers are all suitable excitation sources for SERS experiments. UV lasers have limited applicability in SERS because the dielectric properties of noble metals restrict LSPR excitation above a certain frequency threshold. Tunable lasers provide flexibility because it is possible to match the excitation frequency to the LSPR frequency of the substrate. However, complications arise when one attempts to prevent Rayleigh-scattered photons from reaching the detection components. For pulsed laser systems, peak power and bandwidth must be considered. High peak powers can damage the analyte or substrate, and pulse widths higher than 5 ps are required to achieve a spectral resolution of 1 cm^{-1} . The excitation and collection optics are the same as those used for normal Raman experiments. For example, large camera lenses are needed for maximal efficiency of light collection, or optical microscopes for probing small sample areas [115].

Spectrometers with long focal lengths (≥ 500 mm) are generally used in SERS experiments to resolve a vibrational spectrum. In a single-stage spectrometer, the Rayleigh-scattered light must be efficiently rejected before the scattered photons are coupled into the spectrometer. This step is usually accomplished with notch filters that have high optical density over a narrow bandwidth centered on the laser excitation wavelength [116].

Although notch filters are readily available for specific laser wavelengths, many filters would be required to cover the entire wavelength range of a tunable laser system. In this case, double- and triple-stage spectrometers are preferred to achieve sufficient Rayleigh light rejection [117]. The detectors commonly used for SERS include photomultiplier tubes, photodiodes, and charged coupled devices (CCDs). Though far less common, FT-Raman instruments have also been used to obtain SER spectra [118].

Schematic illustration of instrumental designs used in SERS applications is given in Figure 13. Instrumental design shown in Figure 13a is usually used for experiment which needs low resolution and high intensity. An experiment which needs high resolution, instrumental approach which is shown in Figure 13b is used. In both of the approaches, laser light is focused and gathered directly on a same type of objective and in order to eliminate the Rayleigh scattering a notch filter is used [106].

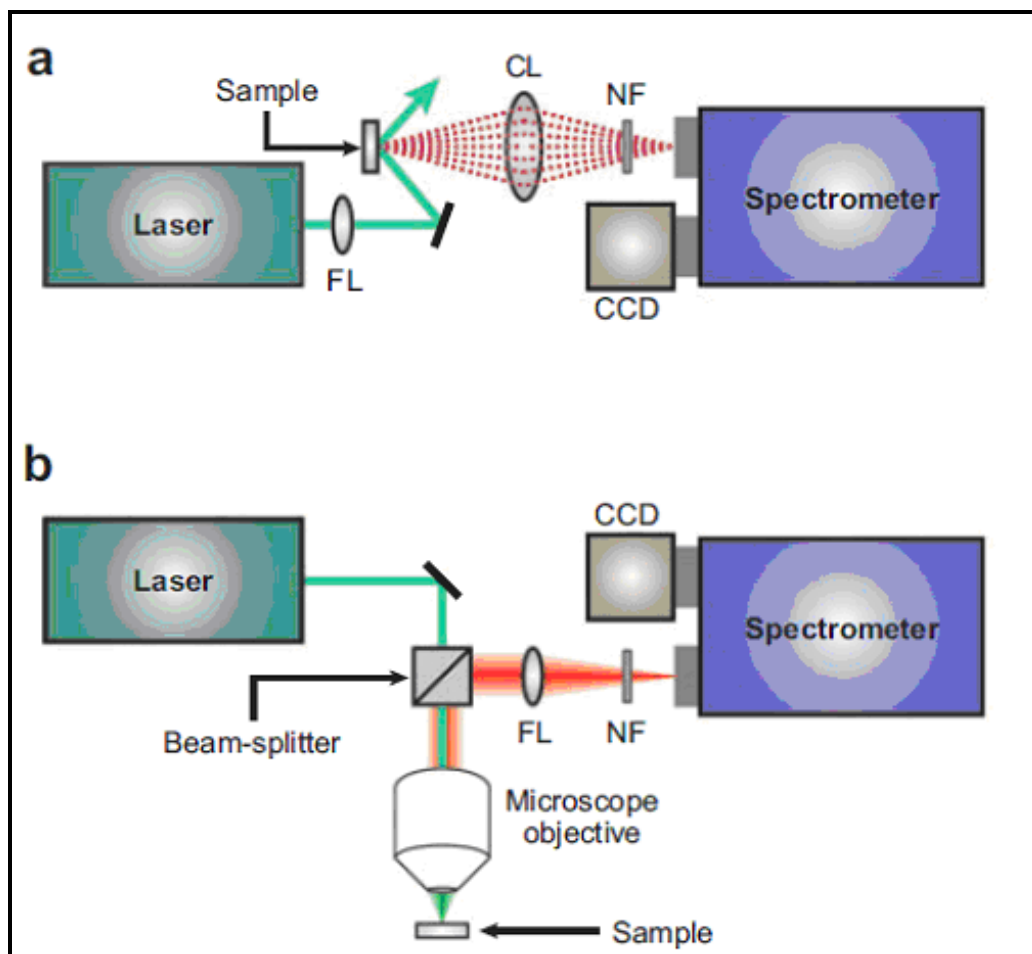


Figure 13. Schematic diagram of representative instrumentation used for surface-enhanced Raman spectroscopy measurements; (a) Macro-Raman setup (b) Micro-Raman setup (Abbreviations: CCD, charge-coupled device; CL, collection lens; FL, focusing lens; NF, notch filter) [118].

1.9.3. Surface Enhanced Resonance Raman Scattering (SERRS)

Surface-enhanced resonance Raman scattering (SERRS) [119,120,121] is an alternative technique, which is also highly sensitive with single molecule detection reported [122,123]. It is a very attractive technique because it produces molecular-specific spectra which make it feasible for easy identification of the components of a mixture without preapplying extensive separation procedures [124].

SERRS is a form of Raman spectroscopy in which a combination of surface enhancement provided by immobilizing an analyte onto a suitable surface and of molecular resonance from a chromophore in the analyte gives a vibrational spectrum at very high sensitivity. A number of different metals such as silver, gold, copper and aluminium can be used to provide the surface, however, silver tends to give the largest enhancement factors when using routinely available visible excitation wavelengths [125,126].

In SERRS, a resonance contribution from the chromophore of the molecule with the excitation light is observed. This is coupled with the surface enhancement effect which can produce an overall enhancement factor of up to 10^{14} . The basic approach to obtain SERRS is to adsorb a molecule onto a suitable roughened metal surface. Also, the molecule must come in contact with or be very close to the metal surface used for the enhancement. The surface is then irradiated with a laser beam and the scattering collected with a standard Raman spectrometer [127].

It is essential that the excitation frequency is close to the absorption maximum of the dye and the plasmon of the metal surface (typically within 100 to 150 nm of the visible region) [128]. Further, due to the sharp vibrational nature of the spectrum, identification of specific components of mixtures in situ without separation is also increased relative to other spectroscopic techniques such as fluorescence. An additional benefit of SERRS is that only the species on the surface will give rise to signals. Therefore by designing strong surface seeking species, background signals can be kept to a minimum [129,130].

There are various formats which can be used in SERRS experiments and these depend on the different types of metal surface used. Electrodes have been used previously [131] as have vapour deposited films [132] and a whole variety of different roughened surfaces [133].

For many of these surfaces, there is little control of the nanoscale roughness features to ensure that enhancement factors across the surface are uniform and reproducible. As such this led to large variations in the enhancement of SERRS when these types of surfaces were used for quantitative analytical work. More recently, engineered surfaces with controlled regularity have been introduced. These can give very good and much more reproducible surfaces [134].

1.10. Surface Modification of Nanostructured Materials

By using physical, chemical, or biological approaches it is possible to modify and functionalizes the surfaces of nanostructured materials with different groups. At the end of the surface modification process, new materials with novel properties such as solubility and stability in aqueous media are often achieved. The affinity toward the nanoparticle can be increased with the modification of its surface by host molecules or cavitands. The host has to fulfill several requirements: (a) display strong affinity to the nanoparticle and the analyte, (b) high selectivity and stability, (c) no self-association or formation of multilayers, and (d) absence or low band overlapping with the Raman features of the target molecule [135,136]. The simple procedure for surface modification of nanoparticles is illustrated in Figure 14.

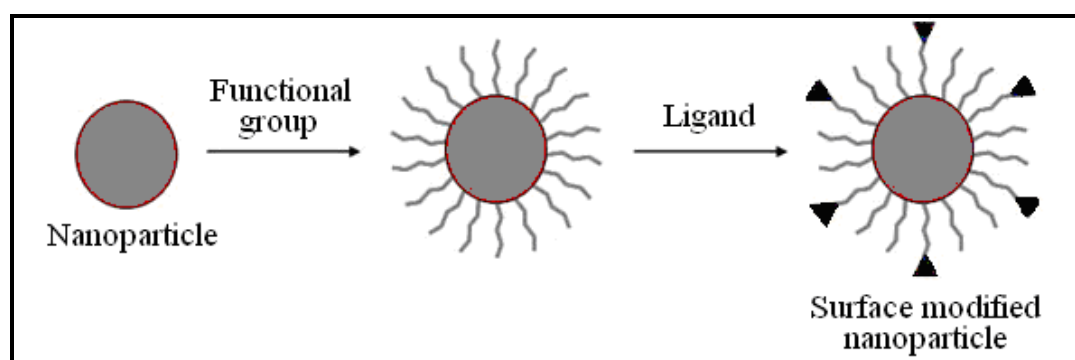


Figure 14. Surface modification of nanoparticles.

Molecular coating or adsorption [137,138], physical treating with plasma, ozone or UV [139] and surface entrapment [140,141] are widely applied physical techniques for surface modifications of nanomaterials.

Molecules with functional groups can be attached covalently to the surfaces of nanoparticles with chemical modification process. Chemical modification methods have several advantages over some physical methods such as activation of the nanostructured material surfaces with higher degrees, creating strong interactions between functional groups and nanomaterial surfaces through stable chemical bonds. Surface oxidation [142], covalent linkers such as carbodiimide, glutaraldehyde and their derivative [143,144], poly (ethylene glycol) (PEG) chemistry [145], silane chemistry [146], and self-assembled monolayer (SAM) [147] are the common applied chemical modification techniques.

Biological modification of nanoparticle surfaces are performed generally via biologically specific reactions, such as like receptor–ligand [148], DNA–DNA hybridization [149], avidin–biotin [150] and antibody–antigen [151].

1.11. Importance of Dopamine (DA) and Common Techniques Used in Dopamine Detection

Development of sensitive and selective techniques for biological and chemical sample detection is an important point in diagnosis of disease. In recent years there has been significant interest in developing methods to investigate the neurotransmitting molecules from neurons deep inside the brain [152]. The analysis of neurotransmitters is of substantial interest for the rapid and early detection of neural disorders.

Catecholamines and their derivatives have received much attention in contemporary scientific research because of their remarkable industrial and biological significance [153]. Dopamine (DA) is one of the most significant neurotransmitters because of its role in the functioning of the cardiovascular, renal, hormonal, and central nervous system. Dopamine (DA) (Figure 15) is the major neurotransmitter for the extrapyramidal motor tracts of the central nervous system (CNS) and is centrally involved in the mechanism of psychostimulant addiction. Its receptors are the major sites of action of antipsychotic as well as anti-Parkinsonism drugs. DA also acts as an isotropic vasopressor agent, and it acts in a specific manner to several various receptor sites in the body depending on the dose [154].

At lower dosages it binds to dopamine receptors in the brain, gut, kidney, and heart causing the blood vessels in these organs to broaden. This enhances the blood flow and thus the amount of oxygen supplied to the organs. β -receptors on the heart muscle are also activated when the dose of DA is increased. Dopamine hydrochloride is a potent drug and is extensively used in heart failure and hypotension [155].

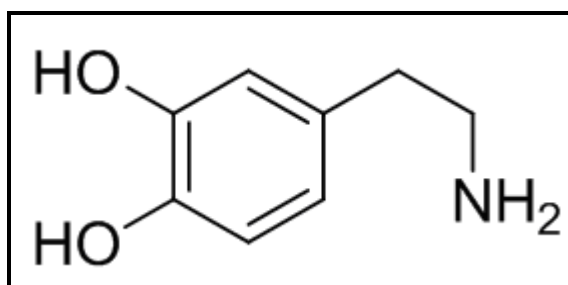


Figure 15. Chemical structure of a Dopamine molecule.

Given the wide range of physiological and pathophysiological effects of dopamine, selective as well as sensitive methods are crucial for the detection and determination of dopamine is of great clinical importance [156].

Finding the amount of catecholamine and their metabolites in body fluids such as serum, plasma and urine has an important function in evaluating the action of the sympathetic nervous system and helping the diagnosis of numerous diseases. Fluorometric, coulometric, chromatographic and electrochemical detection are the most frequently applied methods for measuring DA [157,158,159,160]. In addition, various nanoparticle based techniques have been developed to detect catecholamine [161,162,163]. Fluorometry is sample-consuming technique and lacks selectivity. In the quantitative colorimetric detection of the catecholamines poor selectivity is observed. Chromatography combined mostly with mass spectrometry requires sample pretreatment, lengthy analysis times and high costs.

Dopamine can be easily oxidized electrochemically at conventional electrodes, which have been widely used to detect the neurotransmitter both in vitro and in vivo sensors [164,165,166,167]. However, there are a number of problems with electrochemical methods due to the nature of the oxidative electrode reaction of dopamine. One of the primary problems is that the concentration of dopamine in the extracellular fluid of the caudate nucleus is extremely low (0.01-1 μM) for a healthy individual and in the nanomolar range for patients with Parkinson's disease [164,168] while the concentrations of the main detection interferents, e.g., ascorbic acid, are several orders of magnitude higher and the interferents undergo oxidation within the same potential window as dopamine.

Both sensitivity and selectivity are of equal importance for real applications. For the purpose of improvement of the electrode sensitivity, efforts have been made to adjust the surface of electrodes [169,170] which have shown different degrees of success by inhibiting the interference reactions or promoting dopamine oxidation at different potentials. Inspired by the fact that enzymes can react selectively with their cognate substrates, efforts have also been made to immobilize dopamine-specific enzymes, such as polyphenol oxidase, onto the electrodes to increase the selectivity [171].

However, the main interferent, ascorbic acid (AA), still severely hinders the accurate detection of dopamine because the oxidized dopamine product (dopamine-*o*-quinone) produced from either direct oxidation at the electrode or by the enzymes immobilized on the electrode, can catalytically oxidize ascorbic acid to regenerate dopamine that becomes available again for oxidation [171]. Also due to the same oxidation potential of AA and DA, overlapped voltammetric response has been observed at nearly all electrode materials [159, 160].

Interference problems might be absent or greatly reduced in Raman spectrometric measurements. Vibrational spectroscopy easily distinguishes among substituted benzenes, such as catecholamines and their metabolites. Structurally unrelated species, such as ascorbate, will have different vibrational spectra altogether. At the same time, measurement time could be reduced to about 10 seconds. Interference reductions and a shorter measurement time would be advantageous in most neurochemical studies [172].

Spontaneous Raman spectroscopy is not sufficiently sensitive for neurochemical applications. Adequate sensitivity can be obtained by surface enhancement (SERS) or resonance surface enhancement (SERRS). The study of the mechanisms between SERS or SERRS and surface-plasmon-driven electromagnetic fields has advanced considerably. As a result, the design of materials producing high-quality signals from analytes has been investigated [173,174]. Indeed, one can aim the finding of an analyte in a complex mixture at nano to femto molar level by incorporating a definite functional group on the substrate decorating the surface with molecular systems, that are capable electrostatically, [175] chemically [176] or mechanically [177] for trapping analytes. Such a combination is unique and cannot be achieved with other spectroscopic techniques.

High selectivity and sensitivity offered by SERRS, along with the highly informative characteristics of Raman spectroscopy, allows a SERRS-based method a feasible alternative to more commonly used optical sensing method without having any need to physically remove the interfering species [178,179].

1.12. Nerve Agents (Chemical Warfare Agents)

Nerve agents are one of the most effective groups between the lethal chemical warfare agents. Despite the fact that their use has been prohibited, nerve agents are still manufactured by some countries. Sensitive and precise analysis techniques for nerve agents detection are needed for raising interests over prospective contamination and injury caused by them [180].

Nerve agents are potential inhibitors of acetylcholinesterase enzyme which is responsible for the hydrolysis of the neurohormone acetylcholine in the neural synapses. Inhibition resulting in an increased concentration of acetylcholine at its receptor sites causes the continuous spasm of muscle tissue and finally leads to suffocation [181].

Nerve agents are easily breaking down to the connected alkyl methylphosphonic acids (AMPAs) after exposition to the environment which never exists in nature. For instance, GB (Sarin) and GD (Soman) turns to IMPA (isopropyl methylphosphonic acid) and to PMPA (pinacolyl methylphosphonic acid) respectively. Then they slowly hydrolyze to MPA (methylphosphonic acid), the final product of break down process which is stable and used as reference to show the presence of the nerve agents, as shown in Figure 16 [180,181].

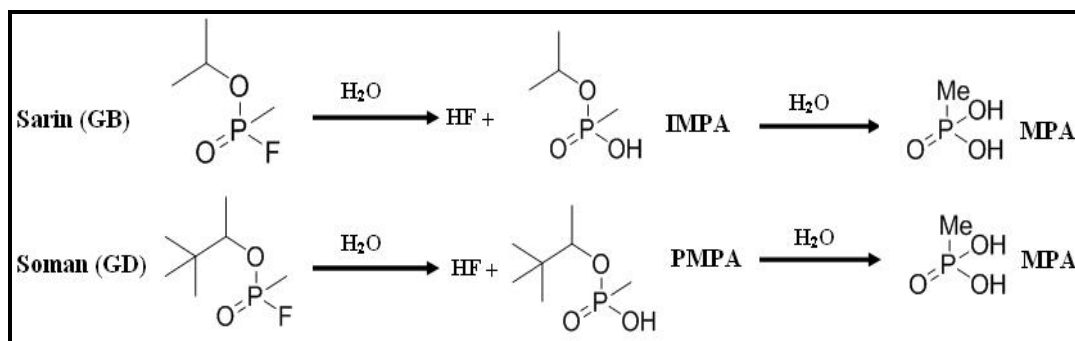


Figure 16. Hydrolysis pathways for G-Series nerve agents.

For the detection of these toxic chemicals, the ideal organophosphonate (OPP) sensor would possess the sensitivity and selectivity of the already-established methods and would reduce the dependence on expensive instrumentation. Robustness, simplicity, the ability to isolate the analyte of interest would be beneficial. Methods for the detection and quantitation of specific species usually involve separate sampling and analysis steps using complex and expensive devices [182,183].

Generally, Gas chromatography-mass spectroscopy (GC-MS) and, high-performance liquid chromatography (HPLC) are used for the quantitative detection of chemical warfare agents [184,185]. However, they are not optimal for rapid detection due to the following limitations: expensive, require sophisticated, often extensive analysis procedures, or nonportability.

Fiber-optic sensors [186], surface acoustic wave devices [187] or biosensors [188,189] may find application to real time monitoring. But they are suffering from low selectivity and sensitivity. The selectivity can be improved with approaches such as a molecular imprinting technique, which possesses specific affinities for guest molecules by using lanthanide ion [190,191] but because of the weak luminescence quantum yield it exhibits low sensitivity.

Raman peaks are much narrower which should aid in the identification of unknowns, such as chemical and biological agents, due to the lesser degree of spectral overlap between peaks. Therefore Raman, in particular SERS, provides a good alternative to conventional sensing modalities for warfare agents. The previous studies where SERS signals could be obtained for OPP's were carried out by using colloidal gold adsorbed onto a silanized quartz surface [192], electrochemically roughened silver oxide substrate [193], silver-doped sol-gels [194,195], silver-oxide thin films and silver nanoclusters [196], silver-coated microspheres [197]. But to increase the sensitivity, affinity of the surface towards the analyte must be improved.

1.13. Scope of the Thesis

The aim of this thesis is to synthesize and characterize the shape-controlled and surface modified noble metal nanoparticles and to measure their performance as substrates in SERS applications. The scope of the research includes:

a) The preparation of shape controlled solid gold, hollow gold, silver, gold-silver core-shell, hollow gold-silver double-shell nanoparticles, iron-nitrilotriacetic acid (Fe(NTA)) modified silver nanoparticles and lanthanide ion (Eu^{3+}) containing silver nanoparticles (Ag-Eu^{3+}) by applying aqueous solution chemistry in a simple and reproducible way.

b) The characterization of nanostructures prepared by an advanced analytical techniques including FE-SEM, SEM-EDX, ICP-OES, UV-Vis spectroscopy, FT-IR spectroscopy and, Raman spectroscopy.

c) Testing the SERS performance of nanostructures prepared. Use of solid gold, hollow gold, silver, gold-silver core-shell, hollow gold-silver double-shell nanoparticles in the detection of dye molecules like BCB and CV in aqueous systems. Application of iron-nitrilotriacetic acid (Fe (NTA)) modified silver nanoparticles in the detection of dopamine (DA) (neurotransmitter) molecules by using surface-enhanced resonance Raman scattering (SERRS). Use of lanthanide ion (Eu^{3+}) containing silver nanoparticles (Ag-Eu^{3+}) for constructing a novel molecular recognition SERS substrate for chemical warfare agents detection. In addition to their SERS and SERRS performance, testing the other important parameters such as reproducibility, sensitivity, stability and reliability of the prepared nanostructures.

CHAPTER 2

EXPERIMENTAL

2.1. Materials

The chemicals used in nanoparticle production and surface modification which are, sodium citrate ($\text{HOC}(\text{COONa})(\text{CH}_2\text{COONa})_2$), chloroauric acid ($\text{HAuCl}_4 \cdot 3\text{H}_2\text{O}$), silver nitrate (AgNO_3), sodium borohydride (NaBH_4), cobalt chloride hexahydrate ($\text{CoCl}_2 \cdot 6\text{H}_2\text{O}$), ascorbic acid ($\text{C}_6\text{H}_8\text{O}_6$), iron trichloride hexahydrate ($\text{FeCl}_3 \cdot 6\text{H}_2\text{O}$), iron nitrate ($\text{Fe}(\text{NO}_3)_3$) and europium dichloride (EuCl_2) were all purchased from Sigma Aldrich, unless otherwise stated and used without further purification. Analytes, dopamine hydrochloride ($(\text{HO})_2\text{C}_6\text{H}_3\text{CH}_2\text{CH}_2\text{NH}_2 \cdot \text{HCl}$), methyl phosphonic acid ($\text{CH}_3\text{P}(\text{O})(\text{OH})_2$), and dyes brilliant crsyl blue ($\text{C}_{17}\text{H}_{20}\text{ClN}_3\text{O}$) and crystal violet ($\text{C}_{25}\text{H}_{30}\text{N}_3\text{Cl}$), were also purchased from Sigma Aldrich. They were all analytical grade and used as received.

Milli-Q water (Millipore) was used throughout the experiments. Milli-Q Elix 5 water purification system was used to produce deionized water. All glassware used in the production of nanoparticles were cleaned with distilled water and ethanol and then dried in an oven at 50 °C before use. Manipulations that require the inert atmosphere were carried out by using Schlenk technique. N_2 and Ar gases used were of high purity (above 99 %).

2.2. Instrumentation

The structural, optical, and spectroscopic properties of prepared nanoparticles were examined using the following measurements. Field Emission Scanning Electron Microscope (FE-SEM) measurements were carried out with a Quanta 400 F field emission scanning electron microscope at METU Central Laboratory. Energy-dispersive X-ray analyses (EDX) were performed with a Quanta 400 F field emission scanning electron microscope equipped with energy-dispersive X-ray analyzer at METU Central Laboratory.

UV-Visible absorption data were recorded over a range of 200-1100 nm with the UV-Vis spectrophotometer (UV-1601 PC, SHIMADZU) at Analytical Chemistry Research Laboratory of the Chemistry Department-METU.

SERS spectra were measured with a Horiba-Jobin-Yvon, model Lab Ram Raman micro spectrometer at Analytical Chemistry Research Laboratory of the Chemistry Department-METU. It has a holographic grating having 1800 grooves mm^{-1} and a 632.8-nm HeNe laser with an exposure time of 10 s. The spectra were collected with Olympus model LMPlanFL, 10X, 50X and 100X microscope objectives. The laser power was approximately 10 mW and Raman signal was detected with a Peltier-cooled CCD camera.

The iron content of the surface modified silver nanoparticles was determined by using a Leeman Direct Reading Echelle inductively coupled plasma optical emission spectrometer (ICP-OES).

FT-IR measurements were performed by using Digilab FTS 3000 Excalibur series instrument in the mid-IR region at the Analytical Chemistry Research Laboratory of the Chemistry Department-METU. The diameter (d) of the resulting nanoparticles was measured with the software called as universal desktop ruler. Results were given as $d \pm s$ (diameter \pm standard deviation).

2.3. Synthesis of Hollow Gold Nanoparticles

2.3.1. Preparation of Cobalt Nanotemplates

Hollow gold nanospheres (HAuNPs) were synthesized using cobalt nanoparticles (CoNPs) which acted as a sacrificial template. Briefly, a solution of 100 mL of water, 400 μ L of 0.1 M sodium citrate, and 100 μ L of 0.4 M cobalt chloride was placed in a round-bottom flask and stirred with a magnetic stir bar. CoNPs were synthesized with the utmost attention paid to cleanliness and exclusion of air.

To obtain air-free solutions, Schlenk line has been used (Figure 17) which was deaerated with pure argon for 10 minutes. A 100 μ L amount of 1 M sodium borohydride was then added with rapid magnetic stirring, resulting in a color change within 30 s from pink to dark brown, indicating the formation of CoNPs (Figure 18). The flask was purged with nitrogen for approximately 20 minutes while waiting for any remaining sodium borohydride to hydrolyze.



Figure 17. Picture of Schlenk line used for producing air-free solution.

2.3.2. Preparation of Hollow Gold Nanoparticles

In a beaker, 10 mL of water with 50 μL of 0.1 M chloroauric acid ($\text{HAuCl}_4 \cdot 3\text{H}_2\text{O}$) were stirred together. A 30 mL amount of CoNPs transferred by cannula into nitrogen purged graduated cylinder, were quickly added at once to the vortexing chloroauric acid solution. The reaction of the gold salt with the cobalt was rapid, changing the solution color to blue within seconds, indicating the formation of HAuNPs. The experimental setup used for the production of the hollow gold nanoparticles is shown in Figure 18.

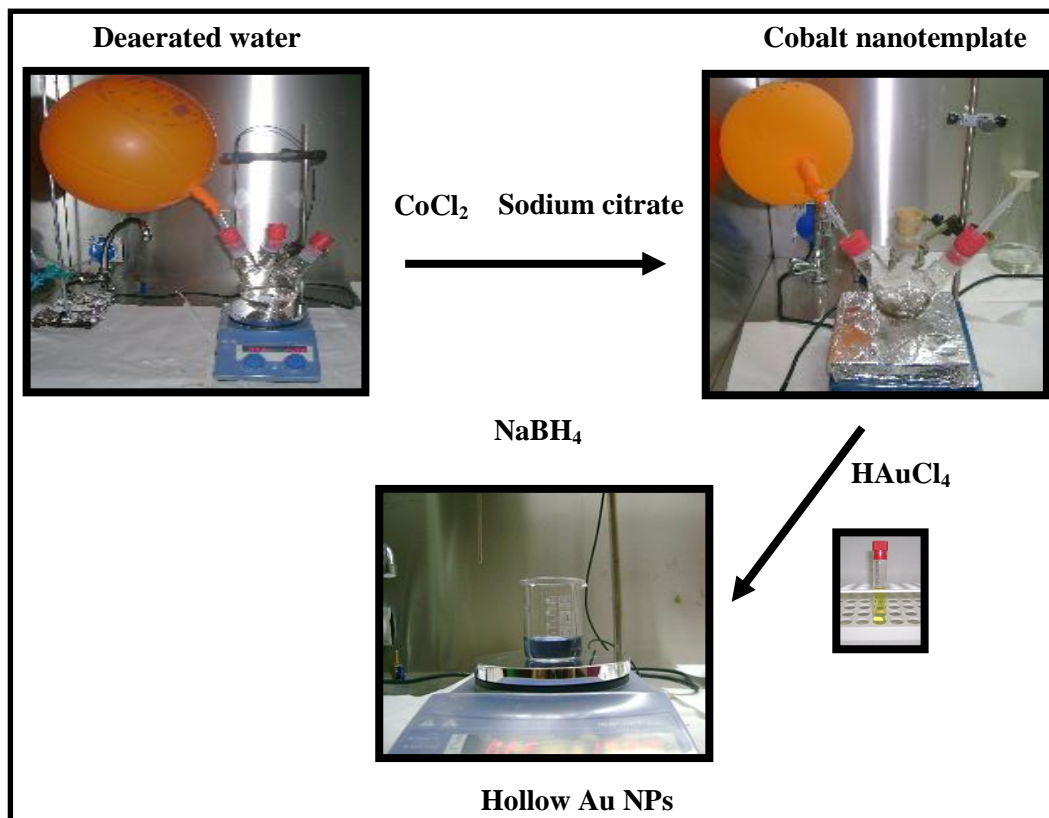


Figure 18. The experimental setup used for the production of the hollow gold nanoparticles (HAuNPs)

2.4. Preparation of Solid Gold Nanoparticles

Gold nanoparticles (AuNPs) were prepared by the citrate-reduction procedure. A 100 mL solution containing 0.01 g $\text{HAuCl}_4 \cdot 3\text{H}_2\text{O}$ was heated to boiling, and then 3 mL of 1% sodium citrate solution was quickly added to the boiling solution. The color of the solution changed from pale yellow to deep red within 1 minute. The solution was further boiled for 1 hour and allowed to equilibrate to room temperature while stirring. The volume was made up to 100 mL by adding water and the solution was cooled at room temperature. Formation of the red colored gold particles was observed at the end of this process. The experimental setup used for the production of the solid AuNPs is shown in Figure 19.

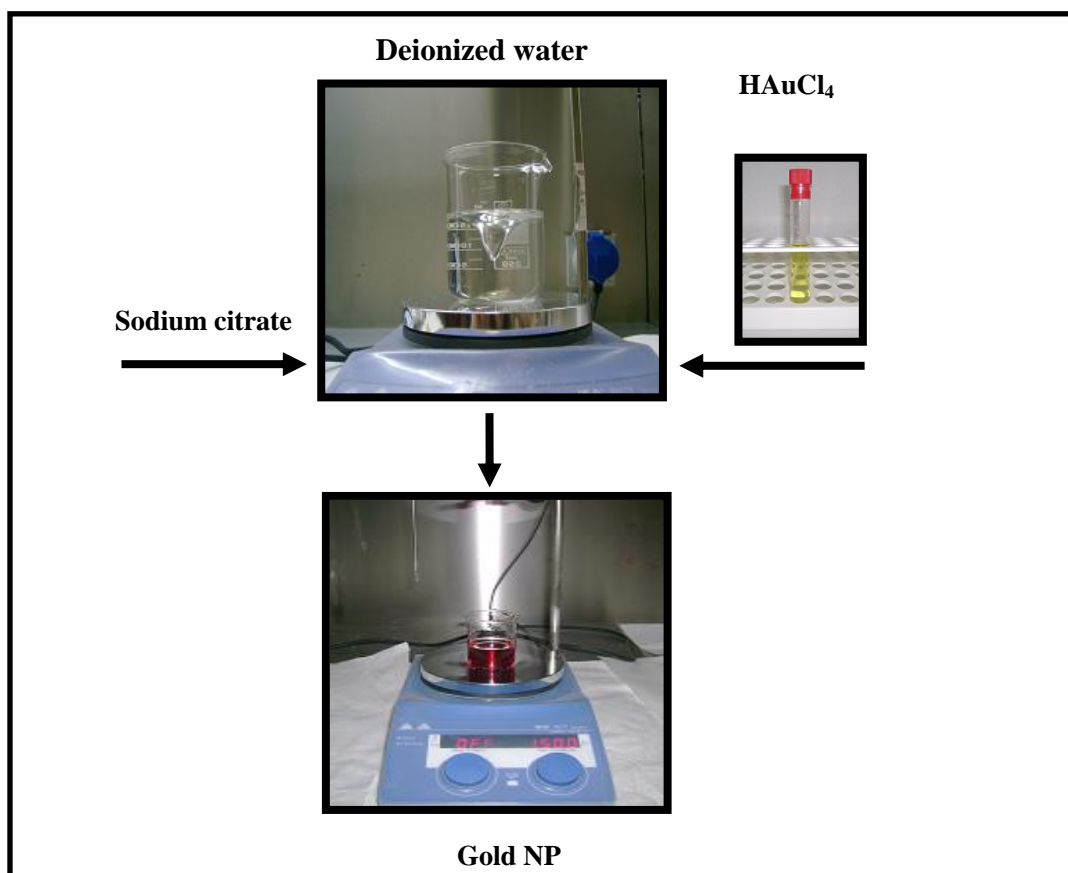


Figure 19. The experimental setup used for the production of the solid gold nanoparticles (AuNPs).

2.5. Synthesis of Hollow Gold-Silver Double-Shell and Solid Gold-Silver Core-Shell Nanoparticles

Silver coated solid gold and hollow gold nanoparticles were prepared following seed growth approach. The ascorbic acid reduction of AgNO_3 was carried out in the presence of the gold seed. 3 mL of as-prepared gold nanostructure solution and 400 μL of 0.1 M ascorbic acid were placed in a glass vial and stirred with a magnetic stir bar. Silver nitrate (1 mM) was then added drop wise (10 μL per addition) to this mixing solution with approximately 30 second between each drop.

By changing the ratio of gold nanoparticles to AgNO_3 , the thickness of silver shell was controlled to arrange the different-sized particles. The solution color changed from pink to deep yellow and from pink to faint brown with the gradual addition of AgNO_3 . The experimental setup used for the production of the silver coated both gold (AuAgNPs) and hollow gold nanoparticles (HAuAgNPs) are shown in Figure 20 and Figure 21.

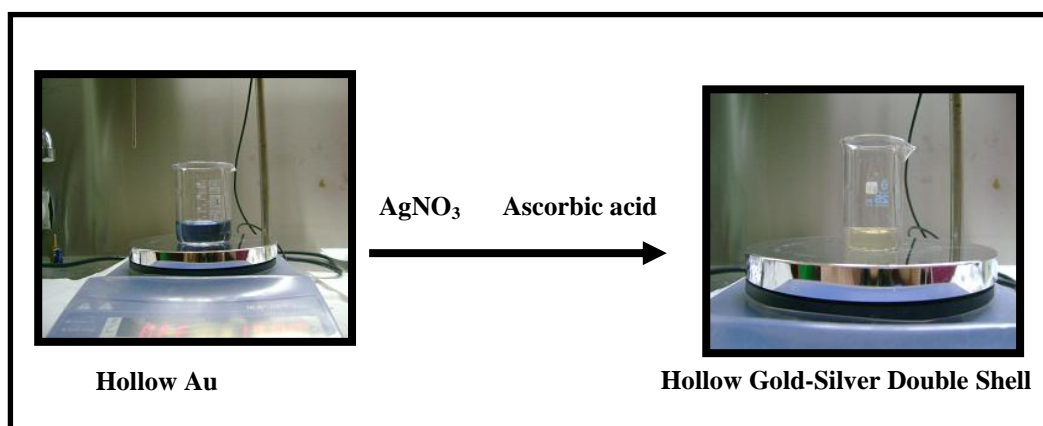


Figure 20. The experimental setup used for the production of the hollow gold-silver double-shell nanoparticles (HAuAgNPs).

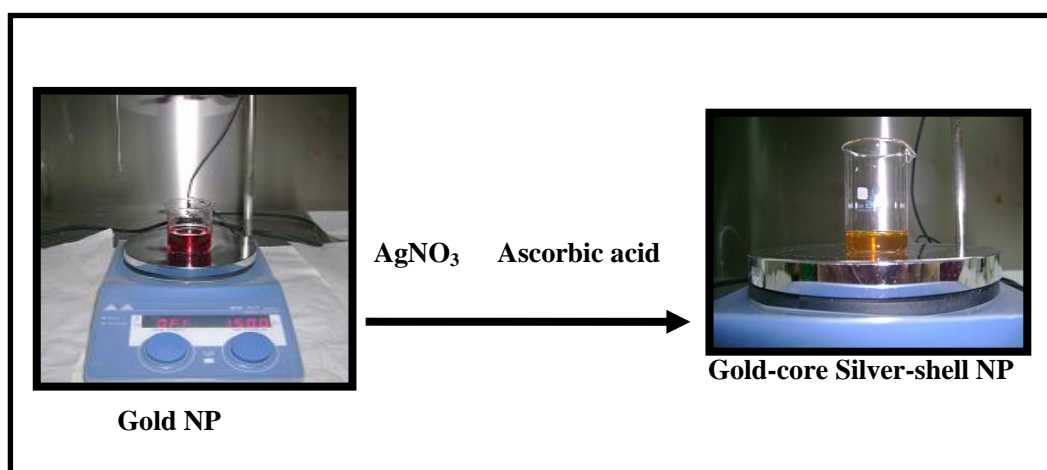


Figure 21. The experimental setup used for the production of the solid gold-silver core-shell nanoparticles (AuAgNPs).

2.6. Synthesis of Silver Nanoparticles with Citrate Reduction

Silver NPs (AgNPs) were synthesized with citrate reduction method as described by Lee and Meisel [198]. 500 mL of 1×10^{-3} M silver nitrate solution was boiled and then 10 mL of 1% sodium citrate solution was added to the boiling solution drop wise and allowed to continue boiling for 1 hour with vigorous stirring. Then it was brought to a final volume of 500 mL. The resulting colloids had yellow/greenish color.

2.7. Surface Modification of Silver Nanoparticles with Iron-Nitrilotriacetic Acid Complex

26.3 mg aminobutylated nitrilo triacetic (AB-NTA) acid and 48.4 mg $\text{Fe}(\text{NO}_3)_3$ were dissolved in 10 mL water separately to obtain 2×10^{-2} M solution. Then 1 mL of 2×10^{-2} M $\text{Fe}(\text{NO}_3)_3$ solution was mixed with 1 mL of 2×10^{-2} M chelate (NTA) solution and the pH was adjusted to 7.0 by the addition of NaOH to achieve the iron nitrilotriacetic acid ($\text{Fe}(\text{NTA})$) complex. After waiting 30 minutes, functionalization of silver nanoparticles with $\text{Fe}(\text{NTA})$ complex was performed by mixing 8 mL of Ag colloids with 2 mL of $\text{Fe}(\text{NTA})$ complex solution at room temperature and allowed to stand for 15 min. The colloidal solution of Ag- $\text{Fe}(\text{NTA})$ was centrifuged twice (15 min, 5000 rpm) to remove excess unbounded $\text{Fe}(\text{NTA})$ and then redispersed in 1 mL water and the pH was adjusted to 7.0 by the addition of NaOH.

2.8. Preparation of Europium (III) Ion Modified Silver (Ag-Eu³⁺) Nanoparticles

The preparation of silver nanoparticles doped with lanthanide ions was undertaken in a one-step redox route. First 85 mg AgNO₃ and 11.1 mg EuCl₂ were dissolved in 5 mL water to obtain 10⁻² M solution. After that 1 mL portion of EuCl₂ and 0.5 mL of AgNO₃ solution were mixed and the Ag-Eu³⁺ nanoparticles were obtained simultaneously.

2.9. Preparation of Substrates for SERS and SERRS Studies

Various fresh stock solutions of analytes were prepared in water in varying concentrations and used for serial dilutions. The substrates for SERS measurements were prepared by simply dropping the prepared nanostructures onto glass slides which were cleaned with ethanol before. Then substrates were used for the measurements of analytes directly or after allowed to dry (Figure 22).

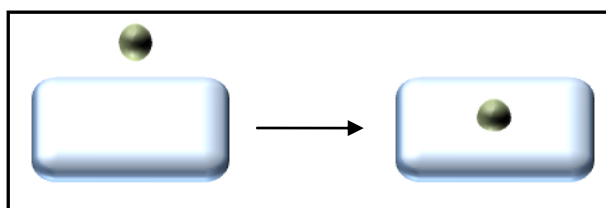


Figure 22. Preparation of SERS and SERRS substrates.

CHAPTER 3

RESULTS AND DISCUSSIONS

3.1. Preparation of SERS Substrates with Tunable Optical Property

SERS enhancement factor depends on the optical absorption of the substrate. Therefore controlling the structure and optical properties of noble metal nanoparticles like silver and gold is particularly important for SERS applications.

In the first part of the study, hollow gold nanoparticles (HAuNPs), hollow gold-silver double shell (HAuAgNPs), solid gold nanoparticles (AuNPs), gold core silver shell nanoparticles (AuAgNPs), and silver nanoparticles (AgNPs), which are shown in Figure 23, were synthesized. These nanoparticles were used as SERS substrate and their Raman enhancement properties were investigated by utilising brilliant cresyl blue (BCB) and crystal violet (CV) dye molecules as model compounds.

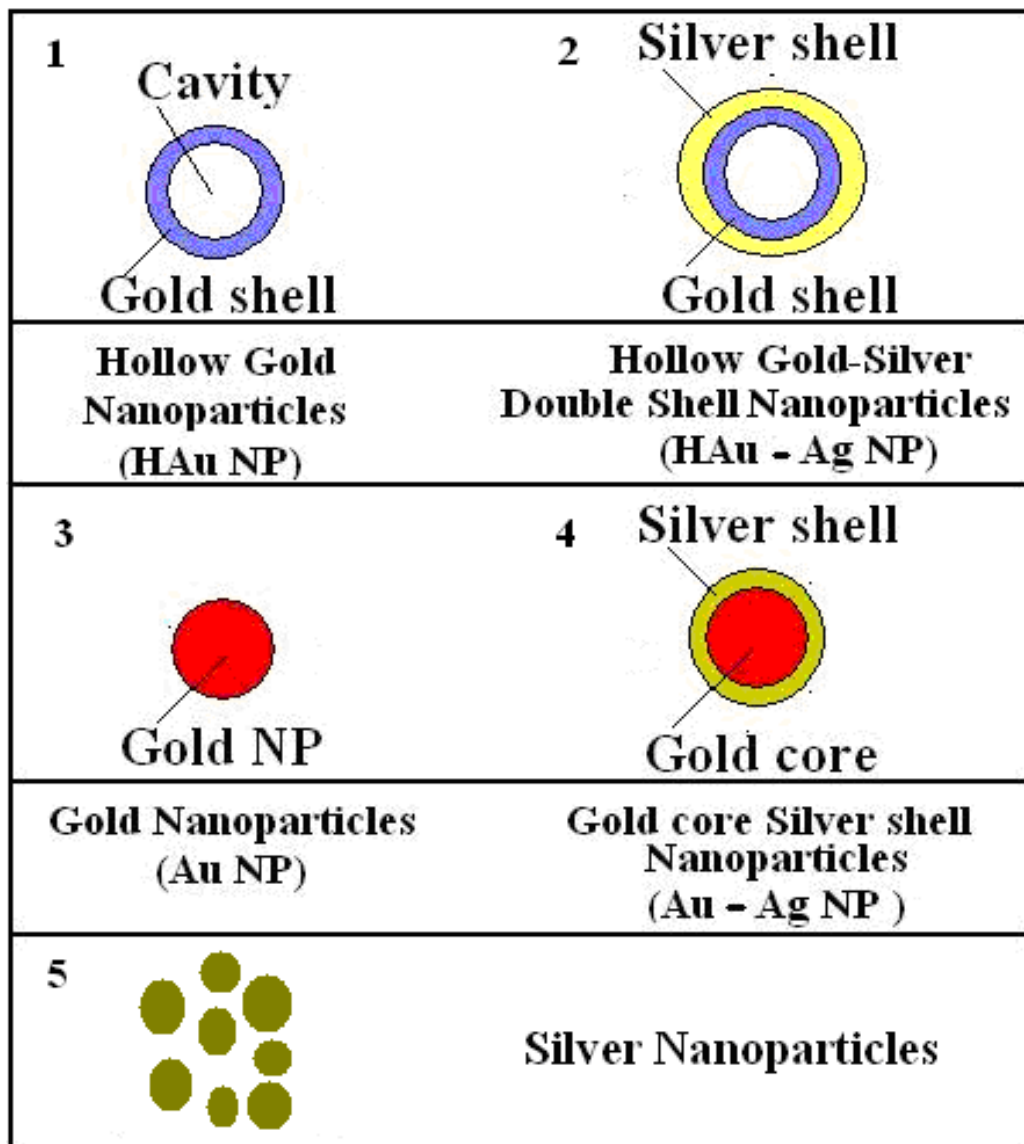


Figure 23. Representations of nanostructures prepared.

3.1.1. Preparation of Hollow Gold Nanoparticles with a Tunable Interior Cavity

3.1.1.1. Preparation of Cobalt Nanotemplates

The size of the hollow interior of the prepared gold nanostructures is directly related to the diameter of cobalt nanoparticles since the reduced gold atoms are mainly confined to the vicinity of the sacrificial template of outer surface. For that reason the production of cobalt nanoparticles is the first critical stage in the preparation procedure.

Cobalt chloride solution was added to citrate solution and then to this solution freshly prepared sodium borohydride solution was added to synthesize cobalt nanoparticles. The formation of cobalt nanoparticles can be easily observed from the color of the solution. The color change of solution from pink to gray demonstrates the reduction of Co (II) ions into cobalt nanoparticles. After the formation of cobalt nanoparticles, solution was kept for several minutes to remove excess NaBH_4 completely from the system.

Characterization of prepared cobalt nanoparticles was done by FE-SEM and EDX. The results are shown in Figure 24 and Figure 25. The average size of the prepared cobalt nanoparticles were measured as 44 ± 4 nm.

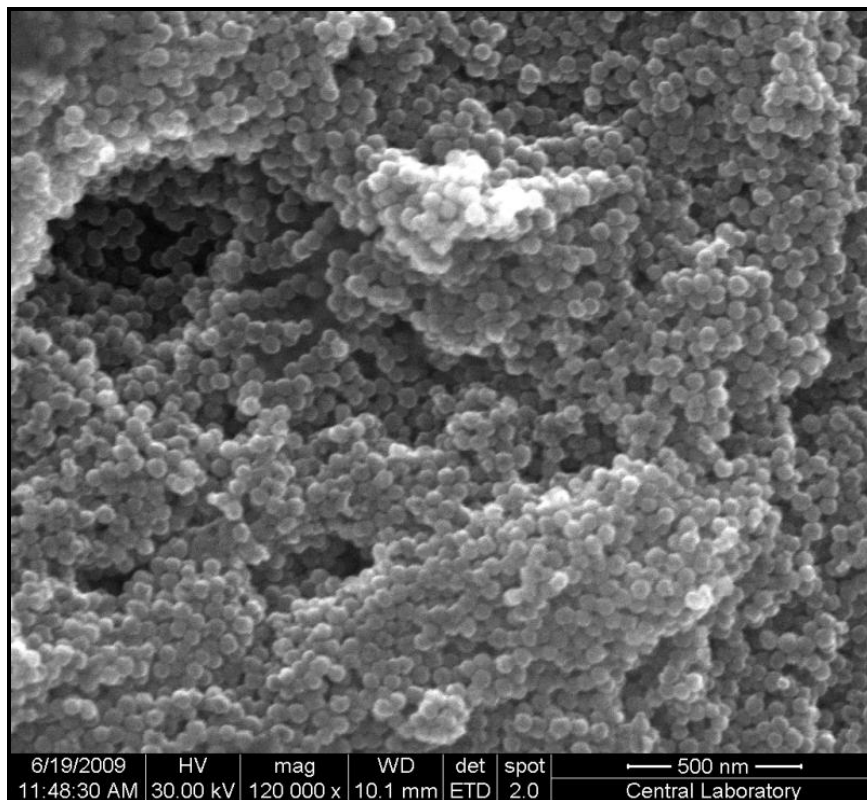


Figure 24. FE-SEM image of cobalt nanoparticles. The average diameter of the cobalt nanoparticles was measured as 44 ± 4 nm by sampling 100 nanoparticles (0.4 M 100 μ L CoCl_2 , 0.1 M 400 μ L sodium citrate and 1 M 100 μ L NaBH_4 were used in the production of cobalt nanoparticles).

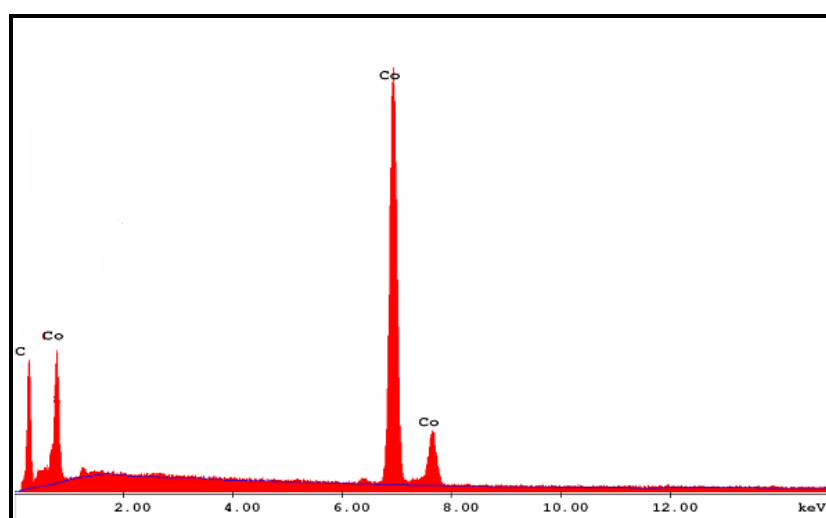


Figure 25. EDX pattern of cobalt nanoparticles.

3.1.1.2. Effect of the Amount of Capping Agent (Sodium Citrate) and Reducing Agent (Sodium Borohydride) on the Particle Size of Cobalt Nanoparticles

In this part of the study, the aim was to control the particle size of cobalt nanostructures by applying aqueous solution chemistry. First the volume of sodium citrate added was altered (400, 600, and 900 μL) while keeping the amount of reducing agent constant to observe the effect of the amount of capping agent on the particle size of CoNPs. The particles were characterized structurally with a FE-SEM. The results are given in Table 3. FE-SEM images of the prepared particles are shown in Figure 24, Figure 26 and Figure 27.

Table 3. Particle size of cobalt nanoparticles as a function of citrate amount

Particle diameter (nm)	Volume of 0.1 M citrate (μL)	Volume of 1 M NaBH_4 (μL)	Figure No.
44 \pm 4	400	100	25
36 \pm 6	600	100	27
25 \pm 3	900	100	28

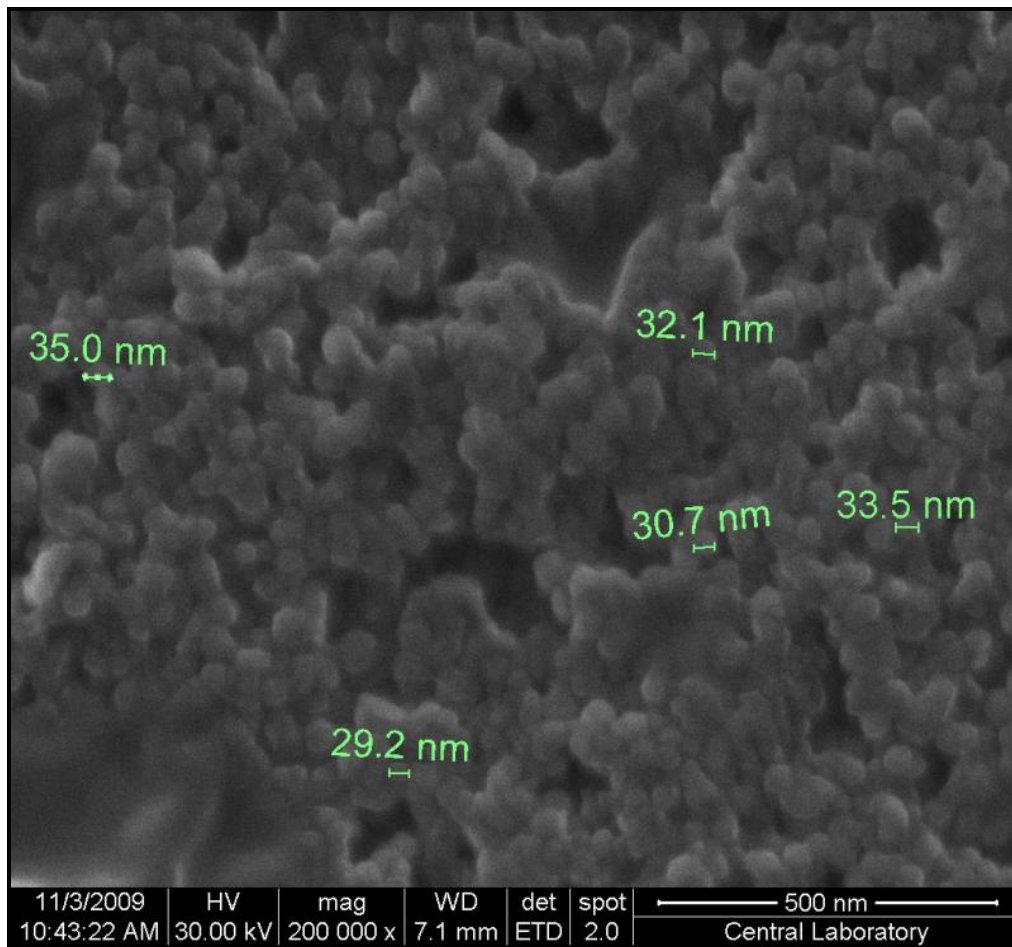


Figure 26. FE-SEM image of cobalt nanoparticles. The average diameter of the cobalt nanoparticles (Table 3) was measured as 36 ± 6 nm by sampling 100 nanoparticles (0.4 M 100 μ L CoCl_2 , 0.1 M 600 μ L sodium citrate and 1 M 100 μ L NaBH_4 were used in the production of cobalt nanoparticles).

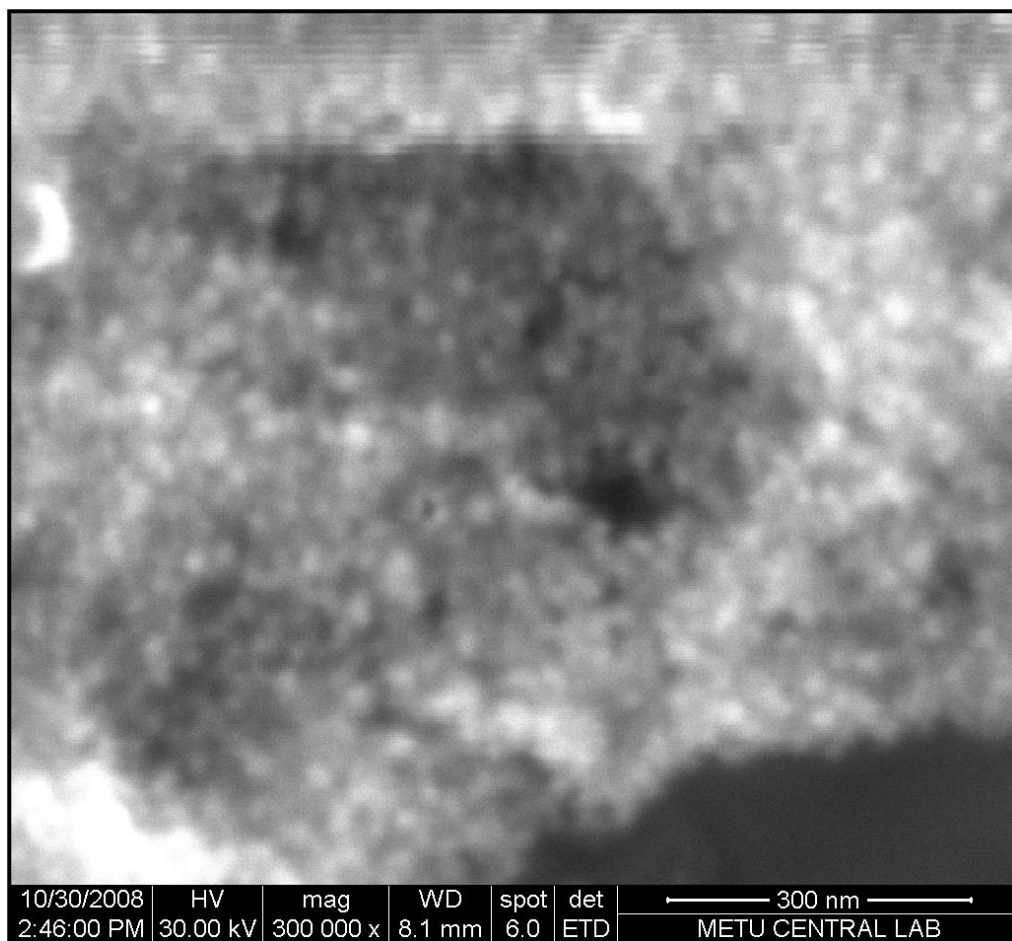


Figure 27. FE-SEM image of cobalt nanoparticles. The average diameter of the cobalt nanoparticles (Table 3) was measured as 25 ± 3 nm by sampling 100 nanoparticles (0.4 M 100 μ L CoCl_2 , 0.1 M 900 μ L sodium citrate and 1 M 100 μ L NaBH_4 were used in the production of cobalt nanoparticles).

As can be seen from Table 3, when small amount of capping agent was used, an increase in the size of the cobalt nanoparticles was observed due to the aggregation of the particles. Increasing the amount of sodium citrate, on the other hand, provided smaller size cobalt nanoparticles due to the formation of more stabilized nuclei which lead to the decrease of aggregation.

The effect of the amount of reducing agent (NaBH_4) on CoNP size was also examined by using two different amounts of NaBH_4 . The experimental results are given in Table 4. The FE-SEM results of the prepared particles are shown in Figure 24 and Figure 28.

Table 4. Particle size of cobalt nanoparticles as a function of sodium borohydride amount

Particle diameter (nm)	Volume of 0.1M citrate (μL)	Volume of 1 M NaBH_4 (μL)	Figure No.
32 \pm 4	400	400	29
44 \pm 4	400	100	25

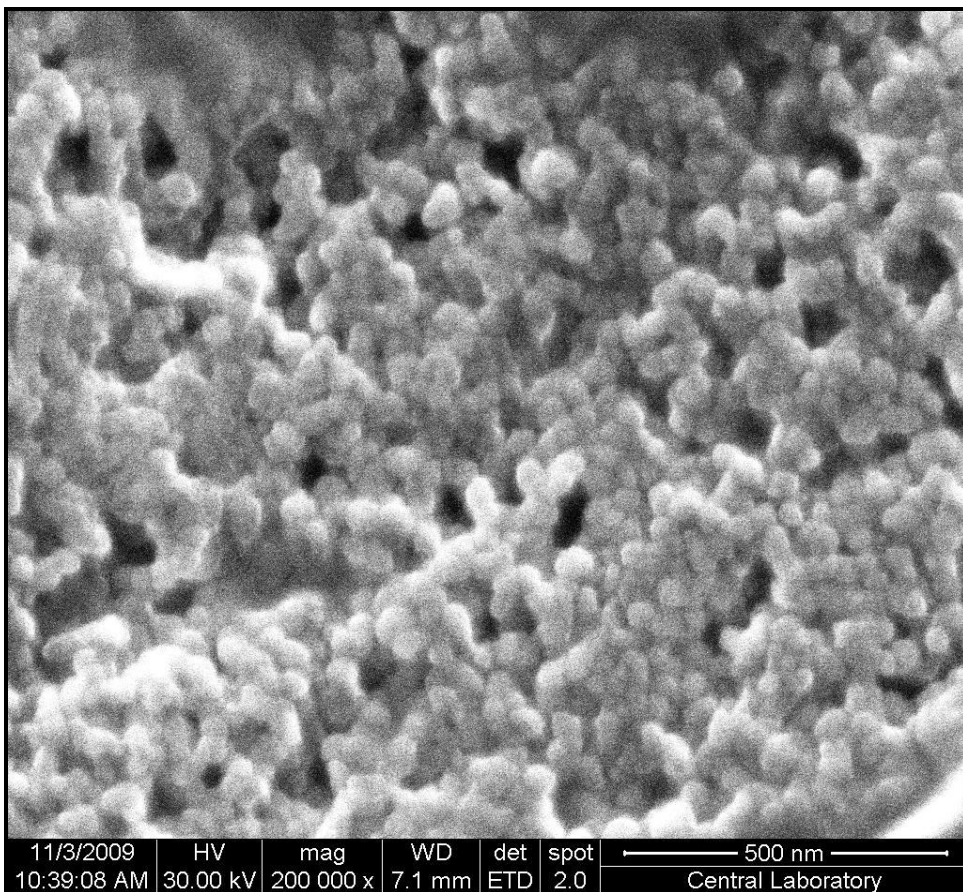


Figure 28. FE-SEM image of cobalt nanoparticles. The average diameter of the Co nanoparticles (Table 4) was measured as 32 ± 4 nm by sampling 100 nanoparticles (0.4 M 100 μ L CoCl_2 , 0.1 M 400 μ L sodium citrate and 1 M 400 μ L NaBH_4 were used in the production of cobalt nanoparticles).

By decreasing the amount of sodium borohydride used (from 400 μ L to 100 μ L), the rate of the reaction was reduced and reaction time was increased significantly. Since the number of seeds, and consequently the size of the resulting particles depends on the rate of reduction [199], formation of larger particles (approximately 35 %) were observed when the reaction rate was slowed down by lowering the amount of reducing agent.

As a summary, in the preparation of cobalt nanoparticles, an inverse relationship was observed between the size of nanoparticles produced and the amounts of the capping (sodium citrate) and the reducing (sodium borohydride) agents used. Thus it was found that, cobalt nanoparticle size can be tuned to a larger or smaller dimension by lowering or raising the concentrations of sodium citrate and sodium borohydride, respectively.

3.1.1.3. Formation of Hollow Gold Nanoparticles (HAuNPs)

Hollow gold nanoparticles were effectively produced by adding cobalt colloidal solution onto aqueous HAuCl₄ solutions. The whole preparation process is illustrated in Figure 29.

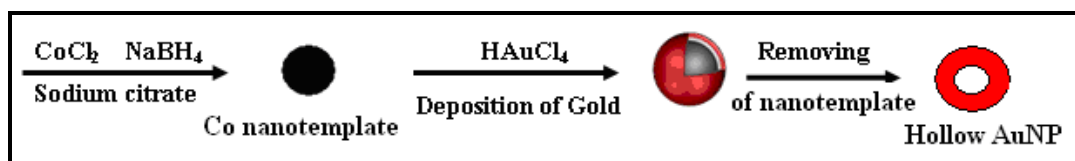


Figure 29. Preparation of hollow gold nanoparticles with a tunable interior cavity.

Gold nanoshell was produced with galvanic replacement reaction and remaining cobalt was removed from the core part by air oxidation. The standard reduction potentials of the Co^{2+} -Co and AuCl_4^- -Au are -0.377 and 0.994 V, respectively. When the AuCl_4^- solutions were added onto Co nanoparticles, AuCl_4^- reduced to Au atoms according to the following replacement reaction



Structural characterizations of the HAuNP were performed utilizing FE-SEM and EDX. Typical FE-SEM images of HAuNPs produced with 44 ± 4 nm

CoNPs are shown in Figure 30 and Figure 31. The EDX pattern shown in Figure 32 gives the elemental composition of prepared hollow gold nanoparticles.

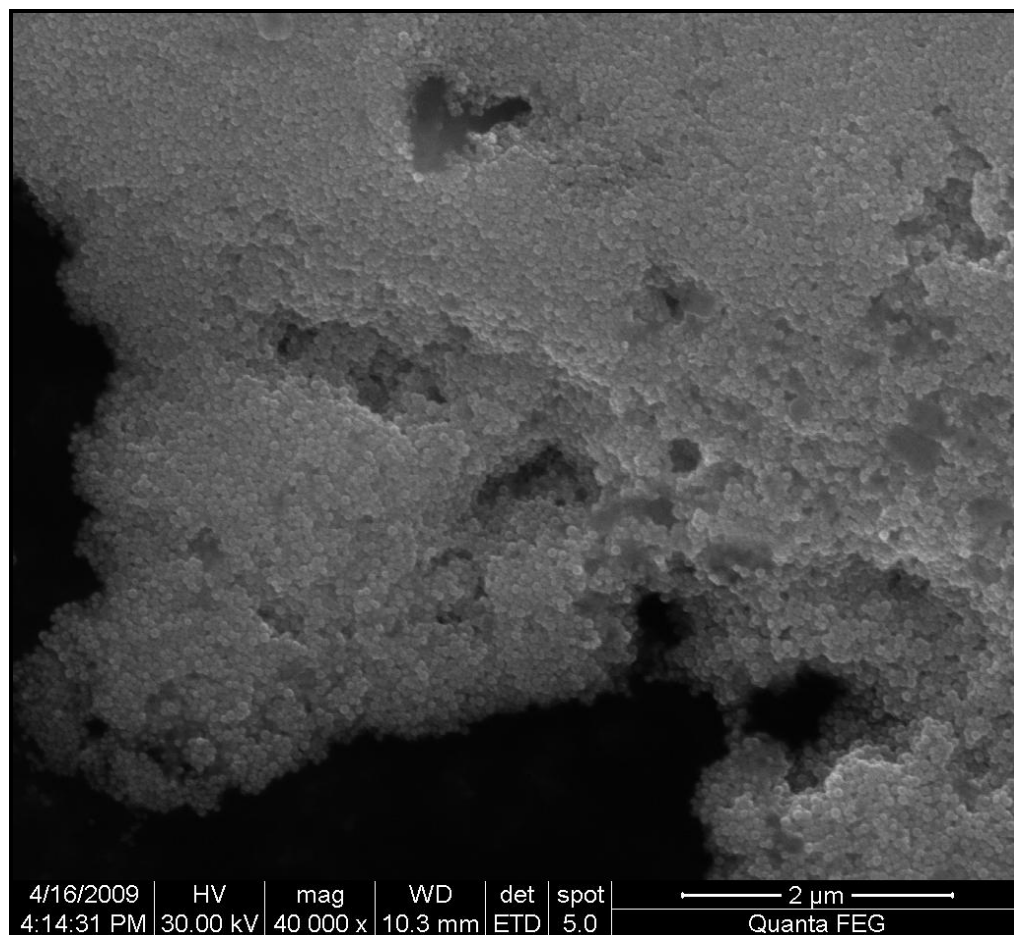


Figure 30. FE-SEM images of hollow gold nanoparticles produced with 44 ± 4 nm CoNP templates and with $50\ \mu\text{L}$ of 0.1 M chloroauric acid ($\text{HAuCl}_4\cdot 3\text{H}_2\text{O}$).

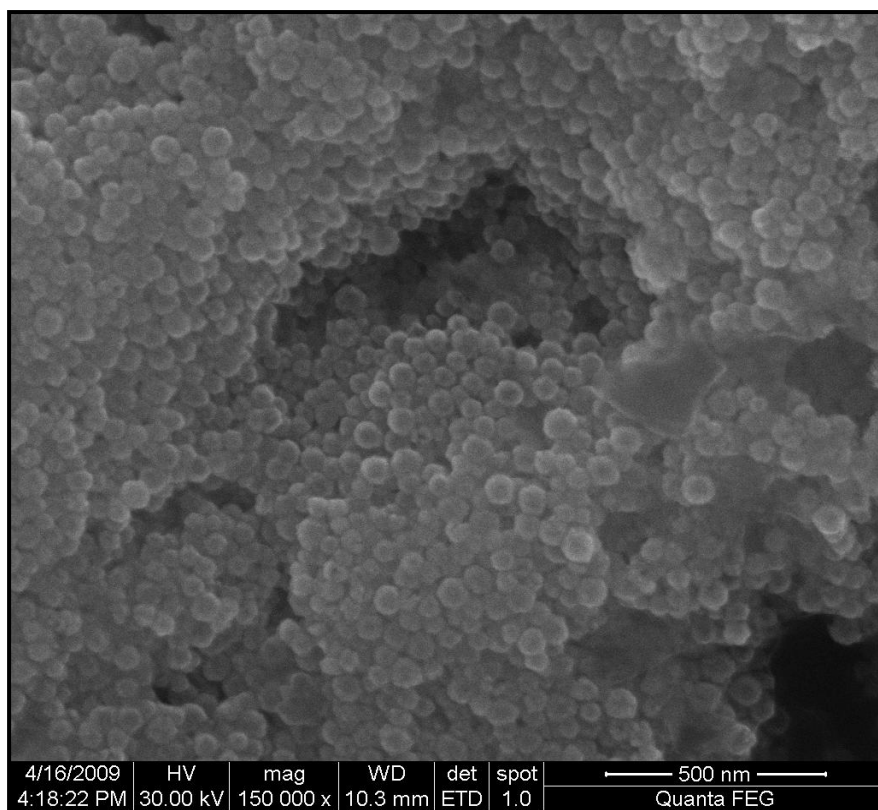


Figure 31. FE-SEM images of hollow gold nanoparticles produced with 44 ± 4 nm CoNP templates and with $50\ \mu\text{L}$ of 0.1 M chlorauric acid ($\text{HAuCl}_4\cdot 3\text{H}_2\text{O}$). The average diameter of the hollow nanoparticles was measured as 52 ± 9 nm by sampling 100 hollow gold nanoparticles.

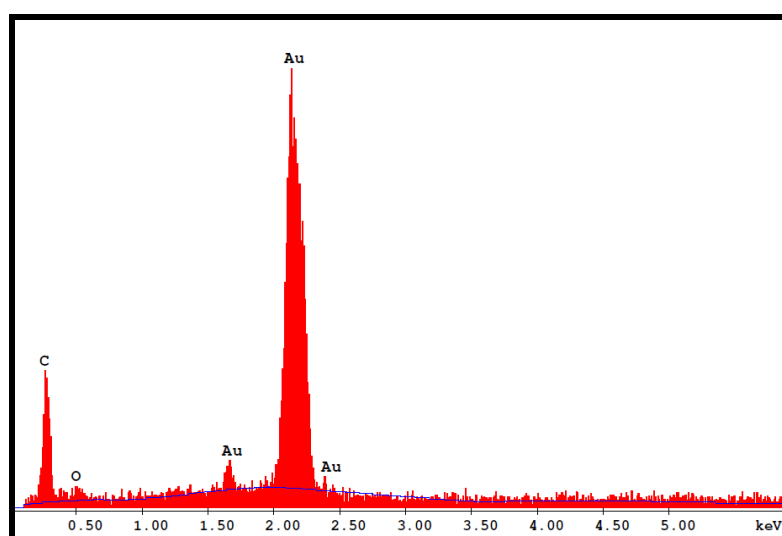


Figure 32. EDX pattern of hollow gold nanoparticles.

The thickness of the gold shell was increased as the replacement between cobalt nanoparticles and HAuCl_4 continued. The resulting large-scale nanoparticles were uniform and the average diameter of the hollow nanoparticles was measured as 52 ± 9 nm by sampling 100 hollow gold nanoparticles. Size separation process was not applied on these HNPs, because of the high monodispersity obtained with the preparation method used. The hollow interior of the prepared nanoparticles can be easily seen from the FE-SEM images, Figure 33 and Figure 34.

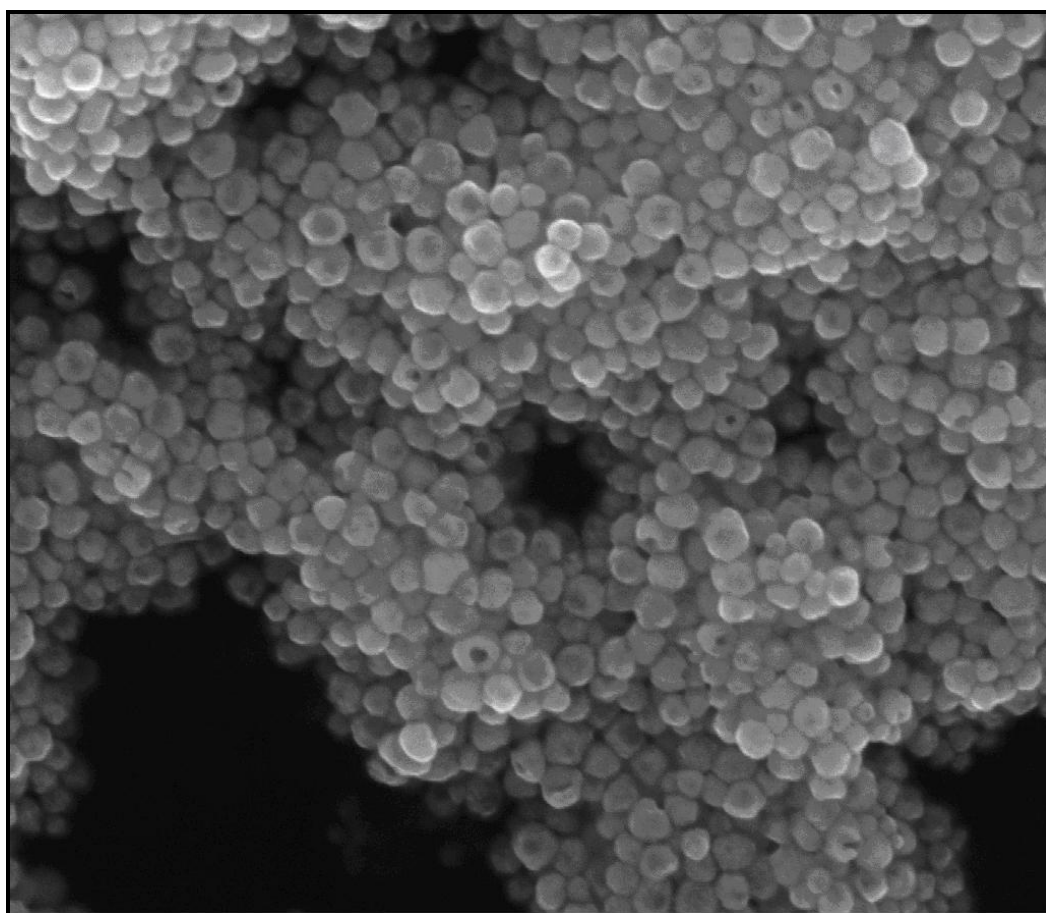


Figure 33. FE-SEM image of the hollow interior of gold nanoparticles.

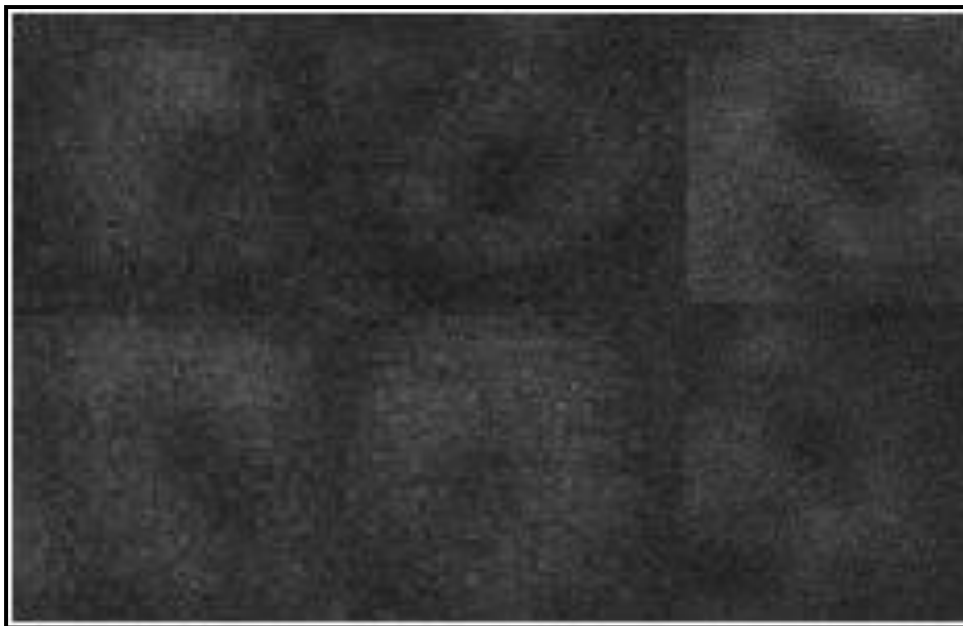


Figure 34. FE-SEM image of the hollow interior of gold nanoparticles.

As can be seen from the results, it was possible to prepare homogeneous hollow gold nanoparticles with tunable hollow and shell diameters by using cobalt nanoparticles as sacrificial templates. Because the gold salt was easily reduced with sodium borohydride and solid gold nanoparticles were formed besides hollow ones, significant amount of time was required to provide the complete hydrolyzation of sodium borohydride before the addition of AuCl_4^- solution.

3.1.1.4. Optical Characterization of Prepared Hollow Gold Nanoparticles

The surface plasmon resonance (SPR) features of gold nanostructures are distinguishable in the UV-visible region. In order to show the shift in absorption maxima of the prepared hollow hold nanoparticles, the UV-visible absorption spectra of aqueous solution of solid and hollow gold nanoparticles were taken. Results are given in Figure 35.

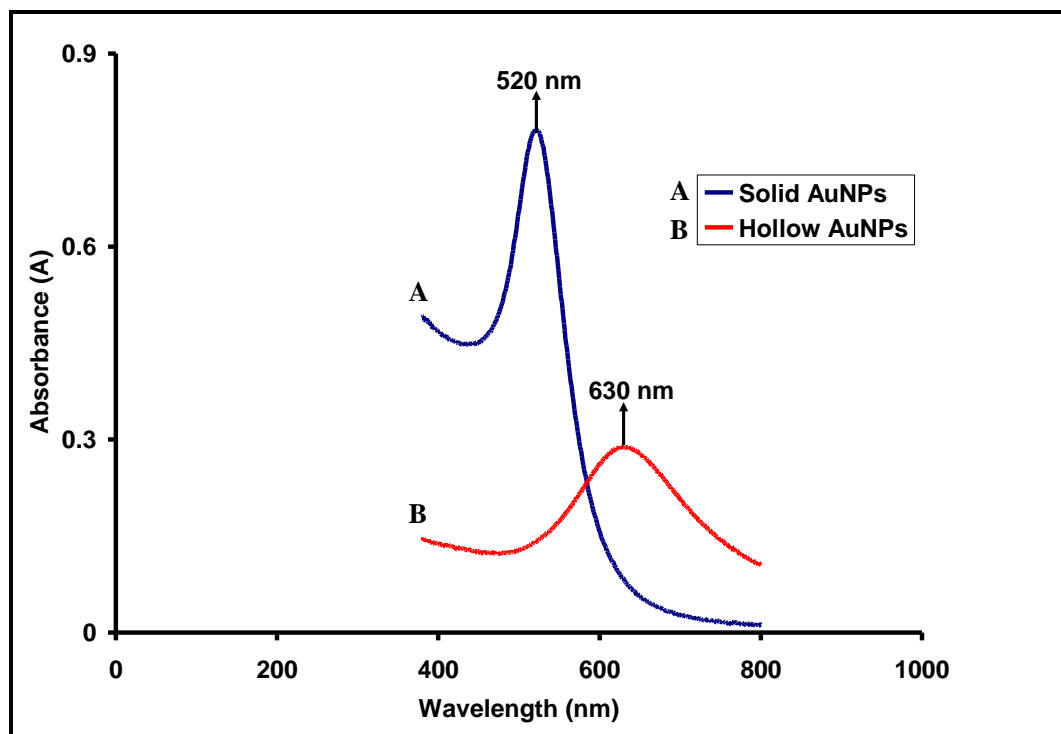


Figure 35. UV–Vis spectra of (A) solid and (B) hollow gold nanoparticles. The sizes of the solid and hollow gold nanoparticles were 20 ± 2 and 52 ± 9 nm respectively.

As can be seen from Figure 35, the SPR peak positions show an apparent red shift from solid gold nanoparticle to hollow gold nanoparticle due to the change in structure of gold nanoparticles. The appearances of AuNP and HAuNP solutions are given in Figure 36.

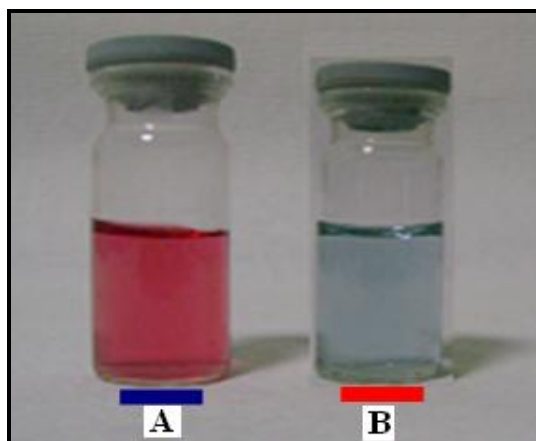


Figure 36. Appearance of (A) solid and (B) hollow gold nanoparticles. The sizes of the solid and hollow gold nanoparticles were 20 ± 2 and 52 ± 9 nm respectively.

The change in color of the nanoparticle solution from red to light blue was another evidence of the change in structure. In order to investigate the effect of size of hollow interior and shell part on optical properties of nanostructures, hollow nanoparticles with different size of shell and core part were prepared by varying the cobalt nanotemplate sizes (25, 36 and 44 nm) at a fixed HAuCl_4 concentration (Figure 37). The appearance of hollow gold nanoparticle solutions with different overall and hollow interior sizes are given in Figure 38 to illustrate the change in color.

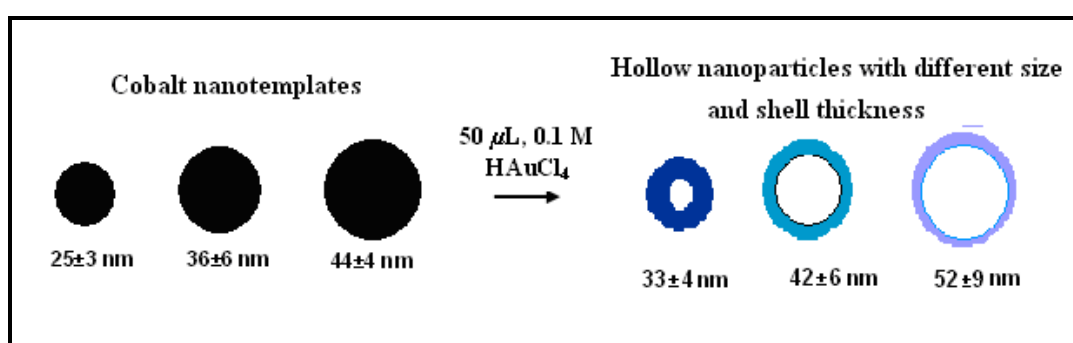


Figure 37. Hollow nanoparticles prepared with different size of cobalt nanotemplates.

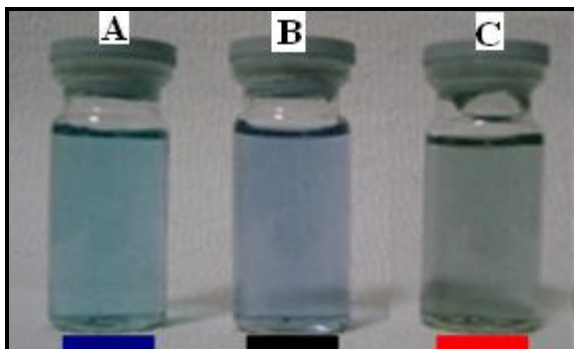


Figure 38. Appearance of hollow gold nanoparticles with different shell thickness and size, prepared using various sizes ((A) 25 ± 3 nm, (B) 36 ± 6 nm and (C) 44 ± 4 nm) of cobalt nanotemplates.

UV-visible absorption spectra of their aqueous solutions were taken. The results are given in Figure 39.

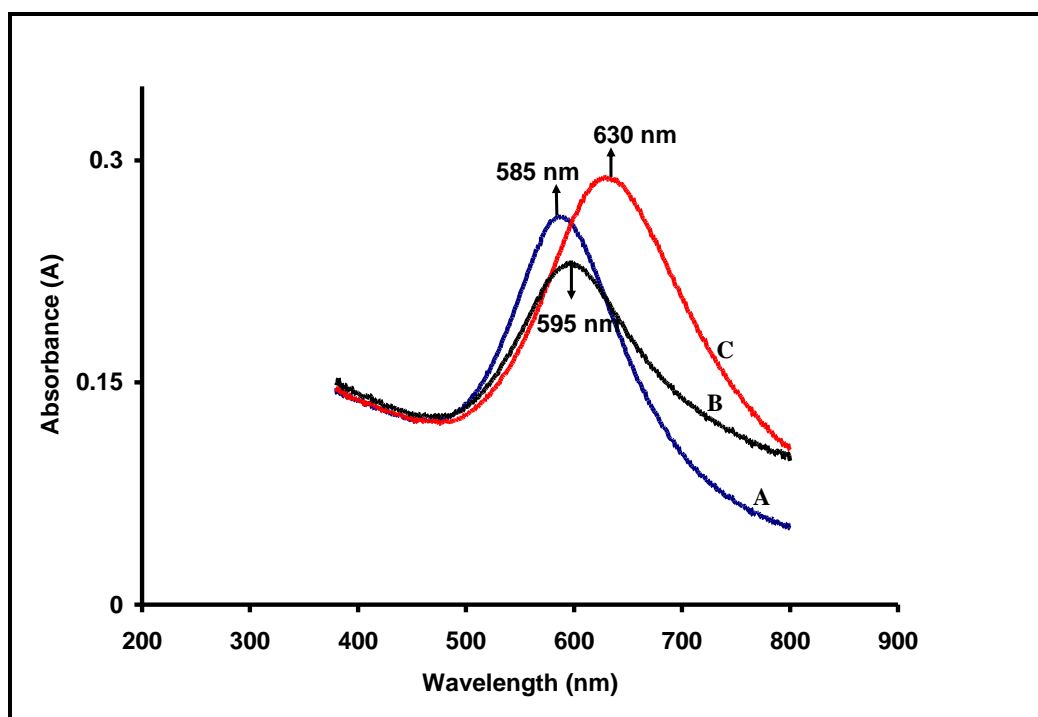


Figure 39. UV-Vis spectra of hollow gold nanoparticles prepared using various sizes ((A) 25 ± 3 nm, (B) 36 ± 6 nm and (C) 44 ± 4 nm) of cobalt nanotemplates.

As can be seen in Figure 39, spectrum of the hollow gold nanoparticles was red shifted by increasing interior-cavity size and overall size of the particles. The effect of wall thicknesses on SPR frequency was also monitored by keeping the template size constant (36 ± 6 nm cobalt nanoparticles, from the same batch) and varying the amount of the gold solution added (50-400 μL of 0.1 M HAuCl_4). The preparation process is illustrated in Figure 40. UV-visible absorption spectra of aqueous solutions of hollow gold nanoparticles were taken. The results are shown in Figure 41.

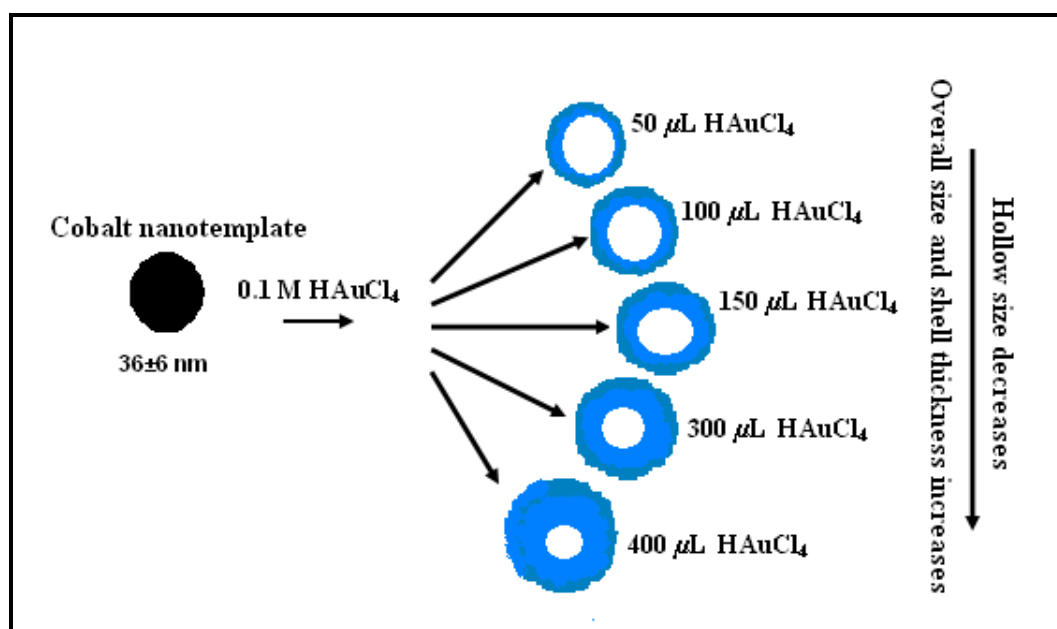


Figure 40. Hollow nanoparticles prepared with different amount of 0.1 M HAuCl_4 .

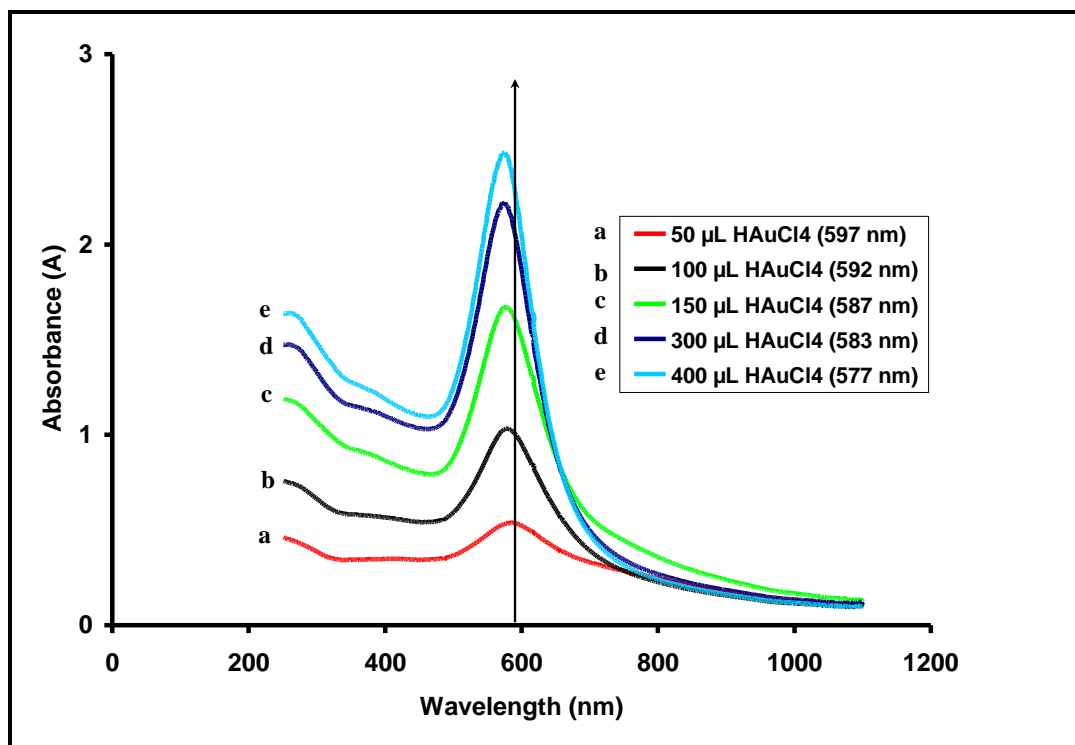


Figure 41. UV–Vis spectra of hollow gold nanoparticles with different shell thickness (0.1 M HAuCl₄).

As can be seen from Figure 41, the SPR absorption maximum of the particles was blue-shifted as the wall thickness was increased. The shortest wavelength of SPR absorption maximum (577 nm) was acquired from the batch of nanoparticles which were prepared using the highest amount of gold salt.

As a result, changes in both shell thickness and the interior-cavity size of gold hollow nanoparticles were resulted in the shift of SPR peaks in both (blue and red) directions. The maximum points of SPR bands of hollow nanoparticles (Figure 37 and Figure 40) thus prepared were covering the visible region from 577 to 630 nm (Figure 39 and Figure 41).

3.1.2. Preparation of Hollow Gold-Silver Double-Shell Nanoparticles (HAuAgNPs)

Plasmon resonance frequency of a nanoshell can also be tuned by changing the precious metal used. To illustrate this effect, HAuAgNPs were prepared by depositing silver on preformed HAuNPs. HAuNPs were acted as a seed to induce the Ag growth by chemical reduction of Ag^+ in the presence of preformed colloid. The preparation process of HAuAgNPs is illustrated in Figure 42.

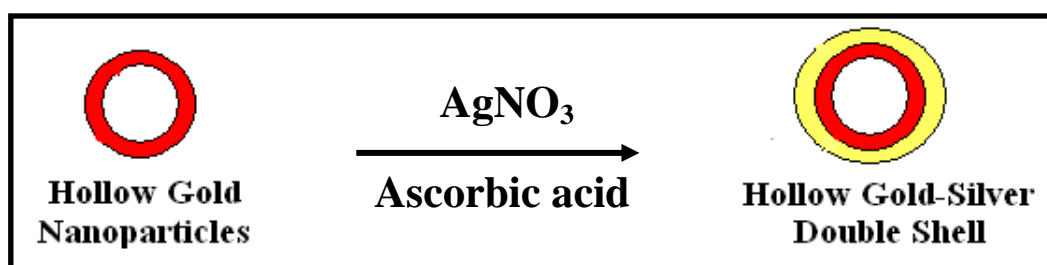


Figure 42. Preparation of hollow gold-silver double-shell nanoparticles with a tunable shell thickness.

52 ± 9 nm HAuNPs were used for the preparation of HAuAgNPs. FE-SEM and EDX were used to determine the structure of hollow gold nanostructures after silver coating. FE-SEM images of the prepared particles are shown in Figure 43 and Figure 44.

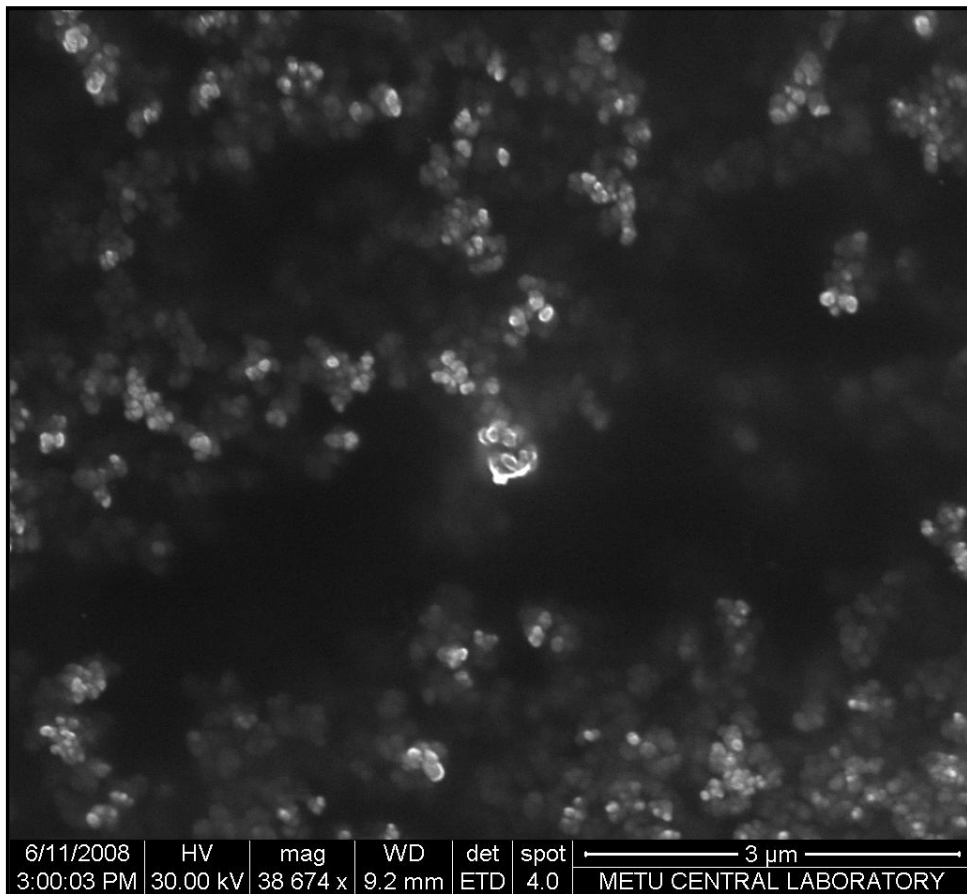


Figure 43. FE-SEM image of hollow gold-silver double-shell nanoparticles produced with 52 ± 9 nm HAuNPs and 1 mM AgNO_3 . The average diameter of the nanoparticles was measured as 87 ± 10 nm.

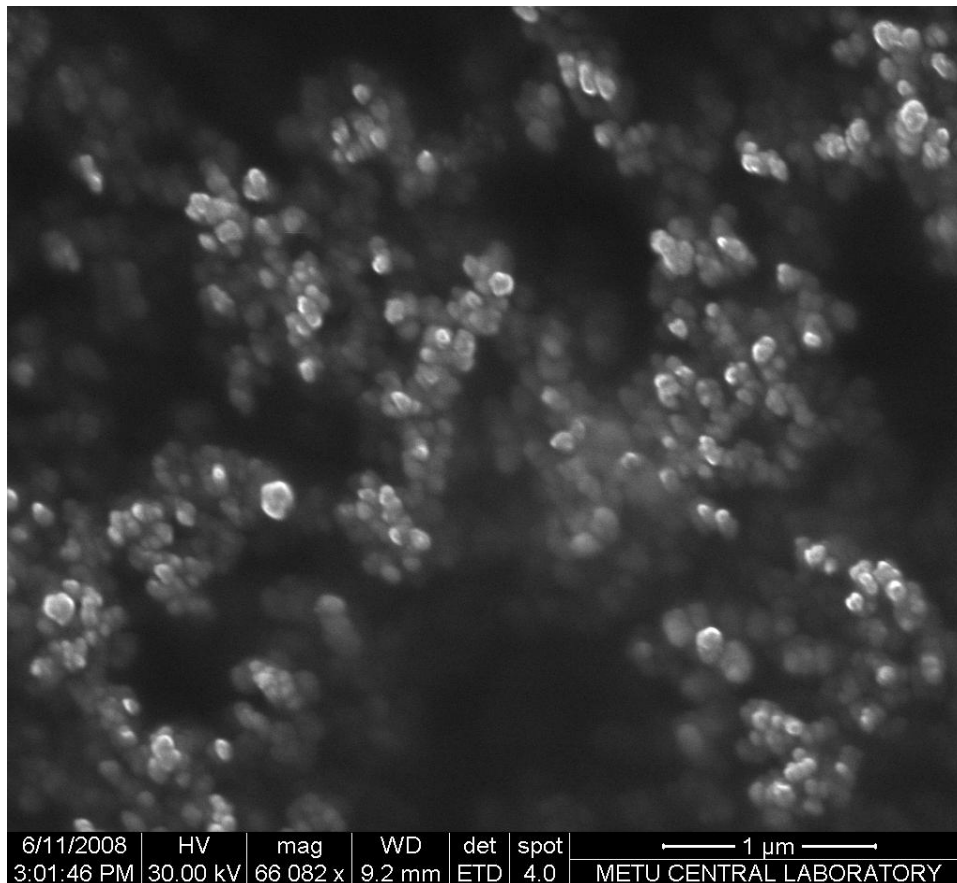


Figure 44. FE-SEM image of hollow gold-silver double-shell nanoparticles produced with 52 ± 9 nm HAuNPs and 1 mM AgNO_3 . The average diameter of the nanoparticles was measured as 87 ± 10 nm.

The resulting large-scale nanoparticles were uniform and the average diameter of the nanoparticles was measured as 87 ± 10 nm by sampling 100 nanoparticles. The uniform structure of H AuAgNPs was largely due to the very uniform size and shape of the initial HAuNPs. Small deviation from the uniformity of HAuNPs was due to grown of new shell layer during the production of H AuAgNPs. The thickness of Ag shell was calculated around 15 nm. The presence of silver shell on gold nanostructure core in EDX measurement (Figure 45) demonstrated the success of seed-mediated growth as a method to coat nanoparticle surfaces.

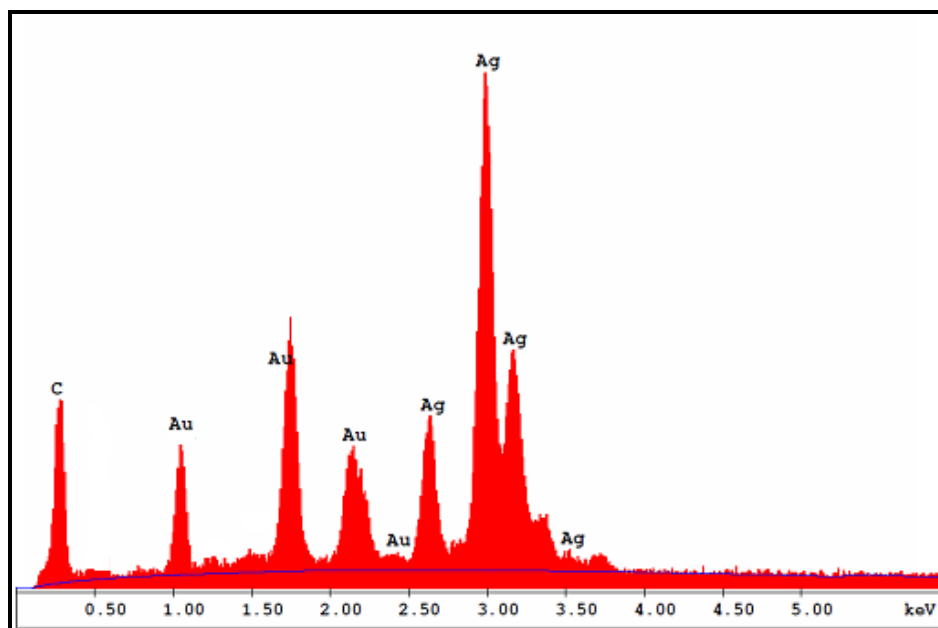


Figure 45. EDX pattern of hollow gold-silver double-shell nanoparticles.

When excessive silver was present during the silver coating process, a single smooth silver shell around each individual gold core became difficult to synthesize. Instead, more than one gold core were encapsulated in the same silver matrix and individual silver nanoparticles of various sizes were formed. Although ascorbic acid is a weak reducing agent, when enough silver ions were present, the silver reduction rate was increased, resulting in nanoparticle formation. Silver coating obtained was more uniform when a lower amounts of silver nitrate and ascorbic acid, and a smaller of dropwise volume addition of silver into the gold solution was applied.

3.1.2.1. Surface Plasmons in Hollow Gold-Silver Double-Shell Nanoparticles

UV-vis spectra of the HAuNPs with and without the silver shell are shown in Figure 46. Also appearance of the prepared nanoparticles with and without silver shell is given in Figure 47.

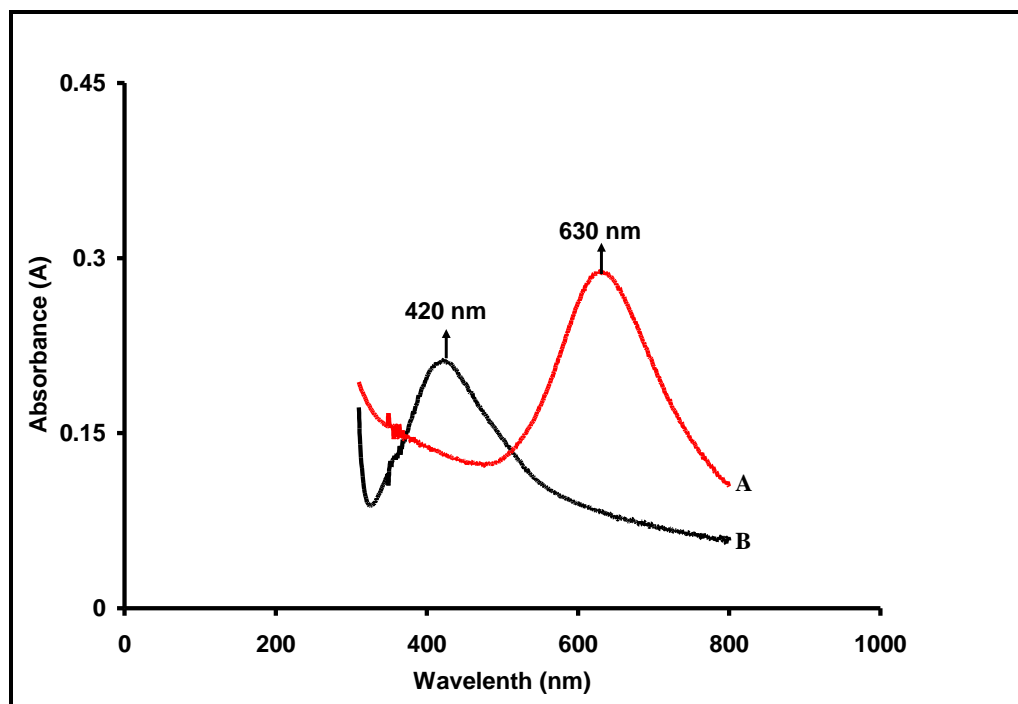


Figure 46. UV-Vis spectra of (A) hollow gold (52 ± 9 nm) and (B) hollow gold-silver double-shell (87 ± 10 nm) nanoparticle solutions.

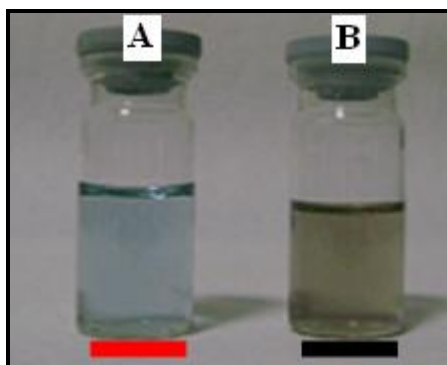


Figure 47. Appearance of (A) hollow gold (52 ± 9 nm) and (B) hollow gold-silver double-shell (87 ± 10 nm) nanoparticle solutions.

The SPR of HAuNP was at 630 nm in aqueous solutions, which was red shifted from the one corresponding to a solid gold nanosphere in water (520 nm). As the thickness of Ag shell increased, the SPR of the hollow gold-silver double-shell nanoparticle was tuned from 630 nm (HAuNP plasmon band) to 420 nm (AgNP plasmon band).

3.1.3. Preparation of Solid Gold Nanoparticles

Gold nanoparticles are used in a wide range of applications because of their electronic and optical properties, and particularly due to their powerful SPR (surface plasmon resonance) present around 520 nm in aqueous medium. Gold seed particles were prepared by citrate-reduction procedure as described in section 2.4. Typical FE-SEM micrograph and EDX pattern of gold nanoparticles prepared in this study are shown in Figure 48 and Figure 49, respectively.

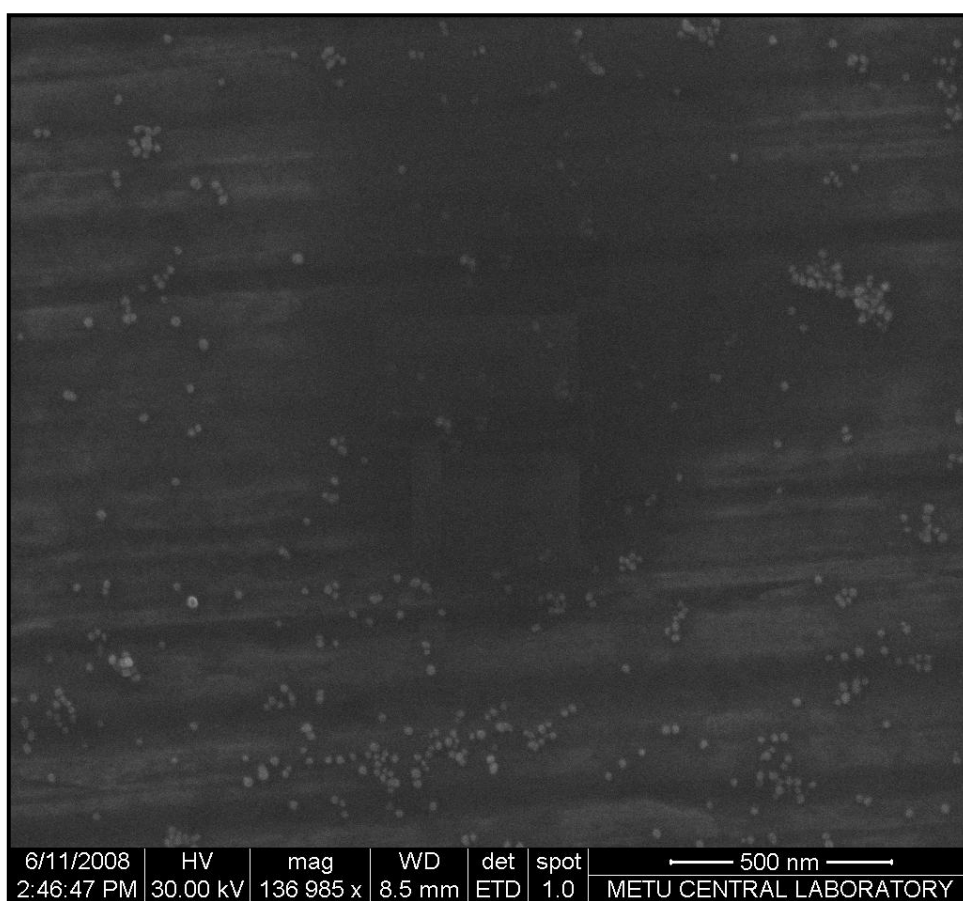


Figure 48. FE-SEM image of 20 ± 2 nm gold nanoparticles.

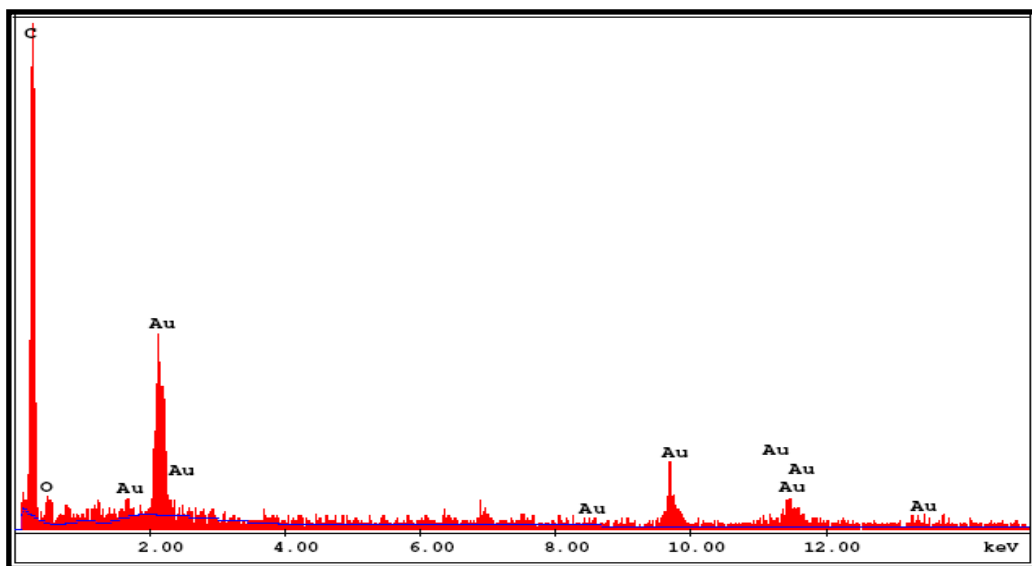


Figure 49. EDX pattern of 20 ± 2 nm gold nanoparticles.

The resulting large-scale nanoparticles were uniform and the average diameter of the solid gold nanoparticles was observed to be 20 ± 2 nm by sampling 100 nanoparticles. They were largely spherical in shape. The key morphological features of them are the size controllability and the size monodispersity. The size of the nanoparticles can be obtained over a 10-100 nm range by changing the reducing agent/gold ratio, and the monodispersity for each sample of the nanoparticles is very high.

3.1.3.1. Effect of Particle Size on Optical Properties of AuNPs

UV-vis spectra of two different sizes gold nanoparticles (20 ± 2 nm and 30 ± 2 nm) are shown in Figure 50.

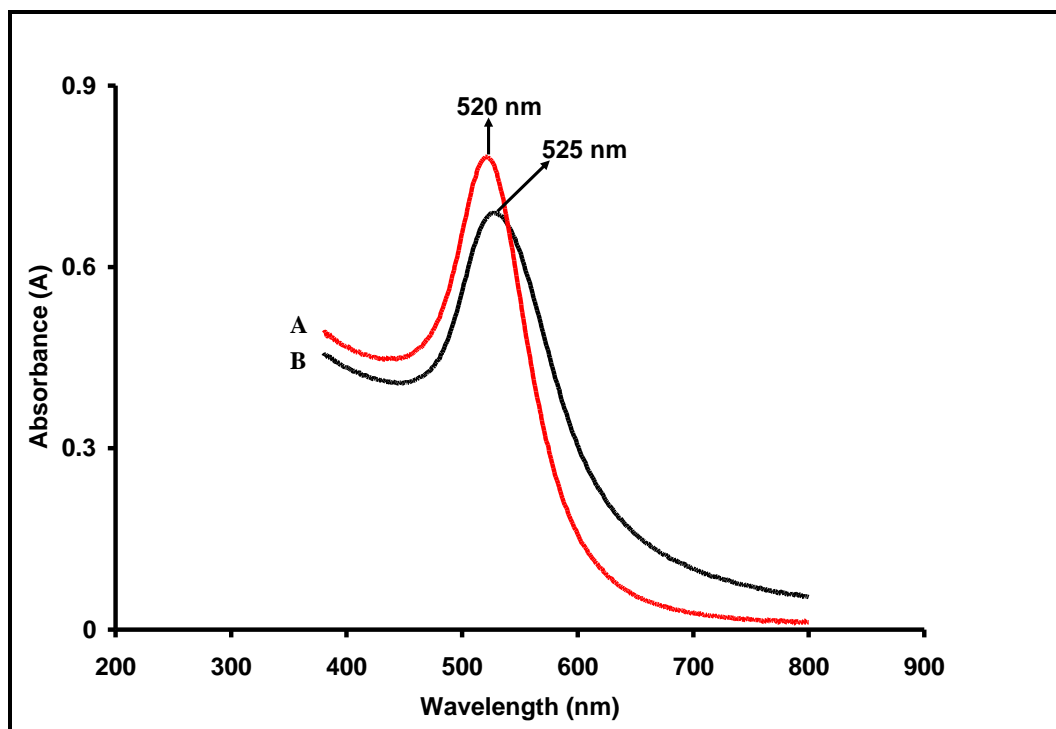


Figure 50. UV–Vis spectra of gold nanoparticles with different size ((A) 20 ± 2 nm and (B) 30 ± 2 nm).

Size of the gold nanoparticles was controlled by varying the reducing agent (sodium citrate)/gold ratio. The wavelengths of the SP bands were clearly dependent on the particle size, as was evidenced by the increase of the wavelength (λ_{max}) at a maximum absorbance of the SP band from 520 to 525 nm for nanoparticles of different sizes.

Representative colors of gold nanoparticles with different sizes are shown in Figure 51. The color exhibited a smooth transition from dark red to pink in going from the size of 20 ± 2 nm to 30 ± 2 nm.

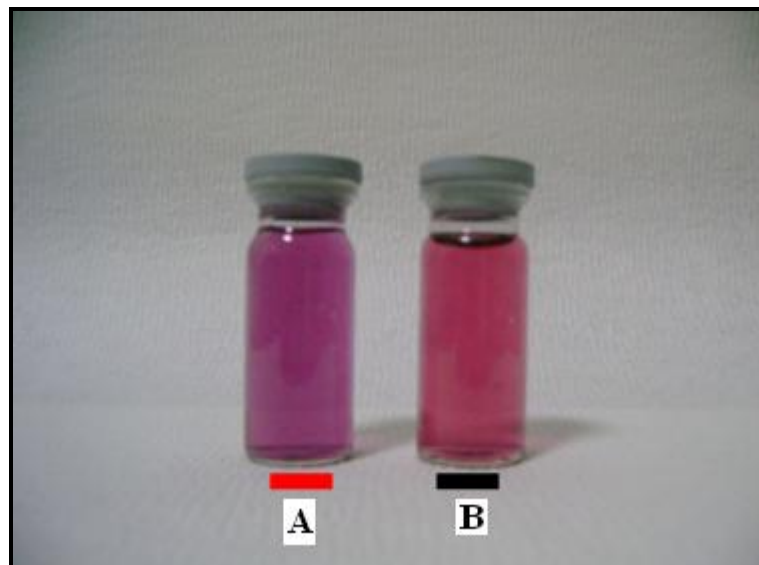


Figure 51. Appearance of solid gold nanoparticles with different size (A) (20 ± 2 nm) and (B) 30 ± 2 nm). Tunable colors generated by controlling the diameter of solid gold nanoparticles.

3.1.4. Preparation of Gold Core-Silver Shell Nanoparticles

Gold core–silver shell nanoparticles (AuAgNPs) were prepared by using seed mediated technique in which nanoparticles at shell region were produced with reducing agent in the presence of gold core part. According to the flow chart given in Figure 52, gold nanoparticles acted as a seed to induce the silver shell growth by chemical reduction of Ag^+ in the presence of preformed colloidal gold.

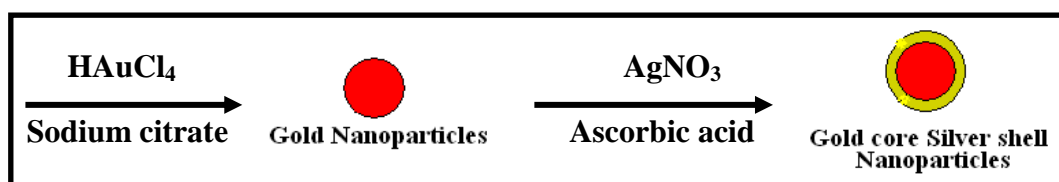


Figure 52. Preparation of gold-silver core-shell nanoparticles with a tunable shell thickness.

3.1.4.1. Characterization of the Gold Core-Silver Shell Nanoparticles

To examine whether a core-shell structure was obtained in the preparation described in the previous section, FE-SEM images of the as-prepared materials were taken which is shown in Figure 53.

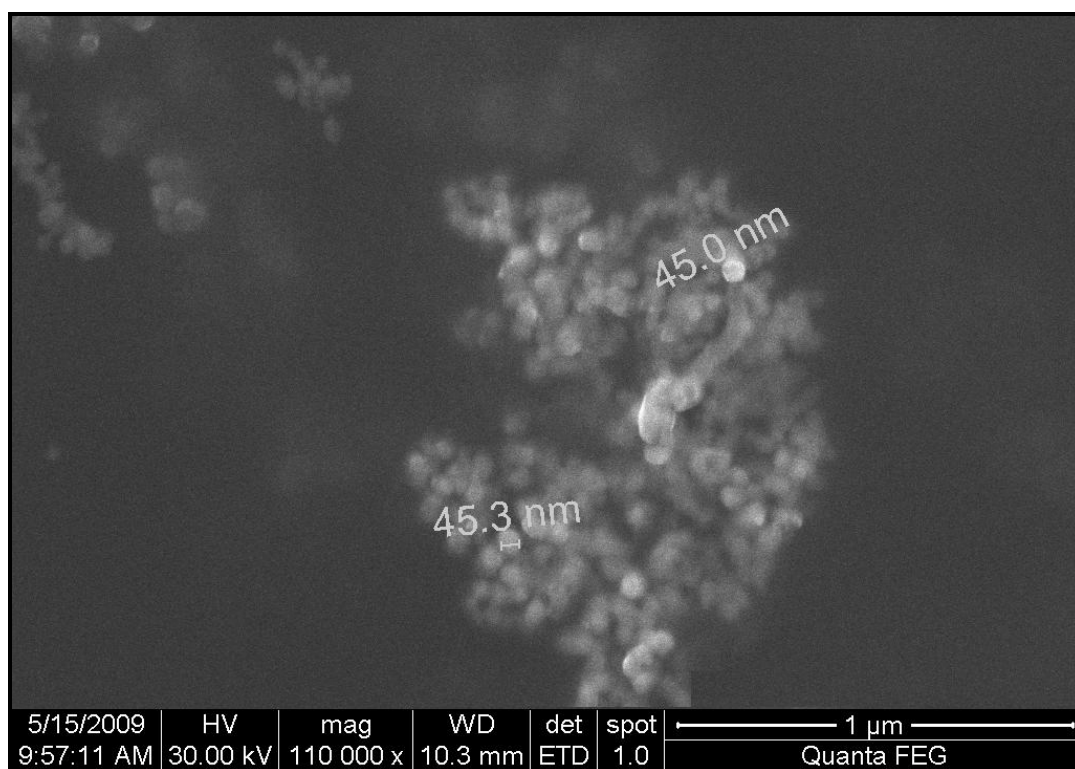


Figure 53. FE-SEM images of gold-core silver-shell nanoparticles produced with 20 ± 2 nm AuNPs and 1 mM AgNO_3 . The average size of the prepared nanoparticles was measured as 51 ± 8 nm.

The average size of the prepared nanoparticles was measured to be 51 ± 8 nm. The observations suggested that Ag^+ ions first being adsorbed on gold nanoparticle surfaces and then being reduced to metallic silver which lead to the formation of gold core silver shell nanoparticles by seed mediated method.

The composition of the particles, determined by energy dispersive X-ray (EDX) analysis shown in Figure 54, confirmed gold core and silver shell structure for the particles. EDX measurement indicated the presence of the metals employed in the preparation procedure.

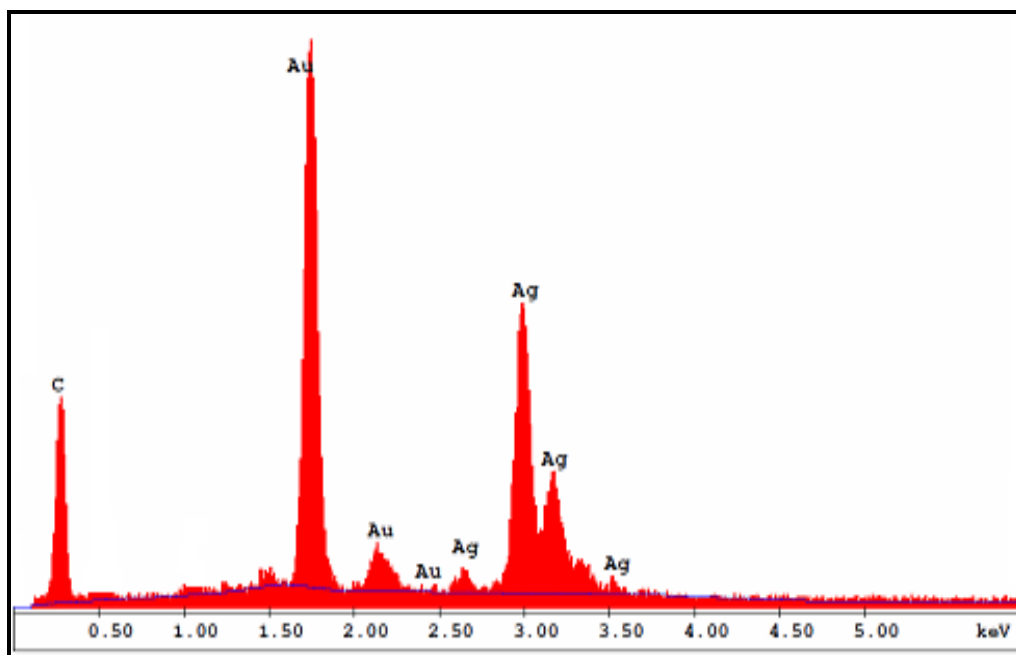


Figure 54. EDX pattern of gold-core silver-shell nanoparticles.

In order to support the formation of AuAgNPs, UV–visible spectra of AuNPs and AuAgNPs were taken. The results are shown in Figure 55.

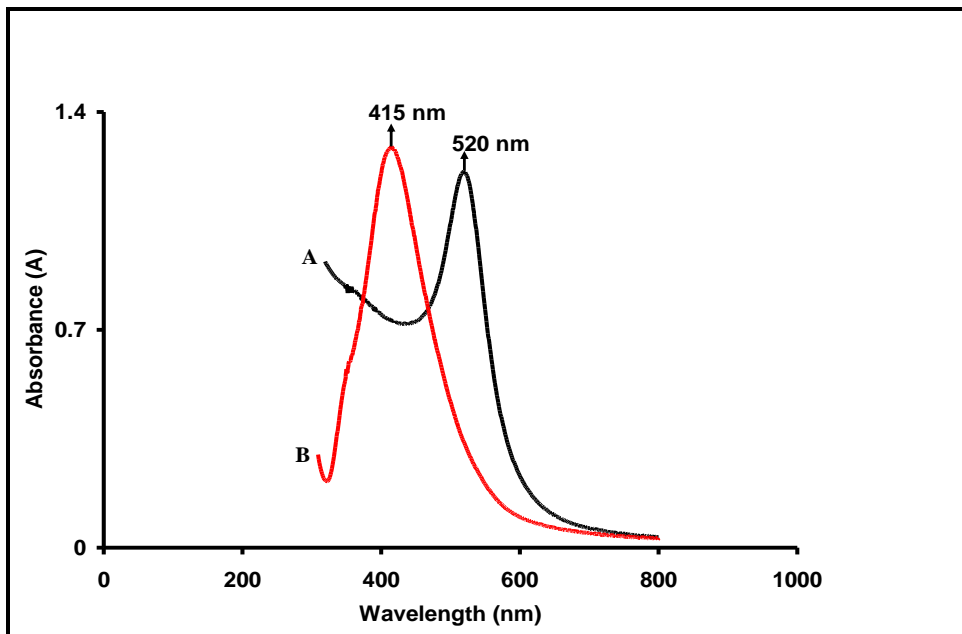


Figure 55. UV-Vis spectra of (A) gold and (B) gold-core silver-shell nanoparticles.

Plasmon band of gold seed particle appeared at 520 nm while the plasmon band of core-shell structure appeared at 415 nm. As a result, deposition of a second metal layer totally altered the resonance condition and changed the color of the nanoparticle solution (Figure 56). The starting gold nanoparticle solution was red however, after deposition of a silver shell, the color of the solution became yellow.

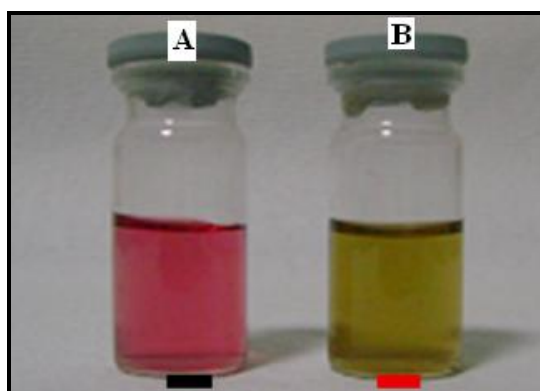


Figure 56. Appearance of (A) solid gold (red in color) and (B) gold-core silver-shell nanoparticles (yellow in color).

The effect of the amount of silver on SPR properties of AuAgNPs was investigated. Three different samples were prepared which the amounts of silver introduced in a simple stepwise manner to show the effect of silver amount on optical property. UV-visible spectra of three different AuAgNPs samples are given in Figure 57.

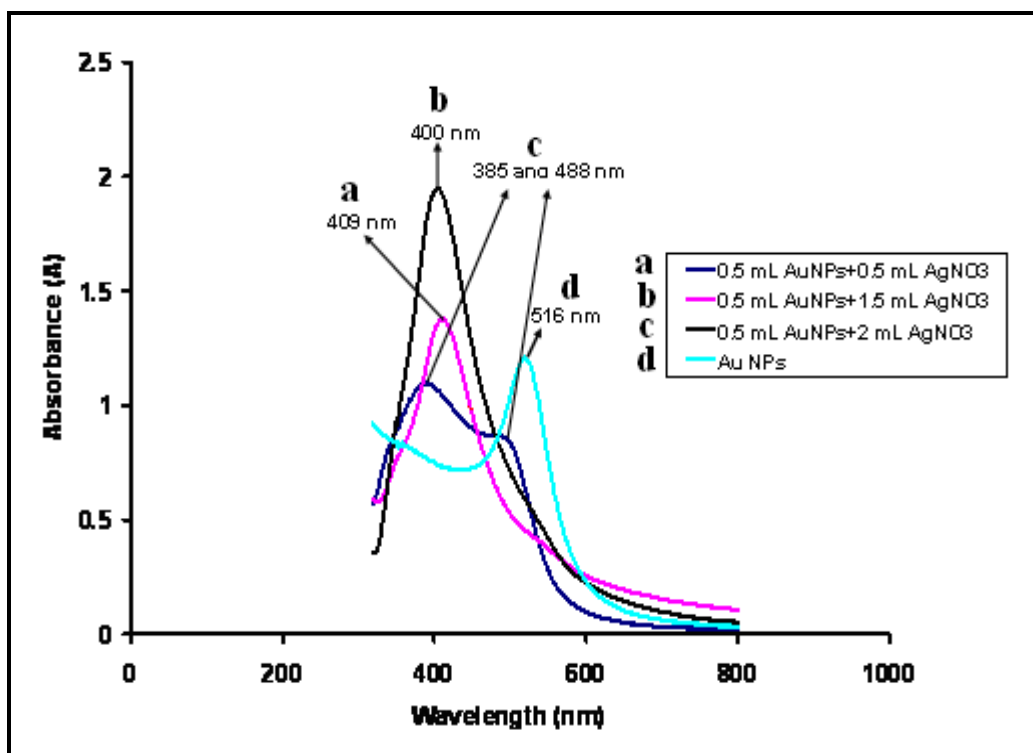


Figure 57. UV–Vis spectra of gold-core silver-shell nanoparticles prepared with different shell thickness (10^{-3}M AgNO_3).

Silver plasmon band appeared when the shell started to form (navy blue line). Finally, the peak shifted to 400 nm, which attributed to the complete encapsulation of gold nanoparticles by silver, i.e., to the formation of AuAgNPs. During the growth of the silver shell around the AuNPs resonance was blue shifted nearly 116 nm from its original position (516 nm).

3.1.5. Production of Silver Nanoparticles with Citrate Reduction Method

The most common synthesis of silver nanoparticles is the chemical reduction of a silver salt solution by a reducing agent such as NaBH_4 , citrate, and ascorbate. In this study, silver nanoparticles were prepared by using a chemical reduction method where silver nitrate was reduced using sodium citrate as reducing agent. The prepared silver nanoparticles were characterized with FE-SEM (Figure 58), EDX (Figure 59) and UV-Vis spectrometer (Figure 60). The average diameter of the silver nanoparticles was measured to be 70 ± 19 nm by sampling 100 nanoparticles. The resulting large-scale nanoparticles were not uniform.

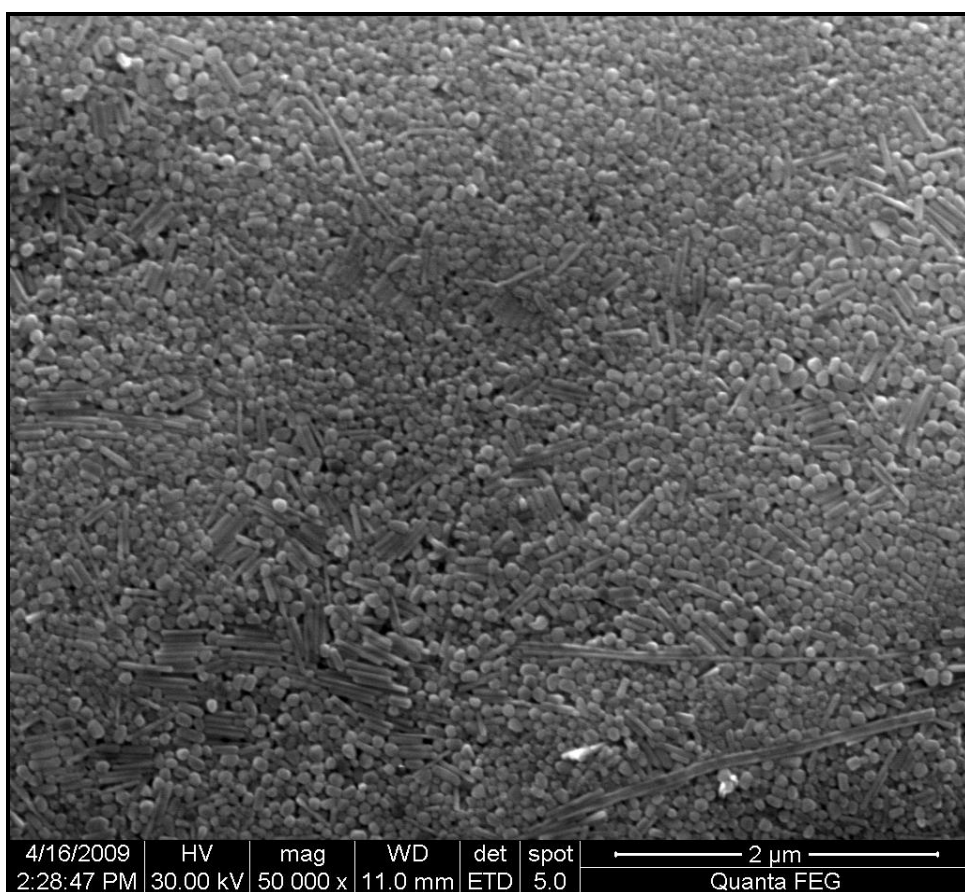


Figure 58. FE-SEM images of silver nanoparticles. The average diameter of the silver nanoparticles was measured to be 70 ± 19 nm by sampling 100 nanoparticles.

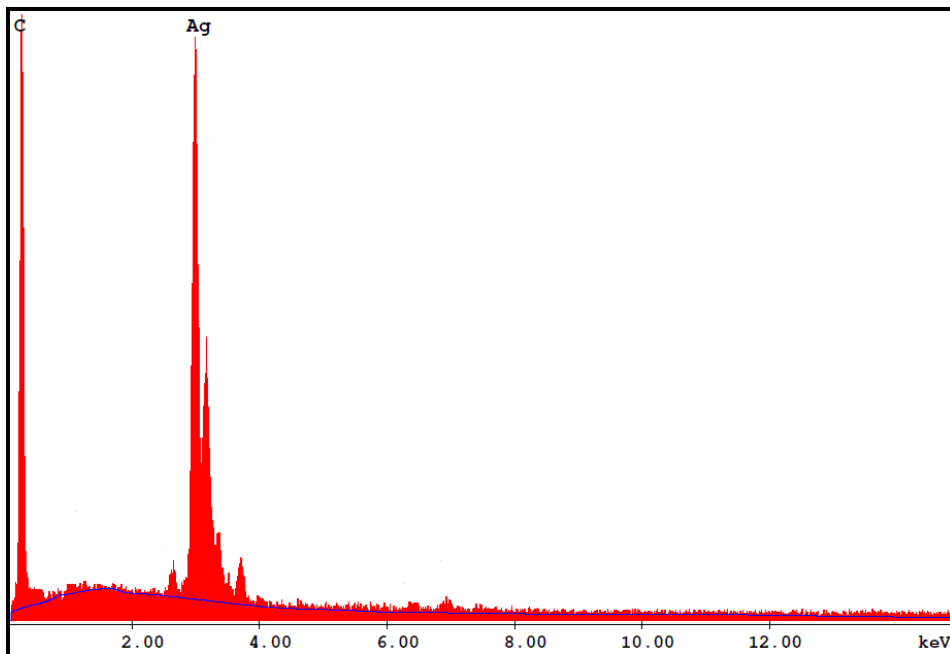


Figure 59. EDX pattern of silver nanoparticles.

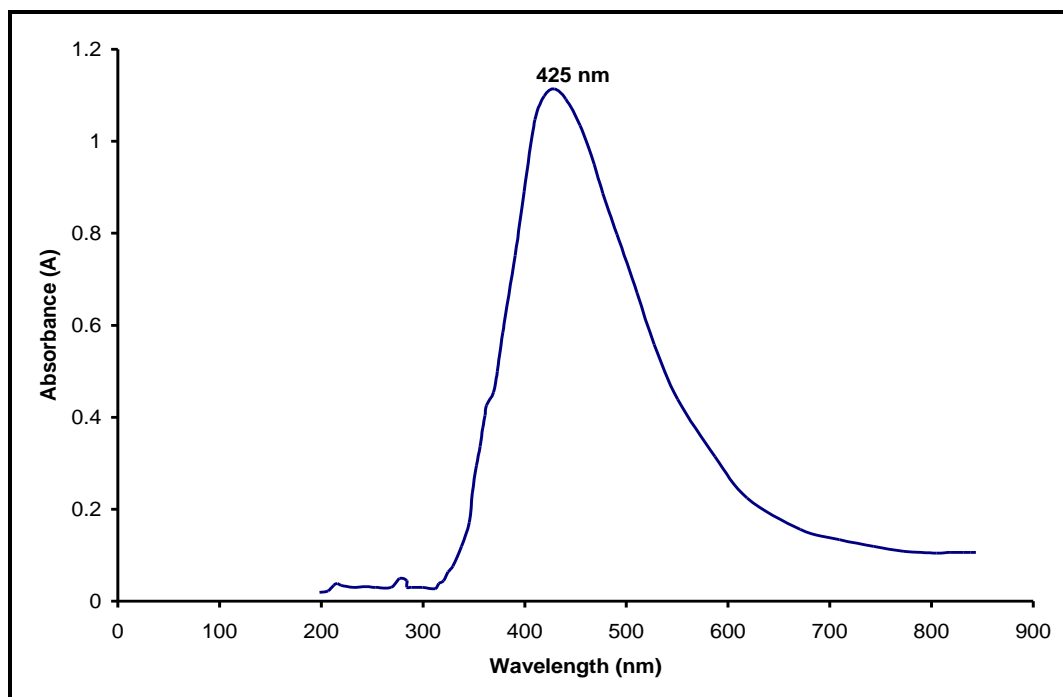


Figure 60. UV-Vis spectrum of silver nanoparticles.

3.1.6. SERS Studies

3.1.6.1. SERS Probe Molecules Used in Comparison Studies

SERS spectra were obtained for all gold containing substrates prepared using the probe molecule brilliant cresyl blue (BCB) and crystal violet (CV) (Figure 61) in order to examine and compare the sensitivity and consistency before and after the formation of silver shell on gold nanostructures (HAuNPs and AuNPs). These spectra were also compared with SERS produced by citrate reduced silver nanoparticles.

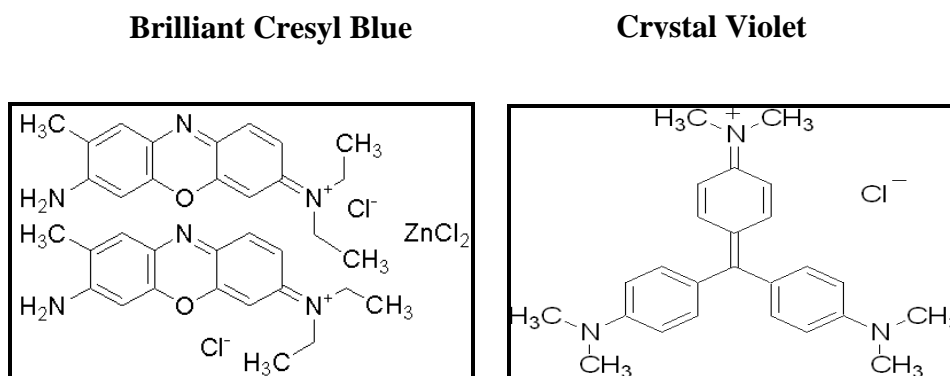


Figure 61. Chemical structures of dye molecules used in SERS measurements.

In the Raman spectrum of solid brilliant cresyl blue, the intense band around 580 cm^{-1} is assigned to the benzene ring deformation mode which is shown in Figure 62. $5 \times 10^{-8}\text{ M}$ BCB was used in all measurements.

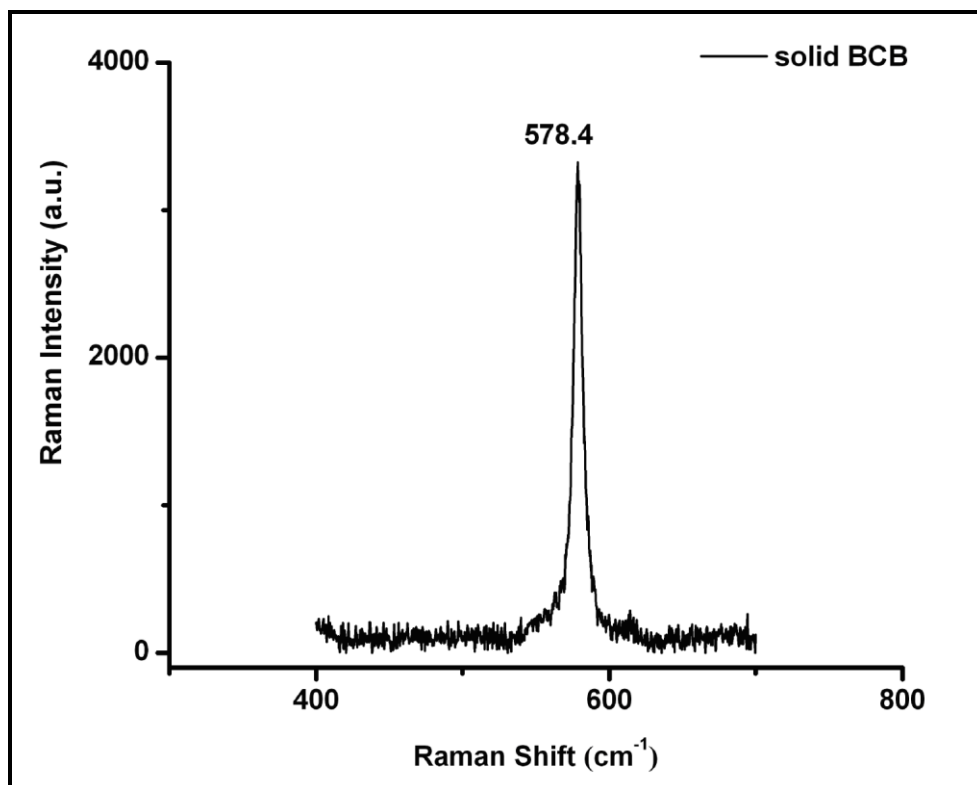


Figure 62. Raman spectrum of solid BCB. 632.8 nm radiation from a Helium–Neon laser was used with an excitation power of 10 mW and spectra was acquired with 10 s integration time.

In the Raman spectrum of solid crystal violet, the band at 1180 cm^{-1} is attributed to C–H in-plane bending vibrations as seen in Figure 63. $5 \times 10^{-7}\text{ M}$ CV was used in all measurements.

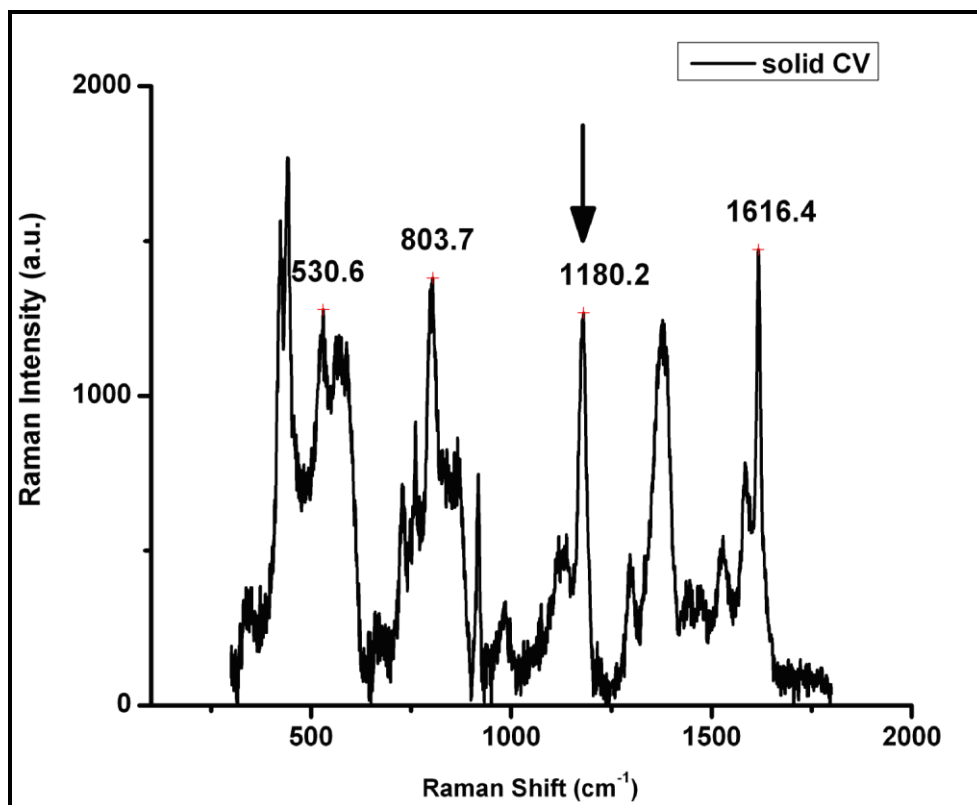


Figure 63. Raman spectrum of solid CV. 632.8 nm radiation from a Helium–Neon laser was used with an excitation power of 10 mW and spectra was acquired with 10 s integration time.

3.1.6.2. SERS Studies with Prepared Nanostructures

The surface-enhanced Raman spectra of BCB and CV absorbed on the solid and hollow gold nanoparticle substrates are given in Figure 64 and Figure 65 respectively.

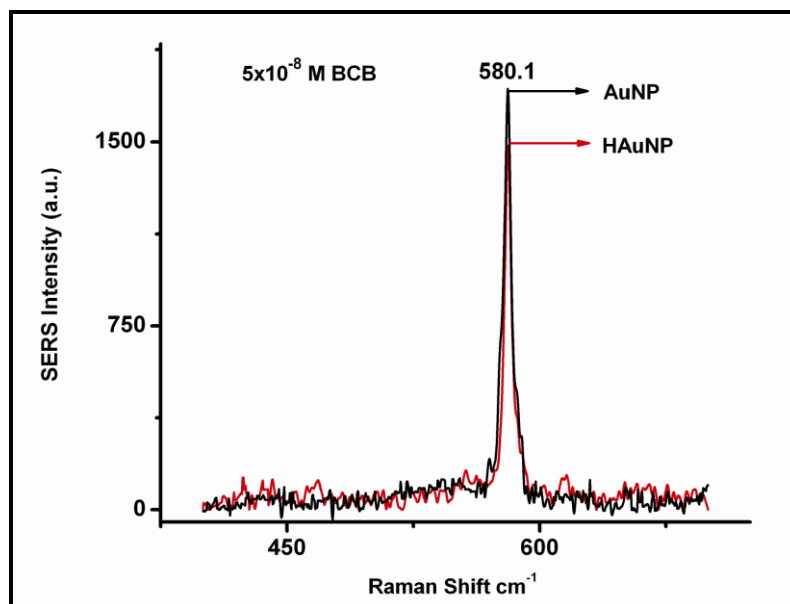


Figure 64. Comparison of SERS spectra of 5×10^{-8} M BCB obtained with solid gold (AuNP) and hollow gold (HAuNP) nanoparticles. 632.8 nm radiation from a Helium–Neon laser was used with an excitation power of 10 mW and spectra was acquired with 10 s integration time.

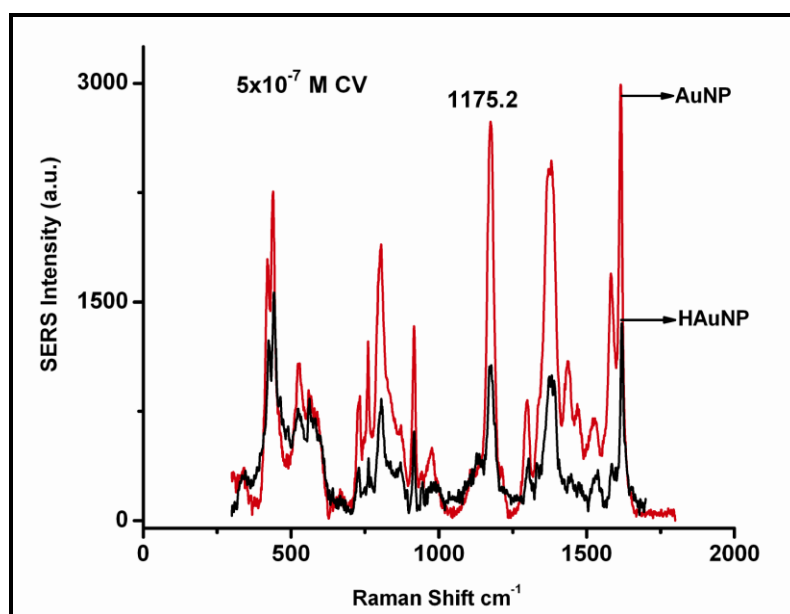


Figure 65. Comparison of SERS spectra of 5×10^{-7} M CV obtained with solid gold (AuNP) and hollow gold (HAuNP) nanoparticles. 632.8 nm radiation from a Helium–Neon laser was used with an excitation power of 10 mW and spectra was acquired with 10 s integration time.

SERS enhancements of both substrates were nearly the same for the measurement of BCB (Figure 64) while, SERS enhancement of CV adsorbed gold nanoparticle was higher than that of CV adsorbed hollow gold nanoparticle (Figure 65).

As it is known, the silver monometallic nanoclusters are good SERS-active substrates, whereas gold monometallic nanoclusters are poorer in SERS activity at visible region. Although HAuNPs have lower enhancement factors in comparison to those of Ag colloids, HAuNPs and AuNPs have the advantage of easier preparation with a high degree of homogeneity. Coating HAuNPs and AuNPs with Ag layer produced more regular structures than citrate reduced AgNPs. So, HAuAgNPs and AuAgNPs may be an alternative substrate for SERS applications at 632.8 nm laser line.

To make this clear the enhancement of Raman signals using gold-core silver-shell and hollow gold-silver double shell nanoparticles were investigated and compared with those of AgNPs. Figure 66 and Figure 67 show the comparison of SERS spectra of 5×10^{-8} M BCB obtained with HAuNPs, HAuAgNPs and AuNPs, AuAgNPs substrates.

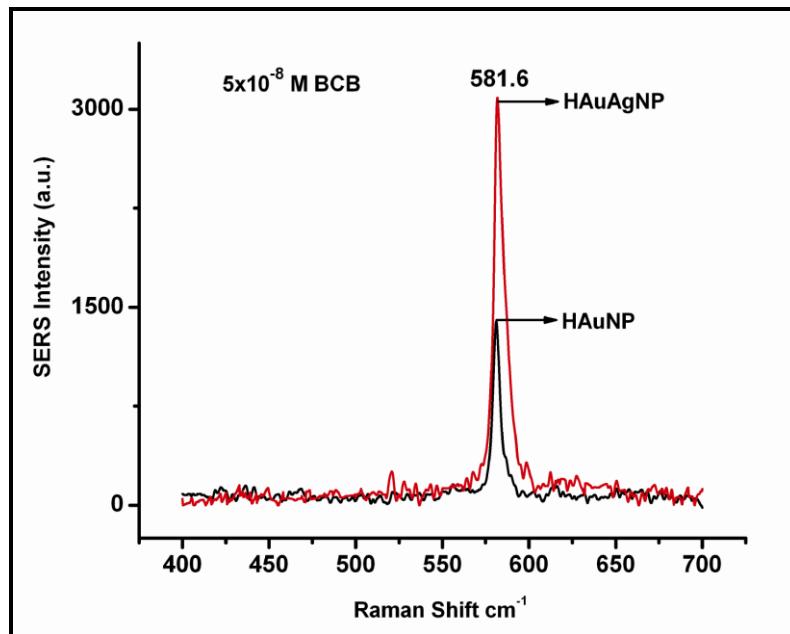


Figure 66. Comparison of SERS spectra of 5×10^{-8} M BCB obtained with hollow gold (HAuNP) and hollow gold-silver double-shell (HAuAgNP) nanoparticles. 632.8 nm radiation from a Helium–Neon laser was used with an excitation power of 10 mW and spectra was acquired with 10 s integration time.

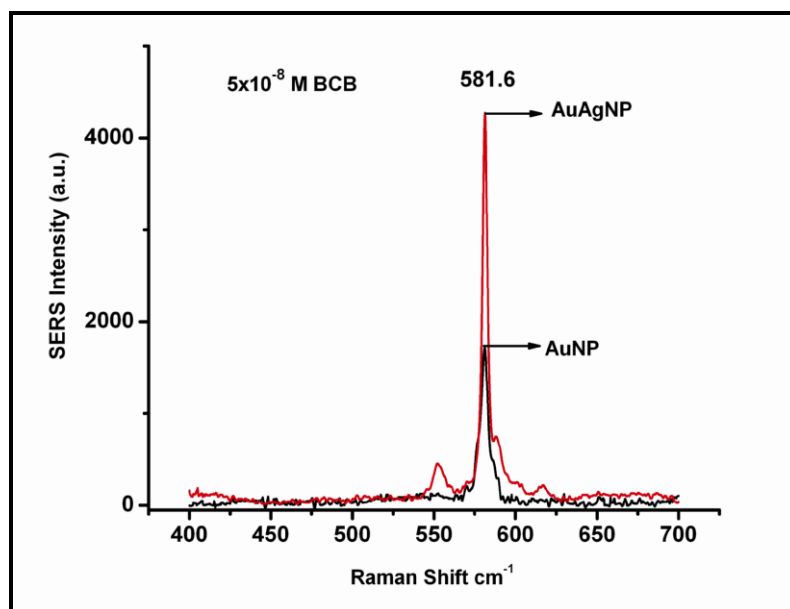


Figure 67. Comparison of SERS spectra of 5×10^{-8} M BCB obtained with gold (AuNP) and gold-core silver-shell (AuAgNP) nanoparticles. 632.8 nm radiation from a Helium–Neon laser was used with an excitation power of 10 mW and spectra was acquired with 10 s integration time.

As seen in Figure 66 and Figure 67, adding a silver shell leads to the enhancement of SERS intensity as expected. The similar behaviour has been observed with the CV solutions also and the results related to SERS measurement of CV are shown in Figure 68 and Figure 69.

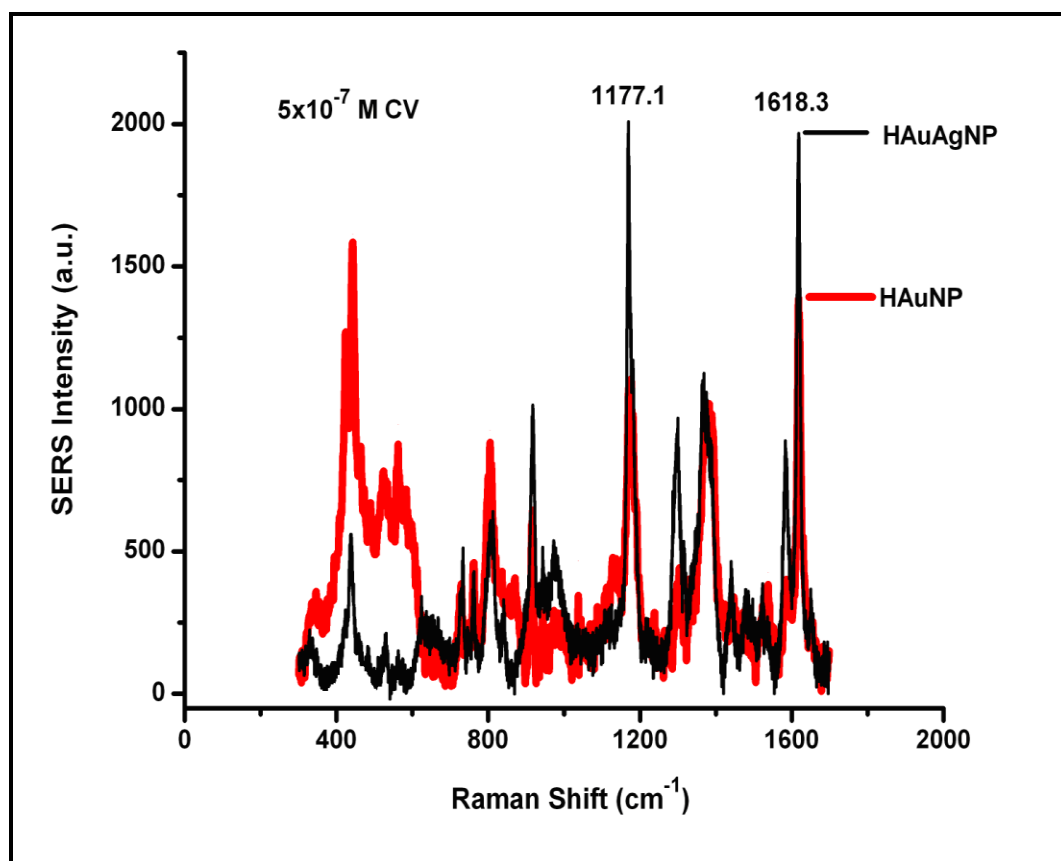


Figure 68. Comparison of SERS spectra of 5×10^{-7} M CV obtained with hollow gold (HAuNP) and hollow gold-silver double-shell (HAuAgNP) nanoparticles. 632.8 nm radiation from a Helium–Neon laser was used with an excitation power of 10 mW and spectra was acquired with 10 s integration time.

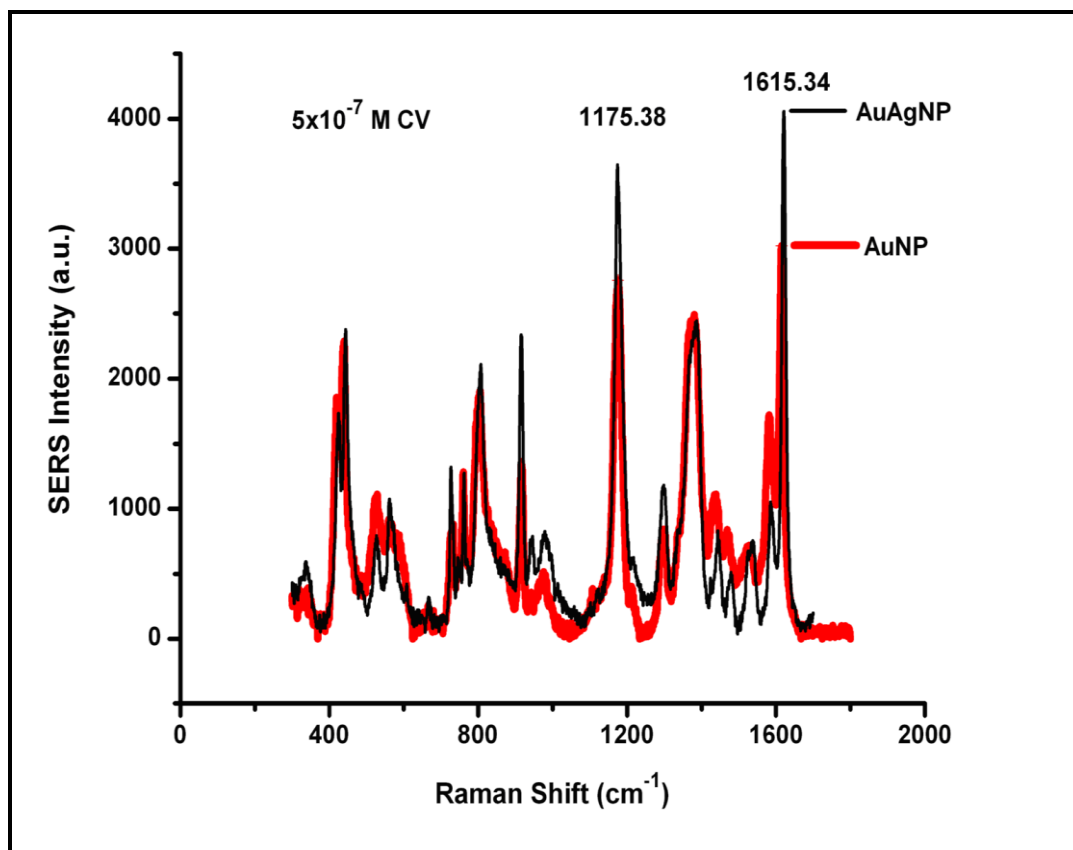


Figure 69. Comparison of SERS spectra of 5×10^{-7} M CV obtained with gold (AuNP) and gold-core silver-shell (AuAgNP) nanoparticles. 632.8 nm radiation from a Helium–Neon laser was used with an excitation power of 10 mW and spectra was acquired with 10 s integration time.

The observed SERS enhancements of H AuAgNPs over H AuNPs and AuAgNPs over AuNPs demonstrated the expected increase in SERS activity of silver shell over gold nanostructures. The spectra of AuAgNPs and H AuAgNPs bimetallic nanoparticles with proportions of silver also compared with the spectrum obtained with pure silver nanoparticles which are shown in Figure 70. AuAgNPs and H AuAgNPs showed similar behaviour with those of monometallic silver particles.

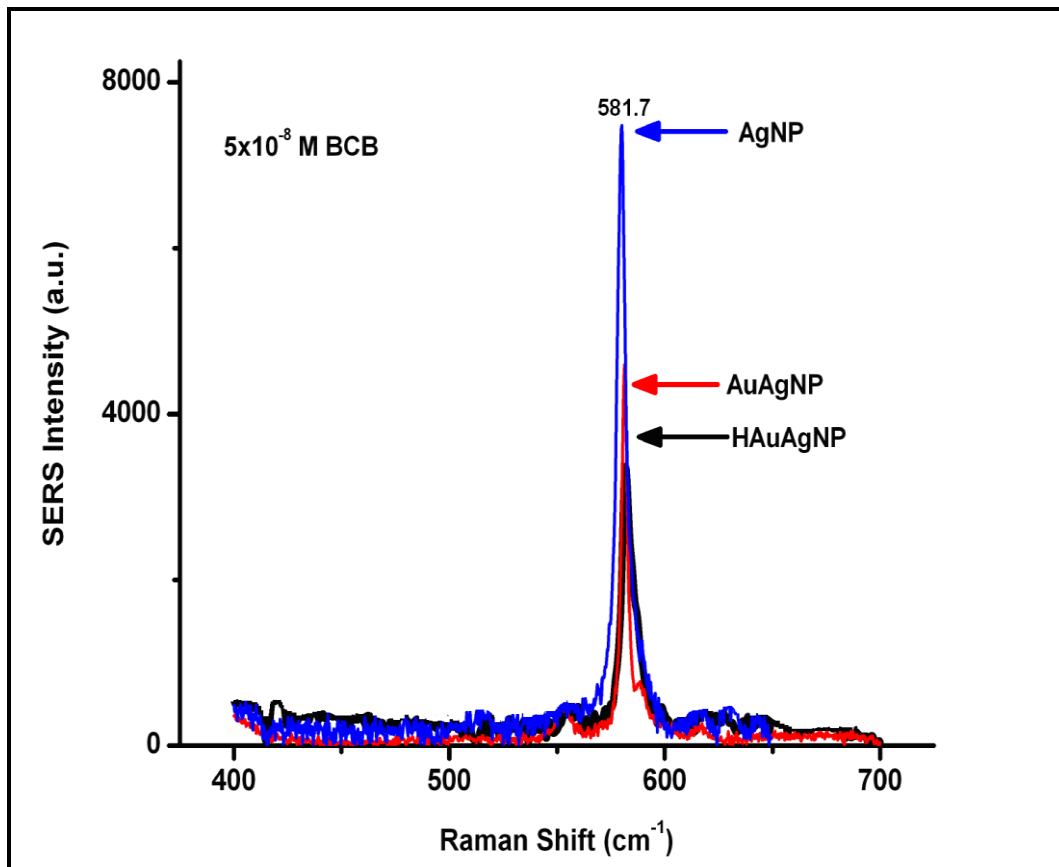


Figure 70. Comparison of SERS spectra of 5×10^{-8} M BCB obtained with solid gold-core silver-shell (AuAgNP), hollow gold-silver double shell (HAuAgNP) and silver (AgNP) nanoparticles. 632.8 nm radiation from a Helium–Neon laser was used with an excitation power of 10 mW and spectra was acquired with 10 s integration time.

The plasmon resonance of gold nanoshells could be properly tuned to contain the region from 600 to 1200 nm, whereas it is difficult to shift the plasmon peak of spherical gold (or silver) nanoparticles by more than 20 nm [200]. So, gold hollow nanoparticles were chosen as a hot research topic because of their special surface property.

In comparison of silver, gold nanoparticle has a lower surface enhancement factor (EF) in the visible region. For that reason, silver shell over gold nanoparticles have been carried out in order to obtain a greater SERS enhancement because preparation of gold core silver shell nanoparticles allows for the combination of the SERS activities of both metals.

Because all substrates gave nearly same SERS response to BCB and CV molecules, one can state that all prepared nanostructures (HAuNPs, AuNPs, HAuAgNPs, AuAgNPs and AgNPs) can be considered to be quite promising substrates in SERS measurements of molecules as they lead to significantly enhanced SERS signals.

3.2. Plasmonic-Based Chemical Sensing Methodologies for the Determination of Dopamine and Chemical Warfare Agents

The general objective of this section was to develop novel plasmonic nanostructures that can improve the analytical figures of merit, such as, detection limit, sensitivity, and selectivity for the determination of dopamine and chemical warfare agents. So the synthesis of silver nanoparticles modified with iron-nitrilotriacetic acid complex groups and Eu^{3+} ions were investigated to provide a way for direct measurements.

3.2.1. Surface Modification of Silver Nanoparticles with Iron-Nitrilotriacetic Acid Complex for the Direct Measurement of Dopamine using SERRS

In this study a new approach for the nanomolar detection of dopamine in the presence of ascorbic acid utilizing SERRS by using NTA-Iron modified silver nanoparticle based SERRS probe is presented. In this approach, the advantages of both the surface modification for specific analytes and the SERRS were integrated into a single functional unit. While the silver nanoparticle core gives the necessary enhancing properties, the NTA-Fe receptors adjoining the silver nanoparticle core can trap dopamine and formed NTA-Fe-dopamine complex provides resonance enhancement.

The analytical performance of the method with respect to reproducibility, sensitivity and selectivity is presented and discussed in detail. To the best of our knowledge, this is the first modified silver SERRS substrate with considerable selectivity and sensitivity for dopamine detection.

3.2.1.1. Preparation and Characterization of Fe(NTA) Modified Silver Nanoparticles

The preparation of SERRS substrate for dopamine detection presented here was based on surface modification of colloidal silver nanoparticle with Fe(NTA) complex which is shown in Figure 71.

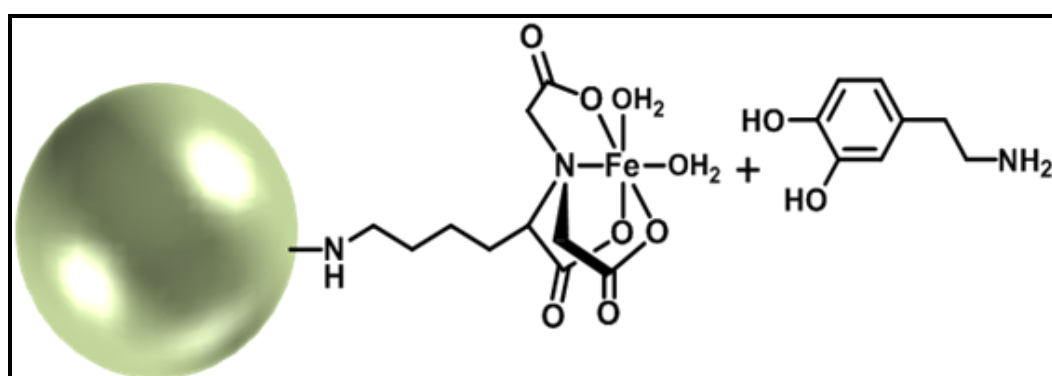


Figure 71. Structure of Fe(NTA) functionalized SERRS labels. Left: silver nanoparticle, middle: bifunctional Fe(NTA) host, right: analyte, dopamine molecule.

Colloidal silver was prepared by using a method of Lee and Meisel [198] as given in section 2.6. The plasmon absorption maximum of the prepared silver colloid was located at 425 nm (Section 3.1.5, Figure 60). The iron(III) nitrilotriacetato moiety 'Fe(NTA)' was readily obtainable in aqueous solution. To prepare Fe(NTA), $\text{Fe}(\text{NO}_3)_3$ was dissolved in water to achieve a molar ratio of 1:1 of Fe(III) to NTA. The prepared complex was then added to an aqueous solution of silver nanoparticles. After the addition of Fe(NTA) to freshly prepared citrate-stabilized silver nanoparticles, the nanosurfaces were modified by Fe(NTA) through the NH_2 arm of the NTA. The whole preparation process is illustrated in Figure 72.

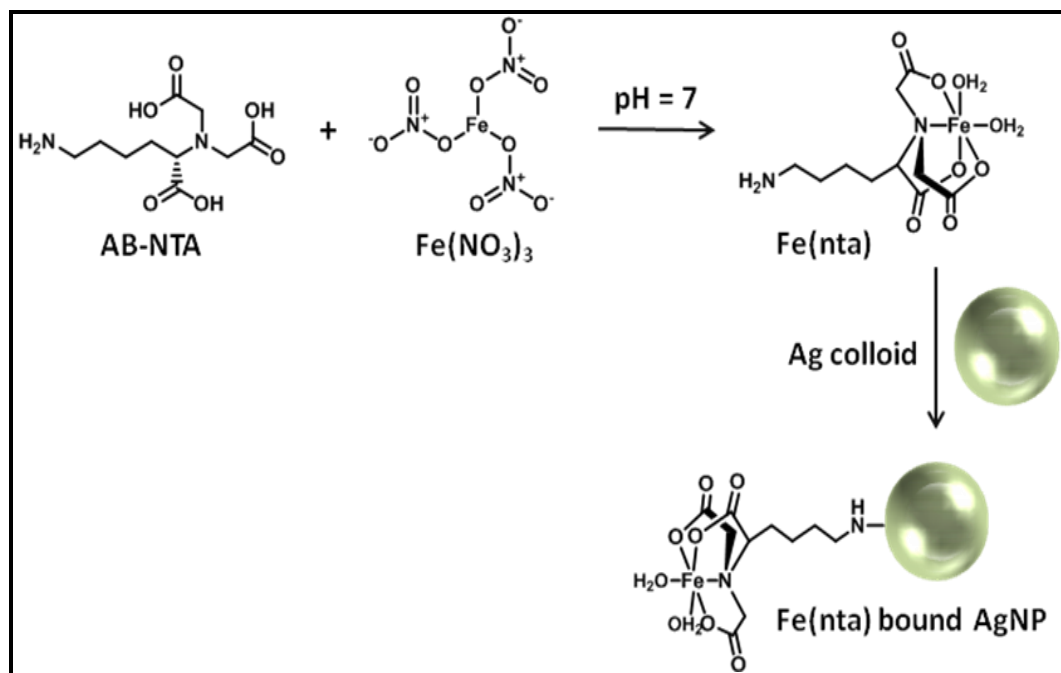


Figure 72. Schematic representation for the production of Ag-Fe(NTA) nanoparticles and possible cross-linking between silver nanoparticle and Fe(NTA) complex.

Nitrilotriacetic acid (NTA) is one of the most widely used and studied organic chelating agents. The higher stability of the NTA complexes is the result of an additional coordination site. Carboxylate donor groups containing a central nitrogen atom allow tetradentate chelation and consequently, hexacoordinated metals such as iron can form ternary complexes with NTA. In our study, four chelating sites of the modified NTA were interacted with iron(III) ions, which result in a tight binding of iron(III) ions. The quadridentate NTA moiety was coupled to the surface of silver nanoparticles via spacer butyl amine arm.

The structural characterization of surface modified silver nanoparticles was done with FE-SEM. The result is shown in Figure 73. The average diameter of the silver nanoparticles was measured as 31 ± 5 nm by sampling 100 nanoparticles.

Attachment of iron complex on silver nanoparticles was revealed by EDX spectrometry, FT-IR spectrometry, and ICP-OES analysis.

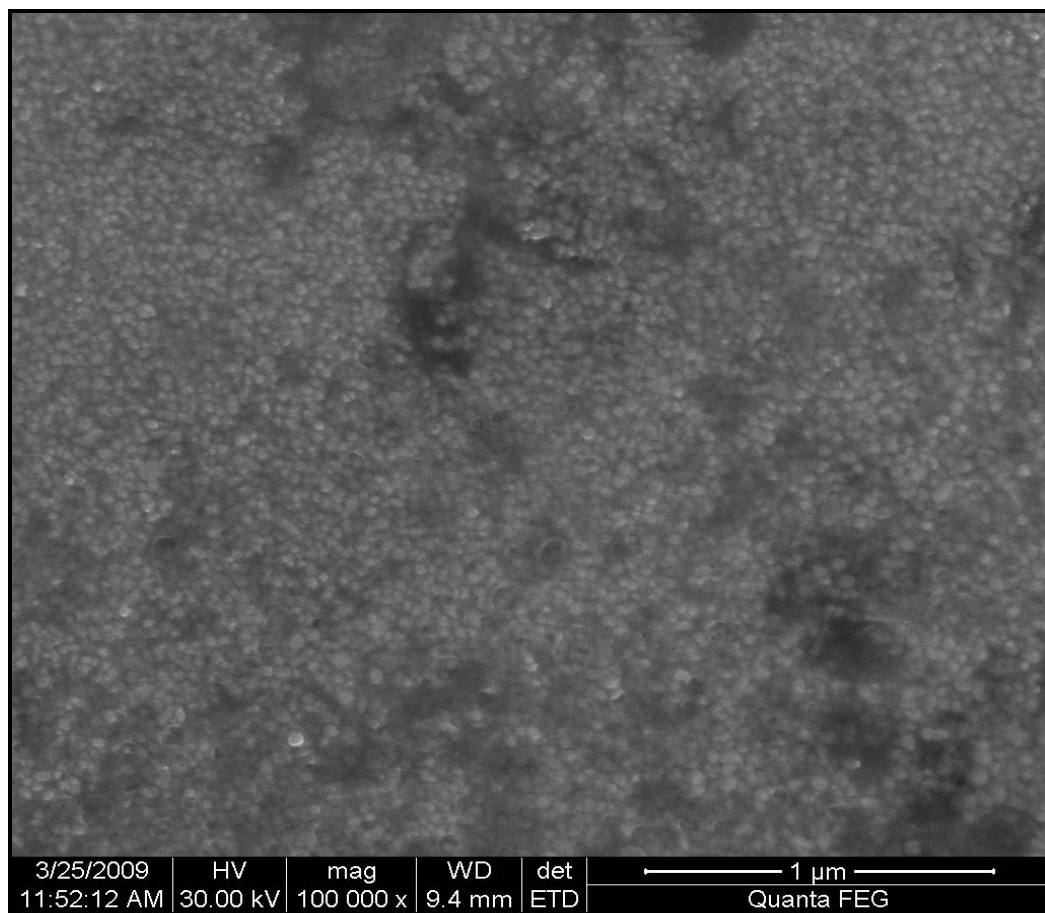
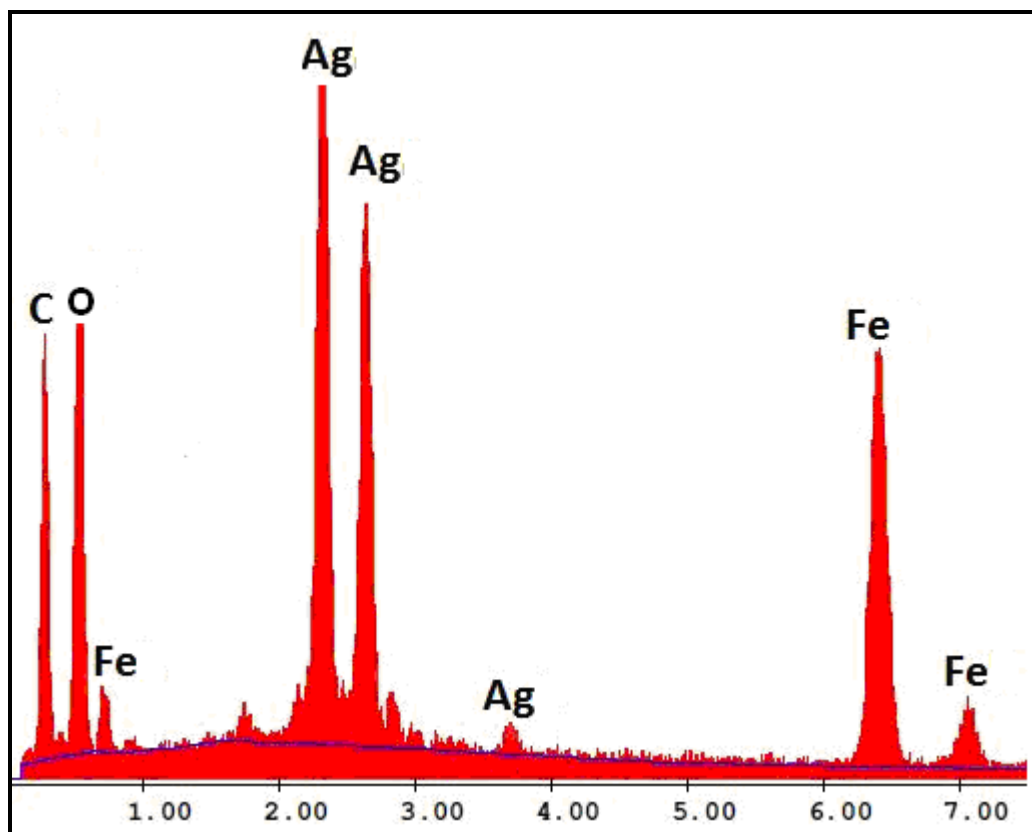


Figure 73. FE-SEM image of Fe(NTA) modified Ag NPs (31 ± 5 nm).

The qualitative elemental composition of the prepared Fe(NTA) modified Ag nanoparticles were analysed with EDX and the results are given in Figure 74.



EDAX ZAF Quantification Element Normalized		
Element	Wt %	At %
AgL	6.79	1.00
FeK	6.69	1.93

Figure 74. EDX pattern of Fe(NTA) modified Ag NPs.

The presence of iron in prepared nanoparticles can be easily observed from EDX pattern (Figure 74). Identification and quantification of Fe(NTA) binding on Ag nanoparticles were also done by inductively coupled plasma optical emission spectrometer (ICP-OES). The initial concentration of $\text{Fe}(\text{NO}_3)_3$ was 1120 mg/L in the mixture. After complex formation, Fe(NTA) was bounded to AgNPs and then Fe(NTA) modified Ag nanoparticles were centrifuged and washed several times.

The remaining parts were combined and analysed with ICP-OES. The ICP-OES measurements were carried out and the average amount of binded Fe on the surface of the AgNPs was found to be 520 ± 20 mg/L (10 replicates).

Functionalization of nanoparticles with nitrilotriacetic groups was confirmed by FT-IR measurements. The FT-IR spectrum of the pure NTA and Ag-Fe(NTA)-assembly are shown in Figure 75.

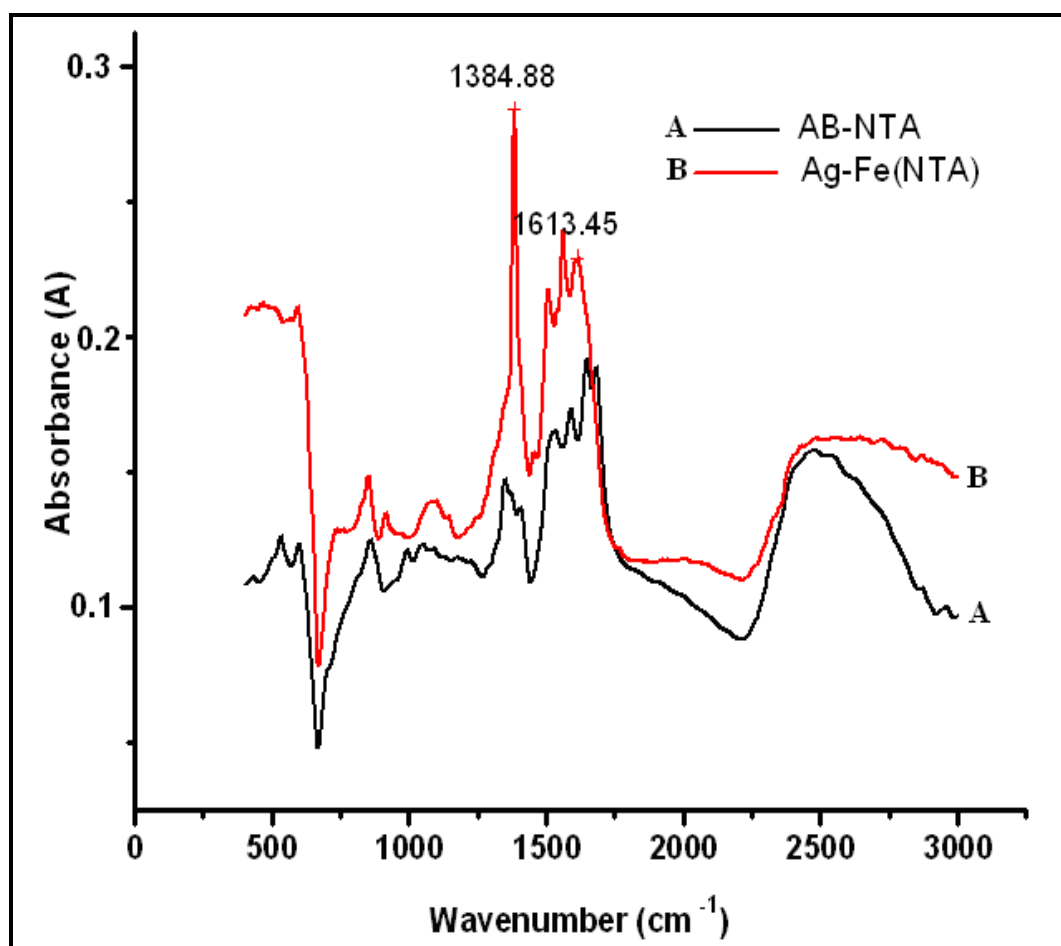


Figure 75. FTIR spectra of (A) AB-NTA (*N_ωN_α*-Bis(carboxymethyl)-L-lysine hydrate) and (B) Fe(NTA) modified Ag NPs.

FTIR spectrum of Fe(NTA) modified Ag NPs displayed characteristic vibrational modes associated with the NTA carboxylate groups [201]. The band at 1614 cm^{-1} and 1385 cm^{-1} were assigned to the asymmetric and symmetric stretching vibration bands of the deprotonated carboxylic acid group of NTA [202,203].

3.2.1.2. Optical properties of the Prepared Particles

Direct determination of dopamine at resting level with SERS substrate made of bare silver or gold is not possible. In order to measure the dopamine at that level, both preconcentration factors must be increased and greater spectral enhancement should be achieved. For this purpose, generally silver electrodes have been used to electrostatically preconcentrate the analytes before SERS measurements [204].

Volkan et al. have first reported the SERS detection of dopamine at micromolar concentration level utilizing a ferric ion doped polymer coated SERS substrate [205]. The enhancement was correlated to the attachment of the dopamine to the surface through Fe(DA) complex formation. This SERS studies have been carried out using He-Ne laser.

Fe(catechol)₃³⁻ complexes has a charge transfer absorption band around 500 nm [204]. Considering the huge contribution of Resonance Raman phenomena for signal enhancement in Raman measurements, the absorption maximum of the Fe(DA)) complex should be shifted toward to 632.8 nm, which is the emission wavelegth of He-Ne laser.

In general tetradentate tripodal ligands are used in order to red shift the absorption maxima of the iron complex. Among them, NTA was preferred due to its convenient absorption maxima for resonance enhancement with He-Ne laser.

Optical and resonance properties of prepared particles were tested with UV-Vis spectrometry. UV-Vis spectrum of Fe(NTA) modified AgNPs with DA is shown in Figure 76. Absorption maxima of both AgNPs at 410 nm and [Fe(NTA)(DA)] complex at 610 nm were observed.

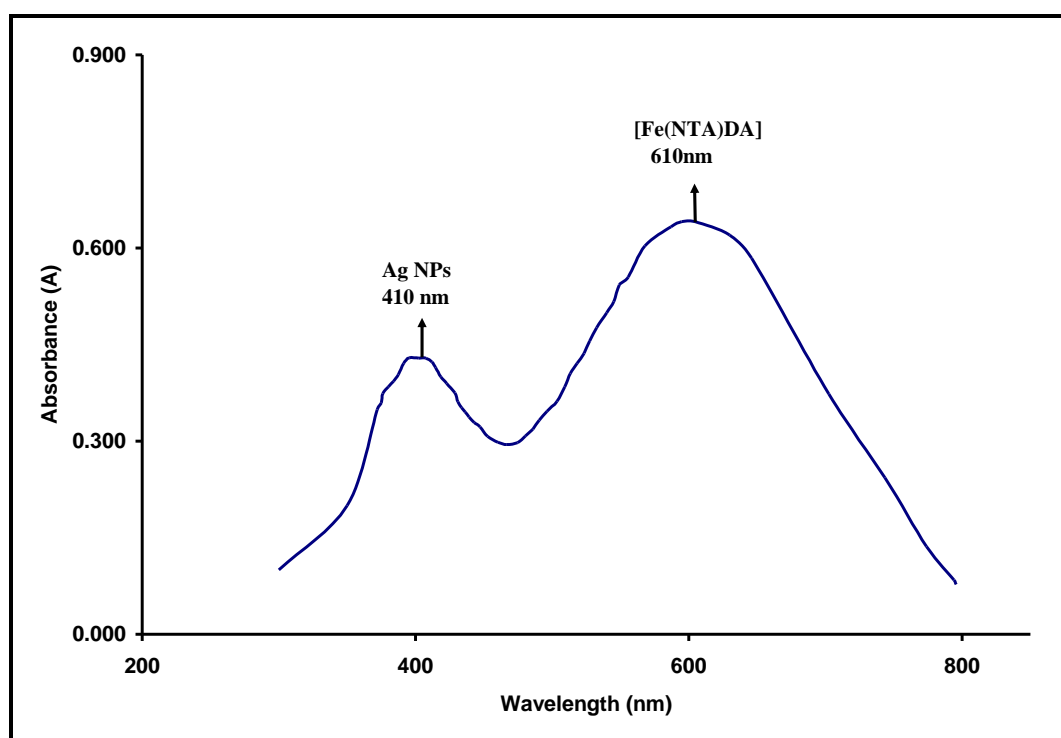


Figure 76. UV-Vis spectrum of [Ag-Fe(NTA)DA] structure in water.

Replacement of two bidentate catechol ligands in $\text{Fe}(\text{catechol})_3^{3-}$ by three carboxylate ligands and an amine ($\text{Fe}(\text{NTA})(\text{catechol})$) increases the Lewis acidity of Fe^{3+} which red shifts the spectrum.

As can be seen from the Figure 76, maximum absorption of the [Fe(NTA)(DA)] was red shifted to 610 nm and overlapped with the emission signal of the He-Ne laser. Hence resonance Raman measurement of [Fe(NTA)(DA)] became possible with He-Ne laser.

3.2.1.3. SERRS Substrate Preparation and Dopamine Measurement

Taking advantage of the molecular trapping and resonance properties of the SERRS substrate, a simple experiment was designed which is presented in Figure 77.

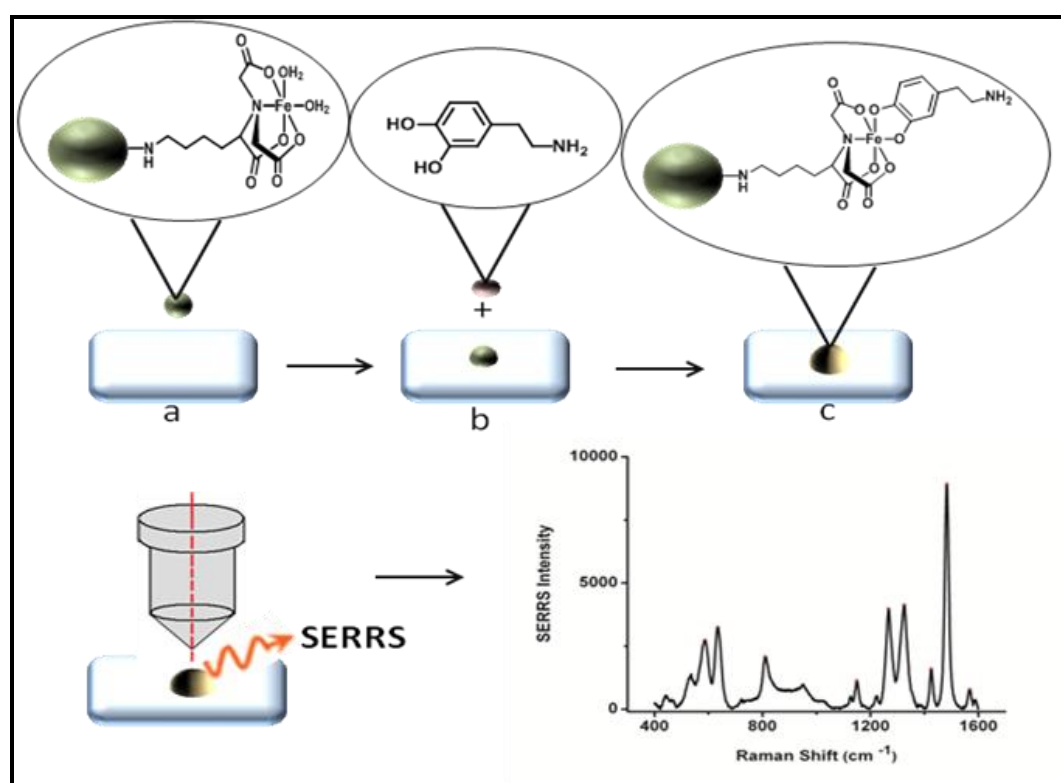


Figure 77. Schematic illustration of the production, and the application of Ag-Fe(NTA) substrate as molecular traps for surface-enhanced resonance Raman scattering (SERRS) of dopamine molecules.

The iron was attached to the surface of silver nanoparticles with NTA. The resulting stable ternary Fe(NTA) complexes on silver nanoparticles were used as a surface trap for DA molecules which increases the intensity of SERRS signal due to both resonance and distance effect. According to the experimental procedure given in Figure 77, SERRS spectrum of 1×10^{-5} M DA solution was taken (Figure 78).

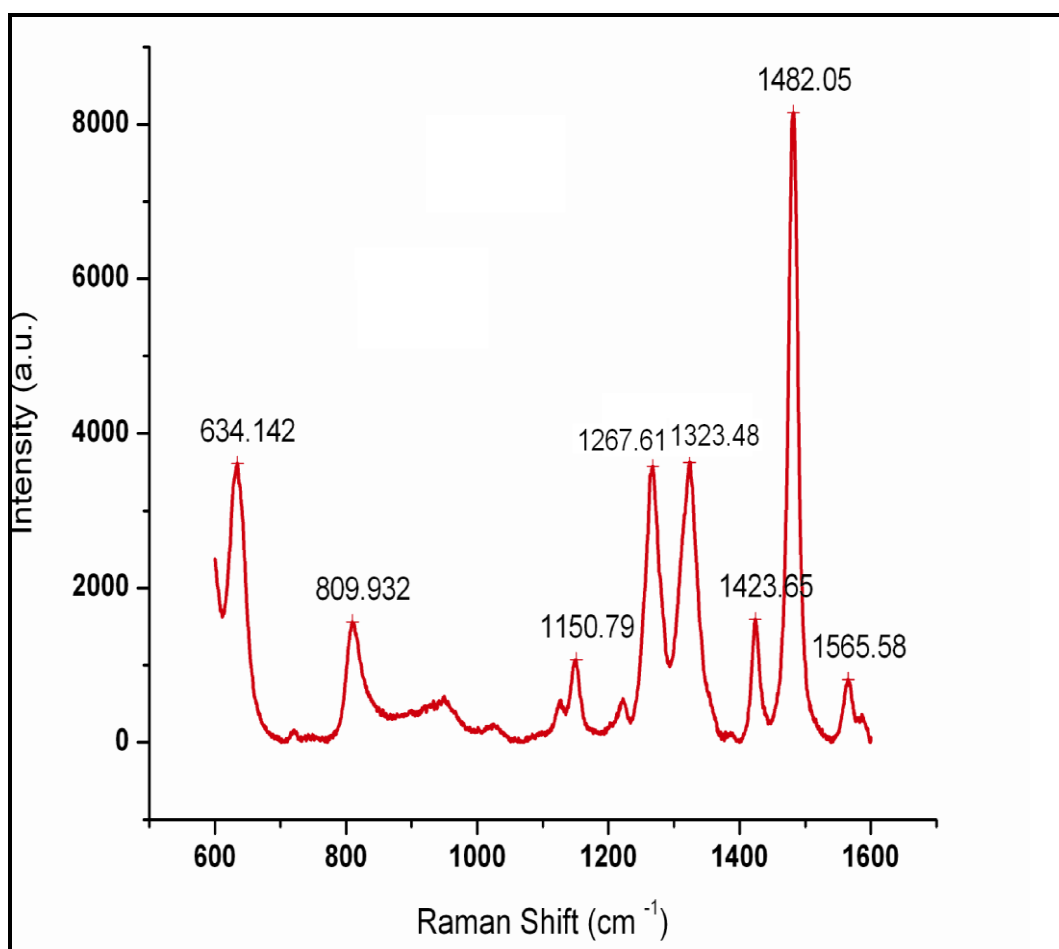


Figure 78. SERRS spectrum of 1×10^{-5} M DA solution. 632.8 nm radiation from a Helium–Neon laser was used with an excitation power of 10 mW and spectra was acquired with 10 s integration time.

The intense 1482-cm^{-1} dopamine band (Figure 78) is easily assigned as ν_{19b} resulting mainly the stretching of the OC–CO bond [206]. This mode occurs at 1479 cm^{-1} in the SERS of catechol (dopamine) itself and in the $1480\text{-}1490\text{ cm}^{-1}$ region in the resonance Raman spectrum of most metal catecholates [205,207]. It is usually the most intense band in a catecholamine surface-enhanced Raman spectrum. The catechol carbon-oxygen stretch, about 1276 cm^{-1} is also intense. The remaining bands are attributable to various ring stretching vibrations [208,209]. For quantitative dopamine measurements the 1482 cm^{-1} band were used through the study.

3.2.1.4. Importance of the Prepared Particles

In order to show the importance of the presence of a NTA-Fe complex on dopamine determination, the strength of bands observed in the corresponding spectra, three different experiments were done. First, SERS signal of DA was measured with silver colloid. Then, SERS signal of Fe(DA) complex was measured with silver colloid. Finally, SERRS signal of DA on Ag-Fe(NTA) substrate was taken. The results are shown in Figure 79.

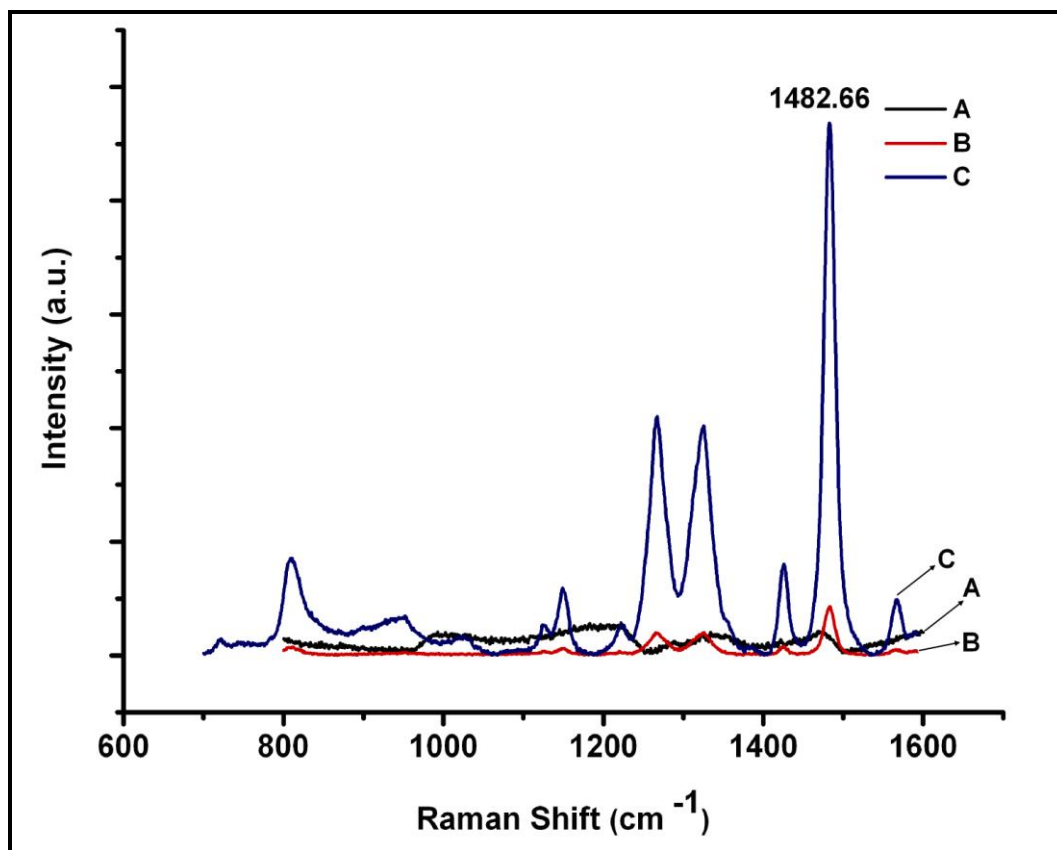


Figure 79. Influence of the surface coverage on the SERRS signal strength: A) SERS signal of 0.5 M DA obtained with silver colloid B) SERS signal of 10^{-4} M DA complexed with Fe^{3+} ion obtained with silver colloid C) SERRS signal obtained with Fe(NTA) modified silver nanoparticle, direct measurement of 10^{-5} M DA. 632.8 nm radiation from a Helium–Neon laser was used with an excitation power of 10 mW and spectra was acquired with 10 s integration time.

It is obvious that the sensitivity of the measurements performed using Ag nanoparticles is strongly effected by the presence of a Fe(NTA) complex. Intense SERRS signals were obtained for 10^{-5} M of dopamine molecules by using Fe(NTA) modified silver nanoparticles whereas no signal was obtained for high molarity dopamine solution (0.5 M) on silver colloid substrate. Added to this, approximately fifty-fold larger signal was obtained with Fe(NTA) modified silver nanoparticles for Fe(DA) complex when compared to those obtained from standard silver nanoparticles.

3.2.1.5. Effect of pH of Complex on the SERRS Signal

Different ferric catecholate complexes are possible in solution and their production and stability are pH dependent. Generally, three different iron(III) catechol complexes are formed as a function of pH. Especially, bis(catecholate)iron(III) complex $[\text{Fe}(\text{cat})_2]$ are formed when the aqueous solutions of the catechol (cat) adjusted to pH 6– 7. The tris(catecholate)iron(III) complex $[\text{Fe}(\text{cat})_3]^{3-}$ is formed at $\text{pH} \geq 9$. The last species, a mono(catecholate)iron(III) complex $[\text{Fe}(\text{cat})]$, can be produced at $\text{pH} < 5$ [210].

In order to show the effect of pH, Fe(NTA) complex were prepared with pH 7 and 9 respectively and used for the determination of DA with SERRS. SERRS spectrum of the complex of Fe(NTA) with dopamine under neutral (black line) and basic (red line) pH conditions are shown in Figure 80.

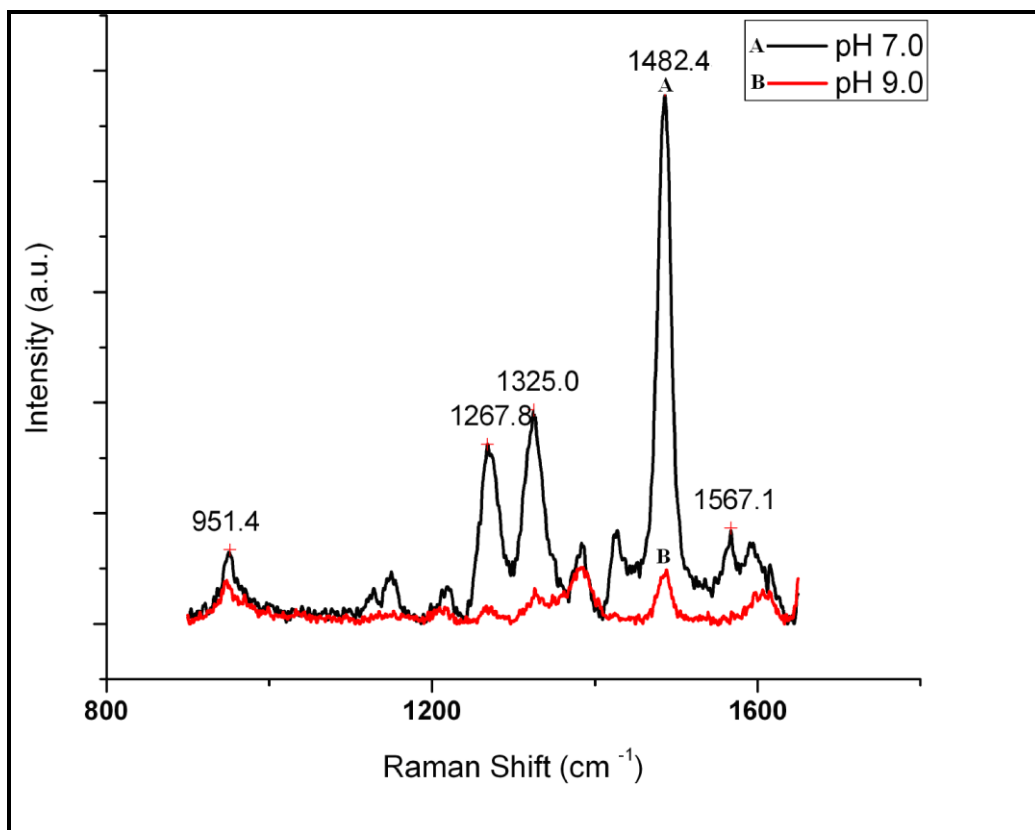


Figure 80. SERRS spectra of 1.0×10^{-5} M DA obtained with Ag-Fe(NTA) substrates at a final pH of (A) 7.0 and (B) 9.0. 632.8 nm radiation from a Helium–Neon laser was used with an excitation power of 10 mW and spectra was acquired with 10 s integration time.

As can be seen from Figure 80, the SERRS intensity was increased approximately ten-fold at neutral pH. Thus, neutral pH was chosen as optimum condition.

3.2.1.6. Choice of the Form of SERRS Substrate

The SERRS spectra of 1.0×10^{-5} M DA was measured utilizing Ag-Fe(NTA) nanoparticles as substrate either in wet or dry conditions. Wet means, SERRS spectrum was recorded as soon as the droplet of Ag-Fe(NTA) and DA mixture was placed on the surface of glass plate (Figure 77). If the droplet of Ag-Fe(NTA) and DA mixture was dried before taking the SERS spectrum it was called as dry condition. The SERRS spectra of DA in wet and dry conditions are shown in Figure 81.

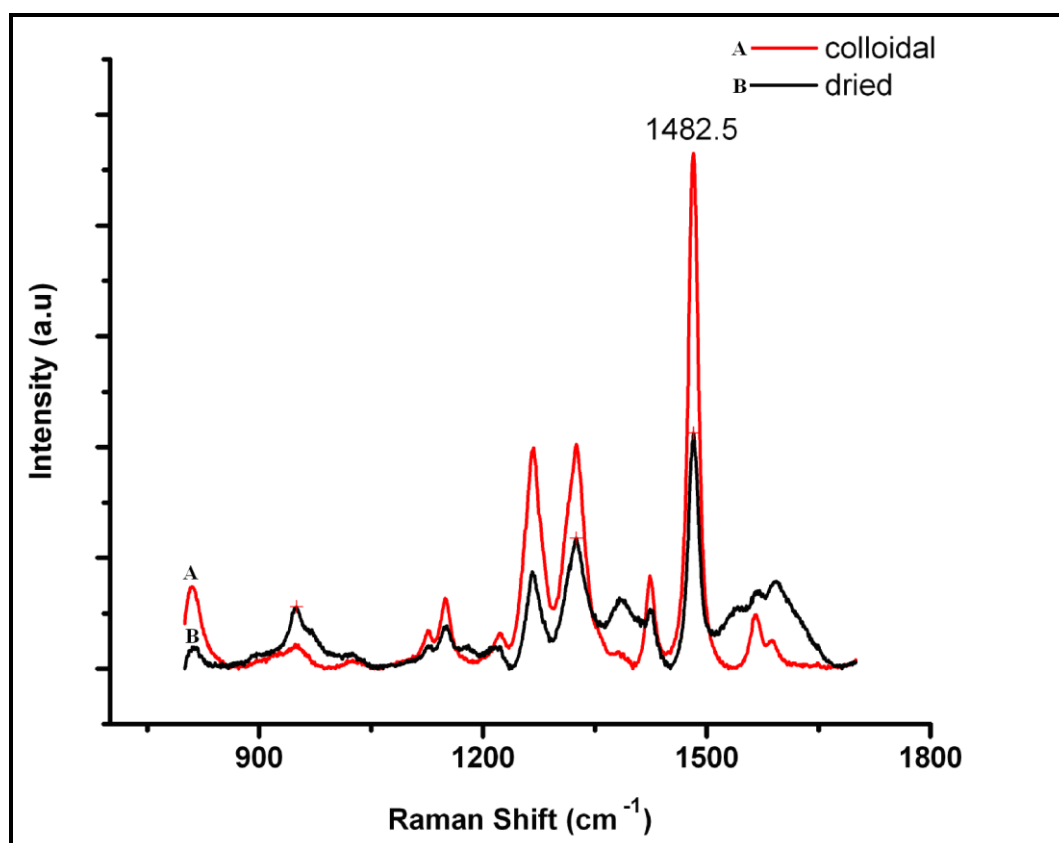


Figure 81. Comparison of SERRS signal of 1.0×10^{-5} M DA obtained with (A) wet and (B) dry conditions. 632.8 nm radiation from a Helium–Neon laser was used with an excitation power of 10 mW and spectra was acquired with 10 s integration time.

As can be deduced from Figure 81, the SERRS signal acquired from wet droplet was twice more intense than that of dried one.

3.2.1.7. Optimization of the Complexation Period

Time dependent SERRS data produced immediately after mixing dopamine solution with the Ag-Fe(NTA) substrate and 15 minutes complexation time indicate that this modified nanobased SERRS assay is very rapid, takes less than 1 min from DA binding to detection (Figure 82).

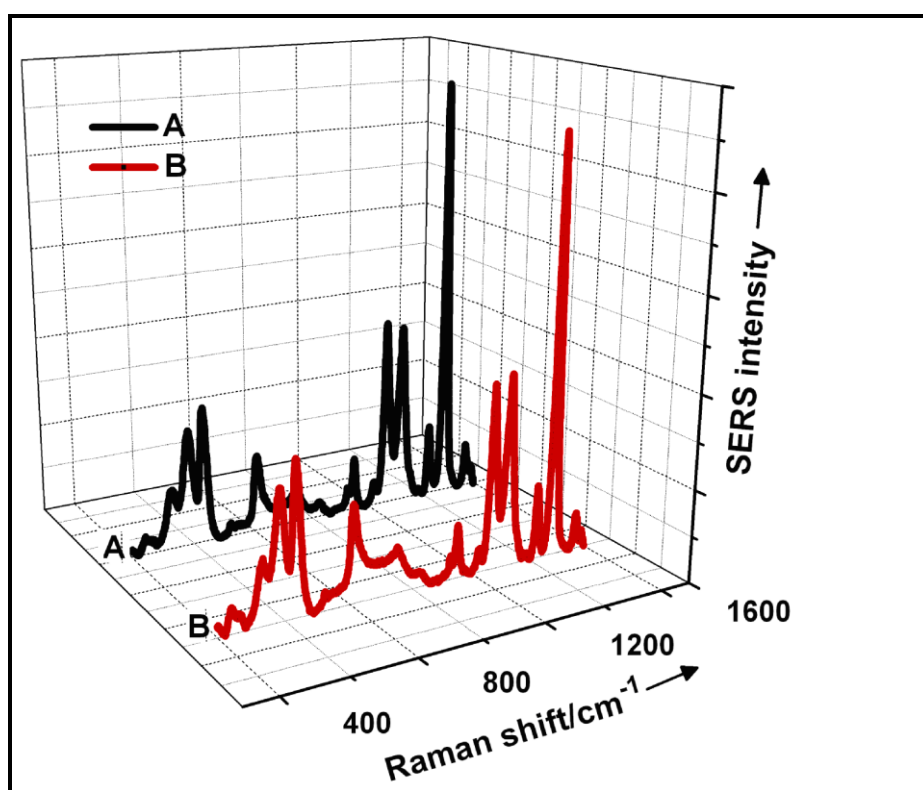


Figure 82. Effect of the complexation time between Fe(NTA) modified silver nanoparticle and 10^{-5} M DA on the SERRS signal strength. SERRS signal of 10^{-5} M DA obtained with Fe(NTA) modified silver nanoparticle after A) as prepared B) 15 minutes. 632.8 nm radiation from a Helium–Neon laser was used with an excitation power of 10 mW and spectra was acquired with 10 s integration time.

3.2.1.8. Reproducibility of the Prepared Substrate

The reproducibility of the substrates is a critical issue in the acceptance of SERS as a mainstream spectroscopic technique [211]. Hence, the reproducibility of this novel SERRS substrate for the determination of dopamine molecules was investigated by collecting spectra of 10^{-5} M DA by using Ag-Fe(NTA) nanoparticles prepared both in the same batch or in different runs. The sample signals are given in Figure 83 a and b.

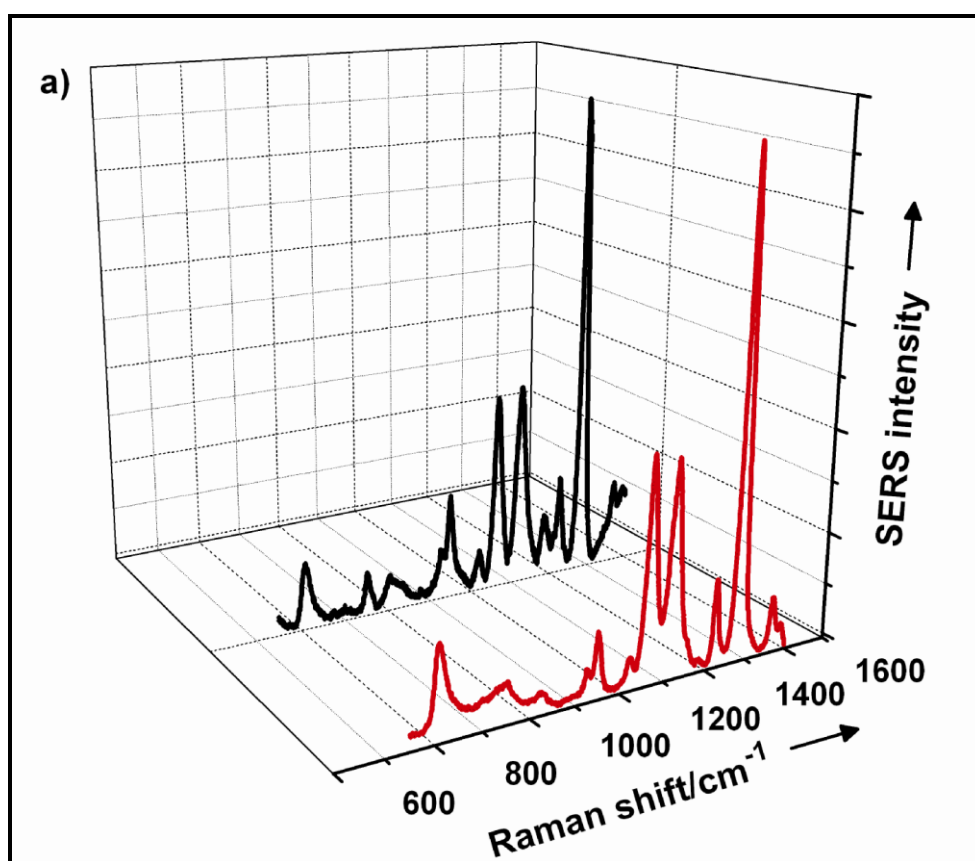


Figure 83. a) SERRS spectra of 10^{-5} M DA by using Ag-Fe(NTA) nanoparticles prepared in the same batch. 632.8 nm radiation from a Helium–Neon laser was used with an excitation power of 10 mW and spectra was acquired with 10 s integration time.

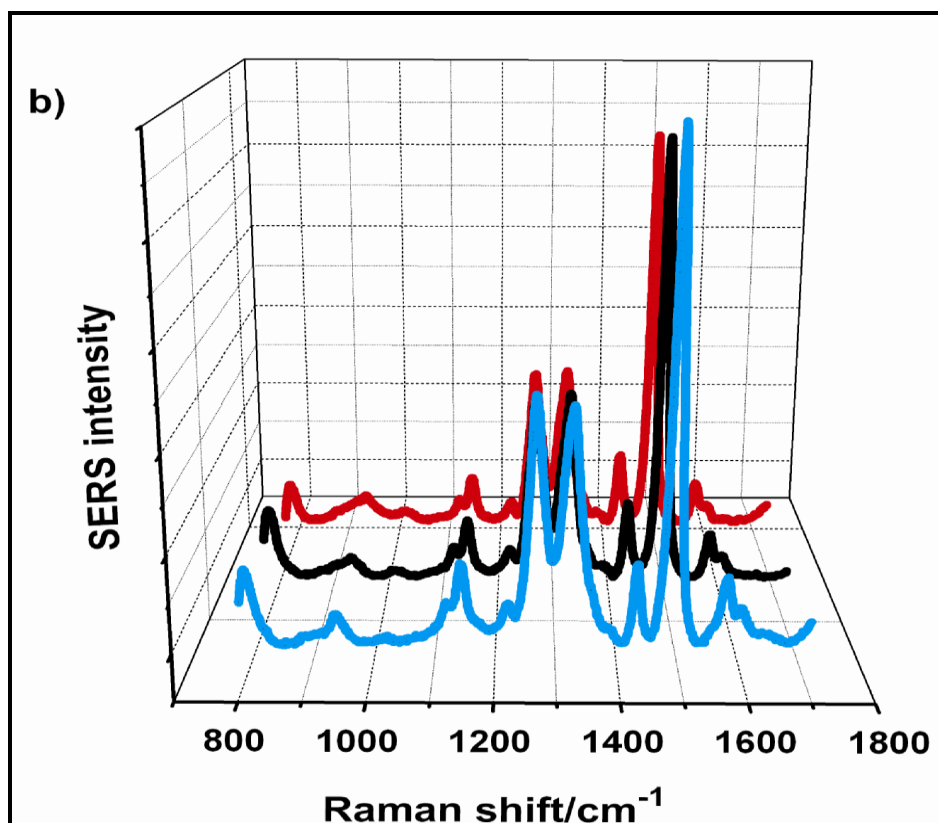


Figure 83. b) SERRS spectra of 10^{-5} M DA by using Ag-Fe(NTA) nanoparticles prepared in different runs. 632.8 nm radiation from a Helium–Neon laser was used with an excitation power of 10 mW and spectra was acquired with 10 s integration time.

The homogeneity of the SERS enhancement properties of the prepared substrates can be seen (Figure 83) from the consistent intensity for the main stretching band of dopamine at 1482 cm^{-1} . Sequential measurements were made for periods of 1-2 min. The percent variation of the peak height of dopamine band at 1482 cm^{-1} (for 20 measurements by using Ag-Fe(NTA) nanoparticles taken either from the same batch or from different batches of the substrates) was below 5.0 %. This outcome has shown the reproducibility of the SERS method utilizing Ag-Fe(NTA) nanoparticles for dopamine detection. Moreover, the substrate

preparation was a simple and single-step process which could be performed very quickly. The latter advantage could be an important factor in the routine analysis.

3.2.1.9. The Shelf-life (Stability) of the Prepared Substrate

The stability of the prepared Ag-Fe(NTA) nanoparticles as a substrate was investigated in a period of 15 days. The SERRS signal of 10^{-5} M DA was taken at various time intervals (1, 5, 7 and 15 days) with the substrates all taken from the same batch of Ag-Fe(NTA) nanoparticles. The results are given in Figure 84.

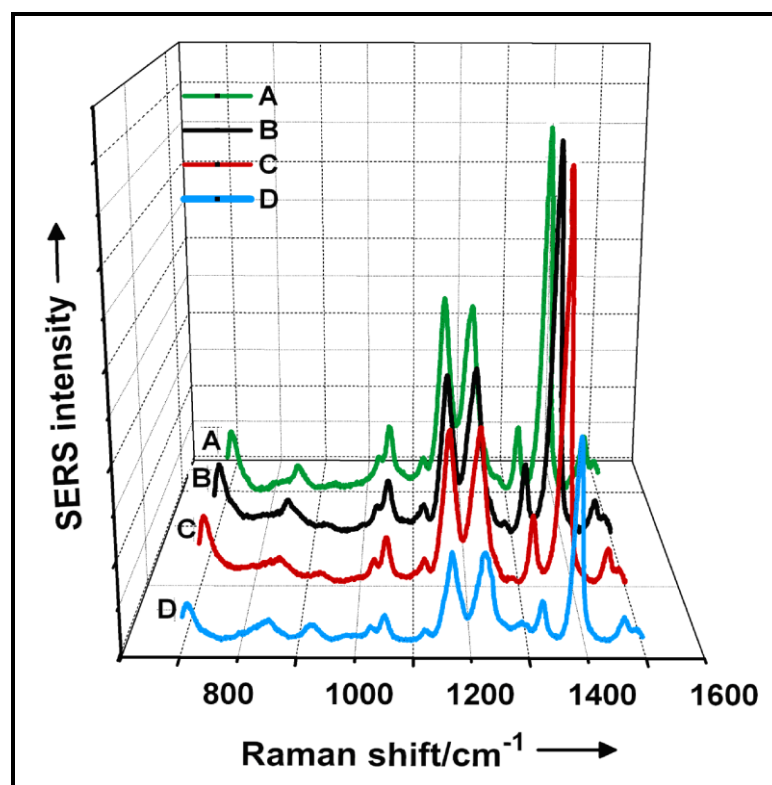


Figure 84. SERRS signal of 10^{-5} M DA acquired with Ag-Fe(NTA) nanoparticles as substrate A) the day B) after 5 days C) after 7 days D) after 15 days of their preparation. 632.8 nm radiation from a Helium–Neon laser was used with an excitation power of 10 mW and spectra was acquired with 10 s integration time.

As can be seen from Figure 84, the substrate did not lose SERRS activity over a period of one week. At the end of the second week, however, surface modified silver nanoparticles in aqueous solution have lost almost half of their initial intensity (Figure 84). The decrease in the signal observed in the usage of silver colloids as SERS or SERRS substrates was probably due to the oxidation of the silver nanoparticles during this period.

3.2.1.10. Selectivity and Interference Studies

As it was mentioned in the introduction part (Sec 1.11), the particularly severe potential interferent is ascorbic acid (AA) because in some body fluids the concentration of AA is several orders of magnitude higher than DA concentration. Therefore, the selectivity of the Ag-Fe(NTA) nanoparticles–dopamine SERRS assay was investigated by getting the spectrum of dopamine solution (10^{-5} M and 10^{-6} M) in the presence of AA concentrations which were one to three order of magnitude higher than those of DA concentrations used. Their spectra are shown in Figure 85.

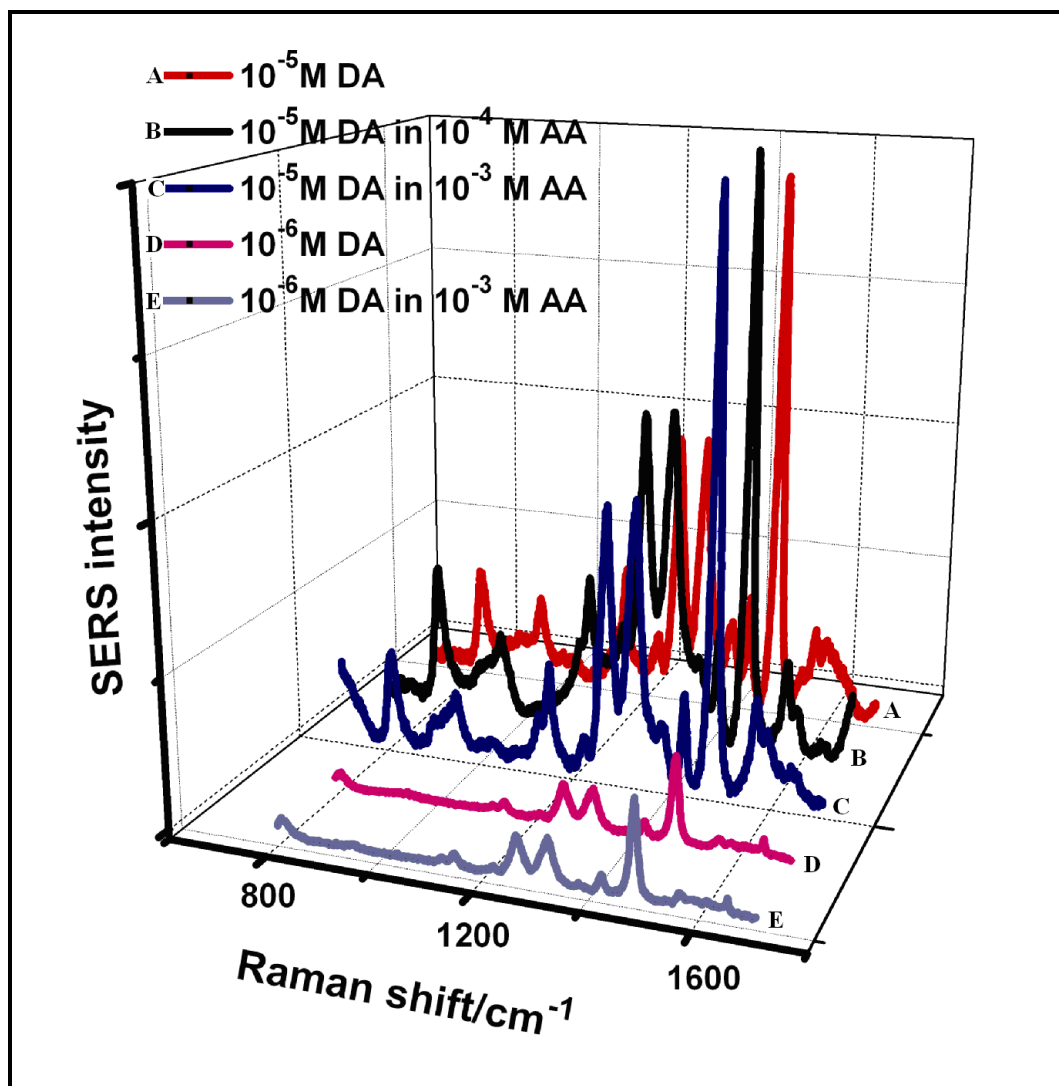


Figure 85. SERRS spectrum of the (A) 1×10^{-5} M DA (B) 1×10^{-5} M DA in 1×10^{-4} M ascorbic acid (AA), (C) 1×10^{-5} M DA in 1×10^{-3} M AA (D) 1×10^{-6} M DA (E) 1×10^{-6} M DA in 1×10^{-3} M AA . 632.8 nm radiation from a Helium–Neon laser was used with an excitation power of 10 mW and spectra was acquired with 10 s integration time.

Results clearly demonstrated that there was no Raman signal from AA. As can be seen from Figure 85, the spectra of dopamine in presence of 10^{-3} and 10^{-4} M AA are very similar to the ones obtained in the absence of AA, which showed excellent selectivity of the substrate over AA.

Adequate selectivity of silver colloid was obtained by overcoating with NTA-Fe complex, which blocked the access of AA.

3.2.1.11. Sensitivity of the Surface Modified (Ag-Fe(NTA)) Nanoparticles as SERRS Substrate

One of the primary problems in dopamine determination is that the concentration of dopamine in the extracellular fluid of the caudate nucleus (physiological resting level) is extremely low (10^{-9} M) [171]. Thus, a sensitive method is required for in vivo and vitro determination of dopamine.

Detection limits of spectrofluorimetric methods are in the range of 30 nM to 60 nM [212,213], whereas electrochemical techniques are of 1 nM to 20 nM [164,171]. In SERS applications, a minimum concentration of 30 μ M [208] was achieved by applying preconcentration. The drawbacks of these techniques were mentioned in section 1.11.

In order to measure the detection capability of Ag-Fe(NTA) nanoparticle as SERRS substrate, 10^{-9} M DA solution was prepared and measured. The result is given in Figure 86.

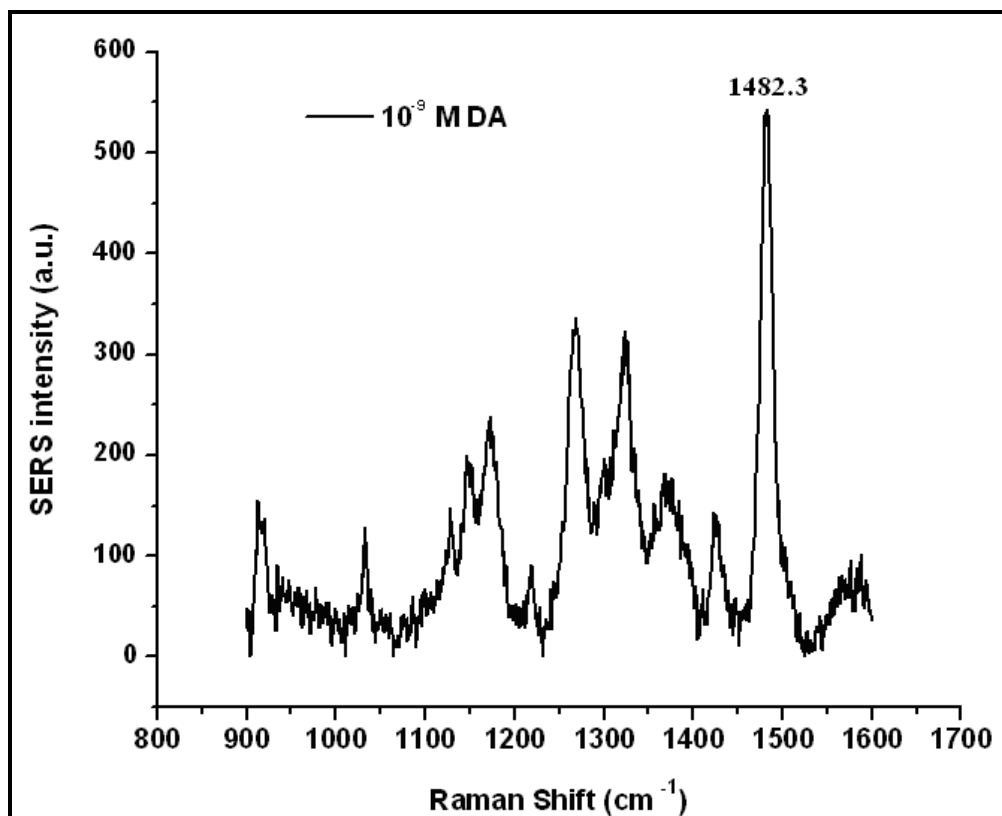


Figure 86. SERRS spectrum of 10^{-9} M DA solution. 632.8 nm radiation from a Helium–Neon laser was used with an excitation power of 10 mW and spectra was acquired with 10 s integration time.

As can be seen from Figure 86, the SERRS spectrum of DA is still completely identifiable at concentration levels down to 10^{-9} M. In other words, the detection capability of our SERS probe for DA was as low as nM level at 10 mW laser power and 10 second integration times, which were considered realistic in a biomedical application [171]. Of course, lower concentration of DA could be achieved by further optimization of the parameters such as increasing laser power and data acquisition time.

Utilizing Ag-Fe(NTA) nanoparticles as SERRS substrate, the detection of dopamine at nano molar levels in the presence of large excess of AA i.e at nearly physiological condition was achieved without any need for separation or elimination of the interfering species. Therefore, the proposed SERRS method has also a great potential for the construction of a dopamine sensor for in vivo applications such as the molecular diagnosis of Parkinson's disease or in the evaluation of the efficacy of the therapeutics designed for its cure.

3.2.2. Preparation of Silver Nanoparticles Modified with Europium (III) Ion for Sensitive and Selective Determination of Chemical Warfare Agents

There has been a progressive need for sensitive and selective techniques for fast detection and recognition of toxic wastes, explosives and chemical and CBW agents. For that reason, great effort has been expended to develop rapid, selective and sensitive detectors for chemical warfare agents and other organophosphate/phosphonate compounds in order to verify fulfilment with the necessities of the contract [214]. Many nerve agents such as sarin, soman and pesticides are in fact organophosphates or organophosphonates.

In this part of the study, the first example of a new class of a europium sensitized SERS method for the determination of nerve agents simulant (methyl phosphonic acid (MPA)) is being presented. This is a novel, simple and fast aqueous method based on the synthesis of silver nanoparticles modified with Eu^{3+} ion for the preparation of nanoparticle based surface enhanced Raman scattering (SERS) substrate, for highly sensitive and selective screening of organophosphates from aqueous solution.

3.2.2.1. Preparation of Europium (Eu^{3+}) Ion Modified Silver Nanoparticles

The preparation of nanocrystalline Ag doped with lanthanide ions (or Ag- Eu^{3+} nanocomposites) was undertaken in a one-step redox step. As the reduction potential of the Ag^+ -Ag redox couple (0.80 V vs SHE) is higher than that of the Eu^{3+} - Eu^{2+} (-0.35 V vs SHE), Ag^+ will be reduced to Ag atoms when Eu^{2+} was added into the solution.

First, the aqueous solution of silver nitrate and europium dichloride were prepared. Then, they were mixed with the same portion and new particles were obtained simultaneously. The size and the structure of the Ag- Eu³⁺ nanoparticles depend on the concentrations of the silver nitrate and europium dichloride solutions. The experimental conditions for the composite particle synthesis have been optimized to allow the uniform Ag-Eu³⁺ formation to be performed in a single step.

3.2.2.2. Characterization of Ag-Eu³⁺ Nanoparticles

The morphology of the prepared nanoparticles was examined by using FE-SEM. The results are given in Figure 87 and Figure 88.

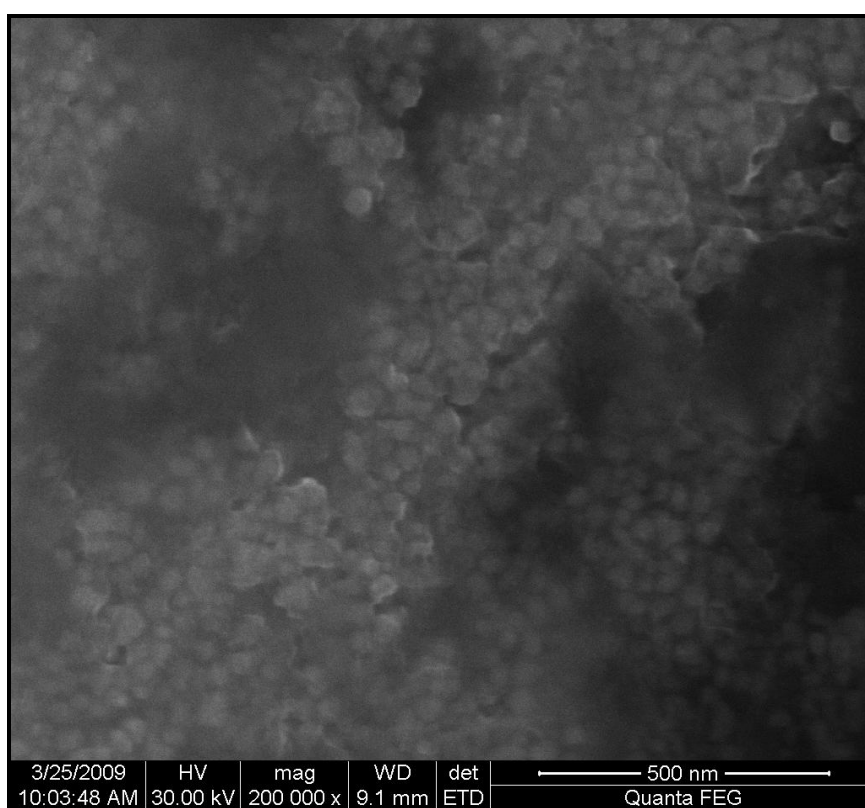


Figure 87. FE-SEM images of Ag-Eu³⁺ nanoparticles (39±5 nm).

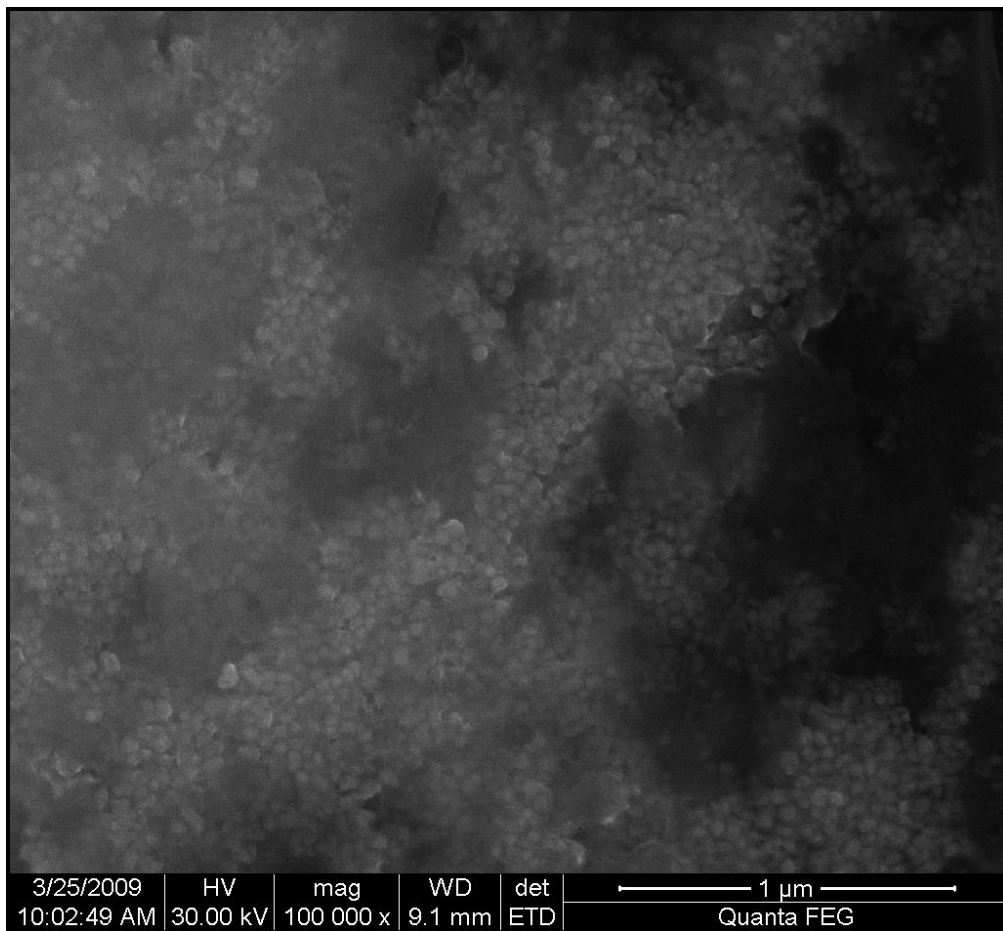


Figure 88. FE-SEM images of Ag-Eu³⁺ nanoparticles.

Eu³⁺ functionalized Ag nanoparticles had a sphere-like morphology with sizes approximately 40 nm (Figure 87 and Figure 88). The monodispersity of prepared nanoparticles was quite high. Incorporation of Eu³⁺ on the surface of silver nanoparticles was verified by taking EDX spectrum as shown in Figure 89.

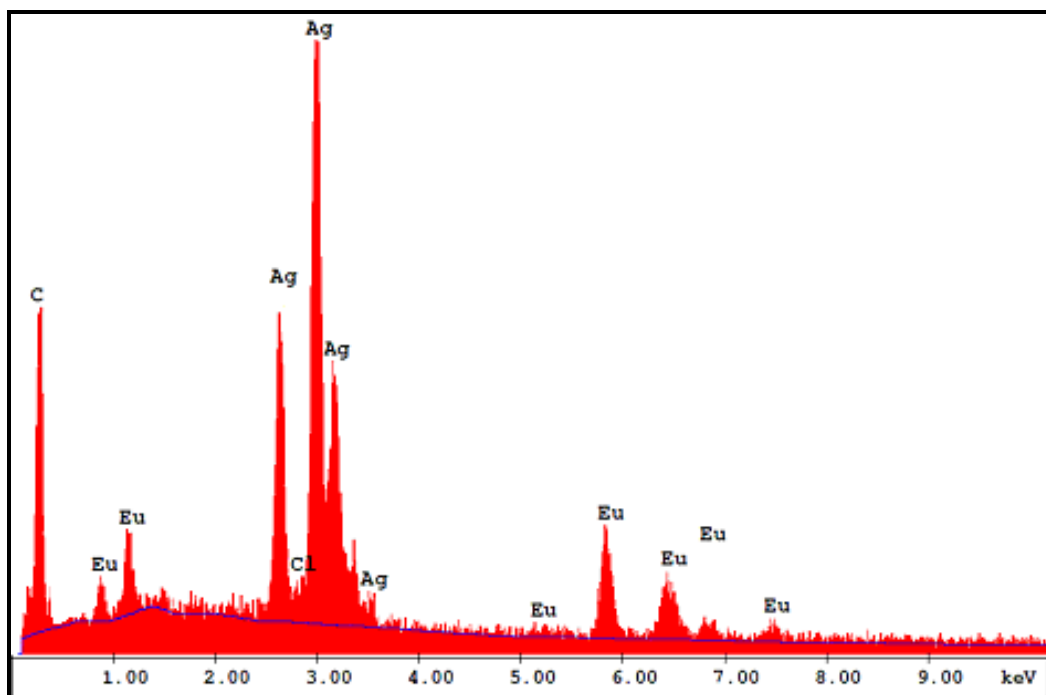


Figure 89. EDX pattern of Ag-Eu³⁺ nanoparticles.

As can be seen from EDX patterns given in Figure 89, the particles contain two diagnostic elements of the precursors, Ag and Eu.

3.2.2.3. Detection of Methylphosphonic Acid (MPA) as Degradation Product of Nerve Agents by Using SERS

A lanthanide ion, Eu³⁺ was employed to functionalize the surface of silver nanoparticles. It allowed the molecule of interest resided near the nanoscale noble metal features for the distance dependent SERS phenomenon. These structures exhibited highly cooperative binding properties that were necessary to achieve high selectivity molecular diagnostic systems based upon nanoparticle probes.

To evaluate the chemical characteristics of these composite nanoparticles in the context of a molecular analysis experiment, the detection of methylphosphonate, a model compound for nonvolatile organophosphate nerve agents was investigated. [215,216].

Herein, a simple experiment was demonstrated that yields high SERS enhancement factors. Ag-Eu³⁺ substrates for SERS analysis were prepared without any pretreatment procedure. A sketch of the experimental system is shown in Figure 90 and involves the steps indicated.

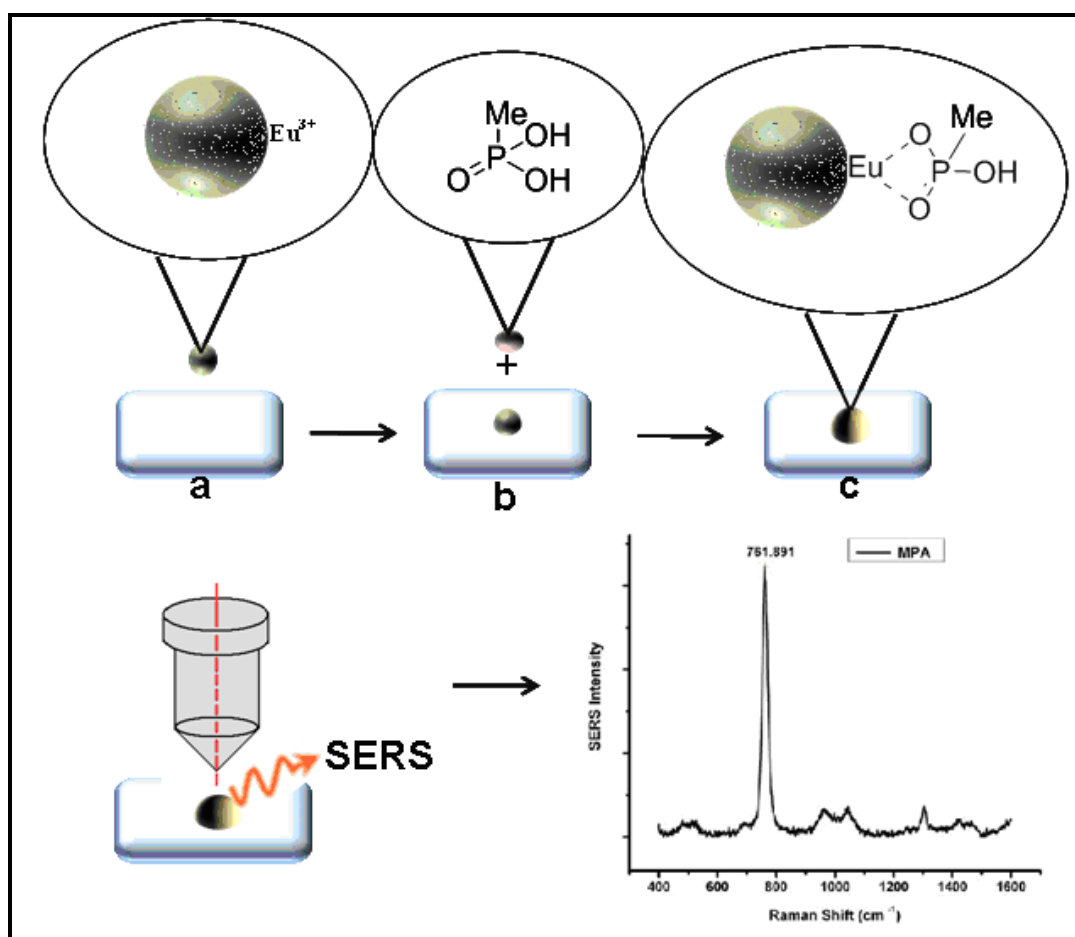


Figure 90. A sketch of the production, and the application of Ag- Eu³⁺ substrate as molecular traps for surface-enhanced Raman scattering (SERS) of MPA molecules.

Ag was functionalized with a Eu^{3+} ion followed by attachment of OPP by dropping its aqueous solution on to the functionalized Ag substrate. The vacant coordination sites of the lanthanide center were occupied by the incoming analyte.

3.2.2.3.1. Raman Spectrum of Methylphosphonic Acid

In most cases, the Raman and SERS spectra for the alkyl methylphosphonic acid degradation products are controlled by one or two peaks between 715 and 775 cm^{-1} , which have been attributed to phosphorus-carbon (P-C) stretching modes [217,218]. In order to see the exact value of P-C stretching modes of methyl phosphonic acid, Raman spectrum of solid MPA was taken which is shown in Figure 91.

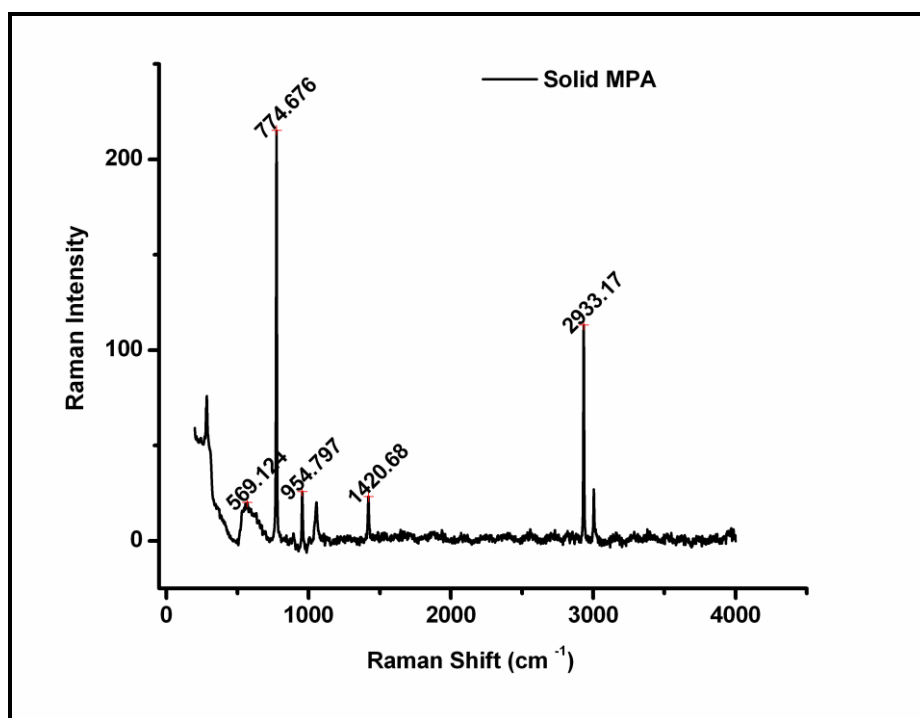


Figure 91. Raman spectrum of solid MPA. 632.8 nm radiation from a Helium–Neon laser was used with an excitation power of 10 mW and spectra was acquired with 10 s integration time.

The peak at 774 cm^{-1} has a higher intensity relative to all of the other peaks which is assigned to P-C stretching modes.

3.2.2.3.2. SERS Measurements of Methylphosphonic Acid

Initially, citrate reduced silver colloid was used as a substrate in order to get the SERS spectra of methyl phosphonic acid solution in water. As can be seen from Figure 92, no peak was observed for this measurement.

Silver-doped sol-gels, silver-oxide thin films and silver islands used for the detection of chemical warfare agents were mentioned in the introduction part (Sec 1.12). Detection capability of these substrates was around 100 mg/L with at least 1 min acquisition time [194]. Among them, silver island has been widely used due to its regular structure. Silver island is produced by evaporating a layer (less than 10 nm thickness) of a metal directly onto a solid support and metal layer forms nanoparticles on the support as separate metal islands. Generally, they are used as standard surfaces to compare the results obtained with other nanostructured materials [113].

In the second trial silver islands were prepared at the Physics Department, METU. SERS signal of 1×10^{-2} M MPA obtained is shown in Figure 92 where the phosphonate fingerprint peaks are clearly recognized at 761 cm^{-1} . 1×10^{-3} M MPA was also examined but no signal was observed for this concentration level. The peak at 774 cm^{-1} which was observed in solid Raman spectrum of MPA shifted to 761 cm^{-1} .

Finally, the SERS measurement of MPA was performed with the prepared Ag-Eu³⁺ nanocomposite. The superiority of enhancement ability of Ag-Eu³⁺ substrate is shown in Figure 92. P-C stretching modes at 761 cm⁻¹ were observed as in the case of silver island without any shift.

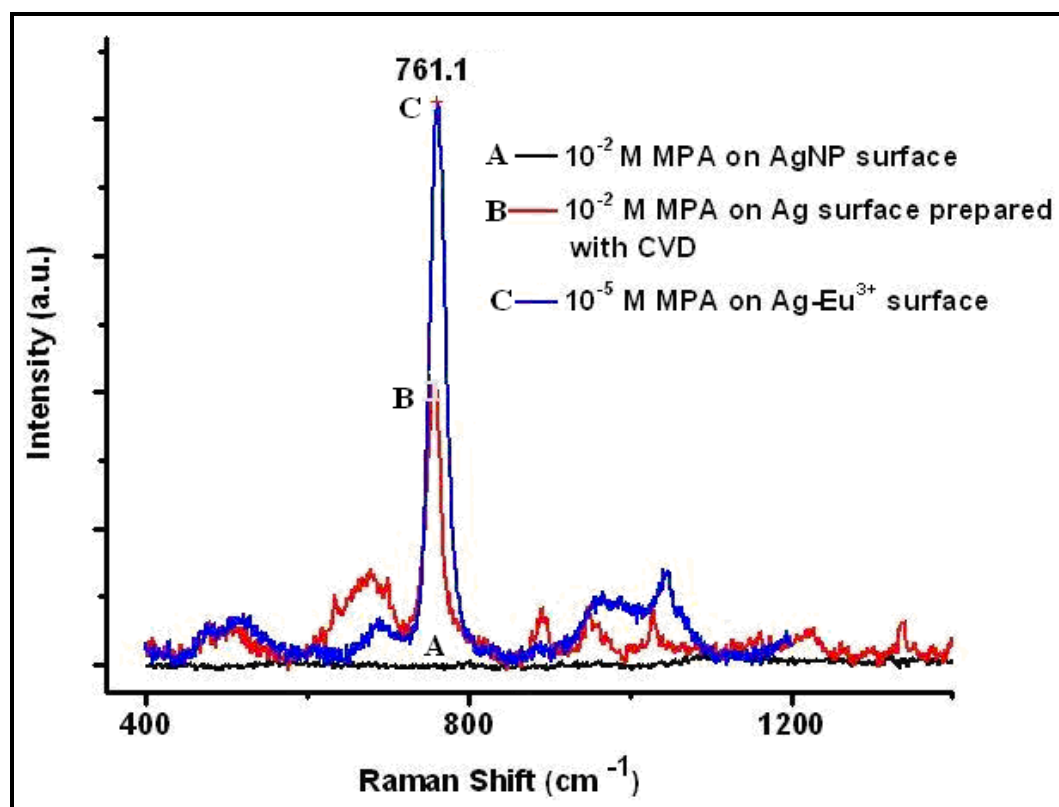


Figure 92. Comparison of SERS intensity of MPA acid measured with three different substrates ((A) 10⁻² M MPA on silver colloid substrate, (B) 10⁻² M MPA on silver island substrate, (C) 10⁻⁵ M MPA on Ag-Eu³⁺ substrate. 632.8 nm radiation from a Helium-Neon laser was used with an excitation power of 10 mW and spectra was acquired with 10 s integration time.

Blank measurements were also performed before the addition of MPA on to Ag-Eu³⁺ substrate. Sample spectrum is given in Figure 93 showing no peaks from the surface of the substrate.

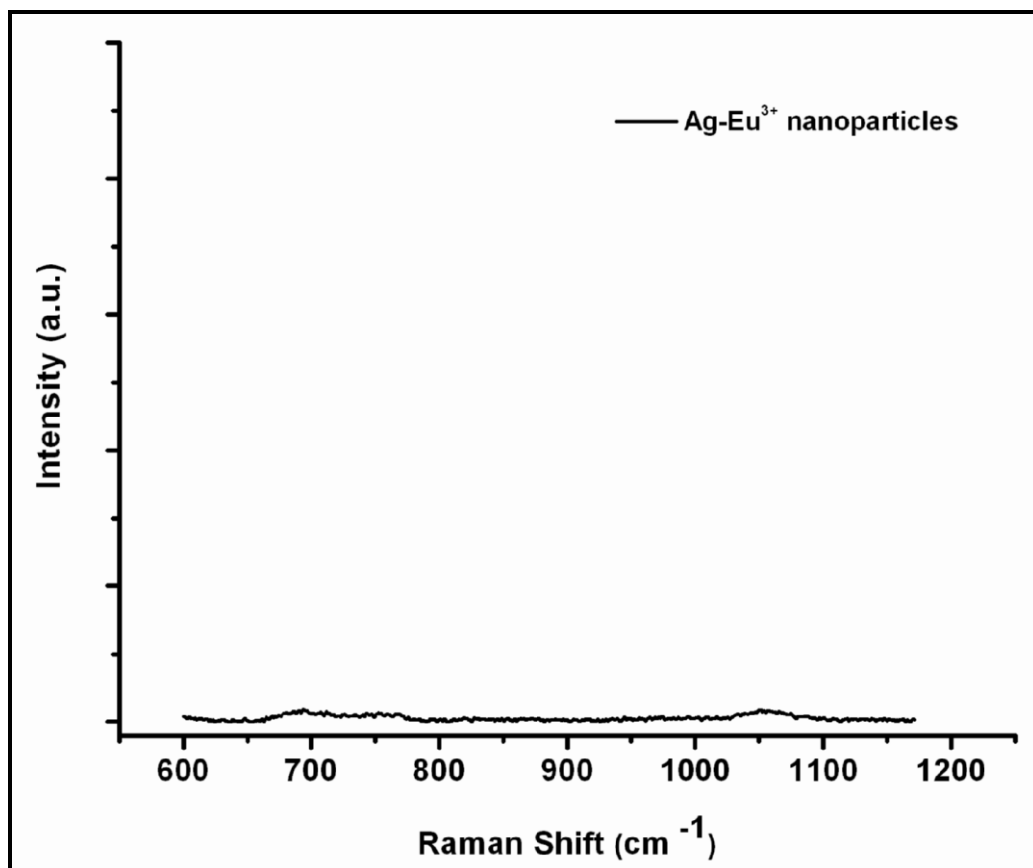


Figure 93. Blank measurement of Ag–Eu³⁺ substrate. 632.8 nm radiation from a Helium–Neon laser was used with an excitation power of 10 mW and spectra was acquired with 10 s integration time.

None of these substrates (silver colloid and silver island) had the combination of sensitivity, reproducibility, and ease of use for routine detection of analytes. Infact, it is extremely difficult to prepare the substrates and not practical at all for routine analyses of samples. On the basis of such a unique feature, it is clear that the Eu³⁺ ion can play a more active role in the molecular recognition events; there is a cooperative action between the Eu³⁺ and Ag. That is, the elaborate utilization of the silver nanoparticles with the europium receptors enables us to establish substrates for phosphate sensing.

3.2.2.4. Optimization of Complexation Period

Complexation time between Ag-Eu³⁺ and MPA acid was investigated by following the SERS signal of MPA at various time intervals after the addition of the MPA onto the substrate. Ag-Eu³⁺ nanoparticle solution was mixed with MPA (of 1x10⁻⁵) solution and then mixture was dropped on to glass slide respectively and SERS signal was taken. The results are given in Figure 94.

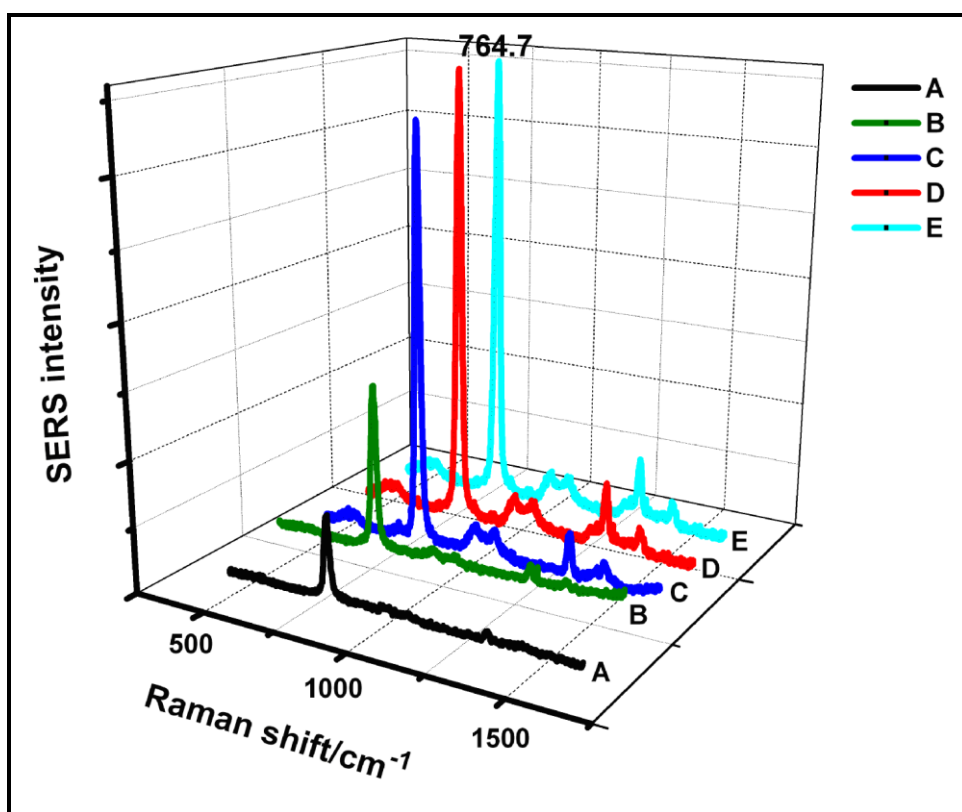


Figure 94. Effect of the complexation time between Ag-Eu³⁺ substrate and 1x10⁻⁵ M MPA on the SERS signal strength. SERS measurements of 1x10⁻⁵ M MPA with Ag-Eu³⁺ substrate were taken after A) 1 minute B) 5 minutes C) 10 minutes D) 15 minutes E) 30 minutes. 632.8 nm radiation from a Helium-Neon laser was used with an excitation power of 10 mW and spectra was acquired with 10 s integration time.

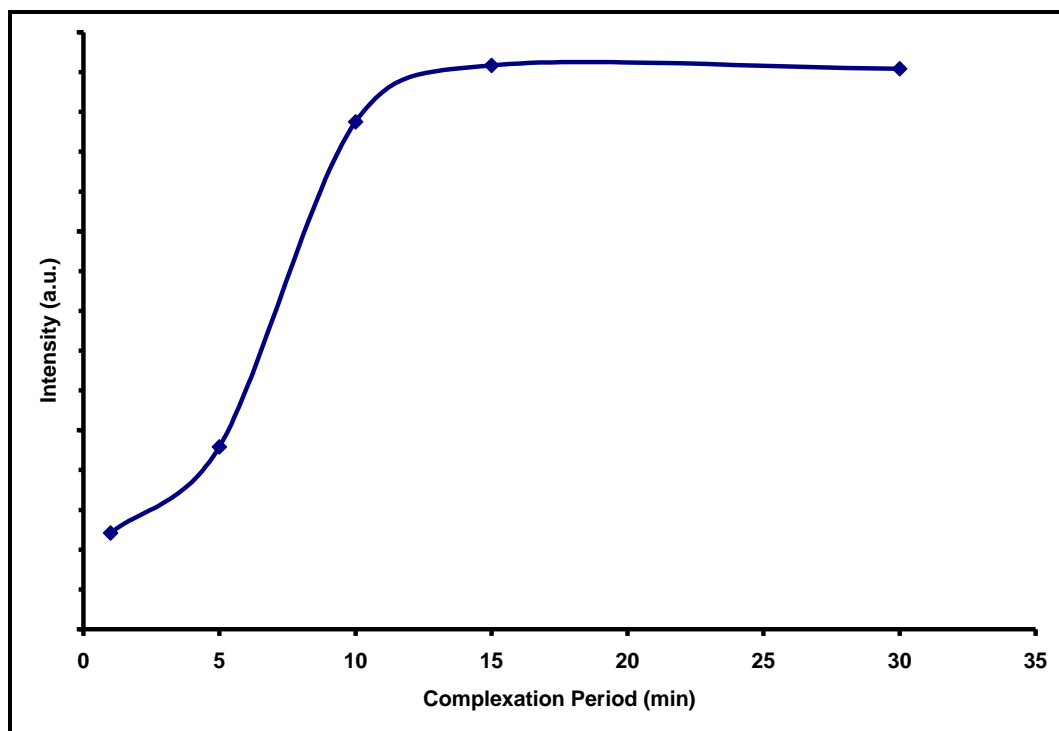


Figure 95. Complexation period between Ag-Eu³⁺ substrate and 1x10⁻⁵ M MPA solution

As can be seen from Figure 95, the SERS intensity values of MPA were reached to a plateau at 15 minutes reaction period. Therefore it was decided that the complexation of MPA onto Ag-Eu³⁺ substrate was completed in 15 minutes.

3.2.2.5. Stability of the Ag-Eu³⁺ Nanostructures

In order to check the stability of Ag-Eu³⁺ substrate, the SERS spectrum of its MPA (of 1x10⁻⁵) complex was taken at the day of preparation and seven days after its preparation (taken from the same batch). The results are given in Figure 96.

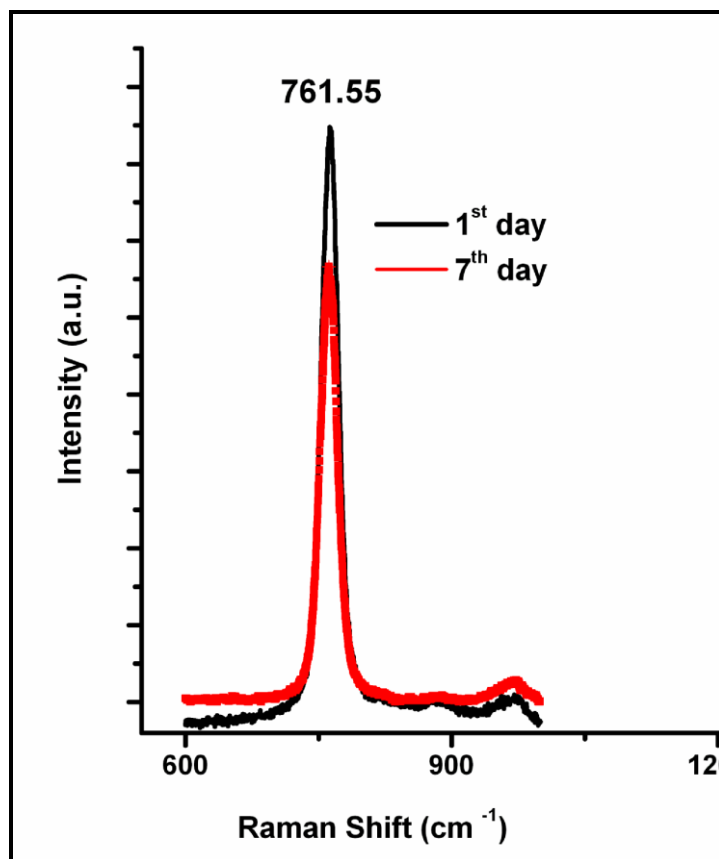


Figure 96. SERS signal of 10^{-5} M MPA obtained with Ag-Eu³⁺ substrate which were taken at the day of preparation and seven days after its preparation. 632.8 nm radiation from a Helium–Neon laser was used with an excitation power of 10 mW and spectra was acquired with 10 s integration time.

As can be seen from Figure 84, the loss in SERS activity was less than 30 % over a period of one week.

3.2.2.6. Reproducibility of the Prepared Substrate

The reproducibility of the SERS substrates for the determination of MPA was investigated by collecting spectra of 1×10^{-5} M MPA by using Ag-Eu³⁺ nanoparticles prepared in different runs. The sample signals are given in Figure 97.

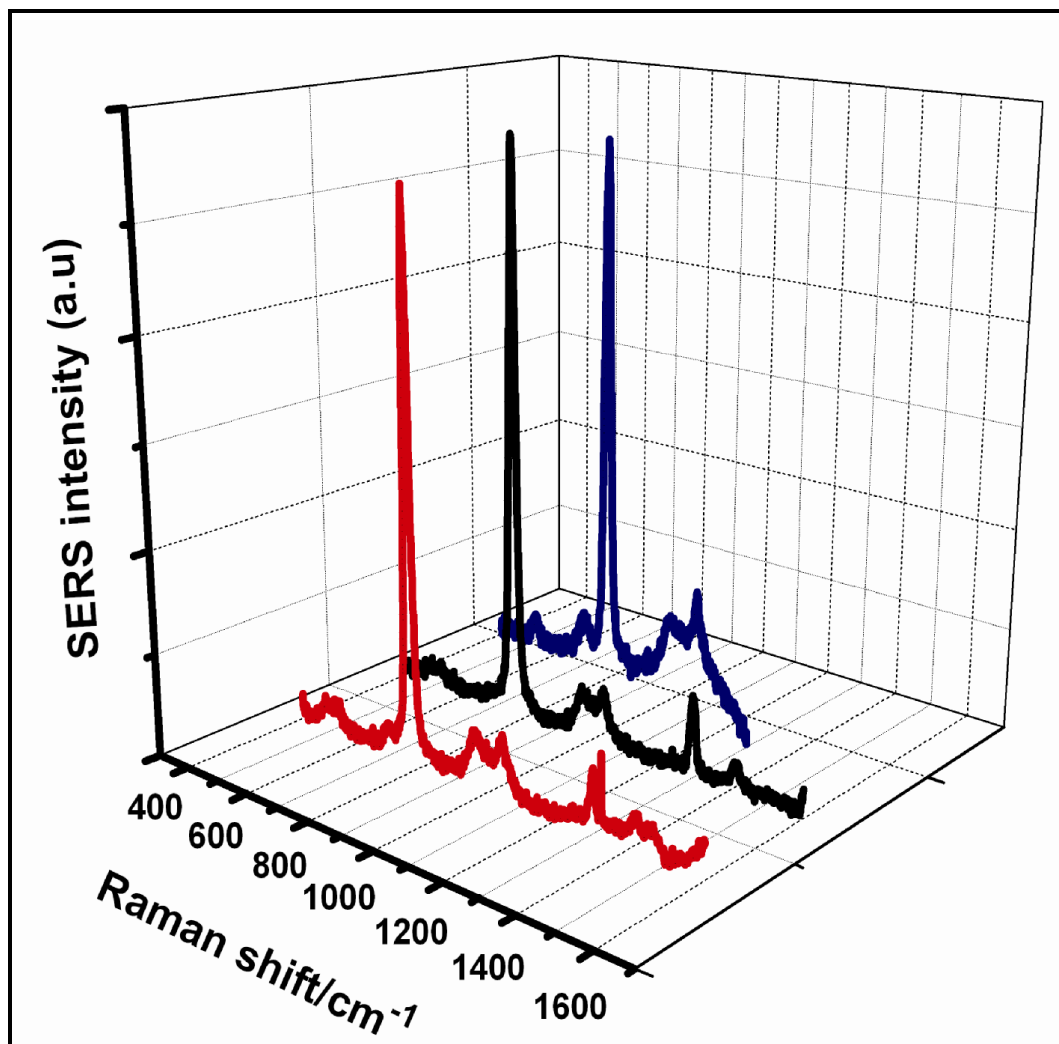


Figure 97. SERS spectra of 10^{-5} M MPA by using Ag-Eu³⁺ nanoparticles prepared in different runs. 632.8 nm radiation from a Helium–Neon laser was used with an excitation power of 10 mW and spectra was acquired with 10 s integration time.

The percent variation of the peak height of MPA band at 761 cm^{-1} for 15 measurements by using Ag-Eu³⁺ nanoparticles taken from different batches of the substrates was below 5.0 %. This outcome has shown the reproducibility of the SERS method utilizing Ag-Eu³⁺ nanoparticles for nerve agent detection.

3.2.2.7. Sensitivity of the Ag-Eu³⁺ Nanostructures as SERS Substrate

To investigate the SERS sensitivity of the Ag-Eu³⁺ substrate, MPA solutions between 1×10^{-7} M and 7×10^{-7} M were prepared and SERS experiment was repeated on Ag-Eu³⁺ substrate. The calibration curve obtained is shown in Figure 98 and SERS signals as a function of MPA concentrations on Ag-Eu³⁺ substrate is shown in Figure 99.

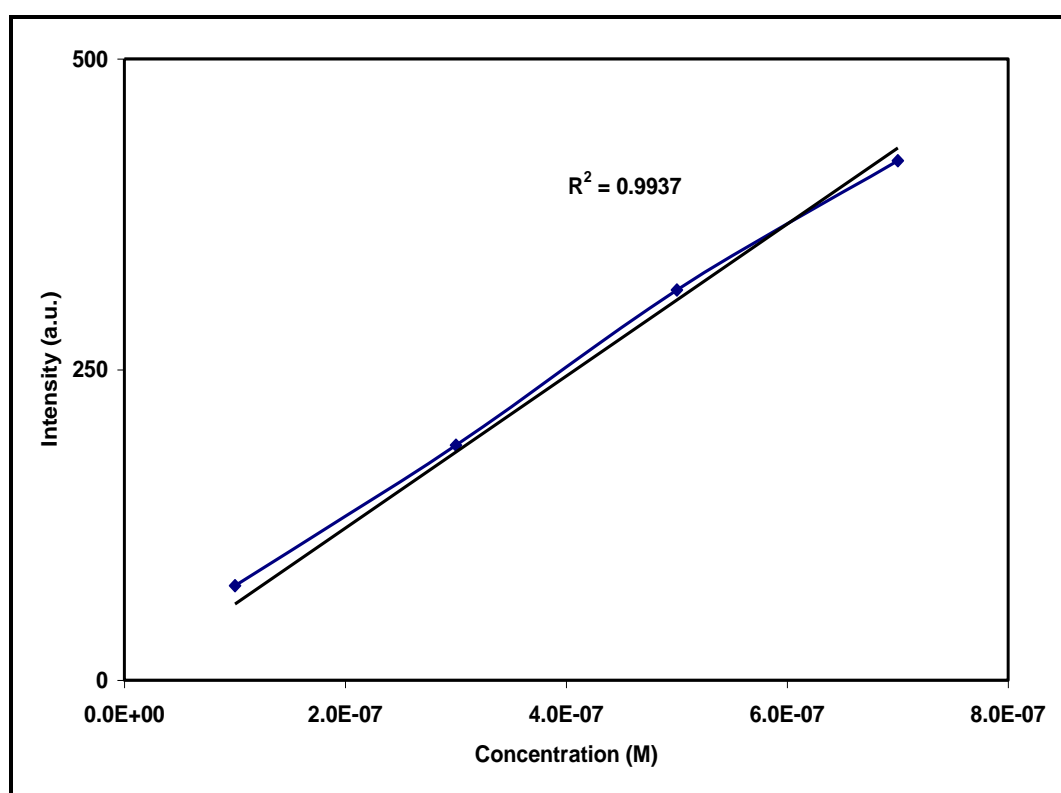


Figure 98. Calibration curve of MPA (1×10^{-7} - 7×10^{-7} M MPA obtained with Ag-Eu³⁺ substrate).

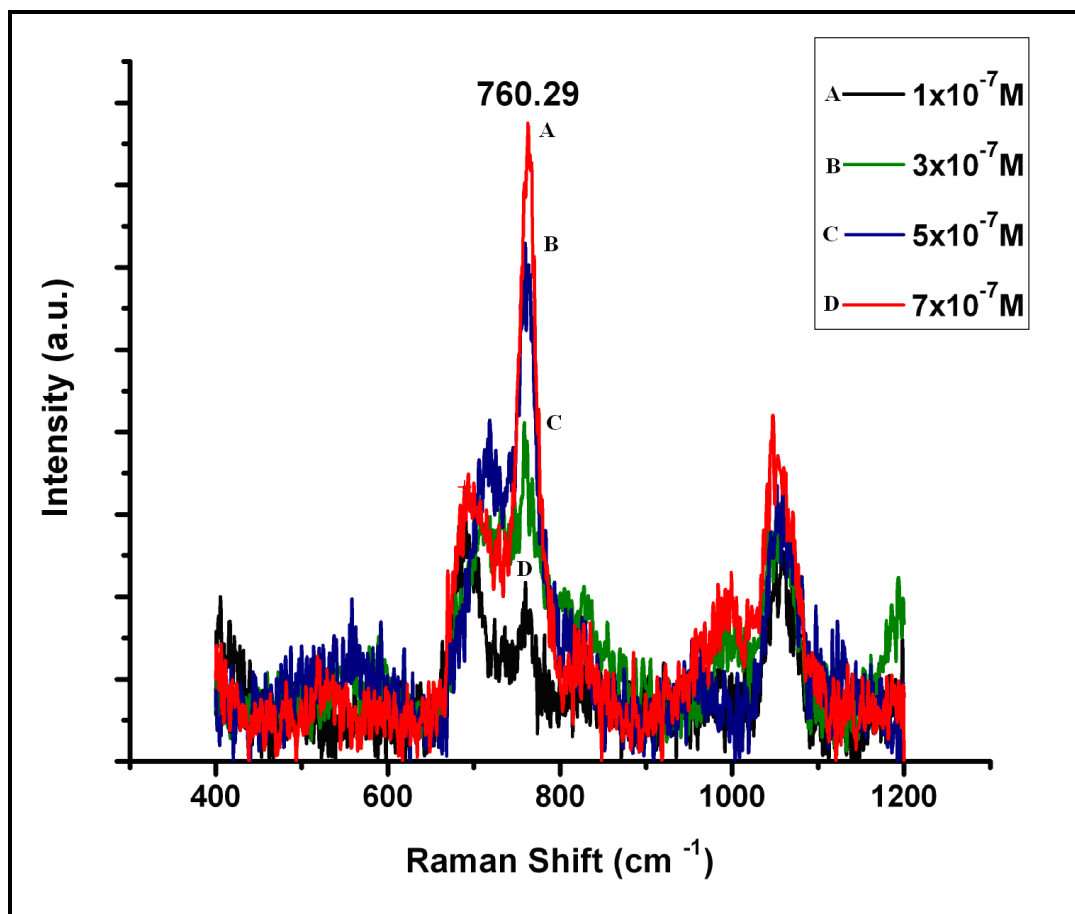


Figure 99. SERS spectrum of 1×10^{-7} – 7×10^{-7} M MPA obtained with Ag-Eu³⁺ substrate. 632.8 nm radiation from a Helium–Neon laser was used with an excitation power of 10 mW and spectra was acquired with 10 s integration time.

The observed response is linear between 1×10^{-7} M and 7×10^{-7} M. A SERS signal of MPA molecules can be observed for concentrations as dilute as 1.0×10^{-7} M and the detection limit of MPA determination was found to be 2.88 ng/L, showing the sensitivity of this SERS technique. The high sensitivity of substrates for CW detection can be attributed to the presence of Eu³⁺. These results showed that Ag-Eu³⁺ SERS substrate can be of practical use for the detection of nerve agents detection. Consequently, a sensitive method for the determination of organophosphonate based on the SERS enhancement effect by the Ag–Eu³⁺ nanocomposites was proposed.

CHAPTER 4

CONCLUSIONS

Monodisperse gold nanoparticles and hollow gold nanoparticles which are almost monodispersed state and having the characteristics of tunable interior and exterior diameter have been synthesized by chemical reduction and by galvanic replacement of cobalt nanoparticles. The position of the surface plasmon band of hollow gold nanoparticles between 570 and 630 nm were controlled by carefully monitoring the particle size and wall thickness. Cobalt nanoparticle size, the template, that controls the resulting hollow gold nanoparticles size, was tuned by simultaneously changing the concentration of sodium borohydride and sodium citrate (the reducing and capping agents) respectively. It was also shown that by the careful addition of gold solution, the thickness of the gold shell varied as well. Then gold core silver shell and hollow gold-silver double-shell nanospheres were synthesized by coating solid gold and hollow gold nanoparticles with silver.

The production of silver shell structures were confirmed using FE-SEM, EDX and UV-Vis spectroscopy, showing the successful coating of silver on the solid AuNPs and AuHNSs. These nanoparticles have been further confirmed to be excellent SERS substrates in terms of spectral consistency. Optical absorption and SERS properties of prepared nanostructures were investigated. SERS enhancement was achieved for nanoparticles with silver shell over Au and AuHNSs. The results demonstrated that complex metal nanostructures synthesized with useful optical properties were generated from such structures in a meaningful and controllable manner.

Secondly, a novel SERRS platform for fast and ultrasensitive analysis of dopamine (DA) molecules through surface enhanced resonance spectroscopy was developed. This is the first time that direct detection of a DA molecule attached to an Ag-Fe(NTA) by using SERRS was achieved. The Ag-Fe(NTA) substrate provided reliable reproducibility, excellent sensitivity, and good time stability. DA was detected quickly and accurately without any pretreatment in nM level with excellent discrimination against AA. Detection level was among the lowest values reported so far, for SERS detection of DA. All of these excellent properties mentioned above made the obtained substrate a perfect choice for routine SERRS detection of DA. This nanotechnology based method could be adapted for the detection of a wide variety of other neurotransmitters.

In the last part of the study, the synthesis of lanthanide ion (Eu^{3+}) containing silver nanoparticles with favorable optical and chemical properties was discussed. These structures exhibited the highly cooperative binding properties that are high selectivity molecular diagnostic systems based upon nanoparticle probes. Furthermore, this approach represented a novel perspective on the use of SERS substrate for a wide range of applications.

The development of highly versatile and SERS active Ag- Eu^{3+} nanocomposites allowed us to incorporate any organophosphates to the Eu^{3+} part while exploiting the benefits of using a silver core for SERS. The procedure reported herein provides a simple way of achieving reproducible and sensitive SERS spectroscopy for OPP detection. The Raman spectra of molecules residing near the surface are strongly enhanced. The detection of the MPA was confirmed by the presence of an intense SERS signal by using Ag- Eu^{3+} substrate. This sensing strategy promises to be useful in a variety of molecular sensing applications.

REFERENCES

1. Bhushan B., Springer Handbook of Nanotechnology, Second Edition, Springer
2. Whitesides G. M., *Small*, 2005, 1(2), 172.
3. Xia Y., Gates B., Yin Y., Lu Y., *Adv. Mater.*, 2000, 10,12.
4. Poole C.P., Jr., Owens F.J., *Introduction to Nanotechnology*, Wiley Interscience, Hoboken, NJ, 2003.
5. Peng X.G., Manna L., Yang W.D., *Nature*, 2000, 404(6773), 59.
6. Li L.S., Hu J.T., Yang W.D., *Nano Lett.*, 2001, 1(7), 349.
7. Buhro W.E., Colvin V.L., *Nat. Mater.*, 2003, 2(3), 138.
8. Burda C., Chen X.B., Narayanan R., *Chem. Rev.*, 2005, 105(4), 1025.
9. Murphy C.J., Sau T.K., Gole A.M., *J. Phys. Chem. B*, 2005, 109(29), 13857.
10. Eastham D.A., Hamilton B., Denby P.M., *Nanotechnology*, 2002, 13, 51.
11. Padovani S., Chado I., Scheurer F., J.P. Bucher, *Phys. Rev. B*, 1999, 59, 11887.
12. Liu C., Wu X., Klemmer T., Shukla N., Roy A.G., Tanase M., Laughlin D., *J. Phys. Chem. B*, 108, (2004), 6121.
13. Sosa I.O., Noguez C., Barrera R.G., *J. Phys. Chem. B*, 2003, 107, 6269.
14. Hu E. L., Shaw D.T., *Nanostructure Science and Technology*, Kluwer Academic Publishing, Dordrecht, 1999, 15.
15. Mijatovic D., Eijkel J. C. T., van den Berg A., *Lab. Chip.*, 2005, 5, 492.
16. Nauellau P., *J. Vac. Sci. Technol. B*, 2002, 20, 2829.

17. Campbell L. C., Wilkinson M. J., Manz A., Camilleri P., Humphreys C. J., *Lab. Chip.*, 2004, 4, 225.
18. A. Notargiacomo, *Mater. Sci. and Eng. C*, 2002, 19, 185.
19. Haneveld J., Jansen H., Berenschot E., Tar N., Elwenspoek M., *J. Micromech. Microeng.*, 2003, 13, 62.
20. Koster G., Rijnders G., Blank D. H. A, Rogalla H., *Appl. Phys. Lett.*, 1999, 74, 3729.
21. Wang D., Mohwald H., *J.Mater. Chem.*, 2004, 14, 459.
22. Wang Y., Xia Y., *Nano Lett.*, 2004, 4(10), 2047.
23. Foos E. E., Stroud R. M., Berry A. D., Snow, A. W., Armistead J. P., *J. Am. Chem. Soc.*, 2000, 122, 7114.
24. Fang J., Stokes K. L., Zhou W. L., Wang W., Lin, J., *Chem. Commun.*, 2001, 1872.
25. Park M., Harrison C., Chaikin P. M., Register R. A., D. H. Adamson, *Science*, 1997, 276, 1401.
26. Lazzari M., Lopez-Quintela M. A, *Adv. Mater.*, 2003, 15, 1583.
27. Burleson D.J., Driessen M.D., Penn R.L., *J. Environ. Science Health A*, 2004, 39(10), 2707.
28. Englert B. C., *J. Environ. Monit.*, 2007, 9, 1154.
29. Egerton R.F., *Electron Energy-Loss Spectroscopy in the Electron Microscope*, Plenum Press, New York, 1996.
30. O'Keefe M. A., *Ultramicroscopy*, 2001, 89, 215.

31. Joseph Y., Besnard I., Rosenberger M., Guse B., Nothofer H. G., Wessels J. M., Wild U., Gericke A. K., Su D., Schlogl R., Yasuda A., Vossmeier T., *J. Phys. Chem. B*, 2003, 107, 7406.
32. Chang H. Y., Cheng S. Y., Sheu C. I., Wang Y. H., *Nanotechnology*, 2003, 14, 603.
33. Lin S. Y., Chen C. H., Lin M. C., Hsu H. F., *Anal. Chem.*, 2005, 77, 4821.
34. Cheng D., Xia H., Chan H. S. O., *Langmuir*, 2004, 20, 9909.
35. Alexeev O. S., Siani A., Lafaye G., Williams C. T., Ploehn H. J., Amiridis M. D., *J. Phys. Chem. B*, 2006, 110, 24903.
36. Dettlaff-Weglikowska U., Skaokalovao V., Graupner R., Jhang S. H., Kim B. H., Lee H. J., Ley L., Park Y. W., Berber S., Tomašnek D., Roth S., *J. Am. Chem. Soc.*, 2005, 127, 5125.
37. Costa P. M., Friedrichs S., Sloan J., Green M. L. H., *Chem. Mater.*, 2005, 17(12), 3122.
38. Kamat P. V., *J. Phys. Chem. B*, 2002, 106, 7729.
39. Murray C. B., Sun S., Doyle H., Betley T., *Mater. Res. Soc. Bull.* 2001, 26, 985.
40. Maier S. A., *Adv. Mater.*, 2001, 13, 1501.
41. Nie S., Emory S. R., *Science*, 1997, 275, 1102.
42. Dick L. A., McFarland A. D., Haynes C. L., Van Duyne R. P., *J. Phys. Chem. B*, 2002, 106, 853.
43. Nicewarner-Pena S. R., *Science*, 2001, 294, 137.

44. Puentes V. F., Krishnan K. M., Alivisatos A. P, *Science*, 2001, 291, 2115.
45. Nicewarner-Peña S. R., *Science*, 2001, 294, 137.
46. Murphy C. J., *Science*, 2002, 298, 2139.
47. Link S., Wang Z. L., El-Sayed M. A., *J. Phys. Chem. B*, 1999, 103, 3529.
48. Liz-Marzan L. M., Philipse A. P., *J. Phys. Chem. B*, 1995, 99, 15120.
49. Treguer M., de Cointet C., Remita H., Khatouri J., Mostafavi M., Amblard J., Belloni J., de Keyzer R. J., *Phys. Chem. B*, 1998, 102, 4310.
50. Vinodgopal K., He Y., Ashokkumar M., Grieser F. J., *Phys. Chem. B*, 2006, 110, 3849.
51. Chen Y. H., Yeh C. S., *Chem. Commun.*, 2000, 371.
52. Anandan S., Grieser F., Ashokkumar M., *J. Phys. Chem. C*, 2008, 112, 15103.
53. Daniel M. C., Astruc D., *Chem. Rev.*, 2004, 104, 293.
54. El-Sayed M. A., *Acc. Chem. Res.*, 2001, 34, 257.
55. Hutter E., Fendler J.H., *Adv. Mater.*, 2004, 16, 1685.
56. El-Sayed I.H., Huang X., El-Sayed M. A., *Nano Lett.*, 2005, 5, 829.
57. Eustis S., El-Sayed M. A., *Chem. Soc. Rev.*, 2006, 35, 209.
58. Zhang J., Matveeva E., Gryczynski I., Leonenko Z., Lakowicz J. R., *J. Phys. Chem. B*, 2005, 109, 7969.
59. Freeman R. G., Grabar K. C., Allison K. J., Bright R. M., Davis J. A, Guthrie A. P., Hommer M. B., Jackson M. A, Smith P. C., Walter D. G., Natan M. J., *Science*, 1995, 267, 1629.

60. Tao A., Kim F., Hess C., Goldberger J., He R. R., Sun Y. G., Xia Y. N., P. D. Yang, *Nano Lett.*, 2003, 3, 1229.
61. Orendorff C. J., Gole A., Sau T. K., Murphy C. J., *Anal. Chem.*, 2005, 77, 3261.
62. Caol J., Matsoukas T., *J. Nanopart. Res.*, 2004, 6, 447.
63. a) Caruso F., Caruso R. A., Mohwald H., *Science*, 1998, 282, 1111. b) Jiang P., Bertone J. F., Colvin V. L., *Science*, 2001, 291, 453.
64. a) Kim S.W., Kim M., Lee W. Y., Hyeon, T., *J. Am. Chem. Soc.*, 2002, 124, 7642. b) Dai Z., Dahne L. Mohwald H., Tiersch B., *Angew. Chem. Int. Ed.*, 2002, 41, 4019.
65. a) Nakashima T., Kimizuka N., *J. Am. Chem. Soc.*, 2003, 125, 6386. b) Fowler C. E., Khushalani D., Mann S., *Chem. Commun.*, 2001, 2028. c) Gao X., Zhang, J., Zhang L., *Adv. Mater.*, 2002, 14, 290.
66. Graf C., Blaaderen A. V., *Langmuir*, 2002, 18, 524.
67. Jackson J. B., Westcott S. L., Hirsch L. R., West J. L., Halas N., *J. Appl. Phys. Lett.*, 2003, 82, 257.
68. Lu W., Wang W., Su Y., Li J., Jiang L., *Nanotechnology*, 2005, 16, 2582.
69. Talapin D.V., Rogach A.L., Kornowski A., *Nano Lett.*, 2001, 1(4), 207.
70. Li J.J., Wang Y.A., Guo W.Z., *J Am Chem Soc*, 2003, 125(41), 12567.
71. Sobal N.S., Hilgendorff M., Mohwald. H., *Nano Lett*, 2002, 2(6), 621.
72. Lee W.R., Kim M.G., Choi J.R., *J Am Chem Soc.*, 2005, 127(46), 16090.
73. Kim H., Achermann M., Balet L.P., *J Am Chem Soc.*, 2005, 127(2), 544.

74. Pellegrino T., Manna L., *Chem. Soc. Rev.*, 2006, 35, 1195
75. Stevens P. D., Fan, J., Gardimalla, H. M. R., Yen, M., Gao, Y. *Org. Lett.* 2005, 7, 2085. b) Doering, W. E., Nie, S. *Anal. Chem.* 2003, 75, 6171.
76. a) Son S. U., Jang Y., Park J., Na H. B., Park H. M., Yun H. J., Lee J., Hyeon T. *J. Am. Chem. Soc.* 2004, 126, 5026. b) Zhou S., Varughese B., Eichhorn B., Jackson G., McIlwrath K., *Angew. Chem. Int. Ed.* 2005, 44, 4539.
77. a) Park J.-I., Cheon J., *J. Am. Chem. Soc.*, 2001, 123, 5743. b) Park J.-I., Kim M. G., Jun Y.-W., Lee J. S., Lee W.-R., Cheon J., *J. Am. Chem. Soc.*, 2004, 126, 9072.
78. a) Reetz M. T., Westermann E., *Angew. Chem. Int. Ed.*, 2000, 39, 165. b) Jansat S., Gomez M., Philippot K., Muller G., Guiu E., Claver C., Castillon S., Chaudret B., *J. Am. Chem. Soc.*, 2004, 126, 1592. c) Joachim C., Gimzewski J. K., Aviram A., *Nature*, 2000, 408, 541.
79. Link S., El-Sayed M., *J. Phys. Chem. B*, 1999, 103, 8410.
80. Kelly K. L., Coronado E., Zhao L. L., Schatz G. C., *J. Phys. Chem. B*, 2003, 107, 668.
81. Jackson J. B., Halas N. J., *J. Phys. Chem. B*, 2001, 105, 2743.
82. Born M., Wolf E., 7th edition, Pergamon Press, Oxford, 1998.
83. Kreibig U., Vollmer M., *Springer Series in Materials Science 25*, Springer, Berlin, 1995.
84. Link S., El-Sayed M. A., *Annu. Rev. Phys. Chem.*, 2003, 54, 331.
85. Haus J. W., Zhou H. S., Takami S., Hirasawa M., Honma I., Komiyama H., *J. Appl. Phys.*, 1993, 73, 1043.

86. Zhou H. S., Honma I., Haus J. W., Komiyama H., Phys. Rev. B, 1994, 50, 12052.
87. Halas N., Opt. Photon. New., 2002, 26.
88. Averitt R. D., Sarkar D., Halas N. J., Phys. Rev. Lett., 1997, 78, 4217.
89. Raman C. V., Krishnan K. S., Nature ,1928, 121, 501.
90. Rao A. M., Richter E., Bandow S., Chase B., Eklund P. C., Williams K. A., Subbaswamy K. R., Menon M., Thess A., Smalley R. E., Dresselhaus G., Dresselhaus M. S., Science, 1997, 275, 187.
91. Ryder A. G., O'Connor G. M., Glynn T. J., J. Raman Spectrosc., 2000, 31, 221.
92. Ferraro J.R., Nakamoto K., Brown C. W., Introductory Raman spectroscopy (second edition), Academic Press Elsevier, California, 2003.
93. Smith E., Dent G., Modern Raman spectroscopy, a practical approach, John Wiley & Sons, England, 2005.
94. Lewis I. R., Edwards H. G. M., Handbook of Raman spectroscopy, from the research laboratory to the process line, Marcel Dekker, 2001.
95. Nakamoto K., Infrared and Raman Spectra of Inorganic and Coordination Compounds. Part A, Theory and Applications in Inorganic Chemistry, John Wiley & Sons, Inc., New York 1997.
96. Jeanmaire, D. L., Duynes, R. P. V. J. Electroanal. Chem. 1977, 84, 1.
97. Albrecht, M. G., Creighton, J. A. J. Am. Chem. Soc. 1977, 99,5215.
98. Kneipp K., Wang Y., Kneipp H., Perelman L. T., Itzkan I., Dasari R. R., Feld M. S., Phys. Rev. Lett., 1997, 78, 1667.

99. Nie S., Emory S. R., *Science*, 1997, 275, 1102.
100. Ibrahim A., Oldham P., Stokes D.L., Vo-Dinh T., *J. Raman Spectrosc.*, 1996, 27, 887.
101. Zeman E.J., Schatz G.C., *J. Phys. Chem.*, 1987, 91, 634.
102. Wokaun A., Gordon J.P., Liao P.F., *Phys. Rev. Lett.*, 1982, 48, 957.
103. Stevenson C.L., Vo-Dinh T., Laserna J.J. (Editor), *Modern Techniques in Raman Spectroscopy*, Wiley, New York, 1996.
104. Moskovits M., *Rev. Modern Phys.*, 1985, 57, 783.
105. Moskovits M., *J. Raman Spectrosc.*, 2005, 36, 485.
106. Stiles P. L., Dieringer J. A., Shah N. C., Van Duyne R. P., *Annu. Rev. Anal. Chem.*, 2008, 1, 601.
107. Chang R.K., Furtak T.E., *Surface-Enhanced Raman Scattering*, Plenum Press, New York, 1982.
108. Tran C.D., *Anal. Chem.*, 1984, 56, 824.
109. Tran C.D., *J. Chromatogr.*, 1984, 292, 432.
110. Sheng R.S., Zhu L., Morris M.D., *Anal. Chem.*, 1986, 58, 1116.
111. Torres E.L., Winefordner J.D., *Anal. Chem.*, 1987, 59, 1626.
112. Haynes C. L., Van Duyne R. P., *J. Phys. Chem. B*, 2001, 105, 5599.
113. Vo-Dinh T., *Trend. Anal. Chem.*, 1998, 17(8), 557.
114. Weaver M. J., *J. Raman Spectrosc.*, 2002, 33, 309.

115. Gerrard D.L., *Anal. Chem.*, 1994, 66, 547R.
116. Kneipp K., Wang Y., Kneipp H., Perelman L. T., Itzkan I., Dasari R., Feld M., *Phys. Rev. Lett.*, 1997, 78, 1667.
117. McCreery R. L., *Raman Spectroscopy for Chemical Analysis*, 1st ed., John Wiley & Sons, New York, 2000.
118. Haynes C. L., McFarland A. D., Van Duyne R. P., *Anal. Chem.*, 2005, 1, 338.
119. Haynes C. L., Yonzon C. R., Zhang X., Duyne R. P. V., *J. Raman Spectrosc.*, 2005, 36 (6-7), 471.
120. Graham D., Smith W. E., Linacre A. M. T., Munro C. H., Watson N. D., White P. C., *Anal. Chem.*, 1997, 69 (22), 4703.
121. Moskovits M., *J. Raman Spectrosc.*, 2005, 36, 485.
122. Emory S. R., Nie S., *Science*, 1997, 275, 1102.
123. Otto A., *J. Raman Spectrosc.*, 2002, 33, 593.
124. Munro C. H., Smith W. E., White P. C., *Analyst*, 1995, 120, 993.
125. Champion A., Kambhampati P., *Chem. Soc. Rev.*, 1998, 27, 241.
126. Kneipp K., Kneipp H., Itzkan I., Dasari R. R., Feld M. S., *Chem. Rev.*, 1999, 99, 2957.
127. Faulds K., Littleford R. E., Graham D., Dent G., Smith W. E., *Anal. Chem.*, 2004, 76, 592.
128. Hildebrandt P., Keller S., Hoffmann A., Vanhecke F., Schrader B., *J. Raman Spectrosc.*, 1993, 24, 791.

129. Emory S. R., Nie S., *Science*, 1997, 275, 1102.
130. Faulds K., Stewart L., Smith W. E., Graham D., *Talanta*, 2005, 67, 667.
131. Albrecht M., Creighton J. A., *J. Am. Chem. Soc.*, 1977, 99, 5215.
132. Douketis C., Haslett T. L., Wang Z., Moskovits M., Iannotta S., *J. Chem. Phys.*, 2000, 113, 11315.
133. Tian Z. Q., Ren B., Wu D. Y., *J. Phys. Chem. B*, 2002, 106, 9463.
134. Abdelsalam M. E., Bartlett P. N., Baumberg J. J., Cintra S., Kelf T. A., Russell A. E., *Electrochem. Commun.*, 2005, 7, 740.
135. Yao j., Le A.-P., Gray S. K., Moore J. S., Rogers J. A., Nuzzo R. G., *Adv. Mater.*, 2010, 22, 1102.
136. Katz E., Willner I., *Angew. Chem. Int. Ed.*, 2004, 43, 6042.
137. Hrapovic S., Liu Y.L., Male K.B., Luong J.H.T., *Anal. Chem.*, 2004, 76, 1083.
138. Lin Y.H., Lu F., Tu Y., Ren Z.F., *Nano Lett.*, 2004, 4, 191.
139. Chin V., Collins B.E., Sailor M.J., Bhatia S.N., *Adv. Mater.*, 2001, 13, 1877.
140. Artyukhin A.B., Bakajin O., Stroeve P., Noy A., *Langmuir*, 2004, 20, 1442.
141. Islam M.F, Rojas E., Bergey D.M., Johnson A.T., Yodh A.G., *Nano Lett.*, 2003, 3, 269.
142. Hu H., Ni Y.C., Montana V., Haddon R.C., Parpura V., *Nano Lett.*, 2004, 4, 507.

143. Haes A.J., Hall W.P, Chang L., Klein W.L., Van Duyne R.P., *Nano Lett.*, 2004, 4, 1029.
144. Qhobosheane M., Santra S., Zhang P., Tan W.H., *Analyst*, 2001, 126, 1274.
145. Moghimi S.M., Hunter A.C., Murray J.C., *Pharmacol. Rev.*, 2001, 53 , 283.
146. Kohler N., Fryxell G.E., Zhang M.Q., *J. Am. Chem. Soc.*, 2004, 126, 7206.
147. Xu S.Y., Han X.Z., *Biosens. Bioelectron.*, 2004, 19, 1117.
148. Oyewumi M.O., Mumper R.J., *Int. J. Pharm.*, 2003, 251, 85.
149. Moghaddam M.J., Taylor S., Gao M., Huang S.M., Dai L.M., McCall M.J., *Nano Lett.*, 2004, 4, 89.
150. Vinogradov S.V., Bronich T.K., Kabanov A.V., *Adv. Drug Deliver. Rev.*, 2002, 54, 135.
151. Zhang C.X., Zhang Y., Wang X., Tang Z.M., Lu Z.H., *Anal. Biochem.*, 2003, 320, 136.
152. Dijkstra R. J., Scheenen W. J. J. M., Dama N., Roubos E. W., Meulen J.J., *J. Neurosci. Meth.*, 2007, 159, 43.
153. Jill V. B., Kevin P. T., Mark W. R., *Anal. Chem.*, 2002, 74, 539.
154. Frederic R., Lionel B., Luc D., Bernard R., *Anal. Chem.*, 1995, 67, 1838.
155. Zhang A., Neumeyer J. L., Baldessarini R., *J. Chem. Rev.*, 2007, 107, 274.
156. Ali S. R., Ma Y., Parajuli R. R., Balogun Y., Lai W. Y. C., He H., *Anal. Chem.*, 2007, 79, 2583.
157. Mo J.W., Ogorevc B., *Anal. Chem.*, 2001, 73, 1196.

158. Raymo F.M., Cejas M.A., *Org. Lett.*, 2002, 4, 3183.
159. Wang H.Y., Sun Y., Tang B., *Talanta* 2002, 57, 899.
160. Fotopoulou M.A., Ioannou P.C., *Anal. Chim. Acta*, 2002, 462, 179.
161. Wu K., Fei J., Hu S., *Anal. Biochem.*, 2003, 318, 100.
162. Willard D.M., Carillo L.L., Jung J., Orden A.V., *Nano Lett.*, 2001, 1, 469.
163. Raj C.R., Okajima T., Ohsaka T., *J. Electroanal. Chem.*, 2003, 543, 127.
164. Venton B. J., Wightman R. M., *Anal. Chem.* 2003, 75, 414A.
165. Phillips P. E. M., Stuber, G. D., Heien M. L. A. V., Wightman R. M., Carelli R. M., *Nature*, 2003, 422, 614.
166. Heien M. L. A. V., Phillips P. E. M., Stuber G. D., Seipel A. T., Wightman R. M., *Analyst*, 2003, 128, 1413.
167. Yoo, J.-S., Park S.-M., *Anal. Chem.* 2005, 77, 3694.
168. O'Neill R. D., *Analyst*, 1994, 119, 767.
169. Wang Z., Liu J., Liang Q., Wang Y., Luo G., *Analyst*, 2002, 127, 653.
170. Rojas M. T., Kaifer A. E., *J. Am. Chem. Soc.*, 1995, 117, 5883.
171. Shah R. A., Yufeng M., Rishi R. P., Yetunde B., Warren Y.-C. L., Huixin H., *Anal. Chem.* 2007, 79, 2583.
172. a) Sanles-Sobrido M., Exner W., Rodriguez-Lorenzo L., Rodriguez-Gonzalez B., Correa-Duarte M. A., Alvarez-Puebla R. A., Liz-Marzan L. M., *J. Am. Chem. Soc.*, 2009, 131, 2699, b) Schmuck P., Wich B., Kstner W., Kiefer S., *Angew. Chem.*, 2007, 119, 4870, *Angew. Chem. Int. Ed.*, 2007, 46, 4786.

173. a) Alvarez-Puebla R. A., Garrido J. J., Aroca R. F., *Anal. Chem.*, 2004, 76, 7118, b) Camden P., Dieringer J. A., Wang Y., Masiello D. J., Marks L. D., Schatz G. C., Van Duyne R. P., *J. Am. Chem. Soc.*, 2008, 130, 12616.
174. a) Laurence T. A., Braun G., Talley C., Schwartzberg A., Moskovits M., Reich N., Huser T., *J. Am. Chem. Soc.*, 2009, 131, 162, b) Ko H., Singamaneni S., Tsukruk V. V., *Small*, 2008, 4, 1576.
175. Alvarez-Puebla R. A., Aroca R. F., *Anal. Chem.*, 2009, 81, 2280.
176. a) Guerrini L., Garcia-Ramos J. V., Domingo C., Sanchez-Cortes S., *Langmuir*, 2006, 22, 10924, b) Guerrini L., Garcia-Ramos J. V., Domingo C., Sanchez-Cortes S., *Anal. Chem.*, 2009, 81, 953, c) Guerrini L., Garcia-Ramos J. V., Domingo C., Sanchez-Cortes S., *Anal. Chem.*, 2009, 81, 1418.
177. a) Alvarez-Puebla R. A., Contreras-Caceres R., Pastoriza-Santos I., Perez-Juste J., Liz-Marzan L. M., *Angew. Chem., Int. Ed.* 2009, 48, 138, b) Abalde-Cela S., Ho S., Rodríguez-González B., Correa-Duarte Miguel A. A'lvarez-Puebla Ramón A., Liz-Marzan Luis M., Kotov Nicholas A., *Angew. Chem., Int. Ed.*, 2009, 48, 5326.
178. Camden J. A., Dieringer J. A., Wang Y., Masiello D. J., Marks L. D., Schatz G. C., Van Duyne R. P., *J. Am. Chem. Soc.*, 2008, 130, 12616.
179. Cao Y. C., Jin R., Mirkin C. A., *Science*, 2002, 297, 1536.
180. Hill H. H., Martin Jr. S. J., *Pure Appl. Chem.*, 2002, 74(12), 2281.
181. Jenkinsa A. L., Uyb O. M., Murray G. M., *Anal Commun.*, 1997, 34, 221.
182. Zhou Y., Yu B., Shiu E., Levon K., *Anal. Chem.* 2004, 76, 2689.
183. Marx S., Zaltsman A., Turyan I., Mandler D., *Anal. Chem.*, 2004, 76, 120.

184. Hooijschuur E. W. J., Kientz C. E., Brinkman U. A. T., *J. Chromatogr. A*, 2002, 982, 177.
185. Black R. M., Muir B., *J. Chromatogr. A*, 2003, 1000, 253.
186. Jenkins A., Uy O. M., Murray G., M., *Anal. Chem.* 1999, 71, 373.
187. Nieuwenhuizen M. S., Harteveld J. L. N., *Sensor Actuat. B*, 1997, 40, 167.
188. Mulchandani A., Mulchandani P., Chen W., Wang J., Chen L., *Anal. Chem.*, 1999, 71, 2246
189. Wang C., Li C., Ji X., Orbulescu J., Xu J., Leblanc R. M., *Langmuir*, 2006, 22, 2200.
190. Southard G. E., Van Houten K. A., Murray G. M., *Macromolecules*, 2007, 40, 1395.
191. Wang C., Li C., Ji X., Orbulescu J., Xu J., Leblanc R. M., *Langmuir*, 2006, 22, 2200.
192. Pearman W. F., Fountain A. W., *Appl. Spectrosc.*, 2006, 60, 36.
193. Taranenko N., Alarie J. P., Stokes D. L., Vo-Dinh T., *J. of Raman Spectrosc.*, 1996, 27, 379.
194. Farquharson S., Gift A., Maksymiuk P., Inscore F., *Appl. Spectrosc.*, 2005, 59, 654.
195. Inscore F., Gift A., Maksymiuk P., Farquharson S., *SPIE*, 2004, 46, 5585.
196. Yan F., Vo-Dinh T., *Sensor Actuat. B*, 2007, 121, 61.
197. Alak A. M, Vo-Dinh T., *Anal. Chem.*, 1997, 59, 2149.

198. Lee P. C., Meisel D. J., *J. Phys. Chem. B*, 1982, 86, 3391.
199. Schwartzberg A. M., Olson T. Y., Talley C. E., Zhang J. Z., *J. Phys. Chem. B* 2006, 110, 19935.
200. a) Mathlowitz E., Jacob J. S., Jong Y. S., Carino G. P., Chickering, D. E., Chaturvedl P., Santos C. A., Vijayaraghavan K., Montgomery S., Bassett M., Morrell C., *Nature*, 1997, 386, 410. b) Huang H., Remsen E. E., Kowalewski T., Wooley K. L., *J. Am. Chem. Soc.*, 1999, 121, 3805. c) Gill I., Ballesteros A., *J. Am. Chem. Soc.*, 1998, 120, 8587.
201. Rigler P., Ulrich W.P., Hoffmann P., Mayer M., Vogel H., *ChemPhysChem.*, 2003, 4, 268.
202. Tural B., Kaya M., Özkan N., Volkan M., *J. Nanosci. Nanotechnol.*, 2008, 8, 695.
203. Rigler P., Ulrich W.-P., Hoffmann P., Mayer M., Vogel H., *ChemPhysChem.*, 2003, 4, 268.
204. McGlashen M. L., Davis K. L., Morris M. D., *Anal. Chem.*, 1990, 62, 846.
205. Volkan M. , Stokes D. L., Vo-Dinh T., *Appl. Spectrosc.*, 2000, 54, 1842.
206. Salama S., Stong J. D., Neilands J. B., Spiro T. G., *Biochemistry*, 1978, 17, 3781.
207. Que L., Heistand Jr. R. H., *J. Am. Chem. Soc.*, 1979, 101, 2219.
208. Lee N. S, Hsieh Y. Z., Paisley R. F., Morris M. D., *Anal. Chem.*, 1988, 60, 442
209. Kneipp K., Wang Y., Dasari R. R, Feld M. S., *Spectrochim. Acta, Part A*, 1995, 52, 481.

210. Sever M. J., Wilker J. J., Dalton Trans., 2004, 1061.
211. Barhoumi A., Zhang D., Tam F., Halas N. J., J. Am. Chem. Soc., 2008, 130, 5523.
212. Zhu X., Ge X., Jiang C., J. Fluoresc., 2007, 17, 655.
213. Ma Y., Yang C., Li N., Yang X., Talanta, 67, 2005, 979.
214. Newman J. D. S., Roberts J. M., Blanchard G. J., Anal. Chem., 2007, 79, 3448.
215. Prathish K.P., Prasad K., Prasada Rao T., Suryanarayana M.V.S., Talanta, 2007, 71, 1976.
216. Ashley J.A., Lin C.H., Wlrching P., Janda K.D., Angew. Chem. Int. Ed., 1999, 38, 1793.
217. Farquharson S., Gift A., Maksymiuk P., Inscore F., Appl. Spectrosc., 2005, 59, 654.
218. Suh J. S., Moskovits M., J. Am. Chem. Soc., 1986, 108, 4711.

APPENDIX

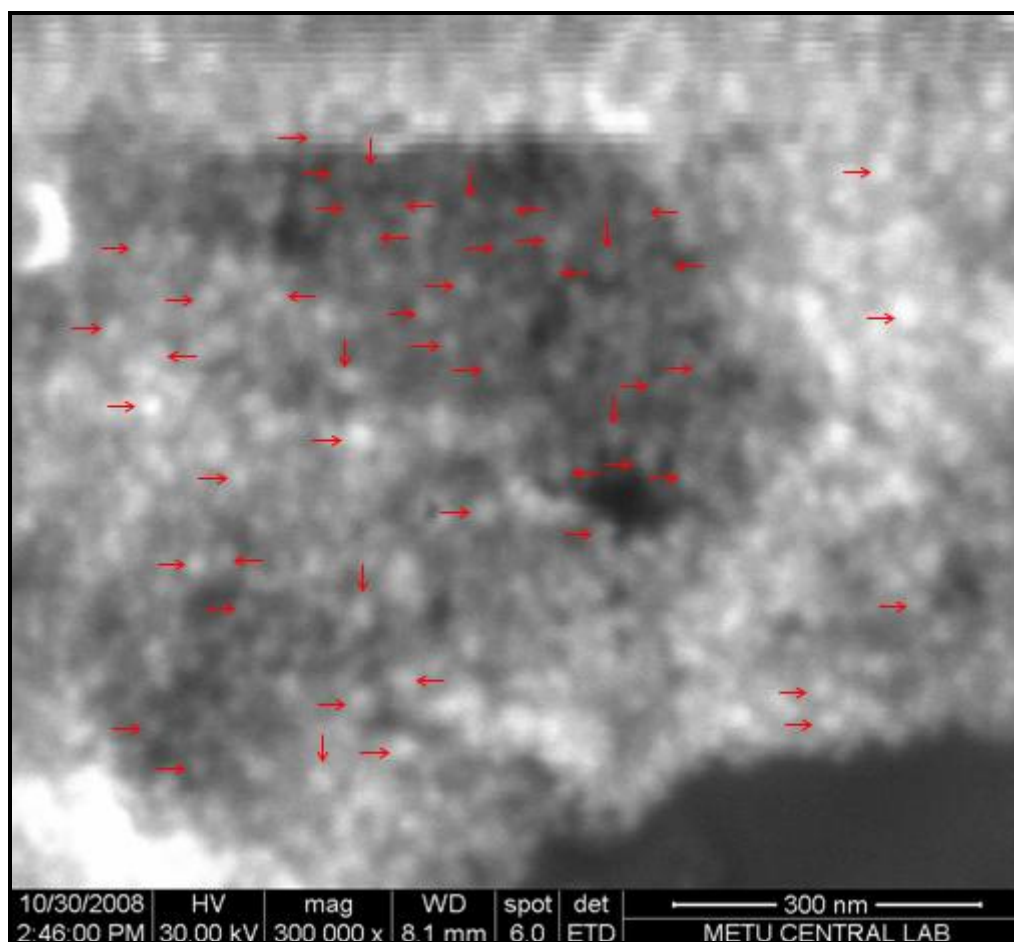


Figure 100. FE-SEM image of cobalt nanoparticles used in the particle size measurement study

Table 5. Particle size (d) measurement results for cobalt nanoparticles (shown in Figure 100)

Label	Particle Size	Label	Particle Size	Label	Particle Size
1	23.20	35	24.32	69	
2	19.30	36	29.43	70	
3	28.90	37	26.19	71	
4	24.10	38	26.41	72	
5	28.90	39	27.10	73	
6	24.10	40	23.55	74	
7	24.90	41	20.32	75	
8	22.20	42	24.12	76	
9	26.00	43	24.34	77	
10	27.10	44	25.71	78	
11	25.16	45	28.56	79	
12	20.32	46	23.12	80	
13	25.16	47	28.16	81	
14	26.77	48	24.68	82	
15	24.45	49	20.54	83	
16	23.55	50	26.35	84	
17	28.71	51		85	
18	22.25	52		86	
19	20.32	53		87	
20	23.12	54		88	
21	21.51	55		89	
22	28.42	56		90	
23	21.64	57		91	
24	30.00	58		92	
25	25.16	59		93	
26	28.39	60		94	
27	28.44	61		95	
28	25.36	62		96	
29	28.19	63		97	
30	29.12	64		98	
31	28.59	65		99	
32	26.27	66		100	
33	28.19	67		Average:	25.31
34	25.00	68		Stdev:	2.81

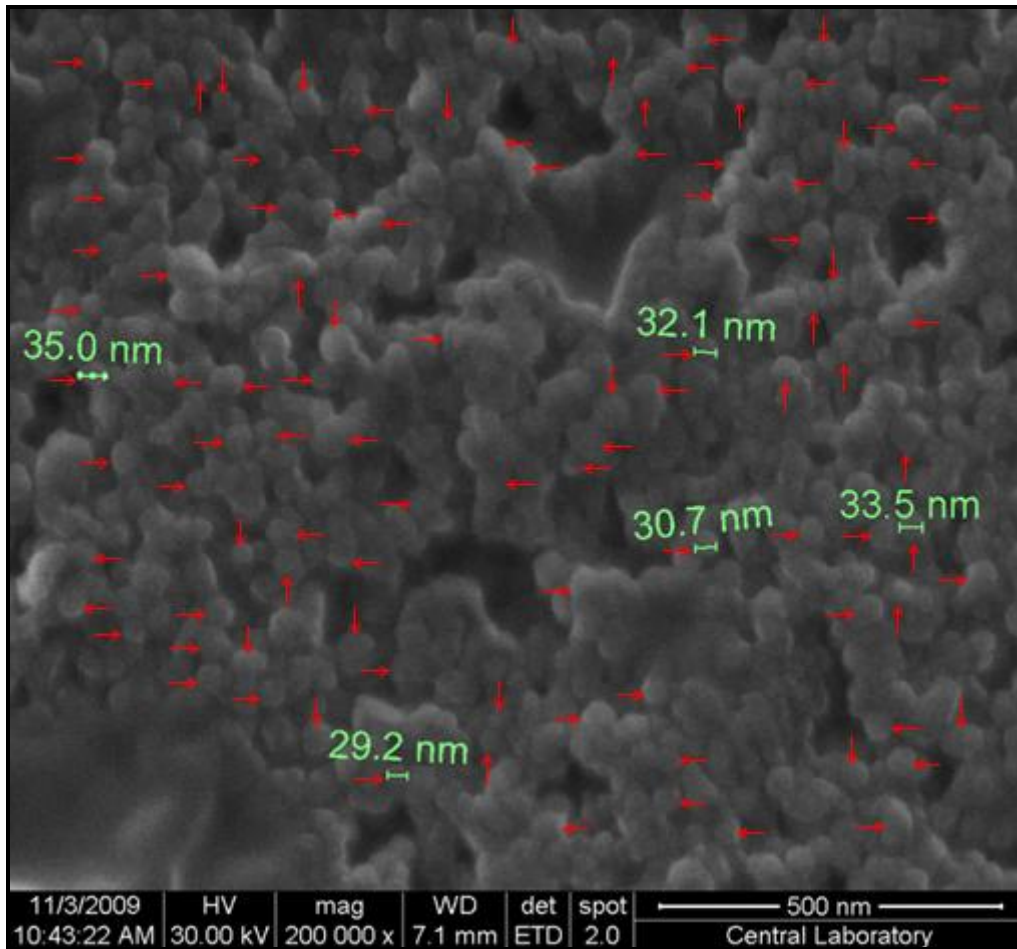


Figure 101. FE-SEM image of cobalt nanoparticles used in the particle size measurement study

Table 6. Particle size (d) measurement results for cobalt nanoparticles (shown in Figure 101)

Label	Particle Size	Label	Particle Size	Label	Particle Size
1	31.98	35	40.70	69	36.34
2	17.44	36	33.43	70	43.60
3	37.79	37	36.34	71	33.43
4	23.26	38	34.88	72	30.52
5	26.16	39	34.88	73	37.79
6	33.43	40	31.98	74	40.70
7	31.98	41	43.60	75	43.60
8	27.62	42	34.88	76	39.24
9	31.98	43	42.15	77	36.34
10	29.07	44	36.34	78	31.98
11	30.52	45	50.87	79	37.79
12	31.98	46	46.51	80	29.07
13	33.43	47	36.34	81	33.43
14	36.34	48	39.24	82	40.70
15	39.24	49	50.87	83	33.43
16	36.34	50	47.97	84	31.98
17	33.43	51	49.42	85	39.24
18	37.79	52	40.70	86	36.34
19	34.88	53	34.88	87	33.43
20	33.43	54	55.23	88	36.34
21	37.79	55	40.70	89	30.52
22	33.43	56	33.43	90	36.34
23	33.43	57	36.34	91	30.52
24	36.34	58	31.98	92	29.07
25	34.88	59	42.15	93	37.79
26	39.24	60	40.70	94	34.88
27	30.52	61	39.24	95	26.16
28	31.98	62	39.24	96	34.88
29	33.43	63	37.79	97	37.79
30	30.52	64	43.60	98	33.43
31	31.98	65	31.98	99	34.88
32	33.43	66	31.98	100	36.34
33	40.70	67	36.34	Average:	35.94
34	37.79	68	36.34	Stdev:	5.77

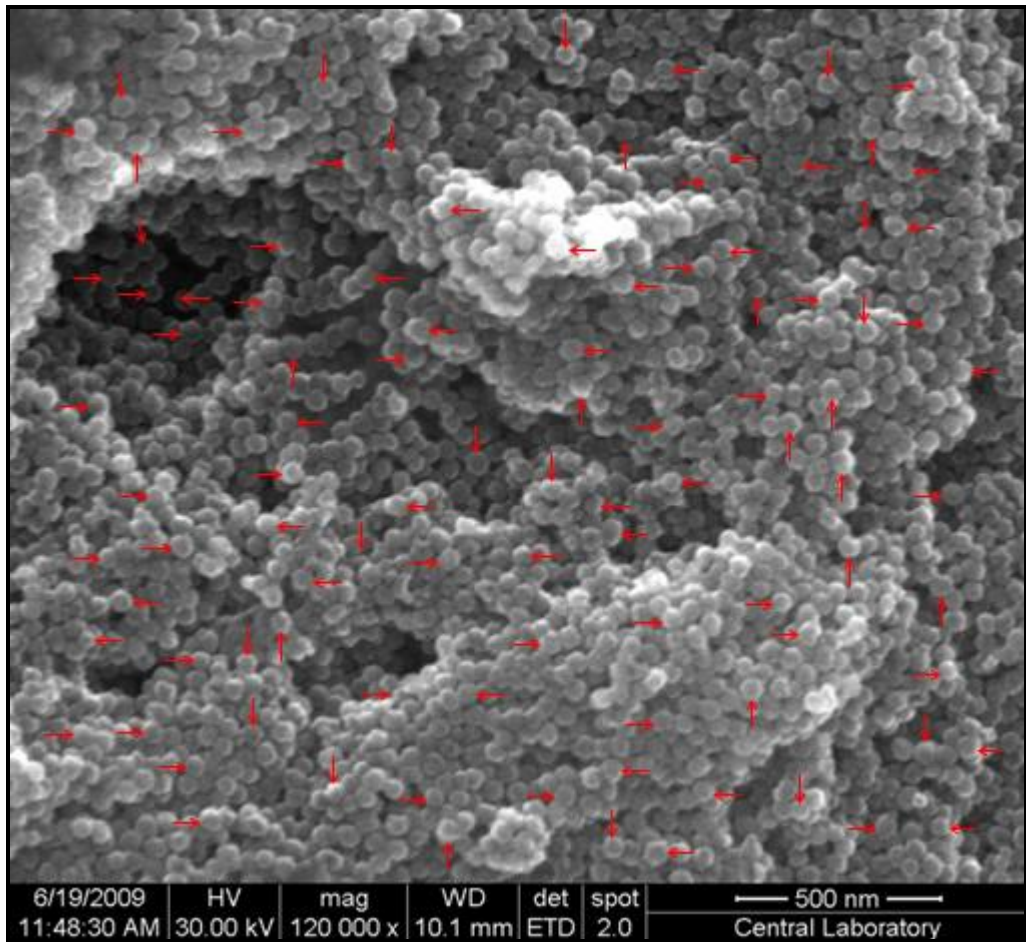


Figure 102. FE-SEM image of cobalt nanoparticles used in the particle size measurement study

Table 7. Particle size (d) measurement results for cobalt nanoparticles (shown in Figure 102)

Label	Particle Size	Label	Particle Size	Label	Particle Size
1	50.12	35	46.88	69	35.48
2	45.17	36	45.16	70	43.55
3	45.21	37	43.55	71	40.32
4	48.39	38	45.16	72	43.55
5	41.94	39	45.22	73	38.71
6	45.16	40	48.39	74	40.32
7	43.55	41	51.61	75	40.32
8	45.16	42	41.94	76	43.55
9	50.00	43	40.32	77	38.71
10	40.32	44	46.77	78	45.16
11	45.16	45	45.16	79	41.94
12	40.32	46	45.16	80	48.39
13	45.16	47	41.94	81	50.00
14	46.77	48	43.55	82	48.39
15	43.55	49	45.16	83	45.16
16	43.55	50	43.55	84	51.61
17	38.71	51	45.16	85	40.32
18	43.55	52	51.61	86	46.77
19	40.32	53	38.71	87	43.55
20	40.32	54	41.94	88	43.55
21	51.61	55	45.16	89	46.77
22	40.32	56	38.71	90	41.94
23	41.94	57	40.32	91	43.55
24	50.00	58	45.16	92	46.77
25	45.16	59	41.94	93	40.32
26	48.39	60	45.16	94	45.16
27	48.44	61	46.77	95	43.55
28	45.16	62	40.32	96	41.94
29	48.39	63	41.94	97	45.16
30	50.00	64	43.55	98	43.55
31	48.39	65	41.94	99	44.22
32	46.77	66	37.10	100	48.15
33	48.39	67	40.32	Average:	44.28
34	50.00	68	37.10	Stdev:	3.58

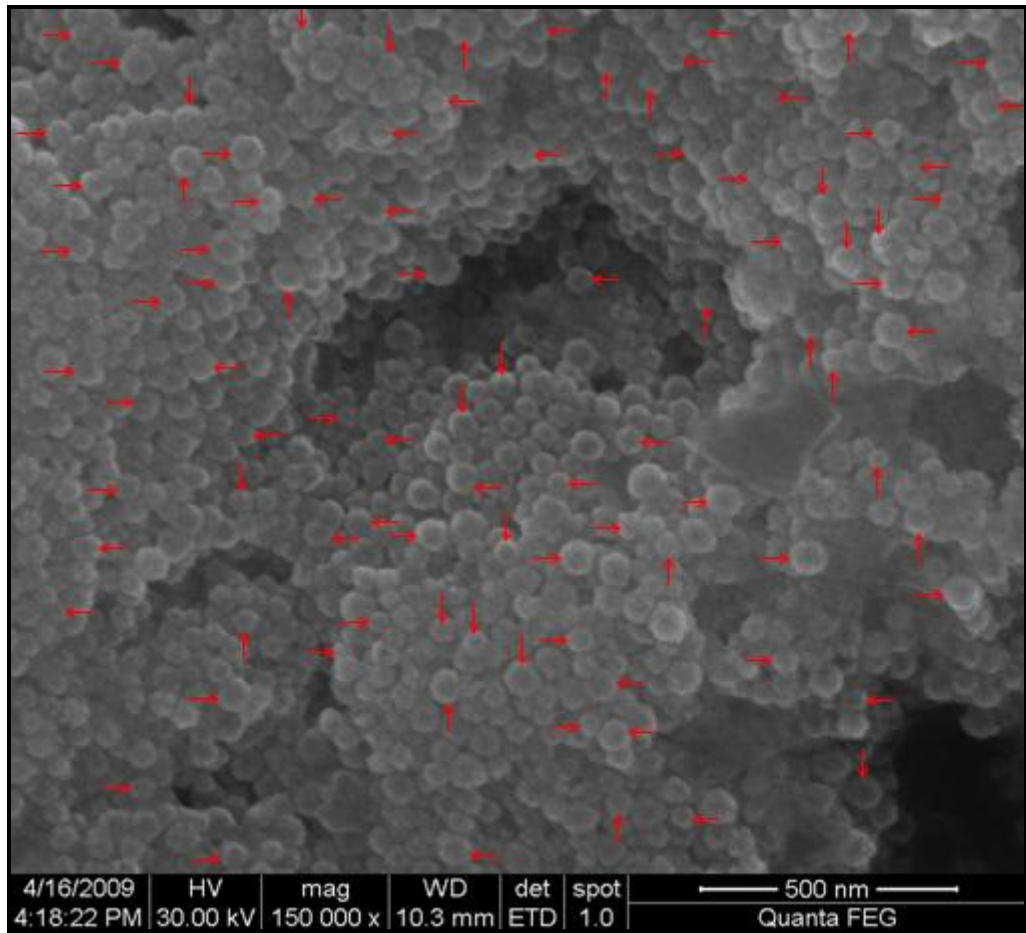


Figure 103. FE-SEM image of HAuNPs used in the particle size measurement study

Table 8. Particle size (d) measurement results for HAuNPs (shown in Figure 103)

Label	Particle Size	Label	Particle Size	Label	Particle Size	Label	Particle Size
1	68.83	35	66.23	69	35.06	103	45.45
2	57.14	36	61.04	70	59.74	104	42.86
3	62.34	37	64.94	71	45.45	105	48.05
4	55.84	38	55.84	72	48.05	106	40.26
5	79.22	39	64.94	73	51.95	107	46.75
6	67.53	40	67.53	74	45.45	108	45.45
7	63.64	41	72.73	75	41.56	109	46.75
8	63.64	42	55.84	76	46.75	110	50.65
9	58.44	43	46.75	77	49.35	111	51.95
10	62.34	44	45.45	78	51.95	112	48.05
11	68.83	45	46.75	79	50.65	113	45.45
12	58.44	46	41.56	80	46.75	114	46.75
13	74.03	47	46.75	81	44.16	115	46.75
14	68.83	48	46.75	82	44.16	116	42.86
15	62.34	49	53.25	83	45.45	117	40.26
16	63.64	50	45.45	84	49.35	118	46.75
17	68.83	51	45.45	85	44.16	119	40.26
18	44.16	52	45.45	86	42.86	120	54.55
19	54.55	53	45.45	87	49.35	121	45.45
20	50.65	54	49.35	88	45.45	122	45.45
21	72.73	55	48.05	89	48.05	123	44.16
22	59.74	56	50.65	90	40.26	124	49.35
23	64.94	57	42.86	91	49.35	125	49.35
24	61.04	58	54.55	92	51.95	126	46.75
25	59.74	59	40.26	93	42.86		
26	55.84	60	42.86	94	53.25		
27	70.13	61	51.95	95	45.45		
28	66.23	62	44.16	96	41.56		
29	58.44	63	48.05	97	42.86		
30	42.86	64	44.16	98	40.26		
31	64.94	65	37.66	99	40.26		
32	63.64	66	46.75	100	38.96		
33	71.43	67	46.75	101	36.36	Avrg:	51.71
34	71.43	68	46.75	102	46.75	Stdv:	9.72

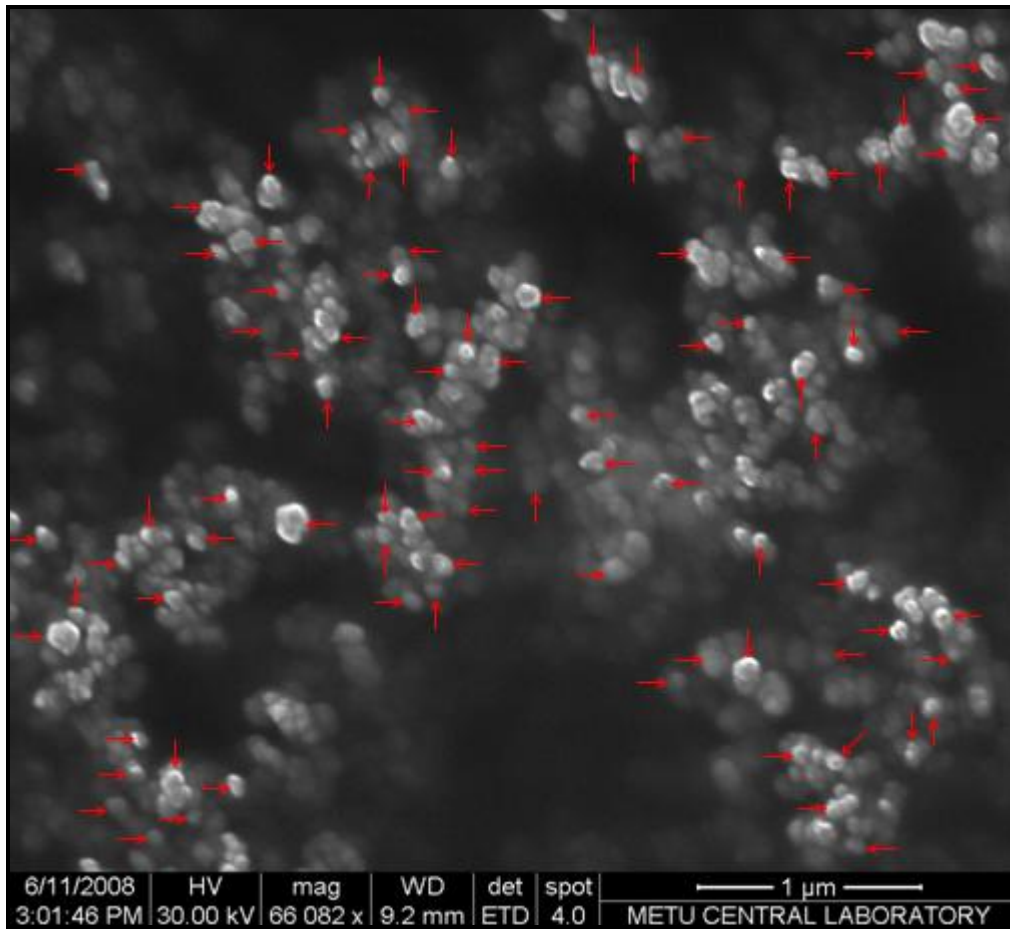


Figure 104. FE-SEM image of HAuAgNPs used in the particle size measurement study

Table 9. Particle size (d) measurement results for H_{Au}AgNPs (shown in Figure 104)

Label	Particle Size	Label	Particle Size	Label	Particle Size
1	119.05	35	86.31	69	86.31
2	92.26	36	80.36	70	95.24
3	89.29	37	86.31	71	86.31
4	92.26	38	98.21	72	74.40
5	89.29	39	86.31	73	80.36
6	98.21	40	89.29	74	80.36
7	86.31	41	83.33	75	74.40
8	101.19	42	89.29	76	74.40
9	71.43	43	107.14	77	74.40
10	101.19	44	83.33	78	89.29
11	77.38	45	95.24	79	86.31
12	74.40	46	86.31	80	65.48
13	92.26	47	86.31	81	89.29
14	74.40	48	77.38	82	95.24
15	83.33	49	83.33	83	83.33
16	80.36	50	80.36	84	83.33
17	95.24	51	89.29	85	89.29
18	71.43	52	86.31	86	92.26
19	83.33	53	80.36	87	83.33
20	95.24	54	86.31	88	71.43
21	83.33	55	77.38	89	89.29
22	80.36	56	86.31	90	86.31
23	92.26	57	92.26	91	89.29
24	104.17	58	107.14	92	65.48
25	92.26	59	98.21	93	77.38
26	98.21	60	86.31	94	92.26
27	74.40	61	101.19	95	92.26
28	74.40	62	92.26	96	83.33
29	86.31	63	80.36	97	101.19
30	86.31	64	92.26	98	83.15
31	113.10	65	74.40	99	89.05
32	89.29	66	89.29	100	94.62
33	77.38	67	74.40	Average:	86.68
34	77.38	68	80.36	Stdev:	9.66

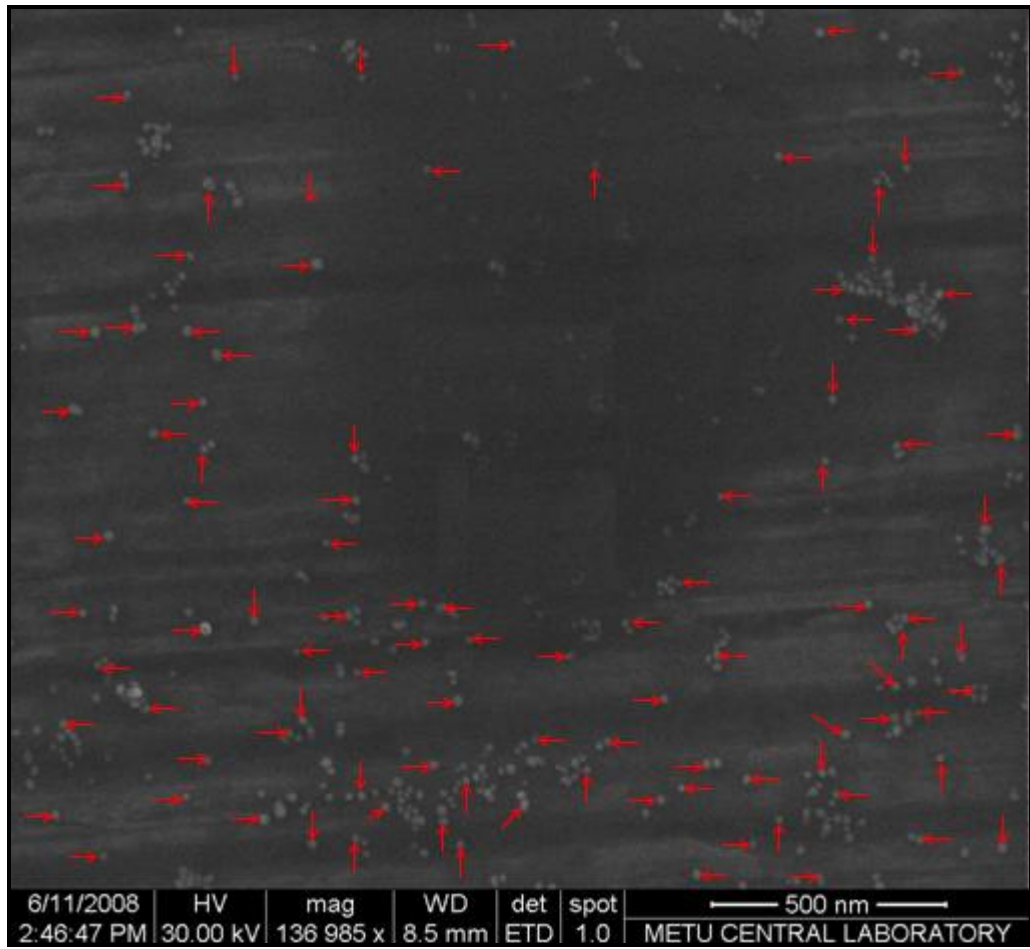


Figure 105. FE-SEM image of AuNPs used in the particle size measurement study

Table 10. Particle size (d) measurement results for AuNPs (shown in Figure 105)

Label	Particle Size	Label	Particle Size	Label	Particle Size
1	19.72	35	21.13	69	21.13
2	23.94	36	19.72	70	19.72
3	22.54	37	19.72	71	21.13
4	21.13	38	19.72	72	21.13
5	19.72	39	16.90	73	22.54
6	16.90	40	21.13	74	19.72
7	19.72	41	18.31	75	21.13
8	18.31	42	19.72	76	19.72
9	19.72	43	19.72	77	18.31
10	21.13	44	21.13	78	19.72
11	19.72	45	18.31	79	15.49
12	19.72	46	19.72	80	25.35
13	16.90	47	25.35	81	19.72
14	21.13	48	15.49	82	19.72
15	21.13	49	21.13	83	18.31
16	18.31	50	19.72	84	23.94
17	19.72	51	18.31	85	18.31
18	21.13	52	16.90	86	21.13
19	21.13	53	18.31	87	22.54
20	19.72	54	15.49	88	22.54
21	19.72	55	23.94	89	19.72
22	22.54	56	18.31	90	21.13
23	21.13	57	21.13	91	18.31
24	19.72	58	21.13	92	21.13
25	21.13	59	19.72	93	16.90
26	21.13	60	21.13	94	18.31
27	19.72	61	23.94	95	16.90
28	18.31	62	21.13	96	21.13
29	22.54	63	19.72	97	19.72
30	21.13	64	19.72	98	22.54
31	21.13	65	22.54	99	28.17
32	22.54	66	22.54	100	21.13
33	18.31	67	25.35	Average:	20.38
34	21.13	68	23.94	Stdev:	2.2

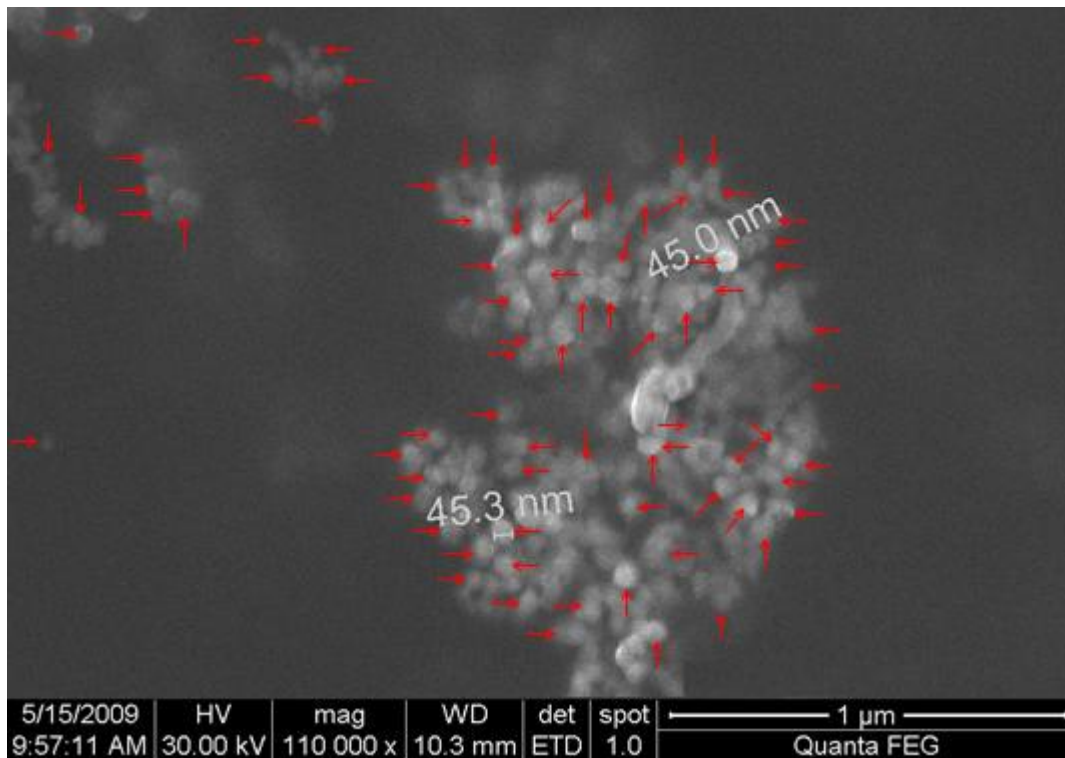


Figure 106. FE-SEM image of AuAgNPs used in the particle size measurement study

Table 11. Particle size (d) measurement results for AuAgNPs (shown in Figure 106)

Label	Particle Size	Label	Particle Size	Label	Particle Size
1	47.01	35	43.66	69	47.01
2	50.37	36	48.69	70	60.44
3	45.34	37	52.05	71	48.69
4	47.01	38	48.69	72	57.08
5	36.95	39	53.72	73	40.30
6	57.08	40	48.69	74	65.47
7	48.69	41	47.01	75	58.76
8	57.08	42	38.62	76	55.40
9	55.40	43	47.01	77	48.69
10	45.34	44	50.37	78	43.66
11	43.66	45	36.95	79	40.30
12	40.30	46	38.62	80	45.34
13	45.34	47	40.30	81	45.34
14	38.62	48	33.59	82	35.27
15	53.72	49	38.62	83	43.66
16	40.30	50	38.62	84	
17	45.34	51	55.40	85	
18	53.72	52	55.40	86	
19	53.72	53	33.59	87	
20	45.34	54	35.27	88	
21	48.69	55	38.62	89	
22	48.69	56	38.62	90	
23	50.37	57	45.34	91	
24	36.95	58	41.98	92	
25	48.69	59	40.30	93	
26	41.98	60	58.76	94	
27	55.40	61	31.91	95	
28	47.01	62	40.30	96	
29	50.37	63	35.27	97	
30	40.30	64	33.59	98	
31	40.30	65	45.34	99	
32	43.66	66	57.08	100	
33	40.30	67	52.05	Average:	45.98
34	38.62	68	55.40	Stdev:	7.38

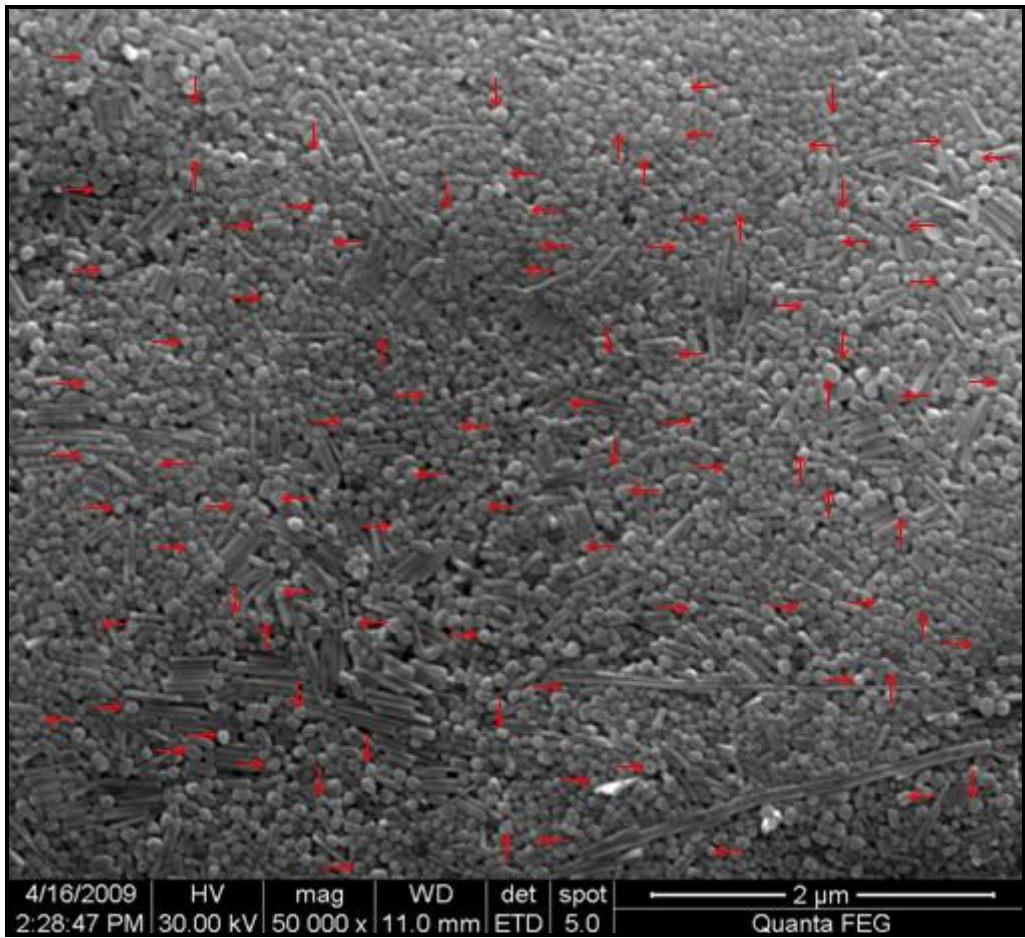


Figure 107. FE-SEM image of AgNPs used in the particle size measurement study

Table 12. Particle size (d) measurement results for AgNPs (shown in Figure 107)

Label	Particle Size	Label	Particle Size	Label	Particle Size	Label	Particle Size
1	69.90	35	81.55	69	85.44	103	50.49
2	66.02	36	66.02	70	97.09	104	62.14
3	93.20	37	100.97	71	85.44	105	66.02
4	89.32	38	85.44	72	73.79	106	66.02
5	81.55	39	81.55	73	54.37	107	69.90
6	69.90	40	69.90	74	69.90	108	69.90
7	58.25	41	108.74	75	54.37	109	66.02
8	46.60	42	81.55	76	62.14	110	58.25
9	34.95	43	89.32	77	73.79	111	50.49
10	54.37	44	100.97	78	73.79	112	50.49
11	58.25	45	116.50	79	62.14	113	66.02
12	69.90	46	77.67	80	77.67	114	58.25
13	50.49	47	73.79	81	69.90	115	69.90
14	34.95	48	93.20	82	54.37	116	62.14
15	50.49	49	58.25	83	89.32	117	58.25
16	46.60	50	77.67	84	81.55	118	97.09
17	85.44	51	77.67	85	89.32	119	62.14
18	93.20	52	100.97	86	50.49	120	66.02
19	116.50	53	73.79	87	85.44	121	58.25
20	89.32	54	77.67	88	100.97	122	58.25
21	38.83	55	62.14	89	100.97	123	77.45
22	31.07	56	97.09	90	100.97	124	93.20
23	54.37	57	66.02	91	54.37	125	81.55
24	58.25	58	69.90	92	58.25	126	38.83
25	66.02	59	66.02	93	38.83	127	42.72
26	69.90	60	66.02	94	54.37	128	34.95
27	58.25	61	69.90	95	62.14	129	34.95
28	62.14	62	81.55	96	62.14	130	38.83
29	69.90	63	89.32	97	73.79	131	38.83
30	54.37	64	93.20	98	104.85	132	38.83
31	54.37	65	81.55	99	93.20	133	46.60
32	58.25	66	62.14	100	73.79	134	38.83
33	97.09	67	62.14	101	85.44	Avrg:	69.58
34	77.67	68	69.90	102	58.25	Stdv:	18.79

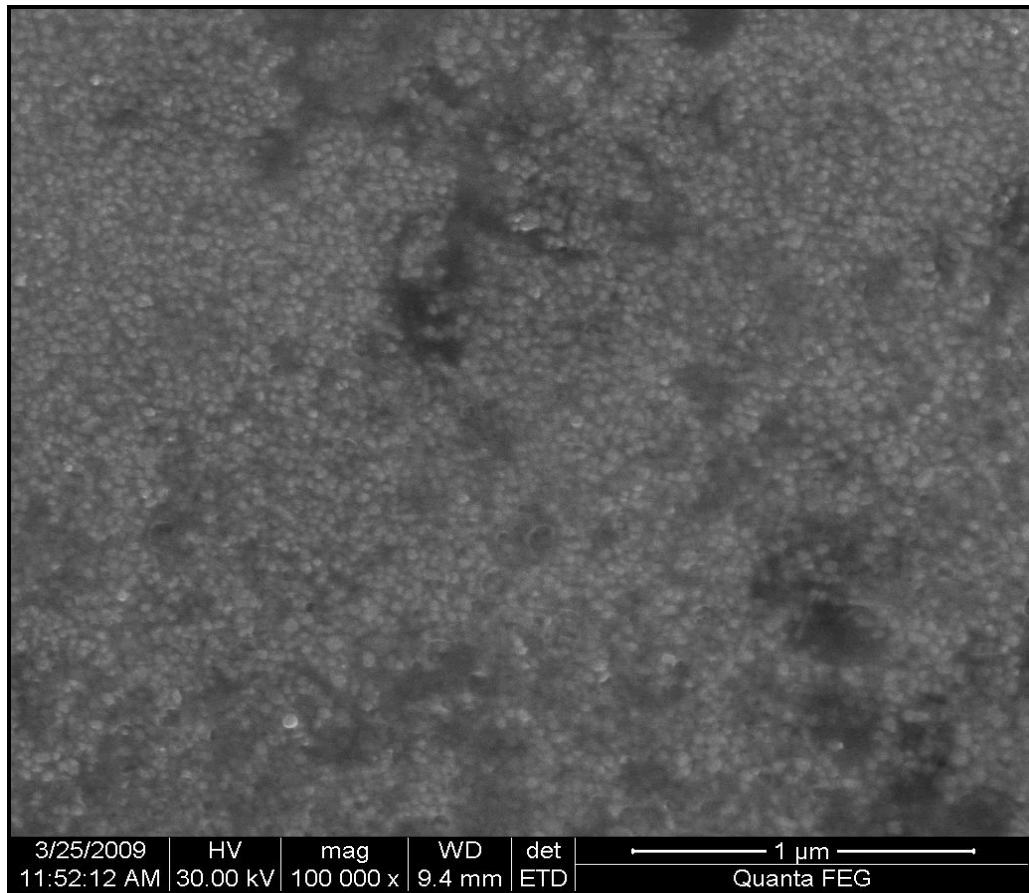


Figure 108. FE-SEM image of Ag-Fe(NTA)NPs used in the particle size measurement study

Table 13. Particle size (d) measurement results for Ag-Fe(NTA)NPs

(shown in Figure 108)

Label	Particle Size	Label	Particle Size	Label	Particle Size
1	39.06	35	37.11	69	31.25
2	42.97	36	27.34	70	29.30
3	44.92	37	27.34	71	35.16
4	31.25	38	23.44	72	23.44
5	41.02	39	29.30	73	25.39
6	33.20	40	33.20	74	33.20
7	35.16	41	25.39	75	27.34
8	39.06	42	29.30	76	29.30
9	33.20	43	23.44	77	25.39
10	29.30	44	29.30	78	29.30
11	29.30	45	25.39	79	23.44
12	31.25	46	37.11	80	33.20
13	39.06	47	31.25	81	29.30
14	29.30	48	29.30	82	25.39
15	31.25	49	35.16	83	33.20
16	35.16	50	29.30	84	27.34
17	31.25	51	25.39	85	31.25
18	27.34	52	27.34	86	31.25
19	31.25	53	29.30	87	33.20
20	21.48	54	33.20	88	25.39
21	25.39	55	21.48	89	27.34
22	37.11	56	25.39	90	35.16
23	41.02	57	29.30	91	29.30
24	21.48	58	27.34	92	25.39
25	27.34	59	21.48	93	31.25
26	31.25	60	23.44	94	33.20
27	39.06	61	33.20	95	37.11
28	31.25	62	23.44	96	27.34
29	31.25	63	31.25	97	33.20
30	48.83	64	33.20	98	31.25
31	31.25	65	29.30	99	27.34
32	23.44	66	31.25	100	37.11
33	25.39	67	25.39	Average:	30.49
34	33.20	68	25.39	Stdev:	5.31

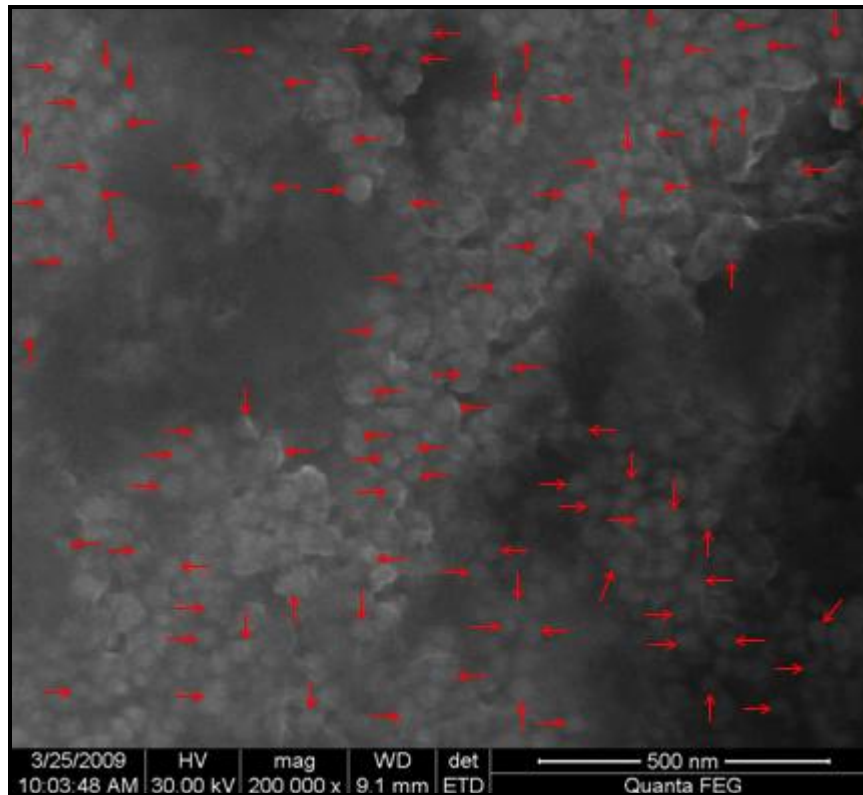


Figure 109. FE-SEM image of Ag-Eu³⁺ NPs used in the particle size measurement study

Table 14. Particle size (d) measurement results for Ag-Eu³⁺ NPs

(shown in Figure 109)

Label	Particle Size	Label	Particle Size	Label	Particle Size
1	37.67	35	42.24	69	42.24
2	35.39	36	45.66	70	36.53
3	38.81	37	35.39	71	36.53
4	33.11	38	37.67	72	35.39
5	31.96	39	37.67	73	36.53
6	36.53	40	38.81	74	42.24
7	42.24	41	37.67	75	46.80
8	37.67	42	44.52	76	41.10
9	30.82	43	39.95	77	41.10
10	31.96	44	46.80	78	37.67
11	36.53	45	42.24	79	42.24
12	36.53	46	42.24	80	45.66
13	37.67	47	38.81	81	50.23
14	37.67	48	37.67	82	41.10
15	33.11	49	36.53	83	42.24
16	36.53	50	39.95	84	30.82
17	38.81	51	37.67	85	38.81
18	31.96	52	41.10	86	39.95
19	35.39	53	44.52	87	42.24
20	41.10	54	38.81	88	31.96
21	46.80	55	41.10	89	34.25
22	30.82	56	50.23	90	41.10
23	36.53	57	45.66	91	43.38
24	34.25	58	41.10	92	33.11
25	42.24	59	39.95	93	34.25
26	39.95	60	43.38	94	33.11
27	35.39	61	41.10	95	36.53
28	36.53	62	42.24	96	45.66
29	36.53	63	41.10	97	41.10
30	38.81	64	38.81	98	28.54
31	37.67	65	44.52	99	31.96
32	37.67	66	46.80	100	39.95
33	37.67	67	44.52	Average:	39.08
34	38.81	68	45.66	Stdev:	4.46

CURRICULUM VITAE

Personal Information

Surname, Name: Kaya, Murat

Nationality: Turkish (TC)

Date and Place of Birth: 10 September 1978, Ankara

Marital Status: Single

Phone: 90 3122103245

Fax: 90 3122103200

e-mail: mmuratkaya@gmail.com

Education

BS	Middle East Technical University, Department of Chemistry	2002
MS	Middle East Technical University, Department of Chemistry	2004
PhD	Middle East Technical University, Department of Chemistry	2011

Work Experience

Lecturer (General Chemistry, Chem102), Atılım University, Chemical Engineering and Applied Chemistry, Ankara, Turkey (2009-2011)

Publications

(1) "Germanium Determination by Flame Atomic Absorption Spectrometry: An Increased Vapor Pressure-chloride Generation System"

Murat Kaya, Mürvet Volkan

Talanta, 2011, 84, 1, 122

(2) “Synthesis of N-Polyethereal Polypyrroles and Their Application for the Preconcentration of Rare Earth Ions “

Bahar Köksel, **Murat Kaya**, Atilla Cihaner, Mürvet Volkan, Ahmet M. Önal

J. App. Poly. Sci., 2008, 108, 2707

(3) “Preparation and Characterization of Ni-NTA Bearing PMAA Coated Superparamagnetic Magnetite Nanoparticles”

Bilsen Tural, **Murat Kaya**, Necati Özkan, Mürvet Volkan

J. Nanosci. Nanotech., 2008, 8, 695

(4) “Silver Nanoparticle-doped Polyvinyl Alcohol Coating as a Medium for Surface-enhanced Raman Scattering Analysis”

Seher Karabıçak, **Murat Kaya**, Tuan Vo-Dinh, Mürvet Volkan

J. Nanosci. Nanotech., 2008, 8, 955

International and National Conference Papers

(1) Zehra Tatlici, Umit Zengin, **Murat Kaya**, Mürvet Volkan, Preparation and Characterization of Silica Coated Magnetite Nanoparticles and Labeling with Tc-99m for Magnetically Targeted Radioactive Imaging, 7th Aegean Analytical Chemistry Days, AACD2010 Conference, 29th September-3th October 2010, Mytilene, Lesvos, Greece (**Best poster award**)

(2) Üzeyir Doğan, **Murat Kaya**, Atilla Cihaner, Mürvet Volkan, Performance of Silver Doped PEDOT Polymer Film as a SERS Substrate, 6th Nanoscience and Nanotechnology Conference (**NanoTR6**), 15-18 June 2010, IYTE, İzmir, Turkey

(3) Gülfem Aygar ,Zeynep Ergül, Lütfiye Sezen Keser , **Murat Kaya** , Mürvet Volkan, Comparison of Magnetic Behavior of Cobalt, Cobalt-Ferrite and Iron

Oxide Nanoparticles with Silica Coatings, 6th Nanoscience and Nanotechnology Conference (**NanoTR6**), 15-18 June 2010, IYTE, İzmir, Turkey

(4) **Murat Kaya**, Mürvet Volkan, Surface Enhanced Raman Scattering (SERS) Detection of Biologically Important Compounds Utilizing Noble Metal Nanoparticles with Tunable Optical Properties, ECASIA'09, 13th European Conference on Applications of Surface and Interface Analysis, October 18-23, 2009, Antalya, Turkey, **Oral Presentation**

(5) Gözde Kerman, Muharrem Timuçin, **Murat Kaya**, Mürvet Volkan, Nuhan Puralı, Petek Korkusuz, Sema Hakkı, Feza Korkusuz, Trace Element Release from Si-HAP Containing Ceramics, BIOTECH 2009 International Symposium on Biotechnology: Developments and Trend, 27-30 September 2009, Middle East Technical University, Ankara, Turkey

(6) **Murat Kaya**, Mürvet Volkan, Synthesis of Hollow Gold-Silver Double Shell and Gold Core Silver Shell Nanoparticles for Molecular Sensing Using Surface-Enhanced Raman Scattering (SERS) Spectroscopy, Colloquium Spectroscopicum Internationale XXXVI - August 30-September 3, 2009, Budapest, Hungary

(7) **Murat Kaya**, Mürvet Volkan, Preparation of Hollow Gold-Silver Double Shell Nanospheres and Gold Core Silver Shell Nanoparticles for SERS Applications, 5th Nanoscience and Nanotechnology Conference (**NanoTR5**), June 08-12, 2009, Eskisehir, Turkey, **Oral Presentation**

(8) Lütfiye Sezen Keser, **Murat Kaya**, Mürvet Volkan, DNA Purification with Aminosilane Modified Magnetic Cobalt Nanoparticles, 5th Nanoscience and Nanotechnology Conference (**NanoTR5**), June 08-12, 2009, Eskisehir, Turkey

(9) Seda Kibar, **Murat Kaya**, Mürvet Volkan, Preparation and Characterization of Silica Coated-Dye Doped Ag Nanoparticles, 5th Nanoscience and Nanotechnology Conference (**NanoTR5**), June 08-12, 2009, Eskisehir, Turkey

(10) Gülfem Aygar, **Murat Kaya**, Mürvet Volkan, Preparation of Silica and PMAA Coated Cobalt Ferrite (CoFe_2O_4) Magnetic Nanoparticles for the Purification of Histidine-Tagged Proteins, 5th Nanoscience and Nanotechnology Conference (**NanoTR5**), June 08-12, 2009, Eskisehir, Turkey

(11) Serap Tekin, **Murat Kaya**, Mürvet Volkan, Sensor Application of Ferrozine Doped Sol-gel Beads for Speciation Studies of Iron, Eurotrode IX – Dublin, March 30th – April 2nd, 2008. Dublin, Ireland (**Best poster award**)

(12) Bahar Köksel, **Murat Kaya**, Atilla Cihaner, Ahmet M. Önal, Mürvet Volkan, Using Poly-1-11-Bis(1-1 Pyrrole)3,6,9-Trioxaundecane in Preconcentrations of Lanthanides, 10th International Spectroscopy Conference, 04-07 July, 2007, IYTE, İzmir

(13) Seher Karabıçak, **Murat Kaya**, Tuan Vo-Dinh, Mürvet Volkan, Silver Nanoparticle-doped Polyvinyl Alcohol Coating as a Medium for Surface-enhanced Raman Scattering Analysis, International Workshop on Nano-structured Materials, NANOMAT 2006, June 21-23, 2006, Antalya, Turkey

(14) Bilsen Tural, **Murat Kaya**, Mürvet Volkan, Preparation and Characterization of Maghemite and Magnetite Nanoparticles Designed Specifically as a Magnetic Platform for Histidine Separation, International workshop on Nano-structured Materials, NANOMAT 2006, June 21-23, 2006, Antalya, Turkey

(15) **Murat Kaya**, Mürvet Volkan, Atomic Spectrometric Method for the Determination of Trace Amounts of Germanium through the Vaporization of Germanium as Germanium Tetrachloride, 2nd Black Sea Basin Conference on Analytical Chemistry, 14-17 September 2003, Sile, Istanbul, Turkey

(16) **Murat Kaya**, Mürvet Volkan, Determination of Germanium at Trace Level by Interference Free Chloride Generation Atomic Absorption Spectrometry, III Aegean Analytical Chemistry Days, Sep 29th-Oct 3rd 2002, Polihnitos, Lesvos, Greece